THE
PHYSICAL REVIEW
A Journal of Experimental and Theoretical Physics
VOL. 46, NO. 5 SEPTEMBER 1, 1934 SECOND SERIES

The Determination of X-Ray Line Shapes by a Double Crystal Spectrometer

LLOYD P. SMITH, *Cornell University*
(Received May 28, 1934)

As a result of a new mathematical analysis of the action of the double crystal spectrometer, a method of using the instrument has been found which makes it possible to determine the spectral energy distribution of an x-ray line and to calibrate the instrument without any previous knowledge of the diffraction patterns of the crystals.

INTRODUCTION

OF late, it has become increasingly important to determine precisely the spectral energy distribution of x-ray lines and of absorption limits. It was hoped that such determinations could be made by means of the double crystal spectrometer but this hope has not as yet been satisfactorily realized. The fundamental difficulty lies in the fact that it has been impossible to calibrate a particular spectrometer, which amounts to saying that the effect of the spectrometer on a strictly monochromatic incident beam of x-rays is not completely known for any spectrometer. Since no source of strictly monochromatic x-rays exists, it is of course impossible to carry out a direct calibration. In lieu of this, a number of investigations have been carried out for the purpose of determining the effect of the component parts of the spectrometer on the incident radiation, in particular, the alteration in the radiation produced by the crystals. Unfortunately an impasse was encountered in this regard also, when it was shown by von Laue[1] that the relevant characteristics or diffraction patterns of two identical crystals cannot be determined in general from the experimentally determined rocking curve in the (1, −1) orders. Lacking such characteristics, investigators have made use of theoretical characteristics developed by Darwin,[2] Ewald,[3, 4] Waller[5] and Prins[6] and certain hypothetical characteristics[7, 8, 9] with the hope that some one of these would give results in agreement with experiment for a given pair of crystals and a suitably restricted wave-length region. The procedure has then been to use the adopted characteristics to compute quantities such as rocking curves, coefficients of reflection, etc., which may be compared with the corresponding experimentally measured quantities. The work of S. K. Allison[10] and L. G. Parratt[11] furnishes an excellent example of how such comparisons have been made. In this connection, it should be noted that in making comparisons it is customary to compare quantities like the widths (at half maximum) of the theoretical and experimental rocking curves or the area under such curves, etc. These are not particularly

[1] M. von Laue, Zeits. f. Physik **72**, 472 (1931).

[2] C. G. Darwin, Phil. Mag. **27**, 325 and 675 (1914).
[3] P. P. Ewald, Ann. d. Physik **54**, 519 (1917).
[4] P. P. Ewald, Phys. Zeits. **26**, 29 (1925).
[5] I. Waller, Upsala Universitets Arsskrift 1925, 11.
[6] Prins, Zeits. f. Physik **63**, 477 (1930).
[7] Ehrenberg and Mark, Zeits. f. Physik **42**, 807 (1927).
[8] Schwarzschild, Phys. Rev. **32**, 162 (1928).
[9] S. K. Allison, Phys. Rev. **38**, 203 (1931).
[10] S. K. Allison, Phys. Rev. **41**, 1 (1932).
[11] L. G. Parratt, Phys. Rev. **41**, 561 (1932).

sensitive to variations in the form of the crystal characteristics and consequently even if they agree with those found experimentally, this does not constitute an adequate test of the correctness of the theoretical crystal characteristic used. Even when the theoretical rocking curves in the (1, −1) orders agree closely with the corresponding curve measured experimentally, it cannot be inferred that the crystal characteristic adopted is the correct one. This fact was realized and mentioned by Allison[10] when he found very close agreement in the (1, −1) rocking curves when the crystal characteristic suggested by Prins[6] was used as the basis for the theoretical curve. The reason for this lack of uniqueness will come out in the subsequent analysis. It is therefore necessary to determine the crystal characteristics experimentally to an extent sufficient for the solution of the problem of determining line shapes. It is the main purpose of this paper to show that there exists a method for doing this which leads to a unique determination of the spectral energy distribution incident on the first crystal of a double crystal spectrometer.

Theoretical and Hypothetical Crystal Characteristics

In order to carry out the subsequent analysis with sufficient generality, the reflected intensity characteristic of a crystal will be defined by means of a function $f(\Phi, \psi, \lambda)$, where Φ denotes the acute angle of incidence of the x-ray beam measured from the crystal surface and ψ is the acute angle between the crystal surface and the direction in which intensity of the reflected radiation is to be measured. It is assumed for the present that the incident and reflected rays lie in a plane perpendicular to the crystal planes. Physically, $f(\Phi, \psi, \lambda)$ is the intensity reflected from a crystal in the angular region between ψ and $\psi+d\psi$ when a beam of radiation of unit intensity whose wave-length lies between λ and $\lambda+d\lambda$ is incident in the angular region between Φ and $\Phi+d\Phi$. It will be noted from this definition that it is contemplated that there will be radiation reflected from an actual crystal at other angles than the angle of incidence; a possibility which has not been taken into account in previous theories of the double crystal spectrometer. As explicitly indicated $f(\Phi, \psi, \lambda)$ is expected to vary with the wave-length of the radiation. In addition to this f will depend on such quantities as the degree of polarization of the radiation, the crystal temperature, etc. In order to justify an assumption with regard to the wave-length variation of the function $f(\Phi, \psi, \lambda)$ which will be made later, it will be necessary to consider briefly the salient features of certain crystal characteristics which have been derived on purely theoretical grounds.

Theoretical derivations of the $f(\Phi, \psi, \lambda)$ have been carried out for certain ideal and special crystals by Darwin,[2] Ewald[3, 4] and Waller.[5] In these derivations it was assumed that an infinitely wide plane parallel monochromatic beam of radiation is incident on a semi-infinite perfect crystal at a glancing angle Φ. It will only be necessary to consider the case where the reflecting planes are parallel to the surface of the crystal and the incident and reflected beams determine a plane perpendicular to the crystal

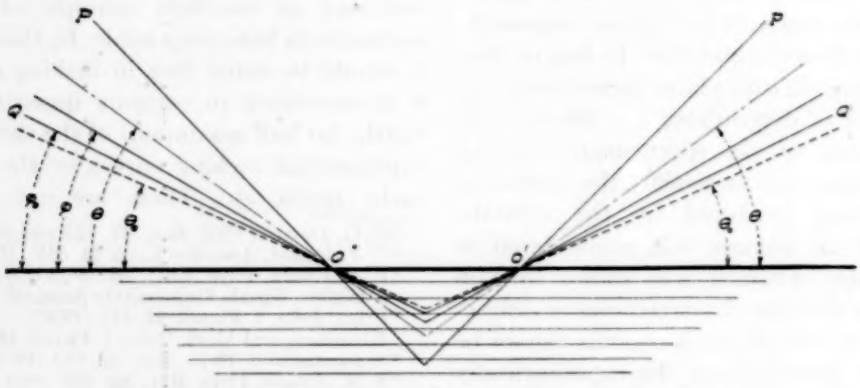

Fig. 1. Diagram showing the tolerance angle of a perfect crystal.

face and finally where the radiation is polarized at right angles to this plane. For this case the above investigations show that there exists an angular region (see Fig. 1) *POQ* in which the incident beam would be totally reflected in contradistinction to the single direction θ_0 given by the Bragg law, $n\lambda = 2d \sin \theta_0$. The angle θ between the bisector of the angle *POQ* and the crystal surface is the Bragg angle corrected for refraction, i.e., $\theta = \theta_0 + 2\delta/\sin 2\theta_0$ where δ is the deviation of the index of refraction from unity. In general the half-width of *POQ* is less than $\theta - \theta_0$. For this ideal arrangement the reflected beam is infinitely wide but accurately plane parallel, making the same glancing angle with the crystal as the initial beam. In terms of the characteristic function this means that $f(\Phi, \psi, \lambda)$ will be zero for all values of ψ except $\psi = \Phi$ and we have a function of one angle only, namely, $f(\Phi, \Phi, \lambda)$. For values of Φ in *POQ*, $f(\Phi, \Phi, \lambda)$ is unity for this ideal case. The actual form of f as computed by Waller for a cubic crystal with identical diffracting centers when Φ is outside of the angle *POQ*, is

$$f_w(\Phi, \Phi, \lambda) = \frac{|\theta - \Phi_0|^2 \sin^2 2\theta_0}{[(\theta - \Phi) \sin 2\theta_0 \pm \{(\theta - \Phi)^2 \sin^2 2\theta_0 - |\theta - \Phi_0|^2 \sin^2 2\theta_0\}^{\frac{1}{2}}]^2}, \tag{1}$$

the plus sign to be taken when $(\theta - \Phi) \sin 2\theta_0 > 0$ and the minus sign when $(\theta - \Phi) \sin 2\theta_0 < 0$. The wave-length dependence is contained in θ and θ_0. $(\theta - \Phi_0)$ depends on a number of factors such as the crystal structure and crystal temperature. The effect of the temperature vibration of the diffracting centers is to make the range $(\theta - \Phi_0)$ smaller.

Darwin's expression for the characteristic function is practically identical with the one given above. In these functions absorption due to quantum processes has not been taken into account. Prins[6] attempted to take such processes into account and arrived at a modified form of Darwin's function, namely

$$f_p(\Phi, \Phi, \lambda) = \left| \frac{a + ib}{\frac{1}{2}(\Phi - \theta) \sin 2\theta_0 - i\beta \pm \{[\frac{1}{2}(\Phi - \theta) \sin 2\theta_0 - i\beta]^2 - (a + ib)^2\}^{\frac{1}{2}}} \right|^2. \tag{2}$$

The additional factors b and β which take into account absorption destroy the symmetry of f about the point $\Phi = \theta$. This function has been plotted by Allison.[10] Another extremely important difference between f_p and f_w is the way in which they depend on the wave-length of the incident beam. As the wave-length is changed the principal alteration of f_w is simply that of displacement along the Φ-axis, while the function f_p is materially changed as can be seen from Fig. 2 in Allison's paper.[10]

Since in the actual crystals used there are surface imperfections as well as lattice structures for which the above functions no longer apply and the incident beam is restricted and not infinite in extent, etc., some investigators have thought that one could come about as near to the correct function by assuming a reasonable type as by trying to use the more complicated ones derived for such ideal conditions. Ehrenburg and Mark[7] and Schwarzschild[8] have assumed that the characteristic function was a Gaussian error function, i.e.,

$$f(\Phi, \Phi, \lambda) = Ae^{-b(\Phi - \theta)^2}. \tag{3}$$

Barnes and Palmer[12] have assumed that the characteristic function was of the same form as that used by Hoyt[13] for representing the shape of an x-ray line, namely,

$$f(\Phi, \Phi, \lambda) = a[1 + (\Phi - \theta)^2/b^2]^{-1}. \tag{4}$$

The above characteristic functions are convenient because in a two crystal spectrometer with identical crystals the rocking curve in the (1, −1) position calculated from them would again be a function of the same form. While rocking curves have been found for certain pairs

[12] S. W. Barnes and L. D. Palmer, Phys. Rev. **43**, 1050 (1933).
[13] A. Hoyt, Phys. Rev. **40**, 477 (1932).

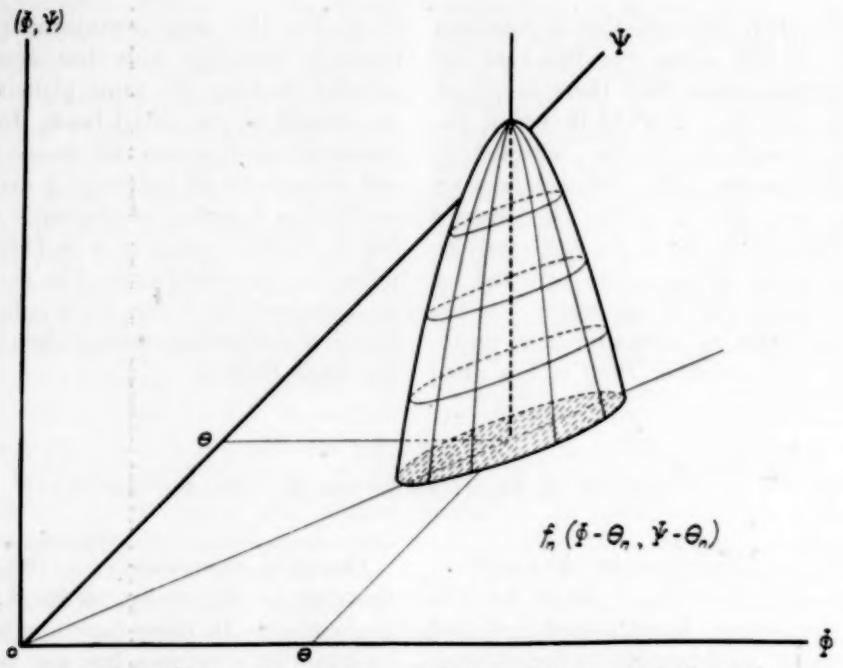

FIG. 2. A schematic representation of the crystal characteristic $f(\Phi, \psi, \lambda)$.

of crystals which agree approximately with one or the other of the functions (3) or (4), this is not universally the case and even if it were it can be shown that there exist asymmetrical crystal characteristics which would yield symmetrical rocking curves of the form (3) or (4).

It should be noted that the form of all of the above characteristic functions precludes the possibility of any radiation being reflected at an angle not equal to the incident angle. In terms of $f(\Phi, \psi, \lambda)$, this means that f is different from zero only when $\psi = \Phi$. This restriction is doubtless justified for the ideal circumstances assumed in the derivation of expressions (1) and (2) but for an actual crystal used in a spectrometer there is considerable departure from the ideal conditions assumed above and it is not *a priori* obvious that ψ should be identically equal to Φ. In fact, evidence is accumulating which makes it unlikely that all the reflected energy leaves the crystal at any one angle. Logically, therefore, it would seem that we should generalize one step further and treat the angles Φ, and ψ as solid angles, which would mean that radiation incident on the crystal at a given angle would be reflected to some extent in all directions in a certain cone. Very likely this is precisely what does occur but, due to the fact that all motions of a properly adjusted double crystal spectrometer are confined to a plane, it will be found that the subsequent analysis can be generalized so as to take account of solid angles. Since this later generalization is possible, it will be much simpler to carry out the analysis treating Φ and ψ as plane angles.

ANALYSIS OF THE DOUBLE CRYSTAL SPECTROMETER

Before proceeding with the analysis it will be necessary to justify an assumption to be made concerning the wave-length dependence of the characteristic function. Geometrically, the function $f(\Phi, \psi, \lambda)$ represents a surface when λ is held fixed. From our general knowledge of the reflecting properties of a crystal this must be a dome-shaped surface having a maximum in the neighborhood where Φ and ψ equal the corrected Bragg angle. This is roughly shown in Fig. 2. In line with the characteristic functions considered above, it is convenient to measure both of the angle variables from the corrected Bragg angle θ. This can be explicitly indicated by writing $f(\Phi-\theta, \psi-\theta, \lambda)$. From experiment, it is known that $f(\Phi-\theta, \psi-\theta, \lambda)$ is appreciably

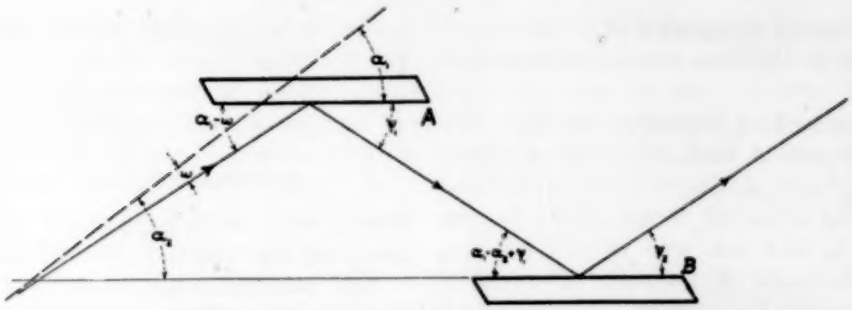

FIG. 3. Crystal arrangement for rocking curves in $(n, -n)$ orders.

different from zero only in a region of the Φ, ψ plane in the vicinity of the point $\Phi=\theta, \psi=\theta$. If we were dealing with a function of the Darwin type Eq. (1) then the wave-length dependence would enter in f principally in the angle θ and we would have $f(\Phi-\theta, \psi-\theta)$. For this case a change in the wave-length would merely displace the dome-shaped surface along a 45 degree line in the Φ, ψ plane. It is definitely known, however, that this simple type of wave-length dependence is untenable in general, which is in accord with f_p of Eq. (2). If the change in the actual surface f, with wave-length, aside from the displacement along the line $\Phi=\psi$, is anything like that of f_p, then f will be a sufficiently slowly varying function of λ so that the change in the shape of the surface over a small wave-length interval may be neglected. This certainly obtains for wave-length intervals covered by a spectral line and for certain crystals f does not change appreciably over intervals many times this size, as is indicated by rocking curves taken in the $(1, -1)$ positions for nearby wave-lengths. Therefore, when the incident radiation is line radiation there will be no loss of generality in assuming that a change in wave-length simply displaces the surface f along the line $\Phi=\psi$. So that we may write

$$f_n(\Phi-\theta_n, \psi-\theta_n),$$

where θ_n denotes the corrected Bragg angle in the nth order. The subscript n attached to f indicates that the surface f will, in general, be different for different orders.

It will be sufficient to compute the intensity of radiation reflected from two crystals when the incident and reflected beams from each all lie in the same plane, since it has been shown by Allison[14] that effects due to crystal alignment and vertical divergence of the incident beam can be made negligibly small. Let the geometrical center of the initial beam (dotted line in Fig. 3) be chosen as the reference line for the angular positions of the two crystals and let the surfaces of A and B make angles α_1 and α_2 with it. Suppose also that a beam of radiation of unit intensity having a wave-length between λ and $\lambda+d\lambda$ falls on crystal A in the angular interval between ω and $\omega+d\omega$ measured with respect to the same reference line. The total intensity reflected from the second crystal will be

$$d\lambda\int_{\Delta\psi_1} d\psi_1 \int_{\Delta\psi_2} f_{n_1}(\alpha_1-\omega-\theta_{n_1}, \psi_1-\theta_{n_1}) \times f_{n_2}\{\pm(\alpha_1-\alpha_2+\psi_1)-\theta_{n_2}, \psi_2-\theta_{n_2}\}d\psi_2,$$

where the $+$ sign is to be used for the orders $(n_1, -n_2)$ and the $-$ sign for the orders $(n_1, +n_2)$ and $\Delta\psi_1$ and $\Delta\psi_2$ denote the angular intervals over which the function f_{n_1} and f_{n_2} are different from zero. Since f_{n_1} and f_{n_2} are zero outside of these intervals, the intervals can be extended from $-\infty$ to $+\infty$. If the intensity of the incident radiation is not unity but $l(\lambda-\lambda_0)k(\omega)$ where $k(\omega)$ is the distribution in intensity with angle and $l(\lambda-\lambda_0)$ is the distribution of intensity with wave-length measured from the wave-length λ_0 of maximum intensity, then the total reflected intensity from crystal B is

$$\int_{-\infty}^{+\infty} l(\lambda-\lambda_0)d\lambda \int_{-\infty}^{+\infty} d\psi_1 \int_{-\infty}^{+\infty} k(\omega) \times f_{n_1}\{\alpha_1-\omega-\theta_{n_1}, \psi_1-\theta_{n_1}\}d\omega \int_{-\infty}^{+\infty} \times f_{n_2}\{\pm(\alpha_1-\alpha_2+\psi_1)-\theta_{n_2}, \psi_2-\theta_{n_2}\}d\psi_2, \quad (5)$$

[14] S. K. Allison, Phys. Rev. **44**, 63 (1933).

where the ranges of integration of λ and ω have been extended for the same reasons as mentioned above.

To compute rocking curves in the $(n_1, -n_2)$ orders with crystal A fixed, it is only necessary to let $\alpha_1=\theta_{n_1}{}^0$ and $\alpha_2=\theta_{n_2}{}^0+\epsilon_2$ where $\theta_{n_1}{}^0$ and $\theta_{n_2}{}^0$ denote the corrected Bragg angles for the wave-length λ_0 and indicated orders, while ϵ_2 then gives the angle of deviation of crystal B from the corrected Bragg angle. Denoting such a rocking curve by $r_{n_1,\,-n_2}(\epsilon_2)$ then

$$r_{n_1,\,-n_2}(-\epsilon_2)=\int_{-\infty}^{+\infty} l(\lambda-\lambda_0)d\lambda\int_{-\infty}^{+\infty} d\psi_1\int_{-\infty}^{+\infty} \times k(\omega)f_{n_1}\{\theta_{n_1}{}^0-\omega-\theta_{n_1},\ \psi_1-\theta_{n_1}\}d\omega\int_{-\infty}^{+\infty} \times f_{n_2}\{\theta_{n_1}{}^0-\theta_{n_2}{}^0-\epsilon_2+\psi_1-\theta_{n_2},\ \psi_2-\theta_{n_2}\}d\psi_2. \quad (6)$$

If the angular range over which $k(\omega)$ is appreciably different from zero is large compared with the region for which f_{n_1} is different from zero and $k(\omega)$ is a slowly varying function of ω over the latter range, then to a sufficient approximation we may write

$$\int_{-\infty}^{+\infty} k(\omega)f_{n_1}\{\theta_{n_1}{}^0-\omega-\theta_{n_1},\ \psi_1-\theta_{n_1}\}d\omega = k(\theta_{n_1}{}^0)\int_{-\infty}^{+\infty} f_{n_1}\{\xi,\ \psi_1-\theta_{n_1}\}d\xi=g_{n_1}(\psi_1-\theta_{n_1}), \quad (7)$$

where $\xi=\theta_{n_1}{}^0-\omega-\theta_{n_1}$.

The conditions leading to this relation are usually fulfilled in practice. Letting

$$h_{n_2}(\psi_1-\epsilon-\theta_{n_2}-\theta_{n_2}{}^0+\theta_{n_1}{}^0) = \int_{-\infty}^{+\infty} f_{n_2}\{\psi_1-\epsilon-\theta_{n_2}-\theta_{n_2}{}^0+\theta_{n_1}{}^0,\ \psi_2-\theta_{n_2}\}d\psi_2 \quad (8)$$

Eq. (6) becomes

$$r_{n_1,\,-n_2}(-\epsilon_2)=\int_{-\infty}^{+\infty} l(\lambda-\lambda_0)d\lambda\int_{-\infty}^{+\infty} g_{n_1}(\psi_1-\theta_{n_1}) \times h_{n_2}(\psi_1-\epsilon_2-\theta_{n_2}-\theta_{n_2}{}^0+\theta_{n_1}{}^0)d\psi_1. \quad (9)$$

This result is very similar to that obtained when the characteristic functions are of the form $f(\Phi,\ \Phi,\ \lambda)$ but the functions appearing in the integrand have wholly different meanings.

Rocking curves in the $(n_1, +n_2)$ orders can be obtained in a similar way by letting $\alpha_1=\theta_{n_1}{}^0$ and $\alpha_2=\theta_{n_2}{}^0+2\theta_{n_1}{}^0+\epsilon_2$ and taking the $-$ sign in Eq. (5), thus

$$r_{n_1,\,+n_2}(\epsilon_2)=\int_{-\infty}^{+\infty} l(\lambda-\lambda_0)d\lambda\int_{-\infty}^{+\infty} g_{n_1}(\psi_1-\theta_{n_1}) \times h_{n_2}(\theta_{n_1}{}^0+\theta_{n_2}{}^0+\epsilon_2-\psi_1-\theta_{n_2})d\psi_1. \quad (10)$$

Henceforth the subscripts on the variable of integration ψ_1 and ϵ_2 will be dropped.

The analysis would have proceeded in the same manner as the above even when Φ and ψ were considered as solid angles. The only difference in the results would have been in the definition of the functions g and h above. Eqs. (7) and (8) would involve double integrations instead of single and the meaning of g and h would be different but, since they are to be determined from experiment anyway, the subsequent analysis holds for the more general case.

It is worth while to notice several important characteristics of Eqs. (9) and (10). First, the right-hand integral of (9) will be a maximum for a given wave-length when ϵ_2 is adjusted to give maximum overlapping of g_{n_1} and h_{n_2}, i.e., to make the common area under the curves g_{n_1} and h_{n_2} a maximum. If $n_1=n_2$ then the amount of overlapping remains constant for all wave-lengths and the form of $r_{n_1,\,-n_1}(\epsilon_2)$ is independent of the form of $l(\lambda-\lambda_0)$ and hence of the shape of the incident line and depends only on the total intensity. On the other hand, if n_1 is not equal to n_2 then the amount of overlapping decreases as λ increases and the origins of g_{n_1} and h_{n_2} are translated in the same direction but by a different amount. g_{n_1} and h_{n_2} therefore separate by an amount measured by $|\theta_{n_2}-\theta_{n_1}|$ so that all curves $r_{n_1,\,-n_2}(\epsilon_2)$ when $n_2\neq n_1$, depend on the line shape. Somewhat similar remarks hold in the case of Eq. (10) except that the amount of overlapping never remains constant as the wave-length changes and consequently all $r_{n_1,\,n_2}(\epsilon_2)$ depend on the form of $l(\lambda-\lambda_0)$. The separation of the origins of the functions g_{n_1} and h_{n^2} is measured by $|\theta_{n_2}+\theta_{n_1}|$ as λ increases. These considerations are important in making use of Eqs. (9) and (10) to determine the line shape $l(\lambda-\lambda_0)$.

Determination of the Line Shape

The possibility of determining the spectral energy distribution of an x-ray line from meas-

urements with an uncalibrated double crystal spectrometer rests on the existence of a unique solution of a set of simultaneous integral equations of the form (9) and (10) and a method for finding it. A method of finding such a solution will now be given.

In order to invert the integral equations it will be convenient to make use of the theory of Fourier transforms. With suitable restrictions (fulfilled for the functions under consideration) a function $f(x)$ can be represented by the Fourier integral

$$f(x)=(2\pi)^{-1}\int_{-\infty}^{+\infty}F(t)e^{-ixt}dt, \qquad (15)$$

where $F(t)$ is the Fourier transform of $f(x)$ defined by the equation

$$F(t)=(2\pi)^{-1}\int_{-\infty}^{+\infty}f(x)e^{ixt}dx. \qquad (16)$$

Throughout the remainder of this paper capital letters will be used to denote the Fourier transforms of the functions denoted by small letters, with the exception of the capital letter L. It should be noted that $F(t)$ is a complex function unless $f(x)$ is an even function in which case $F(t)$ is real. Of the functions to be considered there is a one to one correspondence between the function and its Fourier transform, so that if the transform is known, the function to which it corresponds can be found by Eq. (15).

In addition to the inversion formulae (15) and (16) we shall need to invert a relation of the type

$$\chi(t)=(2\pi)^{-1}\int_{-\infty}^{+\infty}f(x)e^{itu(x)}dx, \qquad (17)$$

where $u(x)$ is an odd function of x. Let $s=u(x)$ and the unique inverse be $x=v(s)$; then

$$\chi(t)=(2\pi)^{-1}\int_{-\infty}^{+\infty}f[v(s)]e^{its}v'(s)ds.$$

Using (15) and (16) we have

$$f[v(s)]v'(s)=(2\pi)^{-1}\int_{-\infty}^{+\infty}\chi(t)e^{-its}dt$$

or since

$$dv/ds=1/(du/dx)$$

$$f(x)=(2\pi)^{-1}u'(x)\int_{-\infty}^{+\infty}\chi(t)e^{-itu(x)}dt. \qquad (18)$$

Eqs. (17) and (18) furnish somewhat more general inversion formulae.

Eq. (9) may be converted into a relation between the Fourier transforms of the functions involved by multiplying through by $e^{-it\epsilon}$ and integrating with respect to ϵ from $-\infty$ to $+\infty$. On inverting the order of integration on the right, the equation becomes

$$\int_{-\infty}^{+\infty}r_{n_1,\,-n_2}r(-\epsilon)e^{-it\epsilon}d\epsilon=\int_{-\infty}^{+\infty}l(\lambda-\lambda_0)\exp\left[it(\theta_{n_2}+\theta_{n_2}^0-\theta_{n_1}-\theta_{n_1}^0)\right]d\lambda\int_{-\infty}^{+\infty}g_{n_1}(\psi)e^{-it\psi}d\psi$$

$$\times\int_{-\infty}^{+\infty}h_{n_2}(\psi-\epsilon-\theta_{n_2}+\theta_{n_1}-\theta_{n_2}^0+\theta_{n_1}^0)\exp\left[it(\psi-\epsilon-\theta_{n_2}+\theta_{n_1}-\theta_{n_2}^0+\theta_{n_1}^0)\right]d\epsilon.$$

Making use of Eqs. (16) and (17) this may be written as

$$R_{n_1,\,-n_2}(t)=2\pi L_{n_1,\,-n_2}(t)G_{n_1}^*(t)H_{n_2}(t), \qquad (19)$$

where the asterisk denotes the complex conjugate and

$$L_{n_1,\,-n_2}(t)=(2\pi)^{-1}\int_{-\infty}^{+\infty}l(\lambda-\lambda_0)\times\exp\left[it(\theta_{n_2}-\theta_{n_1}+\theta_{n_2}^0-\theta_{n_1}^0)\right]d\lambda. \qquad (20)$$

Eq. (10) may be converted to a form similar to (19) by multiplying through by e^{its} and integrating as before. The desired relation is

$$R_{n_1,\,n_2}(t)=2\pi L_{n_1,\,n_2}(t)G_{n_1}(t)H_{n_2}(t), \qquad (21)$$

where

$$L_{n_1,\,n_2}(t)=(2\pi)^{-1}\int_{-\infty}^{+\infty}l(\lambda-\lambda_0)\times\exp\left[it(\theta_{n_2}-\theta_{n_2}^0+\theta_{n_1}-\theta_{n_1}^0)\right]d\lambda. \qquad (22)$$

Of all of the possible relations (19) and (21), six will be required. In order to make the following analysis clear and to save space, the special equations to be used are written below:

$$\left.\begin{aligned}R_{1,\,-1}(t)&=2\pi IG_1^*(t)H_1(t), \quad \text{(a)}\\ R_{2,\,-2}(t)&=2\pi IG_2^*(t)H_2(t), \quad \text{(b)}\end{aligned}\right\}. \qquad (23)$$

$$R_{1,+1}(t)=2\pi L_{1,+1}(t)G_1(t)H_1(t), \quad \text{(a)}$$
$$R_{2,+2}(t)=2\pi L_{2,+2}(t)G_2(t)H_2(t), \quad \text{(b)}$$
$$R_{1,+2}(t)=2\pi L_{1,+2}(t)G_1(t)H_2(t), \quad \text{(c)} \qquad (24)$$
$$R_{2,+1}(t)=2\pi L_{1,+2}(t)G_2(t)H_1(t), \quad \text{(d)}$$

where the relations

$$L_{1,-1}(t)=L_{2,-2}(t)=I$$
$$=(2\pi)^{-\frac{1}{2}}\int_{-\infty}^{+\infty} l(\lambda-\lambda_0)d\lambda=\text{a constant},$$
$$L_{1,+2}(t)=L_{2,+1}(t)$$

have been used.

The immediate problem is to determine one of the functions $L(t)$ in the above equations. In general $L(t)$ is a complex function of the real variable t so that it may be written

$$L_{n_1,n_2}(t)=|L_{n_1,n_2}(t)|\exp[i\Phi_{n_1,n_2}(t)]. \quad (25)$$

$L_{n_1,n_2}(t)$ is real only when the line shape is symmetrical, i.e., $l(\lambda-\lambda_0)$ is an even function of $(\lambda-\lambda_0)$. It is easy to obtain $|L_{n_1,n_2}(t)|$. Multiplying (24a) by its complex conjugate we have

$$|R_{1,+1}(t)|^2=4\pi^2|L_{1,+1}(t)|^2G_1(t)H_1^*(t)G_1^*(t)H_1(t).$$

Making use of Eq. (23a) this becomes

$$|R_{1,+1}(t)|^2/|R_{1,-1}(t)|^2=|L_{1,+1}(t)|^2/I^2$$

or

$$|L_{1,+1}(t)|=I|R_{1,+1}(t)|/|R_{1,-1}(t)|. \quad (26)$$

Similarly

$$|L_{2,+2}(t)|=I|R_{2,+2}(t)|/|R_{2,-2}(t)| \quad (27)$$

and

$$|L_{1,+2}(t)|=I\left[\frac{R_{1,+2}(t)\cdot R^*_{2,+1}(t)}{R^*_{1,-1}(t)\cdot R_{2,-2}(t)}\right]^{\frac{1}{2}}. \quad (28)$$

Eqs. (26) or (27) would constitute a formal solution to our problem if it were known that the initial line shape were symmetrical. Since this is not known it will be necessary to determine the argument of the functions $L_{n_1,n_2}(t)$. To do this, Eqs. (24a) and (24b) are multiplied together and the result divided by the product of (24c) and (24d), so that

$$\frac{L_{1,+1}(t)L_{1,+2}(t)}{L^2_{1,+2}(t)}=\frac{R_{1,+1}(t)R_{2,+2}(t)}{R_{1,+2}(t)R_{2,+1}(t)}$$
$$=S(t)=|S(t)|e^{i\chi(t)}. \quad (29)$$

Taking logarithms of both sides we have

$$\log L_{1,+1}(t)+\log L_{2,+2}(t)-2\log L_{1,+2}(t)$$
$$=\log S(t). \quad (30)$$

In this equation the principal value of the logarithm is meant so that

$$\log L_{1,+1}(t)=\log|L_{1,+1}(t)|+i\Phi_{1,+1}(t). \quad (31)$$

Eq. (30) involving three unknown functions can be reduced to a functional equation involving only one unknown function. To do this, we expand the angles $\theta_{n_2}+\theta_{n_1}$ occurring in Eq. (22) as Taylor's series in the wave-length λ about the point λ_0, thus

$$\theta_{n_2}+\theta_{n_1}=\theta_{n_2}^0+\theta_{n_1}^0+\{d(\theta_{n_2}+\theta_{n_1})/d\lambda\}_{\lambda=\lambda_0}$$
$$\times(\lambda-\lambda_0)+\cdots.$$

Use is now made of the fortunate circumstance that for values of $\lambda-\lambda_0$ over which the function $l(\lambda-\lambda_0)$ is appreciably different from zero, only the first two terms of the above expansion are required to give a good approximation for $\theta_{n_2}+\theta_{n_1}$. Examination shows that this approximation holds for x-ray lines over quite a large wave-length region. We may therefore write

$$\theta_{n_2}+\theta_{n_1}-\theta_{n_2}^0-\theta_{n_1}^0=D_{n_1n_2}(\lambda-\lambda_0)$$

where $$D_{n_1n_2}=(d/d\lambda)(\theta_{n_2}+\theta_{n_1})_{\lambda=\lambda_0}.$$

Substituting the above expression in Eq. (22) we have

$$L_{n_1,+n_2}(t)=(2\pi)^{-\frac{1}{2}}\int_{-\infty}^{+\infty} l(\lambda-\lambda_0)$$
$$\times\exp[itD_{n_1n_2}(\lambda-\lambda_0)]d\lambda$$

or

$$L_{n_1,+n_2}(t/D_{n_1n_2})=(2\pi)^{-\frac{1}{2}}\int_{-\infty}^{+\infty} l(\lambda-\lambda_0)e^{it(\lambda-\lambda_0)}d\lambda.$$

The required relation between $L_{1,+1}(t)$, $L_{2,+2}(t)$ and $L_{1,+2}(t)$ is obtained from this equation, namely,

$$L_{2,+2}(t/D_{22})=L_{1,+2}(t/D_{12})=L_{1,+1}(t/D_{11})$$

or

$$L_{2,+2}(t)=L_{1,+1}(D_{22}t/D_{11})$$

and

$$L_{1,+2}(t)=L_{1,+1}(D_{12}t/D_{11}).$$

Making use of these relations, Eq. (30) reduces to the functional equation

$$\log L_{1,+1}(t)+\log L_{1,+1}(D_{22}t/D_{11}) - 2\log L_{1,+1}(D_{12}t/D_{11})=\log S(t). \quad (32)$$

By equating the real and imaginary parts of this equation in accordance with the relation (31) we have

$$\log |L_{1,+1}(t)|+\log |L_{1,+1}(D_{22}t/D_{11})| - 2\log |L_{1,+1}(D_{12}t/D_{11})|=\log |S(t)|, \quad (33a)$$

$$\Phi_{1,+1}(t)+\Phi_{1,+1}(D_{22}t/D_{11}) - 2\Phi_{1,+1}(D_{12}t/D_{11})=\chi(t). \quad (33b)$$

The unknown argument of $L_{1,+1}(t)$ can be found from the second of the above equations and the Fourier transform of the function $l(\lambda-\lambda_0)$ has been completely determined and consequently the original line shape also.

It does not seem worth while, at the present time, to discuss the solution of Eq. (33b) since the method of procedure will depend on the behavior of the function $\chi(t)$. If, in particular, $\chi(t)$ is an analytic function, an expansion of $\chi(t)$ and $\Phi(t)$ in a power series suggests itself since Eq. (33b) will determine the coefficients in the power series for $\Phi(t)$ uniquely. It should be noticed that if $\chi(t)$ is identically equal to zero, then so is $\Phi_{1,+1}(t)$ since $\Phi_{1,+1}(0)$ is known to be zero and the intensity of the original x-ray line is symmetrical about the point $\lambda=\lambda_0$.

Suggested Procedure in Actual Computations

Since the writer has not as yet carried out the requisite numerical computations to determine the line shape, it cannot be said that the method to be suggested is the best but certain circumstances indicate that it would be a good one to try. In order to carry through the formal mathematical work, it is convenient to have an analytical representation of the various rocking curves. On account of their general form it would appear that they could be represented by a relatively small number of terms in a series of the orthogonal Hermitian functions $\psi_n(x)$ whose generating function is

$$e^{-x^2/2}e^{-(x-t)^2}=\sum_{n=0}^{\infty}(n!)^{-1}\psi_n(x)t^n.$$

Another important reason for employing the functions $\psi_n(x)$ is that they possess the property of being their own Fourier transform except for a possible constant. This should materially facilitate the determination of the Fourier transforms of the rocking curves.

With the function $l(\lambda-\lambda_0)$ thus determined, the functions $G_1(t)$, $H_1(t)$, $G_2(t)$ and $H_2(t)$ can be found from Eqs. (23a), (23b), (24a) and (24b) in an obvious manner. Since these functions depend only on the crystal characteristics the spectrometer can be considered as calibrated for wave-lengths in the neighborhood of λ_0 as soon as they have been determined. It must be remembered, however, that the functions g_1, h_1, etc., whose Fourier transforms are G_1, H_1, etc., are not the diffraction patterns of the crystals as normally defined. It is obvious that it is not possible to determine $f(\Phi, \psi)$ in terms of the functions g, h, etc., but this is not required either to calibrate the spectrometer or to obtain the line shape.

The general problem of determining the spectral energy distribution of an x-ray line and of calibrating the double crystal spectrometer experimentally without appealing to the theoretical diffraction pattern or characteristic function for the crystal has been solved. In conclusion the writer wishes to acknowledge the very considerable help received from very stimulating discussions of this subject with Professor C. C. Murdock.

The Natural Widths of the *K*-Series of W(74)

F. K. RICHTMYER* AND S. W. BARNES, *Department of Physics, Cornell University*
(Received June 28, 1934)

By means of a two-crystal x-ray spectrometer of high resolving power at short wave-length, the full widths at half maximum of the *K*-series of W(74) have been measured. The observed widths W_O in the (1,+1) position of the crystals have been corrected to true widths W_T by use of the formula $W_T = W_O - W_R$ where W_R is the width of the rocking curve of the crystals in the (1,−1) position. It is shown that, in the short wave-length region under consideration the (1,−1) rocking curves obey the Hoyt equation. By using Weisskopf's equation for the shape of a spectral line, the above correction formula results. The following (corrected) full widths at half maximum (in volts) are obtained: $K\alpha_2$, 43.3; α_1, 43.0; β_3, 50.0; β_1, 48.6; γ_3, 37.0; γ_1, 37.0; δ_2, 34.0; δ_1, 34.

I. INTRODUCTION

SEVERAL determinations of the widths of the lines in the *K*-series of W(74) have been previously reported. The authors[1] made an estimate of the true width of W $K\alpha_1$ by extrapolation to higher orders of the apparent true width obtained by means of a two-crystal spectrometer with the crystals in the (2,+2), (3,+3) and (4,+4) positions, respectively, using, to correct for the effect of the crystals, the Schwarzschild formula[2]

$$W_T = (W_O^2 - W_R^2)^{\frac{1}{2}} \qquad (1)$$

where $W_T \equiv$ true width of the line; $W_O \equiv$ observed width; and $W_R \equiv$ width of rocking curve in parallel positions. This formula is now known to be incorrect. Barnes and Palmer[3] arrived at about the same value for *each* of the positions (1,+1), (2,+2), (3,+3) using a correction formula, derived from the Hoyt equation[4] for the shape of a spectral line or a "rocking curve," *viz*:

$$W_T = W_O - W_R. \qquad (2)$$

Williams[5] has given the *uncorrected* widths of the *K*-series of W(74), exclusive of $K\delta$ and the authors[6] have announced preliminary data on the natural widths of these lines. These previously reported results for $K\alpha_1$ are summarized in Table I.

TABLE I. *Width* of the $K\alpha_1$ line of W(74).*

Observers	Correction for crystals	W_R for crystals used	Width of $K\alpha_1$
Williams[5]	None	9″–10″	$W_O = 0.19 \times$ X.U.
Richtmyer[1] and Barnes	$W_T = (W^2_O - W^2_R)^{\frac{1}{2}}$ extrapolated to higher orders	9.6″	$W_T = 0.154$
Richtmyer[6, 3] Barnes, Palmer	$W_T = W_O - W_R$	9.6″	$W_T = 0.15$

* W = full width at half maximum; w = half width at half maximum.

II. APPARATUS

A 60-cycle, 200 kv transformer, supplied with power from a 220-volt, 12 kva generator direct connected to a constant-speed, 60 kva synchronous motor, furnishes the high voltage which is rectified by kenotrons and smoothed out by condensers so that the ripple does not exceed a few percent. The voltage across the x-ray tube is read by an electrostatic voltmeter; and the tube current is measured by a galvanometer arranged to act as a null instrument. Tube voltage and tube current are maintained constant, by manual control, to about 0.1 percent.

The x-ray tube is a commercial-type, tungsten tube, fitted with a linear filament and kept on the pumps. The anode is cooled by a water-oil-water-cooling system.

The two-crystal spectrometer, direct reading as to wave-length, has been briefly described by the authors[7] and, more fully, in a paper now in press.[8]

The ionization chamber is 31 inches long and 6 inches in diameter; and, following the suggestion

* The senior author acknowledges with thanks assistance from the Heckscher Research Council of Cornell University.

[1] F. K. Richtmyer and S. W. Barnes, Phys. Rev. **37**, 1695 (1931).

[2] Schwarzschild, Phys. Rev. **32**, 162 (1928); Ehrenberg and Mark, Zeits. f. Physik **42**, 807 (1927).

[3] S. W. Barnes and L. D. Palmer, Phys. Rev. **43**, 1050 (1933).

[4] Archer Hoyt, Phys. Rev. **40**, 477 (1932).

[5] John H. Williams, Phys. Rev. **40**, 791 (1932).

[6] F. K. Richtmyer and S. W. Barnes, Phys. Rev. **43**, 1049 (1933).

[7] F. K. Richtmyer and S. W. Barnes, Phys. Rev. **35**, 1428 (1931).

[8] Barnes and Richtmyer, Rev. Sci. Inst. **5**, October (1934).

of A. H. Compton,[9] contains a "squirrel-cage" type of grid to reduce the disturbing effect of alpha-particles. The chamber is filled with methyl bromide at a pressure slightly less than one atmosphere. Ionization currents are measured by a two-tube bridge circuit[10] employing a pair of FP-54 tubes.

The slits limiting the vertical divergence of the x-ray beam are 1 cm high and 120 cm apart. The maximum possible angle of divergence ϕ is thus 0.016 rad. Actually ϕ is considerably less than this since the focal spot is only 0.5 cm high and is 150 cm from the second slit.

The calcite crystals, our pair $3A+3B$, have been ground and etched and when prepared gave a $(1,-1)$ rocking curve width[11] of 2.8 seconds of arc (full width) at $\lambda=0.208$A. No $(1,-1)$ rocking curves have been taken recently but, since there has been no measurable increase in the observed widths of lines in the $(1,+1)$ position of these crystals, it is assumed that their characteristics have remained constant.

III. Correcting the Observed Widths of Lines for the Effect of the Crystals

On the assumption that the distribution of energy in an x-ray line as well as the so-called reflection curve of a pair of crystals in the $(1,+1)$ position for strictly monochromatic, unidirectional radiation both follow the Gaussian error curve, Ehrenberg and Mark[2] derived Eq. (1) for the true width W_T of a spectral line. It is now known that this equation is not in agreement with experiment. For example, if Eq. (1) be correct, it should give identical values of W_T for any given line in the several orders. Allison and Williams[12] found that W_T for $K\alpha_1$ of Mo(42), as computed from Eq. (1) was some 13 percent less for the $(2,+2)$ position than for the $(1,+1)$ position of the crystals. Column 6 of Table II of the present paper shows a similar discrepancy of 13 percent for W $K\alpha_1$, as measured by crystals $3A+3B$ in the two orders. Furthermore, as was mentioned by Allison,[13] rocking curves in the parallel as well as in the anti-parallel positions do not, in general, follow the Gaussian error curve upon which Eq. (1) is based. This is shown also by Figs. 1(a) and (b), in which the circles represent the observations on W $K\alpha_1$ in the $(1,+1)$ and in the $(1,-1)$ positions, respectively, and the dotted line represents the Gauss curve. The full line, which, in each case, is seen to agree well with the experimental data, is the plot of the Hoyt equation[4]

$$y=a/[1+(x/b)^2], \qquad (3)$$

where a is the maximum ordinate and b is the half width at half maximum; and $x=0$ when $y=a$.

Now, Weisskopf[14] has shown that the true

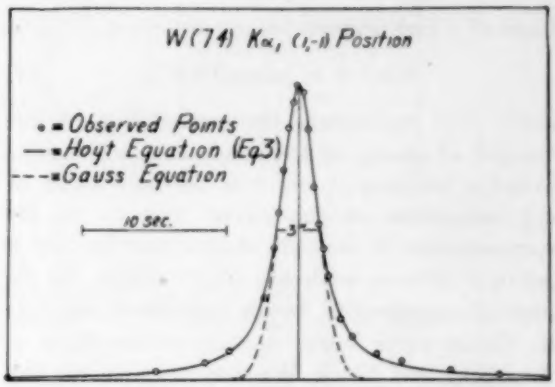

FIG. 1a. Rocking curve in the $(1,-1)$ position for crystals $3A+3B$ at $\lambda=0.208$A, showing that the observed data agree with the Hoyt equation.

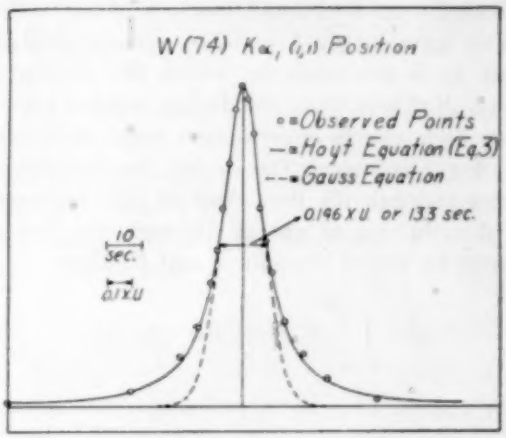

FIG. 1b. The $K\alpha_1$ line of W(74) as obtained by crystals $3A+3B$, showing that the observed shape of the line agrees with the Hoyt equation.

[9] A. H. Compton, Phys. Rev. **7**, 646 (1916).
[10] L. A. DuBridge, Phys. Rev. **37**, 392 (1931).
[11] F. K. Richtmyer, S. W. Barnes and K. V. Manning, Phys. Rev. **44**, 311 (1933).
[12] Allison and Williams, Phys. Rev. **35**, 1477 (1930), Table V.
[13] Allison, Phys. Rev. **38**, 203 (1931).
[14] Weisskopf, Phys. Zeits. **34**, 1 (1933).

shape of a line is given by the equation

$$J(\nu)=b/\pi[(\nu_0-\nu)^2+b^2], \qquad (4)$$

where $J(\nu)$ represents the probability of the emission of energy of frequency ν; ν_0 is the most probable frequency; and b is the half width at half maximum of the curve $J(\nu)$ *vs.* ν. By rearrangement it is easily shown that Eq. (4) is identical in form with Eq. (3),[14a] which, *for the range of wave-lengths herein considered*, replaces the Gauss error curve in the assumptions of Ehrenberg and Mark. We may then derive Eq. (2) as follows:

Let $\Phi_{1,1}(\xi_B)$ represent the "rocking curve" of the pair of crystals A and B in the $(1,+1)$ position for unidirectional, monochromatic radiation of wave-length λ incident upon crystal A; where ξ_B is the angle by which the setting of crystal B differs from the Bragg angle θ appropriate to λ, effects of refraction being neglected. Let $\Psi(\xi_B)$ represent the actual distribution of energy through the line. And let $f(\omega)$ represent the distribution of energy through the line as *observed* by use of crystals A and B. Then

$$f(\omega)=\int_{-\infty}^{+\infty}\Psi(\xi_B)\Phi_{1,1}(\omega-\xi_B)d\xi_B. \qquad (5)$$

We cannot observe $\Phi_{1,1}$ directly but we may use as its equivalent the rocking curve in the $(1,-1)$ position, i.e., $\Phi_{1,-1}$ as may be shown by the following argument:

Allison has shown[15] that the rocking curve $\Phi_{1,1}$ for a pair of identical crystals is given by

$$\Phi_{1,1}(\xi_B)=\int_{-\infty}^{+\infty}F(\alpha)F(\xi_B-\alpha)d\alpha, \qquad (6)$$

where $F(\alpha)$ represents the ratio of the x-ray energy (per second) reflected from either crystal when set at angle α from the Bragg angle, to that reflected when $\alpha=0$; ξ_B is the angle by which crystal B differs from parallelism to crystal A when for it $\alpha=0$. The curve $\Phi_{1,-1}$ for the $(1,-1)$ position is correspondingly given by

$$\Phi_{1,-1}(\xi_B)=\int_{-\infty}^{+\infty}F(\alpha)F(\alpha-\xi_B)d\alpha. \qquad (6a)$$

As pointed out by Allison,[15] irrespective of the nature of the F function, $\Phi_{1,-1}$ must be symmetrical—in agreement with experiment. But if F is unsymmetrical then $\Phi_{1,1}$ cannot be symmetrical. We observe, however, that for W $K\alpha_1 f(\omega)$ of Eq. (5) *is* symmetrical, not only for the (1,1) position but for (2,2) and (3,3). It is, of course, possible that for any given order an unsymmetrical $\Phi_{1,1}$ might combine with a correspondingly unsymmetrical Ψ in Eq. (5) to give a symmetrical $f(\omega)$; but this could hardly be so for several orders, since the relative effect of the crystal diffraction on $f(\omega)$ is less for the higher orders. (See Table II.) We conclude, therefore, that within the limits of error of experiment[16] the F functions are symmetrical and

TABLE II. *Values of W_T for W $K\alpha_1$.*

Order	W_O	W_R	W_T by Eq. (2)		W_T by Eq. (1)
			By crystal pair 3A+3B		
1, +1	13.3″	3.0″	10.3″	0.151 X.U.	0.191 X.U.
2, +2	21.9″	1.6″	20.3″	0.148	0.155
3, +3	34.5″	3.2	31.3	0.151	0.166
			By crystal pair 1A+1B		
1, +1	19.7″	9.6″	10.1	0.149	0.252

[14a] In Eq. (3) b and x, and likewise b in Eq. (4), are measured in frequency units. If b and x are to be measured in wave-length units—call them b_λ and x_λ, respectively—Eq. (3) becomes

$$y=a/[1+(\lambda x_\lambda/\lambda_0 b_\lambda)^2], \qquad (3a)$$

where λ_0 is the wave-length for maximum energy in the line, and λ is the wave-length corresponding to x_λ. If the line is narrow, the ratio λ/λ_0 may be set equal to unity for all values of λ for which y has a measurable value. That is, an equation of the type (3) should give the shape of a *narrow* line whether the plot be on a wave-length, or a frequency, scale. If, however, the line is wide and is symmetrical on a frequency plot, the asymmetry on a wave-length plot may become appreciable.

As was shown by Hoyt,[4] the area under the curve of Eq. (3), i.e., the intensity I of the line, is

$$I=\pi a b_\nu, \qquad (a)$$

where $b_\nu=b$ of Eq. (3).

The ratio of R of the intensities of two lines is

$$R=I_1/I_2=(ab_\nu)_1/(ab_\nu)_2. \qquad (b)$$

If, however, R be determined by comparing the areas obtained from wave-length plots, Eq. (b) becomes

$$R=(\lambda_2/\lambda_1)^2\cdot(ab_\lambda)_1/(ab_\lambda)_2. \qquad (c)$$

That is to say, the ratio of the areas of two lines determined from wave-length plots must be multiplied by $(\lambda_2/\lambda_1)^2$ to give the relative intensities of the lines.

[15] Allison, Phys. Rev. **44**, 63 (1933), Eq. (2).

[16] It should be pointed out that for W $K\alpha_1$ and for our crystals $3A+3B$, $W_T\approx 3W_R$. Any marked asymmetry in $\Phi_{1,1}$ would be more readily observed than when, as is the case for longer wave-lengths, W_R is relatively much smaller.

therefore $\Phi_{1,1}$ is symmetrical and equal to $\Phi_{1,-1}$.

We can now solve Eq. (5) by inserting values of $\Psi(\xi_B)$ and of $\Phi_{1,1}(\omega-\xi_B)$ as follows:

$$\Psi(\xi_B)=h/[1+(\xi_B/w_T)^2] \qquad (7a)$$

in accordance with the conclusions of Weisskopf[14] where h is the maximum ordinate of the energy distribution curve for the line in question and w_T its half width at half maximum; and

$$\Phi_{1,1}(\omega-\xi_B)=a/[1+((\omega-\xi_B)/w_R)^2] \qquad (7b)$$

where a is the maximum ordinate and w_R the half width at half maximum of the $(1,-1)$ rocking curve of the crystals used. Integration then leads to

$$f(\omega)=A/[1+(\omega/(w_R+w_T))^2], \qquad (8)$$

where A is the maximum ordinate. As shown in Fig. 1a, Eq. (8) is in agreement with experiment. The half width at half maximum, namely w_0, of the curve $f(\omega)$ is given by

$$w_O=w_R+w_T.$$

Letting $W_O=2w_O$, $W_R=2w_R$ and $W_T=2w_T$ we have the equation

$$W_T=W_O-W_R$$

in agreement with Eq. (2) above.

An obvious test of Eq. (2) is the constancy of the values of W_T which it yields for any given line in several orders, and with different pairs of crystals. Table II gives data for W $K\alpha_1$, as measured in these orders by crystal pair $3A+3B$; and also by crystal pair $1A+1B$ in first order. A plot of the data in columns 1, 5 and 6 of Table II is shown in Fig. 2. The superiority of Eq. (2) is evident. It is therefore used in determining W_T for the K lines of W(74). But it should be emphasized that when $\Phi_{1,-1}$ departs noticeably from the form of Eq. (3)—as for example[17] at wave-lengths in the neighborhood of $1A$,—Eq. (2) cannot be used.

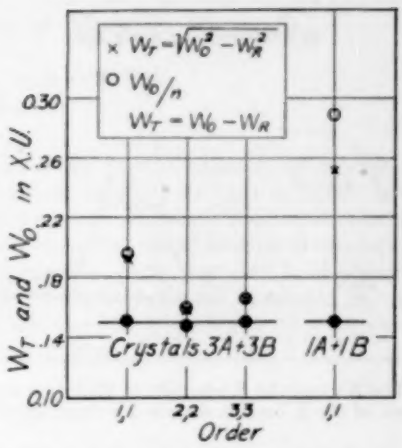

FIG. 2. The true width, W_T of $K\alpha_1$ of W(74) as computed (1) by the Schwarzschild formula and (2) by the equation based on the Hoyt formula, for crystals $3A+3B$ in three orders and for crystals $1A+1B$ in the first order.

RESULTS

The observed values W_O of the width of the several lines of the K-series of W(74) and also the values of the true width W_T as computed by use of Eq. (2) are shown in Table III. The two components of the doublet $K\alpha_{1,2}$ are separated far enough so that the influence of either component on the observed shape of the other may be neglected; and the values of W_O may be read directly from the line as observed. The

TABLE III. *Widths of the lines of the K series of W(74) (in the (1, +1) position of the crystals 3A+3B). $W_R=3.0\pm0.2$ sec. of arc for the (1, −1) position of crystals 3A+3B.*

Line of W(74)	W_O in (1, +1) position X.U.	Sec. of arc	Sec. of arc	$W_T=W_O-W_R$ X.U.	Volts
$K\alpha_2$	0.210±0.002	13.9±0.14	10.9±0.3	0.160±0.004	43.3±1
α_1	0.196±0.001	13.3±0.07	10.3±0.2	0.151±0.003	43.0±0.9
β_3	0.183±0.003	12.4±0.20	9.4±0.3	0.138±0.004	50.0±1.5
β_1	0.178±0.003	12.1±0.20	9.1±0.3	0.133±0.004	48.6±1.5
γ_2	0.140±0.004	9.5±0.27	6.5±0.3	0.095±0.005	37.0±2.0
γ_1	0.140±0.004	9.5±0.27	6.5±0.3	0.095±0.005	37.0±2.0
$\delta_{1,2}$	0.16 ±0.01	10.2±0.6	7.2±0.6	0.106±.01	41.0±3.7

[17] Allison, reference 13. Also unpublished data by the authors.

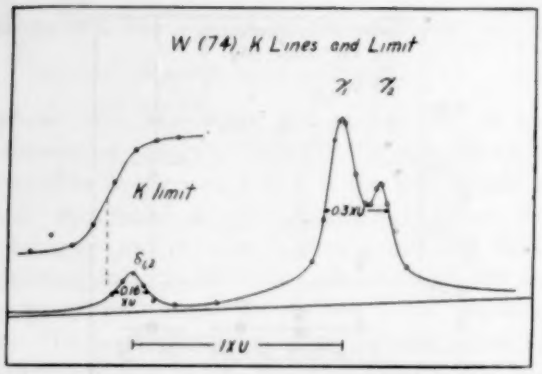

FIG. 3. The $K\gamma$ and the $K\delta$ doublet of W(74) as observed. The location of the K limit is sketched in from unpublished data.

same remark applies to $K\beta_{1,3}$ (Siegbahn's notation). The doublet $K\gamma_{1,2}$ however, is not fully resolved; and the doublet $K\delta_{1,2}(K\rightarrow O_{II,III})$ appears as a single line—as is shown in Fig. 3. Parenthetically, the position and approximate width of the K-limit of W(74), about 37 volts, is shown in Fig. 3, from unpublished data by the authors. It is significant that *it overlaps the doublet* $K\delta_{1,2}$.

The method used in separating the components $K\gamma_1$ and $K\gamma_2$ is clear from Fig. 4. By a trial-and-error method two Hoyt curves (Eq. (3)) were drawn so that the sum of their ordinates gave the envelope that passes through the observed points.

It is to be observed that, *expressed in volts*, the widths of the components of a doublet are the same within the limits of experimental error. We were, however, somewhat surprised to find that the widths of the components of the $K\beta$ doublet are greater than those of either $K\alpha$ or $K\gamma$—a circumstance which finds confirmation in more recent data by the authors, soon to be published, in which it is shown that the energy states $M_{II,III}$ are wider than either $L_{II,III}$ or $N_{II,III}$.

The width of the unresolved $K\delta_{1,2}$ line is put at 41.0 volts. By graphical extrapolation of data given in Siegbahn's *Spektroskopie der Roentgen-*

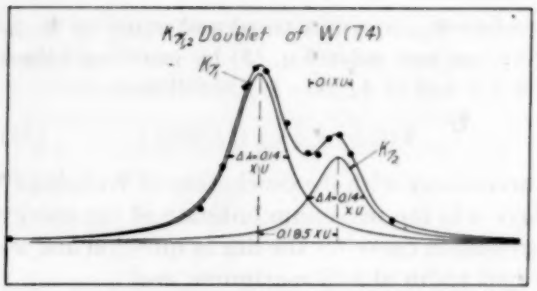

FIG. 4. The $K\gamma$ doublet is resolved into its components by use of two Hoyt curves.

strahlen, it is estimated that the limits O_{II} and O_{III} are separated by approximately 7 volts. If so, $K\delta_1$ and $K\delta_2$ should likewise be separated by some 7 volts. The widths of each of the lines $K\delta_1$ and $K\delta_2$ should therefore be about 34 ± 4 volts.

One concluding remark: The above measurements show that x-ray lines are far less "monochromatic" than are optical lines. The full widths at half maximum of the W K lines are of the order of 0.1 percent of their respective wave-length; whereas for optical lines the corresponding value is more nearly 0.0001 percent or less. From a systematic study of the widths and shapes of x-ray lines we may hope to obtain important information regarding the widths and shapes of the several x-ray energy states of the atom.

ADDENDUM

Our spectrometer is not calibrated to give absolute values of wave-length with high precision. It does however give acceptably precise values of small differences of wave-length. We therefore record the following:

From the graph of Fig. 4, we determine that the wave-length separation of $K\gamma_1$, and $K\gamma_2$ is 0.185 X.U. Siegbahn gives $N_{II}-N_{III}=68$ volts for W(74) corresponding to 0.176 X.U.

From Fig. 3 we find that the difference in wave-length between $K\gamma_1$ and $K\delta_{1,2}$ is 1.00 ± 0.01 X.U. Siegbahn gives, for W(74), $N_{III}-O_{II,III}=381$ volts, corresponding to 0.98 X.U.

The *M*-Series Absorption Spectrum of Metallic Bismuth

WILLIAM D. PHELPS, *University of Iowa, Iowa City*

(Received June 4, 1934)

With a vacuum spectrometer and sputtered bismuth films as absorbers, the five *M*-absorption edges were obtained. The large discrepancies between computed and observed wave-lengths of Bi M_{IV} and M_V were verified. The M_I, M_{II} and M_{III} discrepancies were found to be of the order of experimental error. To explain the M_{IV} and M_V discrepancies it is assumed that electrons from M_{IV} and M_V levels, in an absorption act, go to virtual lattice levels above the filled conduction, or valence, levels of the crystal for the elements Ta73 to Th90. Data on, and Kronig's theory of, secondary x-ray absorption are shown to support this view. The application of the ordinary x-ray selection rule $\Delta l = \pm 1$, $\Delta j = \pm 1$ or 0 in *M* absorption, suggested by Siegbahn, is further discussed. That there is a definite selection rule operating in *M* absorption there is little room to doubt.

MEASUREMENTS on the *M*-series absorption spectra of Ta73 by Whitmer,[1] of W74 by Zumstein[2] and of Os76, Ir77, and Pt78 by Rogers[3] show definite discrepancies between the observed and calculated ν/R values of the M_{IV} and M_V edges. The calculated values[4] are based on L_{III} absorption and emission data, assuming that electrons from the M_{IV}, M_V, and L_{III} levels go out to the same level in an absorption act. Johnson[5] showed, using metallic Pt films, that the M_I discrepancy is not due to chemical binding since the M_I absorption limit agrees with Roger's value obtained with Pt compounds. Lindberg[6] repeated some of the work done in this laboratory and elsewhere[7, 8] using the element in both the combined and uncombined state. He found no effect due to chemical state.

The data show possible discrepancies for the M_I and M_{II} limits, all of positive sign with the exception of Ir M_{II}. But these are in the range of the experimental error.

Not only are the data[9] incomplete with reference to the *M*-absorption limits, but, as will later be explained, there has been presented no satisfactory explanation of the amply verified M_{IV} and M_V "discrepancies." The present work on Bi83 was undertaken to obtain measurements especially on M_I and M_{II}, but on M_{III}, M_{IV}, and M_V as well, and to consider anew the most plausible explanation of the magnitude of the M_{IV} and M_V discrepancies.

Results

The apparatus used is essentially that described by Whitmer[1] though with a few minor changes. The bismuth films used as absorbers were produced by sputtering in an atmosphere of spectroscopically pure hydrogen.

In Table I are tabulated the wave-lengths, ν/R and $(\nu/R)^{\frac{1}{2}}$ values of the *M* limits of bismuth obtained in this research and elsewhere. The emission lines[10] used for reference are shown in Table II.

Discussion

The M_I and M_{II} edges were obtained with the same absorption film. At both edges the visual contrast on the photographic plate was small relative to that at the M_{III}, M_{IV}, or M_V edge, as would be expected from the relatively low electron population of the M_I and M_{II} states.[11] The M_I limit was found more like a line absorption to be expected in transitions between two narrowly defined levels while the M_{II} limit was of the edge type.

The discrepancies found for the bismuth edges M_I, M_{II}, M_{III}, M_{IV} and M_V are, respectively, -8.2, $+6.8$, $+2.7$, $+16.4$, $+19.1$ volts while the

[1] Whitmer, Phys. Rev. **38**, 1164 (1931).
[2] Zumstein, Phys. Rev. **25**, 747 (1925).
[3] Rogers, Phys. Rev. **30**, 747 (1927).
[4] Siegbahn, *Spectroscopy of X-Rays*, 1931 edition, pp. 336 and 346.
[5] Johnson, Phys. Rev. **34**, 1106 (1929).
[6] Lindberg, Zeits. f. Physik **50**, 91 (1928).
[7] Stenström, Dissert. Lund. (1919).
[8] Coster, Phys. Rev. **19**, 20 (1922).
[9] *M*-absorption measurements have been made on Ta73, W74, Os76, Ir77, Pt78, Au79, Hg80, Tl81, Pb82, Bi83, Th90, and U92.
[10] Siegbahn's *Spectroscopy of X-Rays*, 1931 edition, pp. 476–477.
[11] The number of electrons in the M_I, M_{II}, M_{III}, M_{IV} and M_V states are, respectively, 2, 2, 4, 4, 6. See Sidgwick's *Electronic Theory of Valency*, p. 50.

TABLE I. *M limits of Bi83 obtained here and elsewhere.*

Edge	Plate	λ	Reference lines	Average λ	Average ν/R	Average $(\nu/R)^{\frac{1}{4}}$	Author
M_{I}	58	3.102A	Sb $L\alpha_1$; β_1 β_2				
M_{I}	59	3.099	Sb $L\alpha_1$; β_1				
M_{I}	60	3.098	Sb $L\alpha_1$; β_1				
M_{I}	65	3.101	Sb $L\beta_1$; β_2				
M_{I}	88	3.100	Sb $L\alpha_1$; β_1				
M_{I}				3.100A	294.0	17.15	Phelps
M_{II}	58	3.343	Sb $L\alpha_1$; β_1; β_2				
M_{II}	59	3.341	Sb $L\alpha_1$; β_1				
M_{II}	63	3.345	Sb $L\alpha_1$; β_1				
M_{II}	88	3.340	Sb $L\alpha_1$; β_1				
M_{II}				3.342	272.7	16.51	Phelps
M_{III}	106	3.887	K $K\alpha_1$				
M_{III}	112	3.890	K $K\alpha_1$				
M_{III}	118	3.889	K $K\alpha_1$				
M_{III}	119	3.890	K $K\alpha_1$; Ag $L\alpha_1$; β_1				
M_{III}				3.889	234.3	15.31	Phelps
M_{III}				3.893	234.1	15.30	Lindberg
M_{III}				3.894			Coster
M_{IV}	101	4.573	Ag $L\alpha_1$				
M_{IV}	102	4.577	Bi $M\beta$				
M_{IV}	103	4.576	Bi $M\beta$; Cl $K\alpha_1$				
M_{IV}	104	4.571	Bi $M\beta$; Cl $K\alpha_1$				
M_{IV}				4.574	199.2	14.12	Phelps
M_{IV}				4.568	199.5	14.12	Lindberg
M_{IV}				4.569			Coster
M_{V}	102	4.765	Bi $M\beta$; α				
M_{V}	103	4.763	Bi $M\beta$; Cl $K\alpha_1$				
M_{V}	104	4.761	Bi $M\beta$; Cl $K\alpha_1$				
M_{V}				4.763	191.3	13.83	Phelps
M_{V}				4.762	191.4	13.83	Lindberg
M_{V}				4.762			Coster

maximum experimental error for each was estimated to be ±5.1, ±4.4, ±3.2, ±2.4, ±2.2 volts, respectively. These discrepancies are of the order of magnitude to be expected from measurements on other elements.[12]

Different suggestions have been advanced to account for the relatively large discrepancies between the computed and observed ν/R values of the M_{IV} and M_{V} edges. In Table III these discrepancies are listed for the corresponding elements in columns 2 and 3. Sandström[13] has shown experimentally that the ν/R values of the L_{II} and L_{III} edges for the elements Ta73 to Au79 are equal to the ν/R values of lines found by Idei[14] and assigned as the transitions $O_{\mathrm{IV}}L_{\mathrm{II}}$ and $O_{\mathrm{IV,\,V}}L_{\mathrm{III}}$, respectively, thus indicating that electrons from L_{II} and L_{III} go in an absorption act to the incompletely occupied O_{IV} and O_{V} levels for these elements. According to Siegbahn,[15] Sandström's calculations explain the M_{IV} and M_{V} discrepancies, for, assuming the ordinary x-ray selection rule $\Delta l = \pm 1$, $\Delta j = \pm 1$ or 0 to apply in absorption as well as in emission, electrons from M_{IV}[16] and M_{V} are not allowed to go to the incomplete O_{IV} and O_{V} levels to which electrons from L_{II} and L_{III} go but must go to a different atomic level. In this manner he says the M_{IV} and M_{V} discrepancies come about, and there are no M_{II} and M_{III} discrepancies because the selection rule allows electrons from M_{II}, M_{III} and L_{III} to go to the same level. It should be pointed out here

[12] See Table III, columns 2 and 3 for M_{IV} and M_{V} discrepancies. See Siegbahn's *Spectroscopy of X-Rays*, 1931 edition, p. 278 and p. 346 for M_{I}, M_{II} and M_{III} discrepancies.

[13] Sandström, Zeits. f. Physik **65**, 632 (1930).

[14] Idei, Science Reports, Tohoku Imp. Univ. Series I, Vol. 19, No. 5.

[15] Siegbahn, Zeits. f. Physik **67**, 567 (1931).

[16] The l, j values of the levels L_{II}, L_{III}, M_{I}, M_{II}, M_{III}, M_{IV}, M_{V}, O_{IV} and O_{V} are, respectively, 1, 1/2; 1, 3/2; 0, 1/2; 1, 1/2; 1, 3/2; 2, 3/2; 2, 5/2, 2, 3/2; 2, 5/2. See Sidgwick's *Electronic Theory of Valency*, p. 50.

TABLE II. *Wave-length of reference lines.*

Sb $L\alpha_1$	3.432A	K $K\alpha_1$	3.734	Cl $K\alpha_1$	4.718
Sb $L\beta_1$	3.218	Bi $M\alpha$	5.108	Ag $L\alpha_1$	4.146
Sb $L\beta_2$	3.017	Bi $M\beta$	4.899	Ag $L\beta_1$	3.927

TABLE III. M_{IV} *and* M_V *discrepancies in volts.* W—Whitmer, S—Stenström, Z—Zumstein, J—Johnson, R—Rogers, C&V—Coster and Veldkamp, P—Phelps, H—Hanawalt, L—Lindberg, C—Coster, all cited in references.

Element	$M_{IV}'-L_{III}'$	$M_V'-L_{III}'$	*	
Ta73	28.6 W	28.6 W		
W74	41.0 L			
W74	43.2 Z	41.0 Z		
Os76	46.4 R**	54.6 R**		
Ir77	41.0 R	41.0 R		
Pt78	45.1 R	47.8 R		55 C&V
Pt78	43.7 L	45.1 L		
Pt78	58.7 J	58.7 J		
Au79	35.5 L	32.8 L		40 C&V
Au79	45.1 J	38.2 J		
Hg80	28.6 L	28.6 L		29 H
Tl81	25.9 L	24.6 L		
Pb82	20.4 L	23.2 L		
Bi83	16.8 P	19.1 P		
Bi83	20.5 L	20.5 L		
Bi83	20.5 C	19.1 C		
Th90	15.0 L, S	15.0 L, S		
U92	−2.2 L, S	−2.7 L,S		

* Separation in volts of first secondary absorption band from main edge.

** Os M_{IV} and M_V computed from absorption data by Sandström[18] and emission data from Siegbahn's *Spectroscopy of X-Rays*, 1931 edition, pp. 212 and 241.

that the selection rule, as applied by Siegbahn, also requires that electrons from M_I and L_{III} go to different levels while experimentally the M_I discrepancy is as questionable as that for M_{II}. To make this fact consistent with the selection rule explanation, it must be assumed that electrons from M_I and L_{III} go to levels close together. Of course the selection rule explanation alone can not indicate at all how many volts above the O_{IV} and O_V valence levels the M_{IV} and M_V electrons ought to go. Another objection is the assumption that the O_{IV} and O_V valence levels are atomic levels, whereas according to the quantum theory of conduction in metals,[17] the valence electrons fill up the lower of the energy levels common to all the atoms of the crystal lattice. Hence the selection rule that holds between atomic levels may not hold between an atomic and a lattice level. But this objection does not prevent the selection rule from being correct in many cases, for an examination of Idei's[14] careful measurements on the weaker emission lines of the *L*-group for the elements Ta73 to Bi83 shows that transitions connecting the conduction, or valence, levels with atomic levels in all cases appear to be obeying the ordinary x-ray selection rules. For Bi83, for example, the conduction electrons fall into the L_I level, corresponding to the transition $P_{II,\,III}L_I$ (allowed) for the isolated atom, but none fall into the L_{III} level (disallowed). For tungsten 74 occur the transitions $O_{IV,\,V}L_{III}$ and $O_{IV}L_{II}$ (allowed), but not the transition $O_{IV,\,V}L_I$ (disallowed). But for the elements Bi83, Pb82 and Tl81, the selection rule would permit the M_{IV} and M_V electrons to stop at the valence levels[18] and would require the L_{III} electron to go above these levels thus making the M_{IV} and M_V discrepancies for these elements negative. Table III shows these discrepancies to be positive. Hence there is an objection to the application of the emission selection rule unless it can be shown from intensity considerations, or otherwise, that electron transitions from M_{IV} and M_V to the valence levels for bismuth,[19] say, are relatively much less probable than transitions above the valence levels.

Pauling's[20] formula for the shift of the absorption edge of an ion in an ionic crystal gives good agreement with experiment for the halide crystals LiCl, NaCl, KCl and RbCl. However, it cannot account for the M_{IV} and M_V discrepancies since it treats electrons from M_I and M_V the same.

Before proposing an interpretation of the M_{IV} and M_V discrepancies based on secondary x-ray absorption data and other data, the two theories advanced to account for secondary structure will be briefly discussed. The theory of multiple transitions proposed by Ray,[21] Coster,[22] Lindsay and Voorhees[23] and Coster and Wolf[24] is able to account for the positions of the bands but other considerations throw considerable doubt on the correctness of the hypothesis of multiple transitions. For Hanawalt[25] finds no secondary struc-

[17] Bloch, Zeits. f. Physik **52**, 555 (1929).

[18] The l, j values of the valence levels for Bi83, Pb82, and Tl81 are 1, 1/2 and 1, 3/2.

[19] These transitions are $M_VP_{II,\,III}$ (2, 5/2→1, 1/2; 1, 3/2) and $M_{IV}P_{II}$ (2, 3/2→1, 1/2).

[20] Pauling, Phys. Rev. **34**, 954 (1929).

[21] B. B. Ray, Nature **122**, 771 (1928).

[22] Coster, Zeits. f. Physik **25**, 83 (1924).

[23] Lindsay and Voorhees, Phil. Mag. **6**, 910 (1928).

[24] Coster and Wolf, Nature **124**, 652 (1929).

[25] Hanawalt, Phys. Rev. **37**, 723 (1931).

ture in the absorption spectra of the monatomic gases Hg, Zn, Xe and Kr while mercury compounds and solid zinc show a definite structure. Also Hanawalt states that the bands near the main edge are always sharper than those farther out which fact is just the opposite of what would be expected on the multiple transitions theory.[26] Another significant objection to this theory is that it would not account for the M_{IV} and M_V absorption discrepancies.

According to Kronig's[27, 28] theory secondary absorption bands are due to electrons being ejected, in an absorption act, from the x-ray level in question out to lattice levels of the crystal. The energy separation of the secondary absorption bands of a substance depends on its crystal system rather than on the particular atom in the substance. For different substances having the simple cubic structure the energy separation of their secondary absorption bands should be approximately equal when corrected to take account of the difference in the dimensions of the lattice cells. Two different atoms in a mixed crystal, such as a Cu[29]–Au crystal, should give similar secondary absorption spectra. Coster's and Veldkamp's[30, 31] data on the face-centered cubic crystals of Pt, Au, Cu[29] and Ca[29] verify the former conclusion, while their data on the mixed crystals Ni–Fe and Cu–Au very beautifully verify the latter. In addition Veldkamp[30] has examined the secondary absorption spectrum of the compounds[32] $NiF_2 \cdot 2H_2O$ and $CoF_2 \cdot 2H_2O$, the Debye-Sherrer photographs of which indicate the same crystal structure, and finds their absorption spectra to be exactly analogous. The failure of the monatomic gases Hg, Zn, Xe and Kr to show a secondary absorption structure extending beyond the main edge more than the ionization potential of the atom, in disagreement with the theory of multiple transitions, is exactly in accord with the requirements of Kronig's theory. To Hanawalt's[25] data on the monatomic gases may be added that of Coster and Van der Tuuk[33] on argon.

Stephensen[34] concludes that his data on the secondary structure of Br in a KBr crystal agree with those of Lindsay[35] on the secondary structure of K also in a KBr crystal in accord with Kronig's theory.

Assuming the correctness of the view that secondary absorption bands are due to electron transitions to lattice levels of the crystal one may readily account for the M_{IV} and M_V discrepancies. Electrons from the M_{IV} and M_V levels go, in an absorption act giving rise to the M_{IV} and M_V edges, to the first lattice levels available to them above the valence, or filled conduction, levels for the elements Ta73 to Th90. The L_{III} edge is due to electron transitions from L_{III} to the valence levels for the elements Ta73 to Au79 as pointed out by Sandström.[13] Although emission lines involving transitions from the valence levels of Hg80, Tl81 and Pb82 were not obtained by Idei,[14] Sandström's[13] comparison indicates that electrons from L_{III} go to the valence levels or nearby levels for the elements Hg, and Tl also. For Bi83 electrons from L_{III} go to a level close to the valence levels.

In Table III column 4 appears the voltage separation from the L_{III} edge of the first secondary absorption band for the solid substances Hg, Au and Pt. Comparing with the M_{IV} and M_V discrepancies the agreement is within experimental error. One may conclude that, for these elements, electrons from the M_{IV} and M_V levels and the L_{III} level either go to energy zones with the same quantum numbers or to overlapping zones with different quantum numbers.

In view of the fact that the valence, or conduction, levels appear to obey the ordinary x-ray selection rule in emission, it seems worth while to see wherein intensity considerations might help explain why electrons from the M_I level and the M_{IV} and M_V levels, though allowed by the

[26] On this theory the bands farther out from the main edge are due to electrons coming from inner and hence sharper levels.
[27] Kronig, Zeits. f. Physik **70**, 317 (1931).
[28] Kronig, Handb. d. Phys. **24** 1/2, 292 (1933).
[29] The first bands near the main edge in the absorption spectrum of Ca and Cu do not appear in that of Au and Pt. Their explanation is that these bands are due to levels characteristic of the atom and hence not common to the lattice.
[30] Veldkamp, Zeits. f. Physik **82**, 777 (1933).
[31] Coster and Veldkamp, Zeits. f. Physik **74**, 203 (1932).
[32] Brewington, Abstract in Bulletin of the American Physical Society, April, 1934. Brewington reports the secondary absorption spectra of the two elements in a KCl and a CaS compound to be dissimilar. Possibly better agreement may be obtained if secondary structure of ions of the same sign only in different compounds of the same crystal system were compared.
[33] Coster and Van der Tuuk, Zeits. f. Physik **37**, 367 (1926).
[34] Stephensen, Phys. Rev. **44**, 352 (1933).
[35] G. A. Lindsay, Zeits. f. Physik **71**, 735 (1931).

selection rule to do so, do not go to the same level in an absorption act. Applying the x-ray selection rule, $\Delta l = \pm 1$, $\Delta j = \pm 1$ or 0 to the five M levels and the L_{III} level, one readily finds the possible l, j values of the lattice levels to which electrons go, as allowed by this selection rule, in coming from the above x-ray levels in an absorption act. In Fig. 1 the possible l, j values of these experimentally determined levels for bismuth metal are indicated at the right. These levels, also indicated by primed letters at the left, together with the remaining figure constitute a Kronig[27] diagram of energy levels in a crystal (x-ray levels not shown).

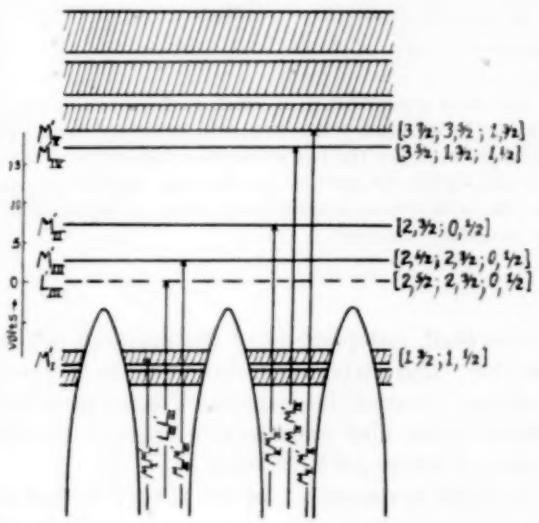

FIG. 1. Part of energy level diagram for bismuth metal (scale for primed levels only).

The separation of any one of the M' levels, which are drawn to scale, from the L'_{III} level gives the corresponding M discrepancy. Thus $M'_V - L'_{III}$ gives the M_V discrepancy in volts. The width of the primed levels is not shown, otherwise there would be overlapping for some levels. The upper and lower lattice levels, which are shown hatched, are not drawn to scale. The lowest zone is supposed to be filled with conduction electrons and the next one-half filled, since bismuth has a valence of three. M'_I is in the middle of the half filled zone.

In Fig. 1 one notes that some of the l, j values for M'_{IV} and M'_V appear also with M'_I although, as already stated, electrons from M_{IV} and M_V and M_I levels do not go to the same level. Before one can hope to investigate the question of relative intensities of the possible transitions concerned from theoretical considerations more must be known about the wave functions representing the lattice states. Turning to emission data one notes that the strongest lines in the K, L and M series are those involving transitions of the type l, $j \rightarrow l-1$, $j-1$. For example $K\alpha_1$ is the 1, $3/2 \rightarrow 0$, $1/2(L_{III}K)$ transition, $L\alpha_1$ is the 2, $5/2 \rightarrow 1$, $3/2(M_V L_{III})$ transition, and $M\alpha_1$ is the 3, $7/2 \rightarrow 2$, $5/2(N_{VII}M_V)$ transition. For absorption these transitions correspond to the type l, $j \rightarrow l+1$, $j+1$. Corresponding to this rule, one would choose the l, j value to the extreme left in each bracket of Fig. 1 for the corresponding primed level. Of course, one may not be justified in extrapolating from the valence levels, which appear to have a definite l, j value as emission data indicate, in assigning l, j values to all or a part of these primed levels. This point cannot be investigated from emission data. Although the discrepancy $L'_{III} - M'_I$ is within experimental error, one would expect the L'_{III} level to lie above M'_I for bismuth since the selection rule allows electrons from M_I to stop at the valence levels but not electrons from L_{III}. Likewise for lead and thallium, M'_I may be expected to lie below L'_{III}.

The same type of diagram as Fig. 1 may be constructed for the elements Ta73 to Hg80 and Th90. U92 does not show M_{IV} and M_V discrepancies. According to the ordinary x-ray selection rule this fact indicates U92 then may have valence levels with quantum numbers 3, 5/2 and 3, 7/2. There is disagreement as to the assignment of quantum numbers to the valence levels of U92[36] and Th90.

In conclusion the large M_{IV} and M_V discrepancies are considered to be definite evidence for the existence of discrete energy levels 20 to 50 volts above the valence, or conduction, levels for the elements Ta73 to Th90. The M_{IV} and M_V edges are here interpreted to be due to electron transitions to virtual lattice levels of the crystal. Data on secondary x-ray absorption are cited in support of this view. The magnitude of the M_{IV} and M_V discrepancies would be greatly reduced for the atom in the monatomic gaseous state.

[36] Ruark and Urey, *Atoms, Molecules and Quanta*, p. 282 and Sidgwick, The *Electronic Theory of Valency*, pp. 46 and 50.

That there is a definite selection rule operating in M absorption there is little room to doubt. No attempt has been made to apply the above reasoning to include elements below Ta73 but if their valence levels obey the selection rule, one may expect to find M_{IV} and M_V discrepancies for Hf72 and Lu71 but none for elements Yb70 to Ce58.

The writer wishes to thank the staff members of the Department of Physics of the University of Iowa for their interest and cooperation. Thanks are especially due to Dr. G. W. Stewart who suggested and directed this research. He also wishes to express his appreciation of the skill and assistance of the instrument maker, Mr. J. G. Sentinella.

The Dependence of Secondary Structure in X-Ray Absorption on Crystal Form

VOLA P. BARTON, *Goucher College* AND GEO. A. LINDSAY, *University of Michigan*

(Received July 6, 1934)

An examination of the Ca K absorption edge in the x-ray absorption spectra of different compounds shows clearly that the secondary structure is not the same in different compounds, and is not even the same in the two crystals calcite and aragonite, which are the same chemically, but of different crystalline form. These facts are in accord with Kronig's theory of the secondary structure. In four other crystals, each of which contains two or more metals, the secondary structure was examined to see if it was the same for the two elements in the same crystal. There is a difference for the two elements, which indicates that the crystal form is not the sole factor in determining the secondary structure.

THE cause of secondary structure in x-ray absorption spectra near the characteristic absorption edges of the elements has been the subject of much investigation and discussion. The present paper considers some points suggested by the wave-mechanical theory of Kronig, which attributes the secondary structure to alternate permitted and forbidden zones in the continuous range of energy values for an electron passing through a crystal. A quantum of energy in the x-ray beam, great enough to remove the electron from the atom, or ion, of the absorbing material, and give it kinetic energy corresponding to one of the permitted zones, may be absorbed; if the kinetic energy corresponds to one of the forbidden zones it will not be absorbed.

The zones of possible absorption are given in Kronig's theory by the expression $W = n^2h^2/8ma^2$, where W is the energy of the electron passing through the network of the crystal, a is the distance between atoms or ions in the direction of motion of the electron. h and m are as usual, Planck's constant, and the mass of the electron, respectively.

This result makes the secondary structure, as far as the limiting conditions of the theory may be accepted, independent of the material of the absorber, and dependent only on the crystal structure. Several investigations have afforded results which give considerable support to the theory as advanced by Kronig.

A simple consequence of the theory is that if the same element occurs in two crystals of different type, then the secondary structure should be different, while two elements occurring in the same crystal should have similar structure in the absorption, because the electron ejected from the atom must pass through the same array of atoms whether it comes from the one element or the other. This last conclusion has been considered by Kronig and others to be invalid in a region near the absorption edge.

Two convenient crystals of different form, and not only containing the same element but consisting of *the same chemical compound* are calcite and aragonite. The formula is $CaCO_3$ and the K absorption edge of Ca, which lies at about 3060 x.u., has been observed for several calcium compounds. The secondary structure of the calcium edge has already been described.[1]

[1] G. A. Lindsay and G. D. Van Dyke, Phys. Rev. **30**, 562 (1927).

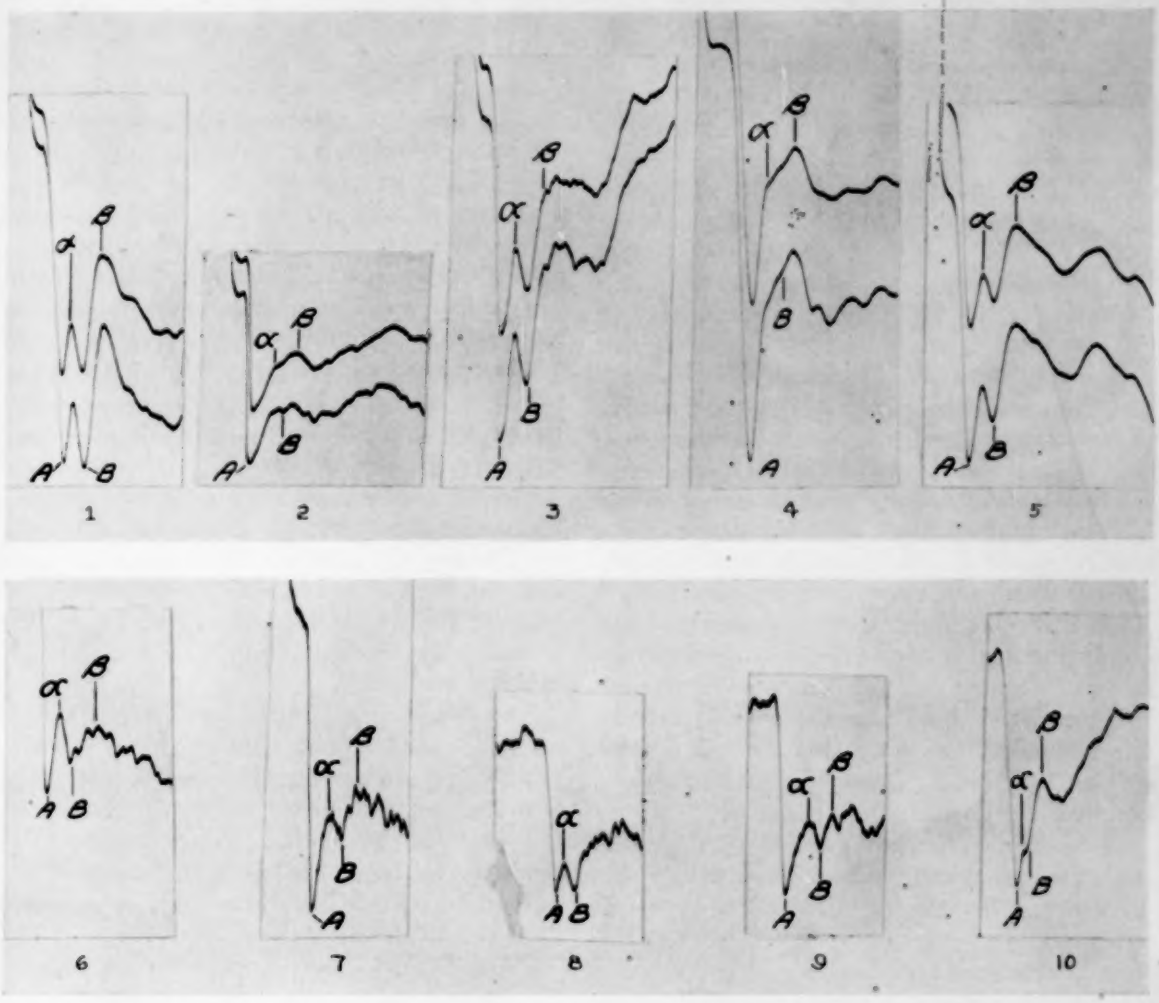

FIG. 1. Photometer curves of the secondary structure. The double curves in the first 5 cases are taken at different levels across the plate. 1, Ca K in calcite; 2, Ca K in aragonite; 3, Ca K in dolomite; 4, Ca K in anhydrite; 5, Ca K in ankerite; 6, Fe K in ankerite; 7, Ca K in perovskite; 8, Ti K in perovskite; 9, Fe K in chromite; 10, Cr K in chromite.

In the present paper the object is not so much to give individual energy separations in the secondary structure for any element or crystal, as to *compare* values and the general appearance of the structure in different crystals or for different elements. However, in order to compare them satisfactorily it is necessary to give a certain amount of data; hence measurements have been made on the photographic plates on successive white (maximum absorption) lines, and dark (minimum absorption) lines. The white lines are denoted in the table by A, B, and the dark ones by α, β as shown in Fig. 1. No attempt was made to measure the structure far from the edge where it is faint and uncertain at the best, but only the well-defined portion nearer the edge has been recorded. The white and the dark lines are here so distinct that there is little doubt of their approximate location. At least two plates of each edge for each absorber were taken and measured.

The appearance of the absorption pattern for calcite, which is hexagonal, and for aragonite, which is orthorhombic, is markedly different. Fig. 1 shows microphotometer traces for the two for comparison. In the case of calcite we have two strong white lines, very nearly equal in intensity, while for aragonite there is only one

TABLE I. *Separations in secondary structure. $A\alpha$, AB, $A\beta$* represent, respectively, the separations in volts between the points A and α, A and B, A and β shown in the photometric records of Fig. 1.

Element	Compound	Crystal Type	$A\alpha$	AB	$A\beta$
Ca	Calcite	Hexagonal	5.7	11.7	20.7
Ca	Aragonite	Orthorhombic	9.3	15.5	22.4
Ca	Dolomite	Hexagonal	6.4	11.9	18 9
Ca	Anhydrite	Orthorhombic	7.2	15.4	23 2
Ca	Ankerite	Hexagonal	6.6	11.9	18 4
Fe	Ankerite		6.6	11.1	23.4
Ca	Titanite	Monoclinic	2.6	4.5	7.4
Ti	Titanite		6.8	12.8	22.6
Ca	Perovskite	Pseudo-cubic	7.3	13.2	20.6
Ti	Perovskite		7.6	14.5	—
Cr	Chromite	Cubic	6.7	13.3	28.0
Fe	Chromite		26.5	57.0	—

of great intensity. The difference is not due to difference in thickness of absorbing screen, for a wide range of thickness shows the same contrast. This marked difference between calcite and aragonite occurs very near the absorption edge, —only about 10 volts away—hence we may base further judgment in regard to other crystals on structure which is as near the edge as this. In this region the measurements are much more definite, for the sharpness of definition decreases rapidly as we go away from the edge.

Since the two forms of calcium carbonate do not differ chemically, we must attribute the difference in the spectra to the different crystal structure. The separation of the first white line from the adjacent dark one is 5.7 volts (see column $A\alpha$ in Table I) for calcite and 9.3 volts for aragonite, while the separations of the first two white lines are 11.7 and 15.5 volts, respectively. This leads to the conclusion that the crystal structure has a marked influence on the secondary structure, even as near the edge as 10 volts. It does not, however, say that other causes may not also influence the secondary structure.

Fig. 2 is a reproduction of two plates; one for calcite and one for aragonite, showing how plainly they differ in the appearance of the calcium absorption.

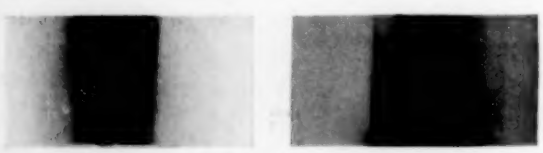

Calcite. Aragonite.

FIG. 2. Structure in calcite and aragonite.

Dolomite (Ca, Mg)CO_3 and ankerite (Ca, Mg, Fe)CO_3 were next observed. Since they were of the same crystal form as calcite there was little difference to be expected, and the photometer diagrams, as well as the values in the table, show almost identical patterns. Anhydrite ($CaSO_4$) which again is orthorhombic, differs greatly from calcite and is much more like aragonite in its secondary structure.

The remaining materials were chosen so as to have two elements in the same compound not too far apart in atomic number. The secondary structure for these two could then readily be compared, and since they are in the same crystal, one might expect the absorption pattern to be very nearly the same for both elements. This idea has been tested by Coster, Veldkamp and Klamer[2] for certain metals, and the secondary structure was found to be in some cases similar, in others dissimilar.

The compounds chosen for this purpose in our work were titanite ($CaSiTiO_5$), perovskite ($CaTiO_3$), and chromite (Fe, Cr) $[(Cr, Fe)O_2]_2$, as well as ankerite, mentioned above. In chromite the edges of Fe and Cr were compared, in ankerite Ca and Fe, while in titanite and perovskite the calcium absorption was compared with that of titanium.

From Table I it may be seen that in ankerite the calcium and iron show patterns which, when reduced to volts are very nearly alike, Ca and Ti in perovskite are quite similar, while Ca and Ti in titanite and Cr and Fe in chromite differ greatly. In the case of titanite there are two strong lines of absorption for calcium and also for titanium. For calcium the white line nearer the edge is plainly divided into two parts by a narrow black line down the middle, although the photometer record does not show this distinctly and it is not included in the figures. No such division could be detected for the titanium. One might think it possible that on account of the lesser resolution at the titanium edge (the wave-lengths of the edges are, Ca 3060 x.u.; Ti 2490 x.u.) a division of the first

[2] D. Coster and J. Veldkamp, Zeits. f. Physik **74**, 191 (1932); J. Veldkamp, ibid. **77**, 250 (1933); ibid. **82**, 776 (1933); D. Coster and G. H. Klamer, Physica **1**, 145 (1934).

white line could escape notice, but the remainder of the structure is also quite out of agreement with that of the calcium. Thus, the distance from the middle of the first absorption line to the middle of the second broad and strong absorption line, ignoring the division of the first line in the case of calcium, is 7.2 volts for Ca, and 12.8 volts for Ti.

In the case of perovskite ($CaTiO_3$), although the separations of the first two white lines agree very well, as may be seen from the table, yet on examining the plates one is not convinced that they are alike, for the two white lines are of nearly equal intensity for Ti, while for Ca the first line is much stronger than the second (see photometer curves).

The absorption due to Cr in chromite differs much from that due to Fe in the same compound. The two strong white lines in the case of Cr are distinct and should be plainly observed a little closer together for Fe on account of the lesser dispersion. The second line is not observed for Fe, but there is another white line of moderate intensity about 57 volts from the first one. No white line appears for Cr at this distance. It seems therefore evident that the secondary structure in absorption, while greatly influenced by crystal structure, is not wholly controlled by that factor.

The x-rays were reflected from the rhombohedral face of a quartz crystal, the grating constant thus being 3336 x.u. The absorbing material was ground into a fine powder and suspended as uniformly as possible in a thin film of collodion. This screen was then placed between the slit and the crystal.

A Quantitative Test of the Waller-Hartree Theory of X-Ray Scattering Applied to the Diffuse Scattering from Crystals

G. G. HARVEY,* *Ryerson Physical Laboratory, University of Chicago*
AND
P. S. WILLIAMS AND G. E. M. JAUNCEY, *Washington University, St. Louis*
(Received July 16, 1934)

The effect of the extra term in the incoherent part of the scattered radiation due to the operation of the Pauli exclusion principle is calculated for neon. It is shown that the inclusion of this term gives considerably better agreement with experimental results for NaF; it is further pointed out that it is probably only in the case of the diffuse scattering from crystals that the effect of this term can be detected experimentally.

A QUANTUM-mechanical theory of the scattering of radiation by a free atom has been given by Wentzel[1] and independently by Waller and Hartree.[2,3] The latter treatment differs from that of Wentzel in that account is taken of the Pauli exclusion principle; this restricts the number of electron transitions possible and leads to a consequent decrease in the intensity of the incoherent part of the scattered radiation. The coherent part of the scattering, on both theories, is given by

$$S_1 = I/ZI_e = f^2/Z, \qquad (1)$$

where S is the scattering per electron in terms of the Thomson value I_e. Wentzel's formula for the incoherent scattering is

$$S_2 = 1 - (\sum_{j=1}^{Z} E_{jj}^2)/Z, \qquad (2)$$

where E_{jj} is the contribution to f "due to the jth electron"; i.e., $f = \sum_{j=1}^{Z} E_{jj}$. The corresponding formula of Waller and Hartree is

$$S_2 = 1 - (\sum_{j=1}^{Z} E_{jj}^2)/Z - (\sum_{j \neq k} |E_{jk}|^2)/Z. \qquad (3)$$

---

* National Research Fellow.

[1] G. Wentzel, Zeits. f. Physik **43**, 1 and 779 (1927).

[2] I. Waller, Phil. Mag. **4**, 1228 (1927); Nature **120**, 155 (1927); Naturwiss. **15**, 969 (1927); Zeits. f. Physik **41**, 213 (1928).

[3] I. Waller and D. R. Hartree, Proc. Roy. Soc. **A124**, 119 (1929).

The quantities E_{jk} are defined by Waller and Hartree (reference 3, Eq. (41)) as

$$E_{jk}=\int \psi_j\psi_k^* e^{i\sigma\mu r}r^2\,dr\,d\mu\,d\varphi, \qquad (4)$$

where $\sigma=4\pi(\sin\phi/2)/\lambda$ and ψ_j is the wave function associated with the jth electron. The summation is to be taken over all pairs of electrons with the same spin and $j\neq k$. Waller and Hartree have compared their calculated values of S_1+S_2 for argon with the experimental results of Barrett.[4] Now the maximum value of the correction term $\sum|E_{jk}|^2$ amounts at most to less than ten percent of the *incoherent* scattering for argon and occurs at a value of $(\sin\phi/2)/\lambda=0.65$. But here the *coherent* scattering is by far the largest part of the whole and so the correction term amounts to only a few percent. At larger and smaller values of $(\sin\phi/2)/\lambda$ its effect rapidly becomes negligible.

The matter is different, however, in the case of the diffuse scattering from crystals. Here the incoherent scattering is always a large part of the whole. It thus seems that this would be the logical place to see whether the inclusion of this term gives better agreement with experiment. The classical theory of the diffuse scattering from a single crystal gives,[5] for a crystal consisting of two kinds of atoms such as NaF,

$$S_{class.}=1-\frac{\sum(E_{jj}^2)_1+\sum(E_{jj}^2)_2}{Z_1+Z_2}+\frac{f_1^2+f_2^2-F_1^2-F_2^2}{Z_1+Z_2}, \qquad (5)$$

where F is the atomic structure factor including the effect of thermal agitation and the numerical subscripts refer to the two kinds of atoms. Taking account of the extra term of the Waller-Hartree theory it is seen that we should subtract from Eq. (5) the quantity

$$\{\sum|E_{jk}|_1^2+\sum|E_{jk}|_2^2\}/(Z_1+Z_2). \qquad (6)$$

We shall now compare the calculated values of $S_{class.}$ taking account of the expression (6) with the recent results of Williams[6] on the diffuse scattering of monochromatic x-rays from NaF at 295°K. To do this it is necessary to calculate the quantities $E_{jk}(j\neq k)$. Since Na^+ and F^- are neon-like and since the E_{jk} are involved only in a correction term we shall not be appreciably in error if we use E_{jk} for neon instead of for Na^+ and F^-. We have

$$\psi_{n,\,l,\,m}=N_{n,\,l,\,m}\chi_{n,\,l}(r)P_l^m(\mu)e^{im\varphi}, \qquad (7)$$

where P_l^m is the associated Legendre function, $\chi_{n,\,l}(r)$ the radial wave function and $N_{n,\,l,\,m}$ a normalizing factor equal to $[(2l+1)(l-m)!/4\pi(l+m)!]^{\frac{1}{2}}$ if $\chi_{n,\,l}(r)$ is taken as already normalized. Analytical approximations to the radial wave functions of neon have been given by Brown.[7] Following Waller and Hartree, we shall neglect values of E_{jk} which involve a change in the total quantum number n; also, E_{jk} vanishes if m is not the same in both wave functions. Since the spin must be the same, this leaves as the only possibility $n=2$, $l=1$, $m=0$, $n'=2$, $l'=0$, $m'=0$ and this occurs four times, *viz.*, (210,200) and (200,210) each taken with + and − spin. Inserting these values in Eq. (4) and integrating with respect to μ and φ, we obtain

$$E_{210,200}=i(3)^{\frac{1}{2}}\int_0^\infty\left(\frac{\sin\sigma r}{\sigma^2r^2}-\frac{\cos\sigma r}{\sigma r}\right)\times r^2\chi_{2,\,0}(r)\chi_{2,\,1}(r)\,dr. \qquad (8)$$

TABLE I.

j	A_j	α_j	j	A_j	α_j	j	A_j	α_j
1	273.38	12.70	3	295.68	8.17	5	38.59	5.60
2	54.21	10.13	4	95.82	6.63	6	18.97	4.06

TABLE II.

$(\sin\phi/2)/\lambda$	$\Sigma\|E_{jk}\|^2$	$(\sin\phi/2)/\lambda$	$\Sigma\|E_{jk}\|^2$	$(\sin\phi/2)/\lambda$	$\Sigma\|E_{jk}\|^2$
0.05	0.140	0.35	1.210	0.70	0.172
0.10	0.467	0.40	1.027	0.75	0.116
0.15	0.852	0.45	0.849	0.80	0.067
0.20	1.199	0.50	0.643	0.90	0.029
0.25	1.324	0.55	0.482	1.00	0.009
0.275	1.340	0.60	0.351	1.10	0.002
0.30	1.324	0.65	0.248	1.20	0.000

[4] C. S. Barrett, Phys. Rev. **32**, 22 (1928).
[5] G. E. M. Jauncey, Phys. Rev. **37**, 1193 (1931); G. E. M. Jauncey and G. G. Harvey, Phys. Rev. **37**, 1203 (1931); Y. H. Woo, Phys. Rev. **38**, 6 (1931); and **41**, 21 (1932); G. E. M. Jauncey, Phys. Rev. **42**, 453 (1932).
[6] P. S. Williams, Phys. Rev. **46**, 83 (1934).
[7] F. W. Brown, Phys. Rev. **44**, 214 (1933).

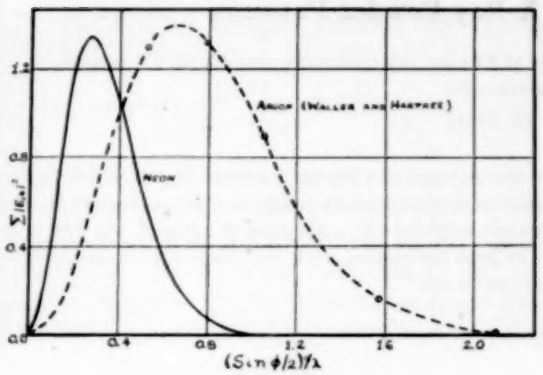

FIG. 1.

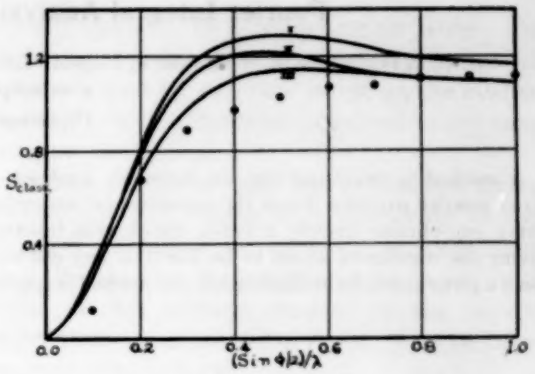

FIG. 2.

But[7]

$$r\chi_{2,0}(r) = 13.60[re^{-8.22r} - r^2(1.08e^{-3.69r} + 0.35e^{-2.15r})]$$

$$r\chi_{2,1}(r) = 20.13r^2(e^{-4.48r} + 0.198e^{-1.91r}),$$

where r is expressed in atomic units; performing the integration with respect to r, we get

$$E_{210,200} = i(3)^{\frac{1}{2}}\left\{\sum_1^2 \frac{8A_j}{\alpha_j^5}\frac{\sigma}{(1+\sigma^2/\alpha_j^2)^3} - \sum_3^6 \frac{(40A_j/\alpha_j^6)\sigma - (8A_j/\alpha_j^8)\sigma^3}{(1+\sigma^2/\alpha_j^2)^4}\right\} \quad (9)$$

and $\sum|E_{jk}|^2 = 4|E_{210,200}|^2$. The A_j and α_j are given in Table I. The value of $\sum|E_{jk}|^2$ is given in Table II as a function of $(\sin\phi/2)/\lambda(\lambda$ in A) and is plotted in Fig. 1 together with Waller and Hartree's values of the same quantity for argon. Although only five values are given for argon it is seen that it is possible to draw a curve through these with considerable accuracy. As might be expected, the curve for neon may be approximately obtained from that for argon by multiplying the abscissae of the latter by $(10-s_1)/(18-s_2)$ where s_1 and s_2 may be considered as average screening constants.

In order to compare the calculated and observed values of S we have used values of E_{jj} and f from the tables of James and Brindley[8] and have obtained F by multiplying f by the Debye-Waller[9, 10] temperature factors, using Shonka's value,[11] 442°K, for the characteristic temperature of NaF and assuming the existence of zero-point energy. The results are shown in Fig. 2. Curve III takes account of the extra correction term while Curve II neglects it. Curve I is based on the assumption that the probability distribution is the same for all electrons so that $\sum E_{jj}^2 = f^2/Z$, i.e., $f'' = f$ in the notation used by Jauncey.[12] The points represent the experimental values.[6] We feel that Curve III agrees with the experimental values within the limits of experimental error and that Curve II, and even more so Curve I, differ by more than the experimental error from the observed values.

[8] R. W. James and G. W. Brindley, Phil. Mag. **12**, 81 (1931).
[9] P. Debye, Ann. d. Physik **43**, 49 (1914).
[10] I. Waller, *Diss. Upsala* (1925); Zeits. f. Physik **17**, 248 (1923).
[11] J. J. Shonka, Phys. Rev. **43**, 948 (1933).
[12] G. E. M. Jauncey, Phys. Rev. **42**, 453 (1932).

Fourier Integral Analysis of X-Ray Powder Patterns

B. E. Warren and N. S. Gingrich, *Eastman Laboratory of Physics, Massachusetts Institute of Technology, Cambridge, Massachusetts*

(Received June 18, 1934)

A method is developed for the harmonic analysis of x-ray powder patterns. From the experimental scattering curve one obtains directly a radial distribution function giving the number of atoms to be found at any distance from a given atom. As an illustration, the method is applied to the pattern of rhombic sulphur. A radial distribution curve is obtained which indicates that each atom has two nearest neighbors at a distance of about 2.3A. The result is in good agreement with the chemist's picture of an S_8 ring molecule.

Introduction

THE determination of the radial distribution of atoms surrounding any given atom, by application of Fourier integral analysis to the experimental x-ray diffraction patterns of liquids, was suggested by Zernike and Prins.[1] The method has been successfully used by Debye and Menke[2] in the study of liquid mercury. It suggests itself immediately that the method should be equally applicable to the x-ray powder patterns of crystalline materials and that, by this method of analysis, the same kind of information should be obtained, namely the radial distribution of atoms about any one atom.

The treatment of x-ray diffraction in crystals by means of a Fourier series representation of the density of scattering matter is well known.[3,4] However, the applicability of the method to a complex crystal has been rather limited because of the fact that one can determine from the intensities of reflection only the magnitudes of the coefficients in the Fourier series. The *phases* are usually unknown and hence the method is not generally applicable. An important feature of the present method of treatment is found in the fact that the coefficients are given in terms of the observed *intensities*, not the amplitudes, and hence there is no ambiguity as to phase. Needless to say since the new method does not require as much diffraction information, it will not yield as much structural information. Instead of determining a complete crystal structure, the new method gives simply the distribution of atoms about any one atom.

[1] Zernike and Prins, Zeits. f. Physik **41**, 184 (1927).
[2] Debye and Menke, *Ergeb. der Tech. Röntgenkunde* II.
[3] A. H. Compton, *X-rays and Electrons.*
[4] W. H. Bragg and W. L. Bragg, *The Crystalline State.*

Theory

For simplicity in presentation we shall assume a crystal containing only one kind of atom, and then later give the corresponding result for the general case. From an array of atoms which takes all orientations in space, the intensity of scattered radiation is given as a function of the angle of scattering by the relation[5]

$$I(s)=I_0\frac{e^4}{m^2c^4R^2}\left(\frac{1+\cos^2 2\theta}{2}\right)\sum_p\sum_q f_p f_q\frac{\sin sr_{pq}}{sr_{pq}}. \quad (1)$$

$s=4\pi\sin\theta/\lambda$, f_p is the atomic scattering factor for atom p and r_{pq} is the distance from atom p to atom q. For a crystal containing only one kind of atom (1) becomes

$$I(s)=\psi(s)N\sum_p \sin sr_p/sr_p, \quad (2)$$

where N is the effective number of atoms in the sample and

$$\psi(s)=I_0\frac{e^4}{m^2c^4R^2}f^2\left(\frac{1+\cos^2 2\theta}{2}\right).$$

Representing the distribution of atoms about any one atom by a density function $\rho(r)$ such that $4\pi r^2\rho(r)dr$ is the number of atoms between r and $r+dr$ from the atom under consideration, Eq. (2) becomes

$$I(s)=N\psi(s)\left\{1+\int_0^\infty 4\pi r^2\rho(r)\frac{\sin sr}{sr}dr\right\}. \quad (3)$$

Let

$$i(s)=(I(s)/N\psi(s))-1$$

$$si(s)=4\pi\int_0^\infty r\rho(r)\sin sr\,dr. \quad (4)$$

[5] P. Debye, Ann. d. Physik **46**, 809 (1915).

By the Fourier integral theorem this can be written

$$r\rho(r)=(2\pi^2)^{-1}\int_0^\infty si(s)\sin sr\,ds. \quad (5)$$

The integration over the scattered intensity $I(s)$ is from zero to large angles and hence includes the diffraction maximum at zero angle (000 order) which is not experimentally observable. Replace $I(s)$ by $I'(s)+I(s)$ where $I'(s)$ is the intensity distribution in the 000 order beam and $I(s)$ is the observable intensity curve.

$$2\pi^2r\rho(r)=\int_0^\infty \frac{sI'(s)}{N\psi(s)}\sin srds + \int_0^\infty s\left\{\frac{I(s)-N\psi(s)}{N\psi(s)}\right\}\sin sr\,ds. \quad (6)$$

The first integral has the same value for either an amorphous or crystalline material and is readily evaluated either from consideration of a spherical sample of continuously distributed scattering matter or by a modification of the usual method of calculating the integrated reflection from a powdered crystal.

$$\int_0^\infty \frac{s^2I'(s)}{N\psi(s)}ds=2\pi^2r\rho_0,$$

where ρ_0 is the average density of the sample in atoms per cc. Our relation takes the final form

$$4\pi r^2\rho(r)=4\pi r^2\rho_0+(2r/\pi)\int_0^\infty si(s)\sin sr\,ds. \quad (7)$$

The $si(s)$ curve is readily constructed from the experimental scattering curve and the operation involved in Eq. (7) is then best carried out with a harmonic analyzer. The final result is a curve of $4\pi r^2\rho(r)$ as a function of r. It might be pointed out that the result is obtained by a purely mechanical, straightforward operation and that it is not even necessary to index the lines of the powder pattern or to have fitted the lines to a quadratic form.

The integral in Eq. (7) can also be expressed in terms of the integrated reflections of the lines in the powder pattern. The relation then becomes a series, with a term for each line in the powder pattern.[6] However, since the number of lines in a powder pattern is usually rather large, the evaluation of the series becomes altogether too laborious; and for practical purposes the evaluation of (7) with a harmonic analyzer is the most satisfactory method.

In the general case, one has a crystal containing several kinds of atoms with scattering factors which do not have the same dependence upon $\sin\theta$. In this case the problem must be set up in terms of the electron density in the crystal rather than the atom density. Eq. (7) then takes the more general form

$$\int_M \rho_m d\sigma_m 4\pi r^2\rho(r)=4\pi r^2\rho_0\sum_M Z_m + (2r/\pi)\int_0^\infty s\{(I/N\psi(s))-\sum_M f_m^2\}\sin sr\,ds, \quad (8)$$

where N is the number of molecules in the sample, Σ_M indicates summation over the atoms per molecule, ρ_m and $\rho(r)$ are electron densities in electrons per cc, and $\psi(s)$ is the intensity per electron. In this case one obtains a distribution curve giving the weighted average density of electrons at distance r from a point, each value being weighted by the electron density at the individual point. The positions of the peaks indicate distances which are slightly larger than the interatomic distances and the areas under the peaks give directly the number of pairs of atoms, having that particular distance of separation, multiplied by the product of the atomic numbers.

Application to Rhombic Sulphur

The method of harmonic analysis has been successfully applied to the powder pattern of rhombic sulphur, the crystalline structure of which had not hitherto been determined. The powdered material was mounted on a thread with dilute collodion and the cylindrical sample placed in a powder diffraction camera of radius 4.75 cm. Since there must be no extraneous background blackening, it is very necessary to use a strictly monochromatic x-ray beam. This was obtained by reflecting the $K\alpha$ line of Mo from a rocksalt crystal placed in front of the camera. With the tube running at 20 m.a. and 35 kv peak an exposure of 25 hours was sufficient.

From the microphotometer record of the film, an intensity curve was derived in the usual way.

[6] N. Gingrich and B. Warren, Phys. Rev. **45**, 762 (1934).

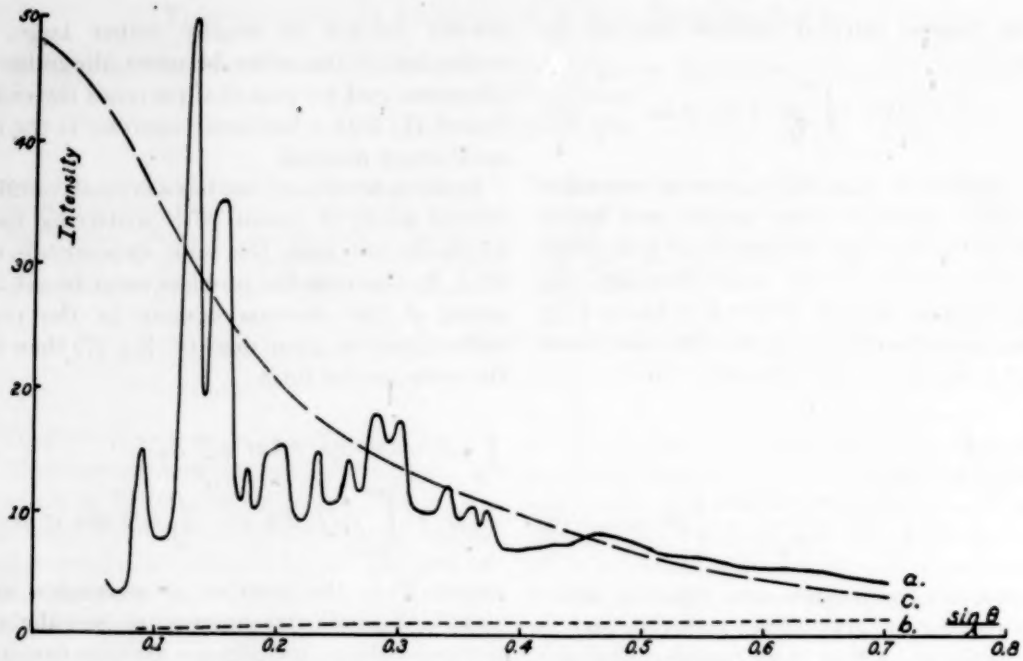

FIG. 1. (*a*) Experimental scattering curve for rhombic sulphur corrected for absorption. (*b*) Modified scattering. (*c*) Independent unmodified scattering $N\psi(s)$.

The experimental intensity curve, corrected for absorption in the cylindrical sample,[7] is given in Fig. 1*a*, the intensity being expressed in arbitrary units.

As seen from Eq. (3), at large angles of scattering $I(s)$ approaches $N\psi(s)$ and hence at sufficiently large values of sin θ the experimental curve is given by the modified and *independent* unmodified scattering of N atoms.

Independent, unmodified

$$I = N\psi(s).$$

Modified[8]

$$I = N\sum_M \{Z_m - \sum(f_n)^2\} I_0 \frac{e^4}{m^2c^4R^2}\left(\frac{1+\cos^2 2\theta}{2}\right).$$

Assuming that the scattering can be taken as independent at sin $\theta/\lambda = 0.7$ the fractional parts of unmodified and modified scattering are calculated. Since $I = I_{\text{unmod.}} + I_{\text{mod.}}$ this determines the ordinates at sin $\theta/\lambda = 0.7$ for both the modified and independent unmodified curves. Both of these curves are readily calculated as a function of the angle, from the tables of scattering factors[9] and, having fixed the scale of ordinates at one point, the two curves are readily plotted on the same scale as $I(s)$. The unmodified part of the experimental scattering curve is then obtained by subtracting 1*b* from 1*a*. The difference divided by 1*c* gives the quotient $I(s)_{\text{coh.}}/N\psi(s)$ from which the curve $si(s)$ is constructed. Although the assumption of independent scattering at large angle is only an approximation, it is nevertheless a sufficiently good one, and affords a very simple method of putting the $si(s)$ curve upon a quantitative basis.

The curve $si(s)$ obtained in this way is plotted against s (Fig. 2) and the integration involved in Eq. (7) carried out on a Coradi harmonic analyzer. The coefficients, which the analyzer delivers for the different harmonics, give directly the values of the integral for various values of r. The scale of abscissae used in Fig. 2 corresponds to 0.4A per harmonic. It might be pointed out that although the $si(s)$ curve has been put upon an absolute basis by several approximations, any errors which have crept in will only result in displacing the curve up or down or in tilting it somewhat. Since these are long period variations,

[7] F. C. Blake, Rev. Mod. Phys. **5**, 180 (1933).
[8] E. O. Wollan, Rev. Mod. Phys. **4**, 233 (1932).
[9] James and Brindley, Phil. Mag. **12**, 81 (1931).

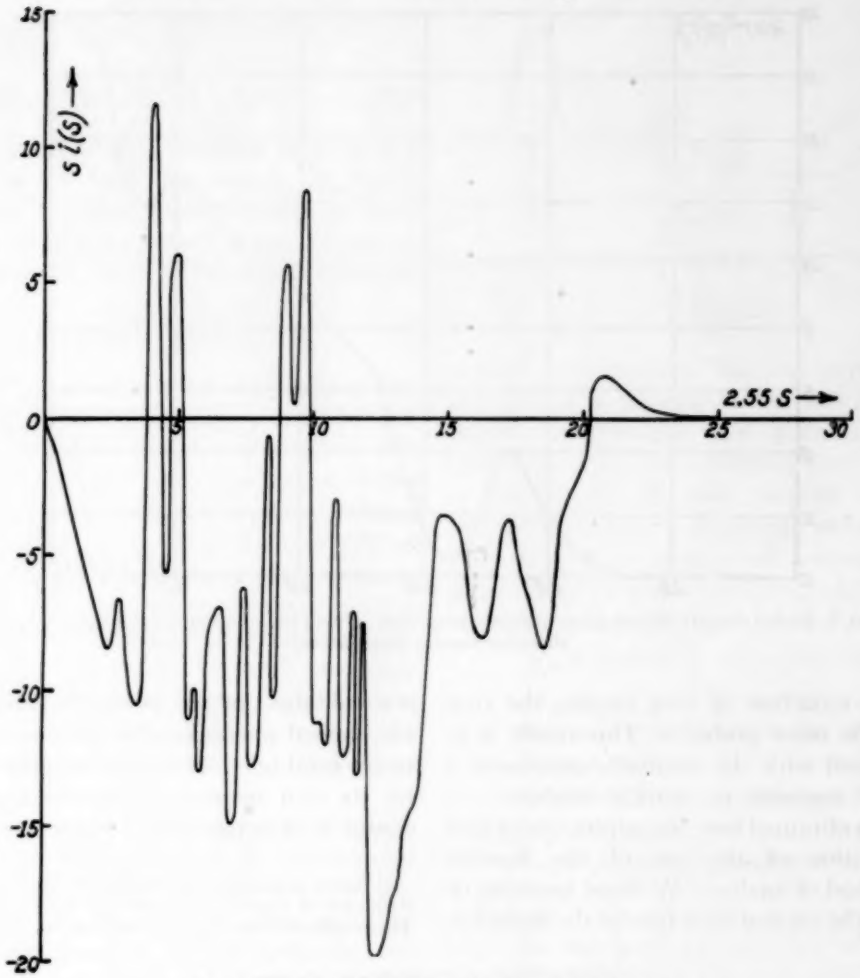

FIG. 2. Curve $si(s)$ against s for rhombic sulphur.

they will affect appreciably only the first one or two harmonics but not the higher ones. Hence only the first two or three points on the $4\pi r^2\rho(r)$ curve will be in error and this does not greatly matter, since this part of the curve is known to have zero ordinate.

The integration involved in Eq. (7) was carried out on the harmonic analyzer for the first 15 harmonics, thus giving points on the r-scale from 0 to 6.0A. The curve obtained is shown in Fig. 3. From the curve one gets directly the concentration of atoms at any distance from a given atom and furthermore, since the work has been carried through on a quantitative basis, the areas under the peaks give directly the number of atoms in that range of distances.

The interpretation of the curve is quite simple. At small distance from an atom there are of course no other atoms. At a distance of about 2.35A there is a peak with area 2.3 atoms. This is interpreted as meaning 2 atoms at a distance slightly less than 2.35A. Beyond these two nearest neighbors, the next nearest atoms are at a distance of 3.25A or more. The S–S distance 2.35A is slightly larger than the distance 2.2A obtained from the Trithionate group[10] but this is not unexpected since the slight overlapping of the next nearest neighbors, which causes a peak area of 2.3 atoms rather than 2.0, will also shift the peak slightly toward larger distances. In order that each atom should have two nearest neighbors, the structure must contain long chains or chains closed into rings and, since there is nothing about the physical properties of sulphur

[10] W. H. Zachariasen, J. Chem. Phys. **2**, 109 (1934).

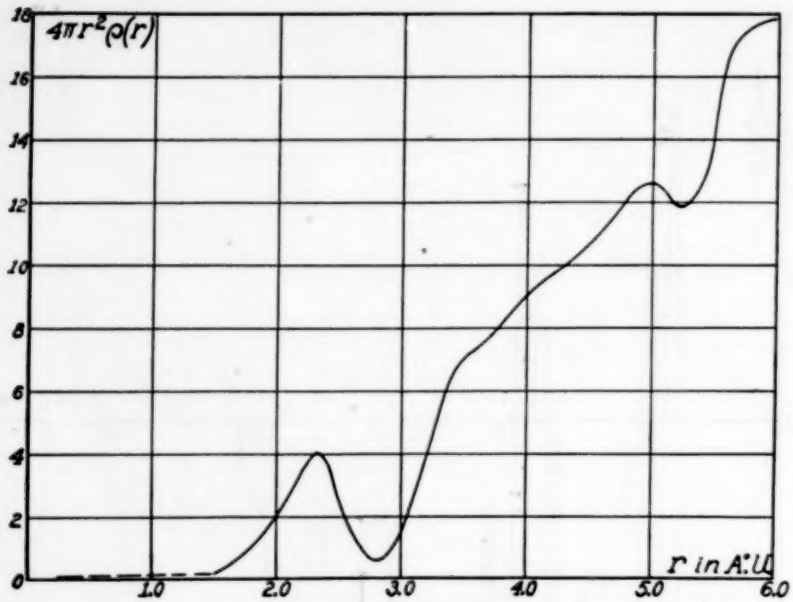

FIG. 3. Radial density distribution in rhombic sulphur, giving the number of atoms per A at any distance from a given atom.

to suggest a structure of long chains, the ring solution is the more probable. This result is in good agreement with the chemist's picture of a closed ring S_8 molecule in rhombic sulphur.

The results obtained here for sulphur serve as a good illustration of the use of the Fourier integral method of analysis. Without knowing or determining the crystal structure of the material, one obtains by a perfectly straightforward mechanical operation the relation of each atom to its neighbors. The value of such information for its own interest, or for its usefulness in a complete structure determination is evident.[11]

[11] Based upon this verification of the ring molecule the structure of rhombic sulphur has since been worked out. The results will be reported elsewhere.

A Fourier Series Method for the Determination of the Components of Interatomic Distances in Crystals*

A. L. PATTERSON, *George Eastman Research Laboratories, Massachusetts Institute of Technology*

(Received June 18, 1934)

A method for the direct determination of the components of interatomic distances in crystals has been developed from a consideration of the properties of the Fourier series whose coefficients are the squares of the F-coefficients for the crystal reflections. Valuable structural information is thus obtained without making any assumptions as to the phase to be allotted to the F-coefficients. The practical application of the method is illustrated by a discussion of the structures of potassium dihydrogen phosphate and hexachlorobenzene.

1. INTRODUCTION

IN any crystal, the density of scattering power for x-rays (electron density) can be represented by a three-dimensional Fourier series of the form[1]

$$\rho(xyz)=\sum_{hkl=-\infty}^{\infty}\sum\alpha(hkl)e^{2\pi i(hx/a+ky/b+lz/c)}. \quad (1)$$

* Presented in part at the Washington Meeting of the American Physical Society, Phys. Rev. **45**, 763A (1934).

[1] For literature references and notation see W. L. Bragg, Proc. Roy. Soc. **A123**, 537 (1929); also A. L. Patterson, Zeits. f. Krist. **76**, 177 (1930).

If this density is real, as is usually the case, we have, in addition,

$$\alpha(h, k, l)=\alpha^*(-h, -k, -l), \qquad (1a)$$

where α^* is the conjugate complex of α. It is a well-known result that the values of $F(hkl)$ obtained from absolute measurements of integrated intensity of x-ray reflection are connected with the coefficients $\alpha(hkl)$ of the series (1) by the relation

$$F(hkl)=|\alpha(hkl)|. \qquad (2)$$

The problem of x-ray crystal analysis is the determination of the appropriate phases for the quantities $\alpha(hkl)$. This involves the use of our knowledge of the atomic scattering powers of the atoms of which the crystal is composed. These atoms are allotted positions in the unit cell in accordance with the space group requirements. Each of these positions, except in very special cases, involves one or more parameters in its specification. In general, a crystal structure investigation will involve the determination of a large number of such parameters and their calculation in most cases can only be carried out by a process of trial and error.

In this paper a method is presented which enables the principal interatomic distances to be directly determined. The directions in which these distances lie can also be obtained. No assumptions are involved in the deduction of these results and they are independent of the space group determination.

These interatomic distances place very definite limits on the values which the unknown parameters can assume. The labor involved in their determination is thus very considerably reduced.

2. One-Dimensional Problem

It is simpler to discuss the one-dimensional problem first. Consider the distribution of electron density normal to a crystallographic plane whose spacing is d. This density can be expressed in the form

$$\rho(x)=\sum_{-\infty}^{\infty}\alpha(n)e^{2\pi inx/a}; \quad \alpha(n)=\alpha^*(-n). \qquad (3)$$

Let the curve of Fig. 1 represent any such distribution function. Consider an element dx at a distance x from the origin. The distribution

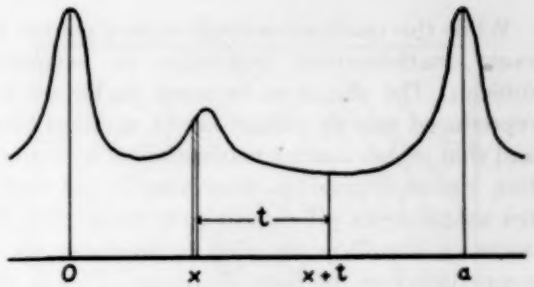

FIG. 1.

around this element can be expressed as a function of a parameter t in the form $\rho(x+t)$. Suppose we weight this distribution by the quantity $\rho(x)dx$, the amount of scattering matter in the element dx, and compute the weighted average distribution about any element dx when x is allowed to assume all values within the period. This average distribution $A(t)$ is given by

$$A(t)=d^{-1}\int_0^d \rho(x)\rho(x+t)dx. \qquad (4)$$

This integral is well known in the modern theory of the Fourier series as the "Faltung" of $\rho(x)$ and can immediately be evaluated by substituting (3) in (4), i.e.,

$$A(t)=\sum|\alpha(n)|^2e^{2\pi int/d}. \qquad (5)$$

This series can obviously be computed directly from the measured intensities of reflection from the various orders of the plane and it will be of great value to crystal analysis if we can obtain a simple physical interpretation of its meaning. This is readily done for the integral form, as follows.

We see that the principal contributions to $A(t)$ will be made when both $\rho(x)$ and $\rho(x+t)$ have large values. Thus if there is a peak in the curve $A(t)$ for a value $t=t_1$, it means simply that there are two peaks in the curve $\rho(x)$ at a distance t_1 apart. This simple qualitative result has a direct interpretation in crystal analysis. If we find a peak in the curve $A(t)$ for a given plane at a distance t_1 from the origin, we know that somewhere in the distribution normal to the plane there are planes of atoms at a distance t_1 apart.[2]

[2] The result obtained here is an extension of the application to crystals of the theory of scattering of x-rays in liquids reported by Gingrich and Warren at the Washington meeting of the American Physical Society and arose in a discussion of that work. Phys. Rev. **46**, 368 (1934).

While this qualitative result is very simple, its exact mathematical expression is extremely difficult. The distances between peaks are not reproduced exactly except in the simplest cases and that makes a strict mathematical interpretation almost impossible. However, a trial with a few simple series will convince the reader that the accuracy is sufficiently good to give very useful approximations for these distances. This is also shown by the examples given below.

3. Three-Dimensional Series

The result of the preceding paragraph can be extended immediately to three dimensions. We evaluate the integral

$$\begin{aligned} A(uvw) &= (abc)^{-1}\int_0^a\int_0^b\int_0^c \rho(xyz) \\ &\quad \times \rho(x+u, y+v, z+w)dxdydz \\ &= \sum\sum\sum |\alpha(hkl)|^2 e^{2\pi i(hu/a+kv/b+lw/c)} \\ &= \sum\sum\sum F^2(hkl)e^{2\pi i(hu/a+kv/b+lw/c)}. \end{aligned} \qquad (6)$$

By a direct extension of the above argument, we can show that if we find a maximum of $A(uvw)$ at some point $(u_1v_1w_1)$, then there are two maxima (atoms) in the distribution $\rho(xyz)$ whose distance apart is given by the vector whose components are $(u_1v_1w_1)$.

4. Two-Dimensional Series

In the practical application of this method to the analysis of crystals, the two-dimensional series promises to be the most fruitful. It is much easier to compute and much easier to represent than the three-dimensional series; and it is much less confused and more easily interpreted than the one-dimensional series. We consider a distribution of the type

$$A(uv) = \sum_{k=-\infty}^{\infty}\sum_{k=-\infty}^{\infty} F^2(hk0)e^{2\pi i(hu/a+kv/b)} \qquad (7)$$

and discuss the components of the interatomic distances which lie in the plane under consideration.

5. Examples of the Method

The practical application of the method is best discussed in the light of known structures. Two such examples have been chosen. Potassium dihydrogen phosphate, which has been very thoroughly investigated by West[3] provides an example of a simple inorganic substance with several atoms in fixed positions and one set of atoms in a general position involving three parameters. A complete set of absolute measurements of intensity is available for the two principal zones of the crystal. The second example is hexachlorobenzene,[4] a relatively simple organic structure whose atoms are all in general positions. For this crystal, Lonsdale has obtained a satisfactory set of relative intensities for the zone [010] from which a picture is obtained of the projection on the (010) face. No original data have been obtained for either of these crystals. The present paper merely involves a rediscussion of the published data, making use of the new method of analysis.

(a) Potassium dihydrogen phosphate

This substance crystallizes in the space group $V_d^{12}(I\bar{4}2d)$. The unit cell, whose dimensions are $a=b=7.43$A; $c=6.97$A, contains four molecules KH_2PO_4. The positions of the potassium and phosphorus atoms are fixed by symmetry conditions. Qualitative consideration of the complexity of the spectra indicates that the sixteen oxygen atoms occupy the sixteen-fold general position[5] requiring three parameters for its specification. We shall confine ourselves here to the application of the new method to the determination of the x and y parameters of the oxygen atoms.

We compute[6] the series

$$\sum\sum F^2(hk0)e^{2\pi i(hu/a+kv/b)},$$

making use of the observed absolute F values published by West. The result of this computation is shown in the form of a contour map in Fig. 2(b). From the positions of the eight peaks surrounding the origin and our knowledge of the space group, we can immediately determine the oxygen parameters in this plane. The maxima

[3] J. West, Zeits. f. Krist. **74**, 306 (1930).
[4] K. Lonsdale, Proc. Roy. Soc. **A133**, 536 (1931).
[5] R. W. G. Wyckoff, *Analytical Expression of the Results of the Theory of Space Groups*, Washington, 1930.
[6] The method of Beevers and Lipson (Phil. Mag. **17**, 855 (1934)) is very convenient.

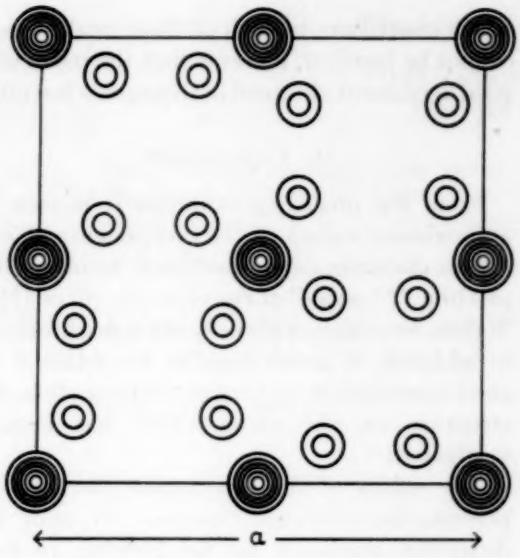

FIG. 2a.

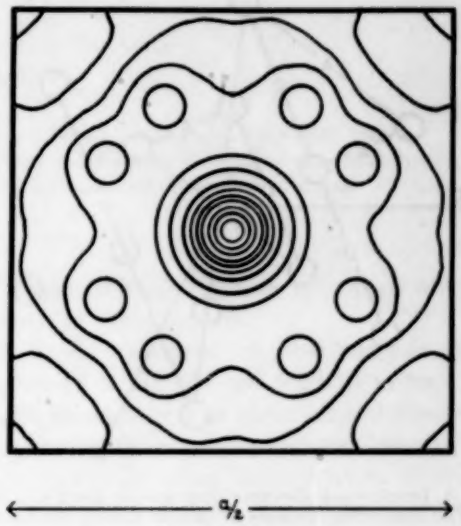

FIG. 2b.

FIG. 2. Potassium dihydrogen phosphate. (*a*) Electron density projected on (001), J. West.[3] (*b*) Contour map of the $F^2(hk0)$ series.

occur for the values[7] $\theta_1 = 29.6°$ and $\theta_2 = 51.4.°$ These are to be compared with the values obtained by West, i.e., $\theta_1 = 29°$, $\theta_2 = 52°$.

(b) Hexachlorobenzene

The space group in this case is $C_{2h}^5(P2_1/c)$. There are two molecules C_6Cl_6 in a cell of dimensions $a = 8.07$A, $b = 3.84$A, $c = 16.61$A, $\beta = 116°25'$. All the atoms are in twofold general positions,[5] the molecules having central symmetry.

In this case we compute the series

$$\sum\sum F^2(h0l)e^{2\pi i(hu/a+lw/c)},$$

using the relative F values observed by Lonsdale. The contour map (Fig. 3) shows the result of this computation. If we assume that peaks of the type *A*, *B* and *C* are due mainly to Cl–Cl distances and make use of the space group data we are led without further assumptions to a slightly irregular hexagon of chlorines arranged with respect to the axes as shown in Fig. 4. To explain other principal peaks we are led to an inner hexagon of carbons. The components of the various interatomic distances are given in Table

[7] $\theta_1 = 360u/a$, etc.

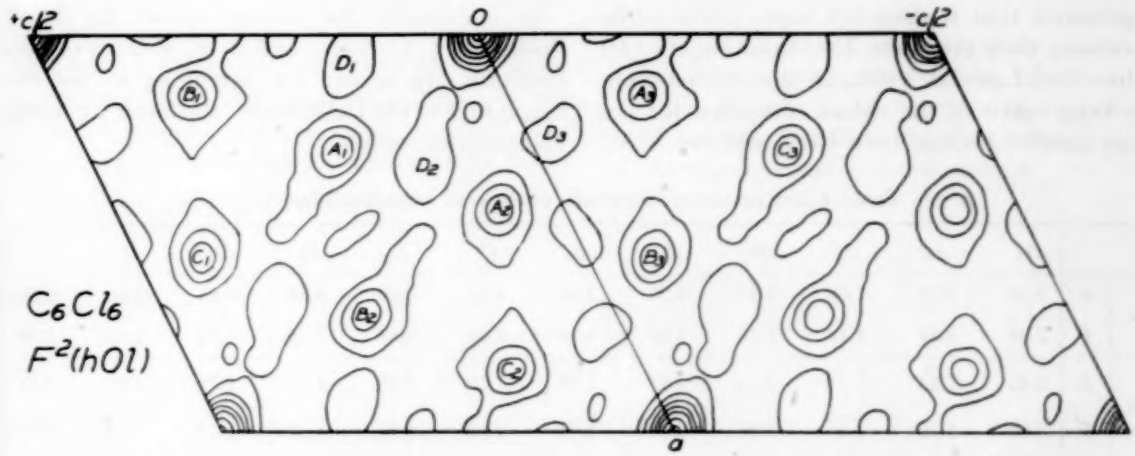

FIG. 3. Hexachlorobenzene. Contour map of the $F^2(h0l)$ series.

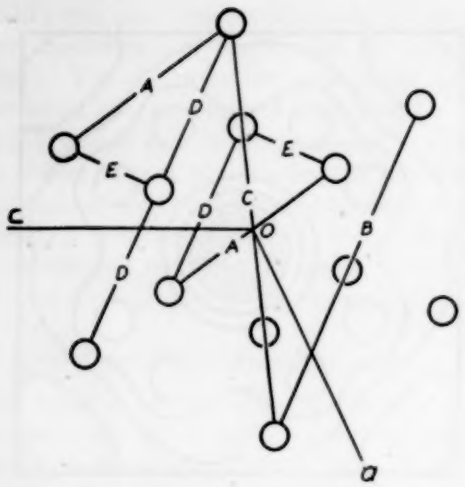

FIG. 4. Interatomic distance diagram for the C_6Cl_6 molecule. The inner ring consists of carbon atoms, the outer of chlorines. The interatomic distances indicated are repeated six times in approximate hexagonal symmetry. The molecule is actually centrosymmetrical. The distances in this diagram give rise to the peaks in Fig. 3 bearing the same letters.

I, as computed from Lonsdale's data (L) and as obtained in the present paper (P). The agreement is, on the whole, very good.

Referring to Fig. 4 we note that the C–C vector (A) is concealed by the similarly labelled Cl–Cl vector. There are also intermolecular Cl–Cl distances very nearly equal to (A) which are largely responsible for the considerable height of peaks of the type (A), (B) and (C) and may also be responsible for their distortion. In Fig. 3 peaks will be seen which correspond to the Cl–C and C–C distances (E) but they are so obviously distorted by neighboring peaks and depressions that it does not seem worth while discussing their positions. In computing the (D) values from Lonsdale's data an unweighted mean has been taken of the values computed for the three parallel vectors (two Cl–C and one C–C) which contribute to each of these peaks. As this cannot be justified, it seems that the particularly good agreement obtained in this case is fortuitous.

6. Conclusion

From the preceding examples it is seen that approximate values of the components of interatomic distances can immediately be obtained by plotting "F^2-series" of the type (5), (6) or (7) and in these two cases, with only the space group data in addition, it seems possible to obtain a very good approximate picture of the projection of the structure on the plane which has been investigated.

The values of the interatomic distance components are obviously subject to error from distortion produced by neighboring peaks. It seems, however, that the presence of such distortion will be recognizable from the nature of the series itself. The final values for the interatomic distances must be obtained from a Fourier analysis or a parameter determination of the usual type but the approximate information provided by the F^2-series will eliminate a great many of the possibilities which normally have to be tested by trial and error.

In addition, it seems that in a great many cases where the structure determination cannot be completed, this method will enable some information as to the molecular structure to be obtained from the x-ray data; and it provides a very convenient means of summarizing the information which can be obtained from that data without any extraneous assumptions.

In conclusion the author wishes to thank Professors J. C. Slater and B. E. Warren of this Institute, the former for extending to me the hospitality of the Laboratory, the latter for many valuable discussions.

TABLE I. *Components of interatomic distances in hexachlorobenzene.*

		A_1	A_2	A_3	B_1	B_2	B_3	C_1	C_2	C_3	D_1	D_2	D_3
u	L	2.25	3.32	1.08	1.17	5.57	4.40	4.53	6.89	2.38	0.64	2.66	2.06
	P	2.38	3.54	1.18	1.18	5.69	4.53	4.49	6.65	2.15	0.57	2.66	2.08
w	L	3.46	1.12	$\overline{2.23}$	5.68	4.57	$\overline{1.11}$	7.10	2.49	$\overline{4.61}$	2.79	2.16	$\overline{0.51}$
	P	3.69	1.20	$\overline{2.49}$	5.81	4.61	$\overline{1.20}$	6.80	2.34	$\overline{4.57}$	2.72	2.15	$\overline{0.57}$

The Singlet Lines of Cl IV

I. S. Bowen, *California Institute of Technology*

(Received July 18, 1934)

Ten singlet and intercombination lines of Cl IV have been classified and the singlet terms of the ground configuration located. Forbidden transitions between the terms of the ground configurations of Cl IV, Cl III and probably S III are not observed in nebulae or novae.

TABLE I lists a small group of strong singlet and intercombination lines which have been identified recently in Cl IV. The corresponding term values, fixed relative to the triplet values previously published,[1] are given in Table II.

TABLE I. *Singlet lines of Cl IV.*

Int.	λ	ν	Classification
2	331.835	301355.	$s^2p^2\ {}^1D-s^2p5s\ {}^1P$
8	486.172	205689.	$s^2p^2\ {}^1D-s^2p4s\ {}^1P$
4	535.039	186902.	$s^2p^2\ {}^1S-s^2p4s\ {}^1P$
2	599.733	166741.	$s^2p^2\ {}^3P_0-sp^3\ {}^1P$
5	601.499	166251.	$s^2p^2\ {}^3P_1-sp^3\ {}^1P$
5	604.590	165401.	$s^2p^2\ {}^3P_2-sp^3\ {}^1P$
4	653.696	152976.	$s^2p^2\ {}^1D-sp^3\ {}^1P$
3	662.454	150954.	$s^2p^2\ {}^1D-sp^3\ {}^3S$
4	745.205	134191.	$s^2p^2\ {}^1S-sp^3\ {}^1P$
1	756.563	132177.	$s^2p^2\ {}^1S-sp^3\ {}^3S$

TABLE II. *Singlet term values of Cl IV.*

$s^2p^2\ {}^1D$	417460
$s^2p^2\ {}^1S$	398676
$sp^3\ {}^1P$	264484
$s^2p4s\ {}^1P$	211772
$s^2p5s\ {}^1P$	116105

This analysis and the previous classifications of Cl III and Cl IV yield the values given in Table III for the wave-lengths of the forbidden transitions from the metastable terms of the ground configurations. As none of these lines have been observed in either nebulae or novae it is evident that chlorine is not an abundant element in these objects.

A similar attempt at the analysis of the singlets of S III did not lead to unambiguous results because two or three crucial lines in the most probable arrangement are blended with other O or S lines and because many of the high level terms are erratic, due to the overlapping of the s^2p3d and s^2p4s configurations. If this most probable arrangement is correct, then the ^1S and ^1D terms of the s^2p^2 configuration occur at 27,601 and 11,322 cm^{-1}, respectively, above the lowest state ($^3P_0$). Transitions between terms with the above values do not correspond to any observed nebular lines. While these values are somewhat uncertain, an interpolation between Si I and Cl IV, as well as the series limits in S II, fix the position of these terms within a few hundred reciprocal centimeters of the above values and thus exclude the identification of any of the stronger unidentified nebular lines with transitions between these terms.

TABLE III. *Forbidden transitions from metastable states in chlorine.*

Cl III		Cl IV	
s^2p^3	λ	s^2p^3	λ
$^4S-{}^2P_{1\frac{1}{2}}$	3342.7	$^3P_1-{}^1S$	3118.3
$^4S-{}^2P_{\frac{1}{2}}$	3353.4	$^1D-{}^1S$	5322.2
$^4S-{}^2D_{2\frac{1}{2}}$	5517.2	$^3P_1-{}^1D$	7531.
$^4S-{}^2D_{1\frac{1}{2}}$	5537.7	$^3P_2-{}^1D$	8046.

[1] I. S. Bowen, Phys. Rev. **45**, 401 (1934).

The Spectra of Neon in the Extreme Ultraviolet

J. C. Boyce, *George Eastman Research Laboratory of Physics, Massachusetts Institute of Technology*

(Received July 6, 1934)

Increased dispersion and resolving power have made possible a revision and extension of previous work on the spectra of neon in the extreme ultraviolet. Lists of classified lines are given for Ne I, Ne II, Ne III and Ne IV in the range from λ2000 to λ282. No new lines were found for Ne I but the accuracy of the wave-lengths is considerably improved. For the other stages of ionization the number of lines identified or resolved has been doubled. Term tables are given for Ne II, Ne III and Ne IV including in them the results of other workers, notably de Bruin, from investigations in the more accessible portion of the spectrum.

WITH the two-meter-focus normal-incidence broad-range vacuum spectrograph[1] the extreme ultraviolet spectra of the electrodeless discharge in neon have been investigated. In addition to lines of Ne I, II, III and IV, lines of hydrogen and of several stages of ionization of carbon, nitrogen and oxygen appeared. These latter lines were easily recognized from Edlén's list[2] and in the region below λ800 his values of their wave-lengths were sometimes used as standards. The principal standards used were the first and intermediate orders of such neon and impurity lines whose higher orders fell on the longer wave-length portion of the plate. Such higher orders were there compared with the lines from an iron arc. The difficulties with the previous standards in the extreme ultraviolet have been mentioned in an abstract[3] and suggested revised values will be published in due course. Excellent agreement was obtained on wave-lengths determined from different exposures or from different orders of the same exposure. For lines whose wave-length is given to three decimal places the probable error is less than 0.01A and in many cases less than 0.005A. In certain cases where the character of the line did not permit precise measurement (as with very strong or very faint lines) the error may be as great as 0.02A and these wave-lengths are given to two decimal places. The plates were independently measured by Dr. Carol A. Rieke and by the writer, each measuring the plate in both directions. The method of reduction used was that discussed in the description of the instrument.[1] As most of the previous measurements of neon lines in the extreme ultraviolet[4, 5, 6, 7] were made with small vacuum spectrographs and depended upon very uncertain wave-length standards, it seems worth while to publish revised values for the lines already known. The lines newly identified or newly resolved in the present investigation are denoted by an asterisk.

Ne I. The revised values for a number of classified lines are given in Table I. The electrodeless discharge is not particularly suitable for the excitation of higher series members of arc spectra and not as many lines were observed as were previously known. The value of the $^1S_0$ ground state of the atom, 173,930 (corresponding to an ionization potential of 21.47 volts) as given by Lyman and Saunders[4] is not appreciably altered. An extensive term table is given by Bacher and Goudsmit[8] to which reference is made for the multiplet designations used.

TABLE I. *Ne I classified lines.*

λ	Int.	ν	Classification
743.70	12	134,463	$(2s)^2(2p)^6\ ^1S_0-(2s)^2(2p)^5\ 3s\ 2_1°$
735.89	30	135,890	$3s\ 4_1°$
629.729	6	158,798	$4s\ 2_1°$
626.819	6+	159,536	$4s\ 4_1°$
619.092	4	161,527	$3d\ 2_1°$
618.668	5	161,638	$3d\ 6_1°$
615.623	5−	162,437	$3d\ 12_1°$
602.712	4−	165,917	$5s\ 2_1°$
600.04	2	166,655	$5s\ 4_1°$
598.86	1	166,984 blend	$4d\ 2_1°$
598.698	2+	167,030	$4d\ 6_1°$
595.911	3	167,810	$4d\ 12_1°$
591.82	2	168,970	$6s\ 2_1°$
589.92	1	169,514 double	$5d\ 6_1°$
			$5d\ 2_1°$
589.16	1	169,733	$6s\ 4_1°$
587.20	1	170,300	$5d\ 12_1°$

[1] K. T. Compton and J. C. Boyce, R. S. I. **5**, 218 (1934).
[2] B. Edlén, Zeits. f. Physik **85**, 85 (1933).
[3] J. C. Boyce, Phys. Rev. **45**, 289 (1934).
[4] T. Lyman and F. A. Saunders, Proc. Nat. Acad. Sci. **12**, 92 (1926).
[5] H. B. Dorgelo and J. H. Abbink, Zeits. f. Physik **37**, 667 (1926).
[6] H. N. Russell, K. T. Compton and J. C. Boyce, Proc. Nat. Acad. Sci. **14**, 280 (1928).
[7] J. C. Boyce and K. T. Compton, Proc. Nat. Acad. Sci. **15**, 656 (1929).
[8] R. F. Bacher and S. Goudsmit, *Atomic Energy States*, McGraw Hill (1932).

TABLE II. *Ne II classified lines.*

λ	Int.	ν	Classification
1938.82	5+	51,577.8	$(2s)^2(2p)^4\ (^3P)\ 3s\ ^2P_{\frac{3}{2}} - (2s)^2(2p)^4\ (^1D)\ 3p\ ^2P_{1\frac{1}{2}}^\circ$
1930.02	7−	51,812.8	$^2P_{\frac{1}{2}} - \quad ^2P_{\frac{1}{2}}^\circ$
1916.09	8	52,189.7	$^2P_{1\frac{1}{2}} - \quad ^2P_{1\frac{1}{2}}^\circ$
1907.49	5	52,424.8	$^2P_{1\frac{1}{2}} - \quad ^2P_{\frac{1}{2}}^\circ$
1688.38	4	59,228.4	$(2s)\ (2p)^6\ ^2S_{\frac{1}{2}} - (2s)^2(2p)^4\ (^1D)\ 3p\ ^2P_{1\frac{1}{2}}^\circ$
1681.70	3	59,463.7	$^2S_{\frac{1}{2}} - \quad ^2P_{\frac{1}{2}}^\circ$
462.388	14	216,269	$(2s)^2(2p)^5\ ^2P_{\frac{1}{2}}^\circ - \quad (2s)\ (2p)^6\ ^2S_{\frac{1}{2}}$
460.725	15	217,049	$^2P_{1\frac{1}{2}}^\circ - \quad ^2S_{\frac{1}{2}}$
• 456.895	5−	218,867	$(2s)^2(2p)^5\ ^2P_{\frac{3}{2}} - (2s)^2(2p)^4\ (^3P)\ 3s\ ^4P_{2\frac{1}{2}}$
456.344	4	219,133	$^2P_{1\frac{1}{2}}^\circ - \quad ^4P_{2\frac{1}{2}}$
455.270	7	219,650	$^2P_{\frac{1}{2}} - \quad ^4P_{1\frac{1}{2}}$
454.648	5+	219,950	$^2P_{1\frac{1}{2}}^\circ - \quad ^4P_{\frac{1}{2}}$
447.813	8	223,307	$(2s)^2(2p)^5\ ^2P_{\frac{3}{2}} - (2s)^2(2p)^4\ (^3P)\ 3s\ ^2P_{1\frac{1}{2}}$
446.591	7	223,919	$^2P_{\frac{1}{2}}^\circ - \quad ^2P_{\frac{1}{2}}$
446.252	8	224,089	$^2P_{1\frac{1}{2}}^\circ - \quad ^2P_{1\frac{1}{2}}$
445.032	7+	224,703	$^2P_{1\frac{1}{2}}^\circ - \quad ^2P_{\frac{1}{2}}$
407.136	8	245,618	$(2s)^2(2p)^5\ ^2P_{\frac{3}{2}} - (2s)^2(2p)^4\ (^1D)\ 3s\ ^2D_{1\frac{1}{2}}$
405.852	9	246,395	$^2P_{1\frac{1}{2}}^\circ - \quad ^2D_{2\frac{1}{2},1\frac{1}{2}}$
362.456	4	275,896	$(2s)^2(2p)^5\ ^2P_{\frac{3}{2}} - (2s)^2(2p)^4\ (^1S)\ 3s\ ^2S_{\frac{1}{2}}$
361.427	5	276,678	$^2P_{1\frac{1}{2}}^\circ - \quad ^2S_{\frac{1}{2}}$
• 357.534	5	279,694	$(2s)^2(2p)^5\ ^2P_{\frac{3}{2}} - (2s)^2(2p)^4\ (^3P)\ 3d\ ^2D_{1\frac{1}{2}}$
• 356.795	5d	280,273	$^2P_{1\frac{1}{2}}^\circ - \quad ^2D_{2\frac{1}{2}}$
• 356.534	3	280,478	$^2P_{1\frac{1}{2}}^\circ - \quad ^2D_{1\frac{1}{2}}$
• 356.436	2	280,555	$(2s)^2(2p)^5\ ^2P_{\frac{3}{2}} - (2s)^2(2p)^4\ (^3P)\ 3d\ ^2P_{\frac{1}{2}}$
• 356.131	4−	280,796	$(2s)^2(2p)^5\ ^2P_{1\frac{1}{2}}^\circ - (2s)^2(2p)^4\ (^3P)\ 3d\ ^2F_{2\frac{1}{2}}$
• 355.946	2	280,942	$(2s)^2(2p)^5\ ^2P_{\frac{3}{2}} - (2s)^2(2p)^4\ (^3P)\ 3d\ ^2P_{1\frac{1}{2}}$
• 355.848	1	281,020	$(2s)^2(2p)^5\ ^2P_{1\frac{1}{2}}^\circ - (2s)^2(2p)^4\ (^3P)\ 3d\ ^4F_{2\frac{1}{2}}$
• 355.647	3	281,178	$(2s)^2(2p)^5\ ^2P_{1\frac{1}{2}}^\circ - (2s)^2(2p)^4\ (^3P)\ 3d\ ^4P_{2\frac{1}{2}}$
• 355.450	2	281,334	$(2s)^2(2p)^5\ ^2P_{1\frac{1}{2}}^\circ - (2s)^2(2p)^4\ (^3P)\ 3d\ ^4P_{\frac{1}{2}}$
• 354.954	4	281,727	$^2P_{1\frac{1}{2}}^\circ - \quad ^2P_{1\frac{1}{2}}$
• 353.922	2+	282,548	$(2s)^2(2p)^5\ ^2P_{\frac{3}{2}} - (2s)^2(2p)^4\ (^3P)\ 4s\ ^2P_{1\frac{1}{2}}$
• 353.206	3	283,121	$^2P_{\frac{1}{2}}^\circ - \quad ^2P_{\frac{1}{2}}$
• 352.946	4	283,329	$^2P_{1\frac{1}{2}}^\circ - \quad ^2P_{1\frac{1}{2}}$
• 352.237	2+	283,900	$^2P_{1\frac{1}{2}}^\circ - \quad ^2P_{\frac{1}{2}}$
• 331.50	2	301,657	$(2s)^2(2p)^5\ ^2P_{\frac{3}{2}} - (2s)^2(2p)^4\ (^3P)\ 4d\ ^2D_{1\frac{1}{2}}$?
• 331.06	1	302,057	$(2s)^2(2p)^5\ ^2P_{\frac{1}{2}}^\circ - (2s)^2(2p)^4\ (^3P)\ 4d\ ^2P_{1\frac{1}{2},\frac{1}{2}}$?
• 330.77	3	302,321	$(2s)^2(2p)^5\ ^2P_{1\frac{1}{2}}^\circ - (2s)^2(2p)^4\ (^3P)\ 4d\ ^2D_{2\frac{1}{2}}$?
• 330.62	2+	302,463	$^2P_{1\frac{1}{2}}^\circ - \quad ^2D_{1\frac{1}{2}}$?
• 330.20	2	302,846	$(2s)^2(2p)^5\ ^2P_{1\frac{1}{2}}^\circ - (2s)^2(2p)^4\ (^3P)\ 4d\ ^2P_{1\frac{1}{2},\frac{1}{2}}$?
• 328.08	2+	304,807	$(2s)^2(2p)^5\ ^2P_{\frac{3}{2}} - (2s)^2(2p)^4\ (^1D)\ 3d\ ^2P_{1\frac{1}{2},\frac{1}{2}}$
• 327.63	2	305,221	$(2s)^2(2p)^5\ ^2P_{\frac{1}{2}}^\circ - (2s)^2(2p)^4\ (^1D)\ 4s\ ^2D_{2\frac{1}{2}}$?
• 327.33	3	305,506	$(2s)^2(2p)^5\ ^2P_{\frac{1}{2}}^\circ - (2s)^2(2p)^4\ (^1D)\ 3d\ ^2D_{1\frac{1}{2}}$
• 327.25	2	305,581	$(2s)^2(2p)^5\ ^2P_{1\frac{1}{2}}^\circ - (2s)^2(2p)^4\ (^1D)\ 3d\ ^2P_{1\frac{1}{2},\frac{1}{2}}$
• 326.77	3	306,022	$(2s)^2(2p)^5\ ^2P_{1\frac{1}{2}}^\circ - (2s)^2(2p)^4\ (^1D)\ 4s\ ^2D_{2\frac{1}{2},1\frac{1}{2}}$?
• 326.54	5	306,240	$(2s)^2(2p)^5\ ^2P_{1\frac{1}{2}}^\circ - (2s)^2(2p)^4\ (^1D)\ 3d\ ^2D_{1\frac{1}{2}}$
• 324.56	2	308,110	$(2s)^2(2p)^5\ ^2P_{1\frac{1}{2}}^\circ - (2s)^2(2p)^4\ (^1D)\ 3d\ ^2F_{2\frac{1}{2}}$

TABLE III. *Ne II term values.*

$(2s)^2\ (2p)^5$	$^2P_{1\frac{1}{2}}^\circ$	0	$(2s)^2(2p)^4\ (^3P)\ 3d$	$^4P_{\frac{1}{2}}$	280,770.2
	$^2P_{\frac{1}{2}}^\circ$	782		$^4P_{1\frac{1}{2}}$	280,991.7
$(2s)\ (2p)^6$	$^2S_{\frac{1}{2}}$	217,050		$^4P_{2\frac{1}{2}}$	281,173.5
$(2s)^2(2p)^4\ (^3P)\ 3s$	$^4P_{2\frac{1}{2}}$	219,133.0	$(2s)^2(2p)^4\ (^3P)\ 3d$	$^2P_{\frac{1}{2}}$	281,334.5
	$^4P_{1\frac{1}{2}}$	219,650.8		$^2P_{1\frac{1}{2}}$	281,722.3
	$^4P_{\frac{1}{2}}$	219,949.9	$(2s)^2(2p)^4\ (^3P)\ 4s$	$^4P_{2\frac{1}{2}}$	282,000.0
$(2s)^2(2p)^4\ (^3P)\ 3s$	$^2P_{1\frac{1}{2}}$	224,089.3		$^4P_{1\frac{1}{2}}$	282,376.7
	$^2P_{\frac{1}{2}}$	224,701.8		$^4P_{\frac{1}{2}}$	282,682.2
$(2s)^2(2p)^4\ (^3P)\ 3p$	$^4P_{2\frac{1}{2}}^\circ$	246,194.8	$(2s)^2(2p)^4\ (^3P)\ 4s$	$^2P_{1\frac{1}{2}}$	283,323.7
	$^4P_{1\frac{1}{2}}^\circ$	246,417.4		$^2P_{\frac{1}{2}}$	283,896.5
	$^4P_{\frac{1}{2}}^\circ$	246,599.9	$(2s)^2(2p)^4\ (^3P)\ 4d$	$^2D_{2\frac{1}{2}}$	302,321 ?
$(2s)^2(2p)^4\ (^1D)\ 3s$	$^2D_{2\frac{1}{2}}$	246,396.5		$^2D_{1\frac{1}{2}}$	302,452 ?
	$^2D_{1\frac{1}{2}}$	246,400.0	$(2s)^2(2p)^4\ (^3P)\ 4f$	$^4D_{3\frac{1}{2}}^\circ$	302,830.6
$(2s)^2(2p)^4\ (^3P)\ 3p$	$^4D_{3\frac{1}{2}}^\circ$	249,110.8		$^4D_{2\frac{1}{2}}^\circ$	302,845.5
	$^4D_{2\frac{1}{2}}^\circ$	249,448.0		$^4D_{1\frac{1}{2}}^\circ$	302,905.2
	$^4D_{1\frac{1}{2}}^\circ$	249,697.7		$^4D_{\frac{1}{2}}^\circ$	302,991.2
	$^4D_{\frac{1}{2}}^\circ$	249,841.8	$(2s)^2(2p)^4\ (^3P)\ 4d$	$^2P_{1\frac{1}{2},\frac{1}{2}}$	302,884 ?
$(2s)^2(2p)^4\ (^3P)\ 3p$	$^2D_{2\frac{1}{2}}^\circ$	251,013.3	$(2s)^2(2p)^4\ (^3P)\ 4f$	$^4F_{4\frac{1}{2}}^\circ$	302,905.8
	$^2D_{1\frac{1}{2}}^\circ$	251,524.7		$^4F_{3\frac{1}{2}}^\circ$	303,511.6
$(2s)^2(2p)^4\ (^3P)\ 3p$	$^2S_{\frac{1}{2}}^\circ$	252,800.8		$^4F_{2\frac{1}{2}}^\circ$	303,530.8
$(2s)^2(2p)^4\ (^3P)\ 3p$	$^4S_{1\frac{1}{2}}^\circ$	252,956.0		$^4F_{1\frac{1}{2}}^\circ$	303,826.6
$(2s)^2(2p)^4\ (^3P)\ 3p$	$^2P_{1\frac{1}{2}}^\circ$	254,167.0	$(2s)^2(2p)^4\ (^3P)\ 4f$	$^4G_{5\frac{1}{2}}^\circ$	303,465.1
	$^2P_{\frac{1}{2}}^\circ$	254,294.0		$^4G_{4\frac{1}{2}}^\circ$	303,475.7
$(2s)^2(2p)^4\ (^1D)\ 3p$	$^2F_{3\frac{1}{2}}^\circ$	274,366.9		$^4G_{3\frac{1}{2}}^\circ$	303,602.3
	$^2F_{2\frac{1}{2}}^\circ$	274,411.3		$^4G_{2\frac{1}{2}}^\circ$	303,701.1
$(2s)^2(2p)^4\ (^1D)\ 3p$	$^2P_{1\frac{1}{2}}^\circ$	276,278.6	$(2s)^2(2p)^4\ (^3P)\ 4f$	$^2D_{2\frac{1}{2}}^\circ$	303,465.4
	$^2P_{\frac{1}{2}}^\circ$	276,514.1		$^2D_{1\frac{1}{2}}^\circ$	303,882.3
$(2s)^2(2p)^4\ (^1S)\ 3s$	$^2S_{\frac{1}{2}}$	276,678.0	$(2s)^2(2p)^4\ (^1D)\ 3d$	$^2G_{4\frac{1}{2}}$	305,336.2
$(2s)^2(2p)^4\ (^1D)\ 3p$	$^2D_{2\frac{1}{2}}^\circ$	277,327.6		$^2G_{3\frac{1}{2}}$	305,337.2
	$^2D_{1\frac{1}{2}}^\circ$	277,346.1	$(2s)^2(2p)^4\ (^1S)\ 3p$	$^2P_{1\frac{1}{2}}^\circ$	305,399.2
$(2s)^2(2p)^4\ (^3P)\ 3d$	$^4D_{3\frac{1}{2}}$	279,139.1		$^2P_{\frac{1}{2}}^\circ$	305,409.3
	$^4D_{2\frac{1}{2}}$	279,220.6	$(2s)^2(2p)^4\ (^1D)\ 3d$	$^2P_{1\frac{1}{2}}$	305,568.9
	$^4D_{1\frac{1}{2}}$	279,326.8		$^2P_{\frac{1}{2}}$	305,584.2
	$^4D_{\frac{1}{2}}$	279,425.1	$(2s)^2(2p)^4\ (^1D)\ 4s$	$^2D_{2\frac{1}{2},1\frac{1}{2}}$	306,018 ?
$(2s)^2(2p)^4\ (^3P)\ 3d$	$^4F_{4\frac{1}{2}}$	280,174.4	$(2s)^2(2p)^4\ (^1D)\ 3d$	$^2D_{1\frac{1}{2}}$	306,244.8
	$^4F_{3\frac{1}{2}}$	280,702.5		$^2D_{2\frac{1}{2}}$	206,689.8
	$^4F_{1\frac{1}{2}}$	280,949.6	$(2s)^2(2p)^4\ (^1D)\ 3d$	$^2F_{3\frac{1}{2}}$	307,992.2
	$^4F_{2\frac{1}{2}}$	281,028.1		$^2F_{2\frac{1}{2}}$	308,103.3
$(2s)^2(2p)^4\ (^3P)\ 3d$	$^2F_{3\frac{1}{2}}$	280,264.0	$(2s)^2(2p)^4\ (^1D)\ 3d$	$^2S_{\frac{1}{2}}$	308,776.8
	$^2F_{2\frac{1}{2}}$	280,799.3	$(2s)^2(2p)^4\ (^1S)\ 3d$	$^2D_{2\frac{1}{2}}$	327,954.7
$(2s)^2(2p)^4\ (^3P)\ 3d$	$^2D_{2\frac{1}{2}}$	280,271.0		$^2D_{1\frac{1}{2}}$	327,968.2
	$^2D_{1\frac{1}{2}}$	280,475.6			

Ne II. The classified lines are given in Table II, the term values in Table III. The first six lines were discovered by Frisch[9] but their present measurements are believed to be more accurate and give a better agreement with the combination principle. Term tables have been given by Russell, Compton and Boyce[6] and more extensively by de Bruin and Bakker.[10] The new results slightly alter the relative position of the sets of terms converging to the different limits, as the only connection between these sets was given by the lines of Frisch and by those around λ400. The series limit (to the $^3P_2$ state of Ne III) as estimated from series of only two members (the $3s$ and $4s$ terms) is 331,350, corresponding to an ionization potential for Ne II of 40.91 volts.

Ne III. Classified lines are given in Table IV and term values in Table V. A number of triplet lines have been measured by von Keussler[11] using a grazing incidence vacuum spectrograph. None of his lines is repeated in Table IV except three at λ313 for which the present measurements are believed to be slightly better. von Keussler's work provides the connection, through the

TABLE IV. *Ne III classified lines.*

λ	Int.	ν	Classification
*1257.190	6	79,542.2	$(2s)^2(2p)^3(^4S).3s\ ^3S_1^\circ-(2s)^2(2p)^3(^2D).3p\ ^3P_2$
*1255.685	5	79,637.8	$^3S_1^\circ-\ ^3P_1$
*1255.026	2	79,679.6	$^3S_1^\circ-\ ^3P_0$
491.050	9	203,645	$(2s)^2(2p)^4\ ^3P_1-2s(2p)^5\ ^3P_2^\circ$
490.310	7	203,953	$^3P_0-\ ^3P_1^\circ$
489.641	4	204,231	$^3P_1-\ ^3P_1^\circ$
489.501	10	204,290	$^3P_2-\ ^3P_2^\circ$
488.868	7	204,554	$^3P_1-\ ^3P_0^\circ$
488.103	8−	204,875	$^3P_2-\ ^3P_1^\circ$
427.840	3+	233,732	$(2s)^2(2p)^4\ ^1S_0-2s(2p)^5\ ^1P_1^\circ$
379.308	7	263,638	$(2s)^2(2p)^4\ ^1D_2-2s(2p)^5\ ^1P_1^\circ$
313.92	1	318,552	$(2s)^2(2p)^4\ ^3P_0-(2s)^2(2p)^3(^4S).3s\ ^3S_1^\circ$
313.677	3	318,799	$^3P_1-\ ^3S_1^\circ$
313.048	4	319,441	$^3P_2-\ ^3S_1^\circ$
* 308.559	1	324,087	$(2s)^2(2p)^4\ ^1S_0-(2s)^2(2p)^3(^2P).3s\ ^1P_1^\circ$
* 301.124	4	332,089	$(2s)^2(2p)^4\ ^1D_2-(2s)^2(2p)^3(^2D).3s\ ^1D_2^\circ$
* 282.50	0+	353,982	$(2s)^2(2p)^4\ ^1D_2-(2s)^2(2p)^3(^2P).3s\ ^1P_1^\circ$

TABLE V. *Ne III term values.*

$(2s)^2(2p)^4$	$^3P_2$	0	$(2s)^2(2p)^3(^4S).3d$	$^3D_1^\circ$	398,189.80
	$^3P_1$	643		$^3D_2^\circ$	398,193.93
	$^3P_0$	922		$^3D_3^\circ$	398,207.84
$(2s)^2(2p)^4$	$^1D_2$	25,841	$(2s)^2(2p)^3(^2D).3p$	$^3P_2$	398,983.64
$(2s)^2(2p)^4$	$^1S_0$	55,747		$^3P_1$	399,079.57
				$^3P_0$	399,122.12
$2s(2p)^5$	$^3P_2^\circ$	204,290	$(2s)^2(2p)^3(^2P).3p$	$^3D_2$	409,842.08
	$^3P_1^\circ$	204,876		$^3D_3$	409,844.53
	$^3P_0^\circ$	205,199		$^3D_1$	409,852.23
$2s(2p)^5$	$^1P_1^\circ$	289,479	$(2s)^2(2p)^3(^2P).3p$	$^3S_1$	410,131.72
$(2s)^2(2p)^3(^4S).3s$	$^3S_1^\circ$	319,442.00	$(2s)^2(2p)^3(^2P).3p$	$^3P_0$	412,290.59
$(2s)^2(2p)^3(^2D).3s$	$^3D_3^\circ$	353,145.00		$^3P_1$	412,310.11
	$^3D_2^\circ$	353,174.16		$^3P_2$	412,317.21
	$^3D_1^\circ$	353,194.40	$(2s)^2(2p)^3(^2D).3d$	$^3F_2^\circ$	435,252.90
$(2s)^2(2p)^3(^4S).3p$	$^3P_1$	356,663.30		$^3F_3^\circ$	435,569.00
	$^3P_{02}$	356,673.62		$^3F_4^\circ$	435,617.80
$(2s)^2(2p)^3(^2D).3s$	$^1D_2^\circ$	357,930	$(2s)^2(2p)^3(^2D).3d$	$^3G_3^\circ$	436,558.35
$(2s)^2(2p)^3(^2P).3s$	$^3P_2^\circ$	374,431.00		$^3G_4^\circ$	436,585.34
	$^3P_1^\circ$	374,457.75		$^3G_5^\circ$	436,608.56
	$^3P_0^\circ$	374,474.66	$(2s)^2(2p)^3(^2D).3d$	$^3D_3^\circ$	436,841.63
$(2s)^2(2p)^3(^2P).3s$	$^1P_1^\circ$	379,834		$^3D_2^\circ$	436,918.39
$(2s)^2(2p)^3(^2D).3p$	$^3D_1$	389,055.24		$^3D_1^\circ$	436,963.49
	$^3D_2$	389,066.37	$(2s)^2(2p)^3(^2D).3d$	$^3P_2^\circ$	444,370.00
	$^3D_3$	389,136.05		$^3P_1^\circ$	444,397.16
$(2s)^2(2p)^3(^2D).3p$	$^3F_2$	391,411.02		$^3P_0^\circ$	444,417.37
	$^3F_3$	391,426.94	$(2s)^2(2p)^3(^2D).3d$	$^3S_1^\circ$	444,625.38
	$^3F_4$	391,447.31			

[9] S. Frisch, Zeits. f. Physik **64**, 499 (1930).
[10] T. L. de Bruin and C. J. Bakker, Zeits. f. Physik **69**, 19 (1931). Also, T. L. de Bruin, Zeits. f. Physik **44**, 157 (1927); **46**, 856 (1928).
[11] V. von Keussler, Zeits. f. Physik **85**, 1 (1933).

TABLE VI. *Ne IV classified lines.*

543.884	7	183,863	$(2s)^2(2p)^3\ {}^4S^\circ_{1\frac{1}{2}} - 2s(2p)^4\ {}^4P_{2\frac{1}{2}}$
542.076	6	184,476	${}^4S^\circ_{1\frac{1}{2}} - {}^4P_{1\frac{1}{2}}$
541.124	5	184,801	${}^4S^\circ_{1\frac{1}{2}} - {}^4P_{\frac{1}{2}}$
*521.810	2−	191,641	$(2s)^2(2p)^3\ {}^2P^\circ_{1\frac{1}{2}} - 2s(2p)^4\ {}^2D_{2\frac{1}{2}}$
*521.730	2−	191,670	${}^2P^\circ_{\frac{1}{2}} - {}^2D_{1\frac{1}{2}}$
*469.865	3−	212,827	$(2s)^2(2p)^3\ {}^2D^\circ_{2\frac{1}{2}} - 2s(2p)^4\ {}^2D_{2\frac{1}{2}}$
*469.817	2	212,849	${}^2D^\circ_{2\frac{1}{2}} - {}^2D_{2\frac{1}{2}}$
			${}^2D^\circ_{1\frac{1}{2}} - {}^2D_{2\frac{1}{2}}$
*421.584	2	237,201	$(2s)^2(2p)^3\ {}^2P^\circ_{1\frac{1}{2}} - 2s(2p)^4\ {}^2S_{\frac{1}{2}}$
388.23	1−	257,579	$(2s)^2(2p)^3\ {}^2P^\circ_{1\frac{1}{2}} - 2s(2p)^4\ {}^2P_{1\frac{1}{2}}$
387.13	0+	258,311	${}^2P^\circ_{\frac{1}{2}} - {}^2P_{\frac{1}{2}}$
*358.70	2−	278,784	$(2s)^2(2p)^3\ {}^2D^\circ_{1\frac{1}{2}} - 2s(2p)^4\ {}^2P_{1\frac{1}{2}}$

TABLE VII. *Ne IV term values.*

$(2s)^2(2p)^3$	${}^4S^\circ_{1\frac{1}{2}}$	0	$(2s)^2(2p)^3$	${}^2P^\circ_{\frac{1}{2}}$	21,202
				${}^2P^\circ_{1\frac{1}{2}}$	21,212
$2s(2p)^4$	${}^4P_{2\frac{1}{2}}$	183,863	$2s(2p)^4$	${}^2D_{2\frac{1}{2}}$	212,852
	${}^4P_{1\frac{1}{2}}$	184,476		${}^2D_{1\frac{1}{2}}$	212,872
	${}^4P_{\frac{1}{2}}$	184,801			
$(2s)^2(2p)^3$	${}^2D^\circ_{2\frac{1}{2}}$	0	$2s(2p)^4$	${}^2S_{\frac{1}{2}}$	258,408
	${}^2D^\circ_{1\frac{1}{2}}$	25			
			$2s(2p)^4$	${}^2P_{1\frac{1}{2}}$	278,786
				${}^2P_{\frac{1}{2}}$	279,518

ground state, between the three independent triplet term systems found by de Bruin.[12] A multiplet has been found at λ1257 − 1255 which gives more accurately this connection between those triplets associated with the ^4S and ^2D limits. For the sake of completeness all of de Bruin's triplet terms have been included in the table but it should be noted that those associated with the ^2P limit are, as a group, not finally located with respect to the remaining group of de Bruin's terms. This uncertainty may be estimated as less than 50 cm^{-1}. As no connection has been found, de Bruin's quintet terms have been omitted from the table. The singlet terms given are located with respect to the ground state of the atom by means of the nebular lines.[13] No series are present to permit the calculation of an accurate ionization potential for Ne III but it may be estimated as 63.3 ± 1 volts.

Ne IV. Classified lines are given in Table VI and term values in Table VII. As no intersystem lines are found the quartet and doublet terms are listed separately, but from the work of von Keussler mentioned above it may be estimated that the $^2D^\circ$ term lies about 34,000 cm^{-1} above the $^4S^\circ$ term. The doublet separations of λ521 and λ469 are both resolved only in higher orders, where they are difficult to measure because of further, still unresolved, structure. The term intervals based on these lines are, therefore, quite tentative and represent one possible interpretation of the line structure. The multiplet intervals in the low states along this isoelectronic sequence from O II to Si VIII show considerable irregularities[14, 15, 16] but all of the Ne IV doublet terms listed would be expected to be inverted with the exception of the $^2P^\circ$. These doublet lines should be investigated under the higher resolving power of a grazing incidence vacuum spectrograph as upon their structure would depend the structure of the forbidden $^2D^\circ - {}^2P^\circ$ transition in Ne IV.[13, 17] The shorter wave-length companion of λ358 is obscured by the adjacent strong line of Ne II. Further comparisons show that combinations between 3*s* and 3*d* electron configurations and the ground configuration will give lines of wave-length shorter than λ200. The ionization potential of Ne IV is about 97 volts.

The spectrograph used in this investigation was built by means of a grant to Dr. K. T. Compton from the Carnegie Institution of Washington, which grant also provided some technical assistance in the measurement and reduction of the plates. It is a pleasure to thank Dr. Compton for his continued interest in this investigation, also Dr. Rieke for her careful collaboration in the measurement of the plates and in their reduction. Mr. D. H. Clewell assisted in a large portion of the computations.

[12] T. L. de Bruin, Zeits. f. Physik **77**, 505 (1932).
[13] J. C. Boyce, D. H. Menzel and C. H. Payne, Proc. Nat. Acad. Sci. **19**, 581 (1933).
[14] O II. B. Edlén, Nova Acta Reg. Soc. Sci. Upsaliensis, Ser. IV, Vol. 9, No. 6 (1934).
[15] F III. I. S. Bowen, Phys. Rev. **45**, 82 (1934).
[16] Na IV to Si VIII. J. Söderquist, Nova Acta Reg. Soc. Sci. Upsaliensis, Ser. IV, Vol. 9, No. 7 (1934).
[17] P. Swings and B. Edlén, Comptes rendus **198**, 1748 (1934).

Wave Numbers of Infrared Spectral Lines Beyond λ10,000

HAROLD D. BABCOCK, *Carnegie Institution of Washington, Mount Wilson Observatory*

(Received June 15, 1934)

Professor Kayser's well-known *Tabelle der Schwingungszahlen* may be used for wave-lengths beyond λ10,000 by merely interchanging the labels of the two quantities tabulated. The vacuum wave number thus derived, though not exactly correct, is sufficiently accurate for most of the data now available. For higher accuracy small corrections are tabulated.

THE extremely useful work of Professor H. Kayser, *Tabelle der Schwingungszahlen*,[1] answers most of the needs of the spectroscopist who must convert wave-lengths measured in air into vacuum wave numbers. This table extends from λ2000 to λ10,000, a range somewhat greater than that of the data on which it was based and that seemed ample at the time it was published. Because of improvements in spectroscopic technique, however, the need is becoming apparent for accurate wave numbers of lines beyond λ10,000 and the purpose of this note is to show a simple way of applying Kayser's table to such lines.

This method is merely to use the table backward and to apply a small correction to the result. Thus the given wave-length greater than λ10,000 is found in the body of the table instead of in the usual place at the left and the corresponding number obtained from the left and upper margins is the approximate vacuum wave number, sufficiently accurate for many purposes without the correction.

Let λ = wave-length measured in air.

n = index of refraction of air corresponding to λ.

c = correction to λ to reduce it to vacuum.

N = vacuum wave number.

Then $$c=\lambda(n-1)$$
$$N=1/(\lambda+c)=1/\lambda n.$$

Let λ', n', c', N' refer to a wave-length greater than λ10,000. If λ' is found in the body of Kayser's table, the corresponding number, N'', found in the left and upper margins, is not exactly equal to N'. Instead, $N''=(1/\lambda')-c$, where c is the correction to vacuum that would apply for a wave-length numerically equal to N''. Values of c are tabulated in the last column on each page of the table.

Since $N'=1/\lambda' n'$,

$$N'-N''=c-(n'-1)/\lambda' n'$$
$$N'=N''+c-(n'-1)/\lambda' n'=N''+C.$$

The table below gives the corrections, C, corresponding to various values of N''. These corrections have been computed by extrapolating the dispersion curve for dry air at 15°C that was found by Meggers and Peters[2] from observations extending as far as λ9000 and that was used by Kayser in preparing his table. Their equation is

$$(n-1)10^7=2726.43+12.288/(\lambda^2\times10^{-8})+0.3555/(\lambda^4\times10^{-16}),$$

for which the curvature is small in the deep red and near infrared, so that the errors of extrapolation are not likely to be serious. The only alternative to choose, so far as I am aware, is

TABLE I. *Corrections required when Kayser's table is inverted for the infrared beyond λ10,000.*

Apparent vacuum wave number (cm^{-1})	Correction add. (cm^{-1})
10,000	±0.000
9500	+0.003
9000	+0.005
8500	+0.007
8000	+0.010
7500	+0.012
7000	+0.014
6500	+0.017
6000	+0.020
5500	+0.022
5000	+0.026
4500	+0.030
4000	+0.035
3000	+0.054
2000	+0.106

[1] Leipzig, 1925.

[2] Meggers and Peters, Bur. Stand. Scientific Papers, No. 327, 1918.

the formula of Perard,[3] which differs appreciably from that of Meggers and Peters in the visible and ultraviolet. Perard's equation, rewritten for the special case of normal pressure and 15°C, in units to correspond with the equation above, is

$$(n-1)10^7 = 2728.13 + 14.038/(\lambda^2 \times 10^{-8}) + 0.3367/(\lambda^4 \times 10^{-16}).$$

If a table of vacuum wave numbers were based on this formula it would show systematic differences from Kayser's table, amounting to about 1 part in 725,000 in the ultraviolet but negligible in the infrared.

It will be noted that the correction to be applied to the inverted table of Kayser is very small between λ10,000 and the present limit of photography, λ12,500, at which point it reaches a magnitude of 1 part in 800,000. For lines whose wave-length is not known with such accuracy the correction may be ignored. Farther in the infrared the relative importance of the correction increases more rapidly. The last entry in the table is of low weight. Observations made in moist air for spectral regions close to the important absorption bands of water vapor or of CO_2 may possibly be affected by anomalies in the index of refraction which are not represented in the equation used for extrapolation.

The writer is indebted to Dr. Charlotte E. Moore, of the University Observatory at Princeton, for checking the computation of the corrections listed in Table I.

[3] Perard, J. de Phys. et le Rad. **6**, 217 (1925).

The Kinetic Energy of Polyatomic Molecules

CARL ECKART, *Ryerson Physical Laboratory, The University of Chicago*

(Received July 5, 1934)

The Lagrangian and Hamiltonian expressions for the kinetic energy of a system of N particles are obtained in such a form that the rotational, vibrational and coupling terms may be distinguished. The principal axes of inertia are used to define rotation. The ordinary moments of inertia appear in the Lagrangian kinetic energy but these are replaced by other functions of the radii of gyration in the Hamiltonian. This throws doubt upon all molecular configurations assigned on the basis of empirical values of the moments of inertia.

INTRODUCTION

IT is proposed to derive the expression for the kinetic energy of a polyatomic molecule, considered as a system of N particles, in such a form that its rotational, vibrational and coupling terms may be distinguished.

I. THE PRINCIPAL AXIS TRANSFORMATION; COORDINATES

It is no loss of generality to suppose the center of mass of the molecule to be at rest, so that its configuration is completely specified by $n = N-1$ vectors $\mathbf{R}_\alpha$, $\alpha = 1, 2, 3, \cdots n$. It is convenient to choose these vectors so that two conditions are fulfilled: (1) the kinetic energy T is given by

$$2T = \mu \sum_\alpha (d\mathbf{R}_\alpha/dt)^2 \qquad (1)$$

and (2) any other vector dimension $\mathbf{X}$ of the configuration is given by

$$\mathbf{X} = \sum_\alpha X_\alpha \mathbf{R}_\alpha, \qquad (2)$$

where the X_α are independent of the $\mathbf{R}_\alpha$. These two conditions may always be satisfied and do not determine the vectors $\mathbf{R}_\alpha$ uniquely. In fact the constant μ is quite arbitrary and the vectors $\mathbf{R}_\alpha$ may be replaced by any n linear functions of themselves, provided that the coefficients of these functions form an orthogonal matrix and are independent of the $\mathbf{R}_\alpha$. It is convenient to set $\mu = 1$ for general considerations.

The length of the vector $\mathbf{X}$ is given by the quadratic form

$$\mathbf{X}^2 = \sum_\alpha \sum_\beta X_\alpha X_\beta \mathbf{R}_\alpha \cdot \mathbf{R}_\beta. \qquad (3)$$

The matrix of this form is also the matrix of the Gram[1] determinant of the vectors $\mathbf{R}_\alpha$. It is known,

[1] Courant-Hilbert, *Methoden der mathematischen Physik*, 1st Ed., p. 20.

or may easily be shown, that this matrix possesses exactly as many non-zero characteristic values as there are linearly independent vectors among the $\mathbf{R}_\alpha$. It is therefore evident that when $n \geqslant 3$, the quadratic form will have three characteristic values which do not vanish identically and $n-3$ which do vanish identically. The triatomic molecule for which $n=2$ thus occupies an exceptional position in the theory; to avoid confusion, it will be discussed separately in Part IV.

With this understanding, let r_1^2, r_2^2, r_3^2 be the non-vanishing characteristic values of the form $\mathbf{X}^2$ and set $r_4^2=\cdots=r_n^2=0$. Then it is known from the general theory of quadratic forms that an orthogonal matrix $c_{\gamma\alpha}$ exists, such that

$$\sum_\alpha c_{\gamma\alpha}\mathbf{R}_\alpha\cdot\mathbf{R}_\beta=r_\gamma^2 c_{\gamma\beta}. \tag{4}$$

The conditions for the orthogonality of the matrix are

$$\sum_\beta c_{\alpha\beta}c_{\gamma\beta}=\delta_{\alpha\gamma}, \tag{5.1}$$

$$\sum_\beta c_{\beta\alpha}c_{\beta\gamma}=\delta_{\alpha\gamma}. \tag{5.2}$$

Its elements will, of course, be functions of the $\mathbf{R}_\alpha$, which distinguishes it from the orthogonal matrices discussed above.

If the n quantities defined by

$$X_\alpha=\sum_\gamma x_\gamma c_{\gamma\alpha} \quad \text{or} \quad x_\alpha=\sum_\gamma c_{\alpha\gamma}X_\gamma \tag{6}$$

are substituted into Eq. (3), it becomes

$$\mathbf{X}^2=\sum_\gamma r_\gamma^2 x_\gamma^2=r_1^2x_1^2+r_2^2x_2^2+r_3^2x_3^2. \tag{7}$$

Again, in distinction to the X_α, the x_γ and r_γ are functions of the $\mathbf{R}_\alpha$. To avoid repetition, it is convenient to introduce the convention that the Latin indices i, j, k have the range 1, 2, 3, while the Greek indices α, β, γ, δ have the range 1, 2, $\cdots$ n. Next consider the three vectors $\mathbf{a}_i$, defined by

$$r_i\mathbf{a}_i=\sum_\alpha c_{i\alpha}\mathbf{R}_\alpha. \tag{8}$$

It is easily seen that they are mutually perpendicular and of unit length, since

$$\begin{aligned} r_ir_j\mathbf{a}_i\cdot\mathbf{a}_j&=\sum_\alpha\sum_\beta c_{i\alpha}c_{j\beta}\mathbf{R}_\alpha\cdot\mathbf{R}_\beta \\ &=\sum_\beta r_i^2c_{i\beta}c_{j\beta} && \text{by Eq. (4),} \\ &=r_i^2\delta_{ij} && \text{by Eq. (5.1).} \end{aligned}$$

These vectors may be used to define a rotating set of coordinate axes, to which the components of the vectors $\mathbf{R}_\alpha$ may be referred. From Eq. (8) it follows that

$$r_i\mathbf{a}_i\cdot\mathbf{R}_\beta=\sum_\alpha c_{i\alpha}\mathbf{R}_\alpha\cdot\mathbf{R}_\beta=r_i^2c_{i\beta},$$

whence

$$\mathbf{R}_\alpha=\sum_i \mathbf{a}_i r_i c_{i\alpha}. \tag{9}$$

It is advantageous to choose the generalized coordinates in such a manner that they correspond to the various elements distinguishable on the right side of Eq. (9). Thus the three quantities r_1, r_2, r_3 may themselves be chosen as three of the $3n$ coordinates. The axes $\mathbf{a}_i$ may be specified by three Eulerian angles according to the usual formulae ($\mathbf{i}$, $\mathbf{j}$, $\mathbf{k}$ are three stationary unit vectors):

$$\begin{aligned} &\mathbf{k}\cdot\mathbf{a}_1=-\sin\beta\cos\gamma, \quad \mathbf{a}_3\cdot\mathbf{i}=\sin\beta\cos\alpha, \\ &\mathbf{k}\cdot\mathbf{a}_2=\sin\beta\sin\gamma, \quad \mathbf{a}_3\cdot\mathbf{j}=\sin\beta\sin\alpha, \\ &\mathbf{k}\cdot\mathbf{a}_3=\cos\beta. \end{aligned} \tag{10}$$

The $3n$ quantities $c_{i\alpha}$ are related by six equations (Eq. (5.1)) so that they can all be specified as functions of $3n-6$ dimensionless quantities q_κ. Thus the total of $3n$ is made up of three different kinds of coordinates.

The further convention that the index κ has the range 1, 2, $\cdots$ $3n-6$, is hereby introduced.

II. The Lagrangian Form of the Kinetic Energy

As the Lagrangian form of the kinetic energy depends on the time derivatives of the coordinates, it will be necessary to express $d\mathbf{R}_\alpha/dt$ in terms of these. To avoid complicated expressions, it is convenient to define certain auxiliary quantities which are linear functions of these derivatives. The first of these is the ordinary angular velocity vector, $\boldsymbol{\omega}$, defined by

$$d\mathbf{a}_i/dt=\boldsymbol{\omega}\times\mathbf{a}_i, \tag{11}$$

or more explicitly by

$$\begin{aligned} \boldsymbol{\omega}&=\sum_i \omega_i\mathbf{a}_i \\ &=\mathbf{a}_1(-\dot{\alpha}\sin\beta\cos\gamma+\dot{\beta}\sin\gamma) \\ &+\mathbf{a}_2(\dot{\alpha}\sin\beta\sin\gamma+\dot{\beta}\cos\gamma) \\ &+\mathbf{a}_3(\dot{\alpha}\cos\beta+\dot{\gamma}). \end{aligned} \tag{11.1}$$

The second set of auxiliary quantities are matrices defined by

$$\Omega_{\beta\gamma}=\sum_\alpha c_{\alpha\beta}\dot{c}_{\alpha\gamma},\quad \omega_{\beta\gamma}=\sum_\alpha \dot{c}_{\beta\alpha}c_{\gamma\alpha}. \tag{12}$$

On differentiating Eq. (5) it appears that both these matrices are skew-symmetric; both are linear functions of the $\dot{q}_\kappa$, so that, e.g.,

$$\omega_{\beta\gamma}=\sum_\kappa \omega_{\beta\gamma,\kappa}\dot{q}_\kappa, \tag{13}$$

where the $\omega_{\beta\gamma,\kappa}$ are functions of the q_κ only. Combining Eq. (5) with Eq. (12), it follows that

$$\sum_\beta c_{\alpha\beta}\Omega_{\beta\gamma}=\dot{c}_{\alpha\gamma}=\sum_\beta \omega_{\alpha\beta}c_{\beta\gamma}, \tag{14.1}$$

and hence that

$$\omega_{\alpha\delta}=\sum_\beta\sum_\gamma c_{\alpha\beta}\Omega_{\beta\gamma}c_{\delta\gamma}. \tag{14.2}$$

The matrices $\Omega_{\beta\gamma}$ and $\omega_{\beta\gamma}$ are the n-dimensional analogues of the angular velocity vector and the q_κ are the analogues of the Eulerian angles. The elements $\Omega_{\beta\gamma}$ are the components of the n-dimensional angular velocity relative to "moving" axes (system of the X_α) and the $\omega_{\beta\gamma}$ are the components of the same quantity relative to "fixed" axes (system of the x_α).

The use of Eqs. (11) and (14.1) now makes it possible to write

$$d\mathbf{R}_\alpha/dt=\boldsymbol{\omega}\times\mathbf{R}_\alpha+\sum_i \mathbf{a}_i\dot{r}_i c_{i\alpha}+\sum_\beta \mathbf{R}_\beta\Omega_{\beta\alpha}. \tag{15}$$

For temporary convenience, call the three terms of this expression $\mathbf{A}_\alpha$, $\mathbf{B}_\alpha$, $\mathbf{C}_\alpha$; then the kinetic energy is

$$2T=\sum_\alpha [(\mathbf{A}_\alpha^2+\mathbf{B}_\alpha^2+\mathbf{C}_\alpha^2) +2(\mathbf{A}_\alpha\cdot\mathbf{B}_\alpha+\mathbf{B}_\alpha\cdot\mathbf{C}_\alpha+\mathbf{C}_\alpha\cdot\mathbf{A}_\alpha)]. \tag{16}$$

The six terms of this sum will be given separate consideration; the first is

$$\sum_\alpha \mathbf{A}_\alpha^2=\sum_\alpha (\boldsymbol{\omega}\times\mathbf{R}_\alpha)^2=\sum_\alpha [\omega^2\mathbf{R}_\alpha^2-(\boldsymbol{\omega}\cdot\mathbf{R}_\alpha)^2]$$
$$=\sum_\alpha\sum_i\sum_j [\omega_i^2r_j^2c_{j\alpha}^2-\omega_i r_i c_{i\alpha}\omega_j r_j c_{j\alpha}]$$

by Eqs. (9) and (11.1);

$$=\sum_i\sum_j [\omega_i^2r_j^2-\omega_i^2r_i^2\delta_{ij}]$$

by Eq. (5.1), so that

$$\sum_\alpha \mathbf{A}_\alpha^2=\omega_1^2(r_2^2+r_3^2)+\omega_2^2(r_3^2+r_1^2)+\omega_3^2(r_1^2+r_2^2).$$

The second term is

$$\sum_\alpha \mathbf{B}_\alpha^2=\sum_\alpha\sum_i \dot{r}_i^2c_{i\alpha}^2=\sum_i \dot{r}_i^2$$

by Eq. (5.1) again; the third term is

$$\sum_\alpha \mathbf{C}_\alpha^2=\sum_\alpha\sum_\beta\sum_\gamma \mathbf{R}_\beta\cdot\mathbf{R}_\gamma\Omega_{\beta\alpha}\Omega_{\gamma\alpha}$$
$$=\sum_\alpha\sum_\beta\sum_\gamma\sum_i r_i^2c_{i\beta}c_{i\gamma}\Omega_{\beta\alpha}\Omega_{\gamma\alpha}$$

by Eq. (9), whence

$$\sum_\alpha \mathbf{C}_\alpha^2=\sum_\alpha\sum_i r_i^2\omega_{i\alpha}^2$$

by Eqs. (14.1) and (5.1). The fourth and fifth terms vanish, since

$$\sum_\alpha \mathbf{A}_\alpha\cdot\mathbf{B}_\alpha=\sum_\alpha\sum_i \boldsymbol{\omega}\times\mathbf{R}_\alpha\cdot\mathbf{a}_i\dot{r}_i c_{i\alpha}$$
$$=\boldsymbol{\omega}\cdot\sum_\alpha\sum_i \mathbf{R}_\alpha\times\mathbf{a}_i\dot{r}_i c_{i\alpha}$$

and

$$\sum_\alpha \mathbf{R}_\alpha\times\mathbf{a}_1c_{1\alpha}=\sum_\alpha (\mathbf{a}_3r_2c_{2\alpha}-\mathbf{a}_2r_3c_{3\alpha})c_{1\alpha}=0$$

by Eq. (5.1); also

$$\sum_\alpha \mathbf{B}_\alpha\cdot\mathbf{C}_\alpha=\sum_\alpha\sum_\beta\sum_i \mathbf{a}_i\cdot\mathbf{R}_\beta\dot{r}_i c_{i\alpha}\Omega_{\beta\alpha}$$
$$=\sum_\alpha\sum_\beta\sum_i \dot{r}_i r_i c_{i\alpha}c_{i\beta}\Omega_{\beta\alpha}$$

by Eq. (9),

$$=\sum_i \dot{r}_i r_i\omega_{ii}=0$$

by Eq. (14.2). The last term does not vanish:

$$\sum_\alpha \mathbf{C}_\alpha\cdot\mathbf{A}_\alpha=\boldsymbol{\omega}\cdot[\sum_\alpha\sum_\beta \mathbf{R}_\alpha\times\mathbf{R}_\beta\Omega_{\beta\alpha}];$$

since the $\mathbf{a}_1$-component of $\mathbf{R}_\alpha\times\mathbf{R}_\beta$ is

$$r_2r_3(c_{2\alpha}c_{3\beta}-c_{3\alpha}c_{2\beta})$$

(by Eq. (9)), it is easily seen upon referring to Eq. (14.2) that

$$\sum_\alpha \mathbf{C}_\alpha\cdot\mathbf{A}_\alpha=-2(r_2r_3\omega_1\omega_{23}+r_3r_1\omega_2\omega_{31}+r_1r_2\omega_3\omega_{12}).$$

Combining all these results according to Eq. (16), the Lagrangian form of the kinetic energy appears:

$$2T=\dot{r}_1^2+\dot{r}_2^2+\dot{r}_3^2+\omega_1^2(r_2^2+r_3^2) +\omega_2^2(r_3^2+r_1^2)+\omega_3^2(r_1^2+r_2^2)-4r_2r_3\omega_1\omega_{23} -4r_3r_1\omega_2\omega_{31}-4r_1r_2\omega_3\omega_{12} +\sum_\alpha (r_1^2\omega_{1\alpha}^2+r_2^2\omega_{2\alpha}^2+r_3^2\omega_{3\alpha}^2). \tag{17}$$

From the form of this expression, it is possible to draw certain conclusions as to the significance of the coordinates which were introduced at the end of Part I. Since there are no terms containing $\omega_1\omega_2$, etc., it follows that the vectors $\mathbf{a}_i$ are along the principal axes of inertia of the instantaneous

configuration of the N particles; this justifies the title of Part I. From the mode of calculation it also follows that

$$A_1=r_2^2+r_3^2, \quad \text{etc.}, \tag{18}$$

are the three Eulerian moments of inertia. The three coordinates r_1, r_2, r_3 may therefore be called the radii of gyration of the instantaneous configuration, although this deviates slightly from the usual definition of the term.

III. The Hamiltonian Form of the Kinetic Energy

Eq. (17) may be rearranged into the form

$$\begin{aligned}2T=&\dot r_1^2+\dot r_2^2+\dot r_3^2\\&+(r_2\omega_1-r_3\omega_{23})^2+(r_3\omega_1-r_2\omega_{23})^2\\&+(r_3\omega_2-r_1\omega_{31})^2+(r_1\omega_2-r_3\omega_{31})^2\\&+(r_1\omega_3-r_2\omega_{12})^2+(r_2\omega_3-r_1\omega_{12})^2\\&+\textstyle\sum^n{}_{\alpha=4}(r_1^2\omega_{1\alpha}^2+r_2\omega_{2\alpha}^2+r_3\omega_{3\alpha}^2),\end{aligned} \tag{17.1}$$

which is more convenient for the calculation of the momenta. In case $n=3$ (tetra-atomic molecule), the residual sum on the last line vanishes. On calculating the momenta in the usual manner, one finds that

$$P_i=\partial T/\partial\dot r_i=\dot r_i \tag{19}$$

and on referring to Eq. (13):

$$\begin{aligned}p_s=&\partial T/\partial\dot q_s\\&=\omega_{23,s}[-r_3(r_2\omega_1-r_3\omega_{23})-r_2(r_3\omega_1-r_2\omega_{23})]\\&+\omega_{31,s}[-r_1(r_3\omega_2-r_1\omega_{31})-r_3(r_1\omega_2-r_3\omega_{31})]\\&+\omega_{12,s}[-r_2(r_1\omega_3-r_2\omega_{12})-r_1(r_2\omega_3-r_1\omega_{12})]\\&+\textstyle\sum^n{}_{\alpha=4}(r_1^2\omega_{1\alpha}\omega_{1\alpha,s}+r_2^2\omega_{2\alpha}\omega_{2\alpha,s}\\&\qquad+r_3^2\omega_{3\alpha}\omega_{3\alpha,s}).\end{aligned} \tag{20}$$

These are $3n-6$ equations; the $3n-9$ quantities $r_i^2\omega_{i\alpha}$ and the three square brackets may be treated as unknowns and expressed as linear functions of the p_s upon solution of the equations. Supposing this to have been accomplished, it follows that

$$r_i^2\omega_{i\alpha}=N_{i\alpha}=\textstyle\sum_s N_{i\alpha,s}p_s, \quad \alpha=4\cdots 3n-6, \tag{21.1}$$

where the $N_{i\alpha,s}$ are functions of the q_s only. Similarly

$$\begin{aligned}&-r_3(r_2\omega_1-r_3\omega_{23})-r_2(r_3\omega_1-r_2\omega_{23})=N_{23},\\&N_{23}=\textstyle\sum_s N_{23,s}p_s, \quad \text{etc.}\end{aligned} \tag{21.2}$$

On dealing with the ordinary angular velocity in the same manner as has just been done with the n-dimensional one, it follows that

$$r_2(r_2\omega_1-r_3\omega_{23})+r_3(r_3\omega_1-r_2\omega_{23})=M_1, \quad \text{etc.}, \tag{22}$$

where[2]

$$\begin{aligned}M_1=&\ \cos\gamma(-p_\alpha+p_\gamma\cos\beta)/\sin\beta+p_\beta\sin\gamma,\\M_2=&-\sin\gamma(-p_\alpha+p_\gamma\cos\beta)/\sin\beta+p_\beta\cos\gamma,\\M_3=&\ p_\gamma.\end{aligned} \tag{23}$$

In passing, it may be remarked that the total angular momentum (three dimensional) of the system can be shown to be

$$\mathbf{M}=\mathbf{a}_1M_1+\mathbf{a}_2M_2+\mathbf{a}_3M_3 \tag{24}$$

in accord with the well-known formula. On solving Eqs. (21.2) and (22) for the two parentheses, one sees that

$$\begin{aligned}&r_2\omega_1-r_3\omega_{23}=(r_2M_1-r_3N_{23})/(r_2^2-r_3^2),\\&r_3\omega_1-r_2\omega_{23}=(r_3M_1-r_2N_{23})/(r_3^2-r_2^2), \quad \text{etc.}\end{aligned} \tag{25}$$

On substituting Eqs. (19), (21.1) and (25) into Eq. (17.1), the Hamiltonian form appears:

$$\begin{aligned}2T=&P_1^2+P_2^2+P_3^2\\&+M_1^2/B_1+M_2^2/B_2+M_3^2/B_3\\&-2(M_1N_{23}/C_1+M_2N_{31}/C_2+M_3N_{12}/C_3)\\&+N_{23}^2/B_1+N_{31}^2/B_2+N_{12}^2/B_3\\&+\textstyle\sum^n{}_{\alpha=4}(N_{1\alpha}^2/r_1^2+N_{2\alpha}^2/r_2^2+N_{3\alpha}^2/r_3^2),\end{aligned} \tag{26}$$

where

$$B_1=(r_2^2-r_3^2)^2/(r_2^2+r_3^2), \quad \text{etc.}, \tag{27.1}$$

$$C_1=(r_2^2-r_3^2)^2/(2r_2r_3), \quad \text{etc.} \tag{27.2}$$

The first, fourth and fifth lines of Eq. (26) represent the vibrational kinetic energy; the rotational is given by the second and the coupling by the third. It will be noted that the Eulerian moments of inertia A_i, do not enter into the

[2] The indices α, β, γ in Eq. (23) refer to the Eulerian angles and are not the same as those used in the n-dimensional geometry.

second line as expected, but are replaced by the coefficients B_i.

In order to set up the wave equation, it is also necessary to know the element of volume in configuration space. This is proportional to the square root of the discriminant of the Lagrangian form[3] and a simple calculation shows that

$$d\tau=(r_2^2-r_3^2)(r_3^2-r_1^2)(r_1^2-r_2^2)(r_1r_2r_3)^{n-3}$$
$$\sin\beta J(q_\kappa)dr_1dr_2dr_3d\alpha d\beta d\gamma dq_1\cdots dq_{3n-6}, \quad (28)$$

where $J(q_\kappa)$ is the determinant of $(3n-6)$th order whose κ-th row is

$$\omega_{23,\kappa},\ \omega_{31,\kappa},\ \omega_{12,\kappa},\ \omega_{14,\kappa}\cdots\omega_{3n,\kappa}. \quad (29)$$

IV. The Triatomic Case

The investigation of the triatomic case parallels the preceding in all essential respects. Since $n=2$, there are only two vectors $\mathbf{R}_1$ and $\mathbf{R}_2$, which satisfy the same conditions (Eqs. (1) and (2)) as before. The orthogonal transformation of Eq. (6) is introduced in the same manner but can be written out explicitly:

$$X_1= x_1\cos q+x_2\sin q,$$
$$X_2=-x_1\sin q+x_2\cos q, \quad (6.3)$$

where the parameter q is the sole representative of the coordinates q_κ. There are only two radii of gyration, r_1 and r_2, and only two unit vectors can be defined:

$$r_1\mathbf{a}_1=\mathbf{R}_1\cos q-\mathbf{R}_2\sin q,$$
$$r_2\mathbf{a}_2=\mathbf{R}_1\sin q+\mathbf{R}_2\cos q, \quad (8.3)$$

so that the third must be defined by

$$\mathbf{a}_3=\mathbf{a}_1\times\mathbf{a}_2.$$

Eqs. (8.3), when solved for $\mathbf{R}_1$ and $\mathbf{R}_2$ become

$$\mathbf{R}_1= \mathbf{a}_1r_1\cos q+\mathbf{a}_2r_2\sin q,$$
$$\mathbf{R}_2=-\mathbf{a}_1r_1\sin q+\mathbf{a}_2r_2\cos q. \quad (9.3)$$

The Eulerian angles are defined as before by Eq. (10) and complete the total of six coordinates.

The n-dimensional angular velocities are here one-dimensional and need not be discussed explicitly. The kinetic energy is readily found to be

$$2T=\dot r_1^2+\dot r_2^2+\omega_1^2r_2^2+\omega_2^2r_1^2+\omega_3^2(r_1^2+r_2^2)$$
$$-4r_1r_2\omega_3\dot q+(r_1^2+r_2^2)\dot q^2. \quad (17.3)$$

The Hamiltonian form is readily derived from this by the same methods as before and is

$$2T=P_1^2+P_2^2+M_1^2/r_2^2+M_2^2/r_1^2$$
$$+M_3^2/B_3+2M_3p/C_3+p^2/B_3. \quad (26.3)$$

The element of volume is

$$d\tau=r_1r_2(r_1^2-r_2^2)\sin\beta dr_1dr_2d\alpha d\beta d\gamma dq. \quad (27.3)$$

A more extended investigation of the triatomic molecule was begun prior to the investigation reported in this paper. On encountering the unexpected form of the coefficient of M_3^2 in Eq. (26.3) it seemed advisable to examine the general case before continuing. The present results throw doubt on molecular configurations previously assigned on the basis of empirical values of the moments of inertia. These empirical values are presumably closer to the equilibrium values of the B_i than the A_i, as has been supposed.

[3] A. Sommerfeld, *Wellenmechanischer Ergänzungsband*, pp. 148, 152; A. Landé, *Handbuch der Physik*, XX, p. 330.

Hartree Fields of Carbon

C. C. TORRANCE, *Institute for Advanced Study, Princeton, New Jersey*

(Received June 4, 1934)

A new method of integrating the Hartree equations for the charge distributions of the electrons in an atom is described and the wave functions for the ground state and the first excited state of carbon are tabulated.

INTRODUCTION

IN Hartree's method for determining a "self-consistent" field of an atom, a set of charge distributions is assumed for the various electrons in the atom, the potentials are computed from them, the radial parts of the wave equations are solved and the resulting charge distributions compared with those assumed. If the two sets of distributions disagree, a new distribution is assumed and the process repeated. In this paper a method is developed whereby the variation of functions (charge distributions) is reduced to the variation of two parameters for each type of electron present in the atom. By this method it is possible to calculate the requisite changes in the assumed values of the parameters so that the convergence of the successive approximations to the charge distributions is very rapid.

THEORY

The radial part of the wave equation for a stationary state of an electron in an atom can be reduced to the form[1]

$$d^2P/dr^2+\{2v(r)-\epsilon-l(l+1)/r^2\}P=0, \quad (1)$$

where $v(r)$ is the (negative) potential of the field in which the electron is moving, ϵ is the energy of the electron in Hartree units, and l is the orbital angular momentum quantum number. The ground state of carbon has the configuration $(1s)^2\ (2s)^2\ (2p)^2$. Let $R(r)$, $S(r)$ and $T(r)$ be the solutions of the (radial parts) of the wave equations for these electrons; then the squares of these solutions represent the charge distributions of these electrons. It is readily seen that Eq. (1) can be put in the following forms for the $1s$, $2s$ and $2p$ electrons, respectively:

$$\frac{d^2R}{dr^2}+\left\{\frac{12}{r}+2\int_0^r\frac{1}{s^2}\int_0^s(R^2+2S^2+2T^2)dtds-E\right\}R=0, \quad (2a)$$

$$\frac{d^2S}{dr^2}+\left\{\frac{12}{r}+2\int_0^r\frac{1}{s^2}\int_0^s(2R^2+S^2+2T^2)dtds-F\right\}S=0, \quad (2b)$$

$$\frac{d^2T}{dr^2}+\left\{\frac{12}{r}-\frac{2}{r^2}+2\int_0^r\frac{1}{s^2}\int_0^s(2R^2+2S^2+T^2)dtds-G\right\}T=0, \quad (2c)$$

where

$$E=2\int_0^\infty(1/r)(R^2+2S^2+2T^2)dr+\epsilon$$

and where F and G are defined in an analogous manner. The three Eqs. (2) must be solved under the following boundary conditions:

$$R(0)=S(0)=T(0)=R(\infty)=S(\infty)=T(\infty)=0, \quad (3)$$

$$\int_0^\infty R^2dr=\int_0^\infty S^2dr=\int_0^\infty T^2dr=1. \quad (4)$$

The numerical integration of the Eqs. (2) is simple and needs no explanation. It should be noted that the computation of the integrals (4) is merely an incidental part of the integration of the Eqs. (2) and hence involves no extra labor. The solutions of (2) are determined most con-

[1] J. McDougall, Proc. Roy. Soc. **A138**, 552 (1932).

veniently by conditions of the form

$$R(0)=S(0)=T(0)=0,$$
$$R(0.01)=R_1,\quad S(0.01)=S_1,\quad T(0.01)=T_1, \tag{5}$$

where R_1, S_1 and T_1 may be any assigned values. Hence it is necessary only to determine the values of the six parameters E, F, G, R_1, S_1 and T_1 so that the conditions (3) and (4) are satisfied. The best method for determining these values is as follows: let $R^\circ(r)$, $S^\circ(r)$ and $T^\circ(r)$ satisfy conditions (3) and (4) and approximate the desired solutions of (2). (R°, S° and T° were obtained for carbon by interpolation from other atoms.) Assuming that R°, S° and T° constitute a solution of (2a) it is possible to tabulate with the aid of (2a) the variations of R°,

$$\int_0^r R^{\circ 2}ds, \quad \text{and} \quad \int_0^r s^{-2}\int_0^s R^{\circ 2}dtds$$

TABLE I. *Tabulated one-electron functions for carbon.*

	Ground State $1s^2\,2s^1\,2p^3$			Excited State $1s^2\,2s\,2p^3$		
	$1s$	$2s$	$2p$	$1s$	$2s$	$2p$
r	R	S	T	R	S	T
0.01	0.2602	0.0575	0.0005	0.2607	0.0578	0.0005
2	.4902	.1083	.0020	.4911	.1088	.0020
3	.6928	.1529	.0043	.6941	.1536	.0044
4	.8704	.1919	.0075	.8720	.1927	.0076
5	1.0254	.2255	.0114	1.0273	.2265	.0116
6	1.1599	.2544	.0160	1.1619	.2555	.0162
7	1.2758	.2789	.0212	1.2780	.2801	.0215
8	1.3749	.2994	.0269	1.3772	.3006	.0273
9	1.4588	.3161	.0332	1.4611	.3174	.0337
.10	1.5289	.3295	.0399	1.5313	.3308	.0405
1	1.5866	.3397	.0470	1.5890	.3411	.0477
2	1.6332	.3471	.0545	1.6355	.3485	.0554
3	1.6697	.3518	.0624	1.6719	.3532	.0633
4	1.6971	.3542	.0705	1.6993	.3555	.0716
5	1.7165	.3544	.0790	1.7186	.3557	.0802
6	1.7286	.3525	.0877	1.7306	.3538	.0890
7	1.7343	.3488	.0966	1.7361	.3500	.0981
8	1.7342	.3435	.1057	1.7358	.3446	.1073
9	1.7289	.3366	.1150	1.7304	.3376	.1168
.20	1.7191	.3283	.1244	1.7204	.3292	.1264
.22	1.6879	.3080	.1437	1.6888	.3088	.1459
4	1.6443	.2834	.1634	1.6449	.2840	.1659
6	1.5913	.2554	.1833	1.5916	.2558	.1861
8	1.5316	.2247	.2034	1.5315	.2249	.2064
.30	1.4670	.1917	.2235	1.4666	.1917	.2268
2	1.3994	.1570	.2435	1.3987	.1567	.2472
4	1.3301	.1210	.2635	1.3291	.1206	.2674
6	1.2602	.0841	.2832	1.2590	.0834	.2874
8	1.1905	.0466	.3026	1.1892	.0458	.3071
.40	1.1219	+.0088	.3217	1.1204	+.0078	.3265
2	1.0549	−.0290	.3405	1.0532	−.0302	.3455
4	.9898	.0667	.3589	.9880	.0681	.3641
6	.9269	.1040	.3768	.9251	.1056	.3823
8	.8666	.1409	.3942	.8647	.1426	.4000
.50	.8090	.1771	.4111	.8070	.1790	.4172
2	.7541	.2125	.4275	.7521	.2146	.4338
4	.7020	.2471	.4434	.7000	.2493	.4499
6	.6527	.2808	.4587	.6508	.2831	.4655
8	.6061	.3139	.4735	.6043	.3160	.4805
.60	.5623	.3451	.4876	.5605	.3477	.4949
.64	.4826	.4050	.5143	.4809	.4079	.5220
.68	.4128	.4603	.5387	.4112	.4634	.5468
.72	.3520	.5109	.5608	.3506	.5142	.5693
.76	.2994	.5567	.5807	.2981	.5603	.5896
.80	.2540	.5979	.5985	.2529	.6017	.6077
.84	.2151	.6345	.6142	.2141	.6385	.6238
.88	.1818	.6668	.6280	.1809	.6709	.6378
.92	.1534	.6949	.6399	.1526	.6992	.6500
.96	.1292	.7190	.6501	.1285	.7234	.6604
1.00	.1087	.7395	.6587	.1082	.7439	.6691
1.04	.0913	.7564	.6657	.0909	.7609	.6762
1.08	767	.7701	.6713	763	.7747	.6819
1.12	643	.7808	.6756	640	.7854	.6862
1.16	538	.7887	.6787	536	.7932	.6892
1.20	451	.7941	.6806	449	.7985	.6911
1.28	315	.7980	.6815	314	.8022	.6916
1.36	221	.7941	.6788	220	.7980	.6885
1.44	155	.7839	.6732	154	.7874	.6823
1.52	108	.7686	.6652	108	.7716	.6736
1.60	76	.7494	.6552	76	.7518	.6628
1.68	53	.7270	.6435	53	.7288	.6502
1.76	37	.7023	.6306	37	.7035	.6363
1.84	26	.6760	.6167	26	.6765	.6214
1.92	18	.6486	.6020	18	.6484	.6056
2.00	13	.6205	.5866	13	.6197	.5892

	Ground State $1s^2\,2s^2\,2p^3$			Excited State $1s^2\,2s\,2p^3$		
	$1s$	$2s$	$2p$	$1s$	$2s$	$2p$
r	R	S	T	R	S	T
2.08	9	0.5922	0.5709	9	0.5908	0.5724
2.16	6	.5640	.5548	6	.5620	.5553
2.24	4	.5360	.5386	4	.5334	.5380
2.32	3	.5085	.5223	3	.5054	.5207
2.40	2	.4816	.5060	2	.4781	.5034
2.48	2	.4555	.4898	2	.4516	.4863
2.56	1	.4303	.4738	1	.4260	.4693
2.72	1	.3825	.4422	1	.3776	.4362
2.88	0	.3387	.4117	0	.3334	.4043
3.04		.2988	.3824		.2933	.3738
3.20		.2628	.3544		.2572	.3449
3.36		.2306	.3279		.2250	.3176
3.52		.2018	.3029		.1963	.2920
3.68		.1763	.2794		.1710	.2681
3.84		.1537	.2573		.1486	.2457
4.00		.1337	.2366		.1289	.2249
4.16		.1162	.2173		.1117	.2057
4.32		.1008	.1994		.0966	.1878
4.48		.0874	.1827		835	.1713
4.64		756	.1673		720	.1562
4.80		654	.1530		621	.1422
4.96		564	.1398		535	.1294
5.12		487	.1277		460	.1176
5.28		419	.1165		395	.1068
5.44		361	.1061		339	.0969
5.60		311	.0967		291	879
5.76		267	880		250	797
5.92		229	800		214	722
6.08		197	728		183	653
6.24		169	661		157	591
6.40		145	600		134	535
6.72		107	494		98	437
7.04		79	406		72	356
7.36		58	333		53	290
7.68		42	273		39	236
8.00		31	223		28	192
8.32		23	182		21	156
8.64		17	149		15	127
8.96		12	122		11	103
9.28		9	100		8	84
9.60		7	82		6	68
9.92		5	67		4	55
10.24		4	54		3	45
10.56		3	45		2	37
10.88		2	36		2	30
11.20		1	30		1	24
11.52		1	24		1	20
11.84		1	20		1	16
12.16		1	16		1	13
12.48		0	13		0	11
12.80			11			9
13.12			9			7
13.44			7			6
13.76			6			5
14.08			5			4
14.40			4			3
14.72			3			2
15.04			3			2
15.36			2			2
15.68			2			1
16.00			1			1
16.32			1			1
16.64			1			1
16.96			1			1
17.28			1			0
17.60			0			

arising (1) from the variation ΔE° of E° (where E° is an approximate value of E obtained, for example, by interpolation from other atoms) and (2) from the variation of R_1° to kR_1° (where $R_1^\circ = R^\circ(0.01)$ and k is a constant of proportionality which is nearly unity). Similar tabulations of the variations of S°,

$$\int_0^r S^{\circ 2}ds, \quad \int_0^r s^{-2}\int_0^s S^{\circ 2}dtds, \quad T^\circ, \quad \int_0^r T^{\circ 2}ds$$

and

$$\int_0^r s^{-2}\int_0^s T^{\circ 2}dtds,$$

may be made with the aid of (2*b*) and (2*c*). Although theoretically it would be necessary to tabulate all the variations of R°, S° and T° caused by variations of each of the six parameters, experience shows that only two more tabulations are needed: the variations of S°,

$$\int_0^r S^{\circ 2}ds \quad \text{and} \quad \int_0^r s^{-2}\int_0^s S^{\circ 2}dtds,$$

caused by variation of T_1° to kT_1° and the variations of T°,

$$\int_0^r T^{\circ 2}ds \quad \text{and} \quad \int_0^r s^{-2}\int_0^s T^{\circ 2}dtds,$$

caused by variation of S_1° to kS_1°.

The integration of Eqs. (2) may now be effected quickly. Values are assigned to E and R_1 and (2*a*) is integrated (by using S° and T°). By using the tabulated variations of R it is possible to calculate the requisite changes in E and R_1 so that the new solution of (2*a*) satisfies (3) and (4). Eqs. (2*b*) and (2*c*) are then integrated simultaneously, the proper parameter values are determined from the tabulated variations and the equations re-integrated. When fairly approximate solutions S and T are known it is possible to return to (2*a*) and determine R to the accuracy desired; this solution in turn permits of the final determination of S and T.

Table I gives the solutions of Eqs. (2) for the ground state of carbon and also the wave functions for the configuration $(1s)^2\ (2s)\ (2p)^3$. All figures given are correct to within a few units in the fourth decimal place; six figures were used in the computations to avoid cumulative errors. Table II gives the parameter values and the electron energies. While the ground state $2s$ electron checks with that obtained by Brown, Bartlett and Dunn,[2] the $2p$ electron differs considerably. The excitation energy works out to be 0.320 but this figure must be corrected for interactions of the electrons.

TABLE II. *Values of parameters and electron energies.*

	Ground State	
$E = 40.5753$	$F = 28.4866$	$G = 28.2215$
$R_1 = 0.260205$	$S_1 = 0.057543$	$T_1 = 0.00051238$
$\epsilon = 22.8377$	$\epsilon = 1.2100$	$\epsilon = 0.6089$
	Excited State	
$E = 40.4110$	$F = 28.2951$	$G = 28.0153$
$R_1 = 0.260686$	$S_1 = 0.057801$	$T_1 = 0.00052057$
$\epsilon = 22.9087$	$\epsilon = 1.2454$	$\epsilon = 0.6435$

The author wishes to thank Professor E. U. Condon for his suggestions in connection with this work.

[2] Brown, Bartlett and Dunn, Phys. Rev. **44**, 298 (1933).

Approximate Wave Functions for High Energy Electrons in Coulomb Fields

W. H. FURRY,* *University of California, Berkeley*

(Received June 28, 1934)

In this paper we construct approximate solutions of the Dirac equations for an electron in a Coulomb field of force, which reduce at large distances to plane waves. For very high energy electrons these functions satisfy the wave equations to terms of the orders $(\alpha^2/r)\sin^2\theta/2$, $(\alpha^2/r)\sin\theta/2$. Thus they are everywhere at least as accurate as the functions obtained by first order approximation methods, and for $\theta\to 0$ they satisfy the equations exactly. They therefore give an improved method for treating problems in which high energy electrons are ejected in a narrow angular range. The functions are simple in form and quite similar to the Gordon-Temple solutions of the Schrödinger equation in parabolic coordinates.

I. INTRODUCTION

PROBLEMS in which an electron moving in a Coulomb field makes transitions to or between states of very high energy present great difficulties when one attempts their solution with the use of exact Dirac wave functions for the high energy states of the electron. These difficulties have been pointed out by Hall and Oppenheimer[1] in the case of the photoelectric effect; they occur also in the problems of production of high energy electron pairs by γ-rays or electrons, of the radiative impacts of electrons with nuclei and of the scattering of very hard radiation by bound electrons.

As remarked by Hall and Oppenheimer,[1] the difficulties result from the fact that the system of spherical coordinates, in which alone exact Dirac wave functions are available, is not at all adapted to the conditions of these problems. This is so because the high energy wave packets with which one has to deal are concentrated into very small angles and could have a simple description only in terms of wave functions having essentially the character of plane waves. Their resolution in terms of spherical waves requires the use of spherical harmonics of very high order, the order becoming infinite with the energy of the electron under consideration. This means that in calculating transition probabilities one is concerned with a sum of squares of matrix elements in which a great many terms contribute appreciably; all these terms refer to very large values of the angular momentum quantum number and the evaluation of any single term is extremely difficult.

A knowledge of the predictions of quantum electrodynamics regarding such processes is highly desirable in the present state of experiment and theory. Such information has usually been sought by the use of the plane wave functions of a high energy free electron, the Coulomb potential of the nucleus being taken into account by the Born approximation method in case the binding of the high energy electron is essential to the occurrence of the effect.[2] This procedure avoids the use of an unfortunate coordinate system and makes the calculation reasonably manageable in most cases. On the other hand, its approximate nature makes it necessary to consider carefully the limitations beyond which we can no longer have complete confidence in the correctness of the results.

The Coulomb binding of the electron is characterized by a certain length, the Bohr radius $a=h^2/(4\pi^2 mZe^2)$. This length becomes infinite for vanishing nuclear charge Z; and the ratios of other lengths appearing in the problem to the length a are the parameters characterizing the effect of the binding. It seems reasonable to suppose that when these are small the approximate procedure just described gives correct results. Now the lengths occurring are first of all the de Broglie wave-lengths of the electron in its

* National Research Fellow.

[1] Harvey Hall and J. R. Oppenheimer, Phys. Rev. **38**, 57 (1931); Harvey Hall, Phys. Rev. **45**, 620 (1934).

[2] The plane wave calculation for the photoelectric effect is described in the first paper of reference 1. Correctly carried through, it leads to the result first obtained by F. Sauter (Ann. d. Physik **11**, 454 (1931)) using a different approximate method. Definitive results of the Born approximation calculations for production of pairs by γ-rays and for radiative impacts of fast electrons with nuclei were first obtained by Heitler and Sauter; for preliminary notice see Nature **132**, 892 (1933).

different states and the wave-length of the light quantum, and for high energies these are small. But one must consider also the de Broglie wave-lengths corresponding to differences of the various momenta, in particular to the momentum imparted to the nucleus. At high energies, $h\nu \gg mc^2$ for the light quantum, this gives the parameter

$$\lambda \sim \alpha(1-\alpha^2)^{-\frac{1}{2}}, \quad \alpha = 2\pi Ze^2/hc \sim Z/137$$

for the photoelectric effect and

$$\lambda \sim \alpha(h\nu/2mc^2)$$

for pair production and radiative impacts.[3] Thus even for light elements we cannot be sure that the results of the Born approximation treatment of these latter problems are right for very large $h\nu/mc^2$. At such large energies important contributions to the matrix integrals come from the region of space straight forward from the nucleus; and in this region within and near the caustic of the classical trajectories[4] the Born wave functions become completely unreliable.

In the present paper we shall construct approximate Dirac wave functions for a high energy electron in a Coulomb field which, like the Born functions, have a type of symmetry adapted to the problems mentioned above and which are superior to the Born functions in just the respect which seems essential for the obtaining of more reliable answers to these problems; namely, they satisfy the Dirac equations everywhere in space to the first power of α and in the region of very small angles—within and near the caustic—they satisfy the equations to a much higher degree of approximation.

The construction of these functions follows closely the procedure which Gordon used originally to obtain the nonrelativistic wave function in parabolic coordinates.[5] This he did by forming a suitable linear combination of the spherical coordinate solutions. When one starts with normalized functions and chooses the coefficients so that a normalized function results, this procedure is essentially the application of a unitary transformation; it suffices to carry through explicitly the application of one row of the transformation matrix, which gives the linear combination used by Gordon. In the relativistic case there exists a similar unitary transformation which takes us from the spherical coordinate wave functions of a free electron to the plane wave functions. But the application of this transformation to the spherical wave functions of an electron in a Coulomb field leads to series which have no simple analytical expressions. To obtain the desired result we must resort to approximations. The approximations in question consist in the neglect of terms of the order α^2/l^2 compared to those kept and should not impair the usefulness of the results for problems in which only the contributions from large values of l need to be treated accurately.

II. Construction of the Functions

In our calculations we shall make exclusive use of the system of units which is best adapted to the problems of the high energy electron. Energies are measured in units mc^2, momenta in units mc and lengths in units $h/(2\pi mc)$, where m is the rest mass of the electron. Equations in these natural units may be obtained from those in c.g.s. units by setting $h/2\pi$, m and c equal to unity and e, the charge of the electron, equal to the square root of the fine structure constant; the return to c.g.s. units may readily be made by dimensional considerations. We use α to denote Z times the fine structure constant and write ϵ and k, respectively, for the absolute values of the energy and momentum of the electron when infinitely distant from the nucleus. Thus $k=(\epsilon^2-1)^{\frac{1}{2}}$.

We take as our starting point the spherical coordinate wave functions in the form given by Hulme,[6] writing l for the quantum number which he calls k. In our present units and notation, the values of some of Hulme's symbols are:

$$|B|/A = k/(\epsilon+1); \quad a=k; \quad b=\epsilon\alpha/k; \quad c=\alpha/k.$$

[3] By similar considerations one can determine the possible effects of screening on the results. Since the length characteristic of the screening is $Z^{\frac{1}{3}}a$, screening can scarcely come into account for the photoelectric effect, and for the pair production and radiative impacts it can be important only at energies much higher than that at which the validity of the Born approximation results first becomes open to question.

[4] Cf. first part of Gordon's paper (reference 5).

[5] W. Gordon, Zeits. f. Physik **48**, 180 (1928).

[6] H. R. Hulme, Proc. Roy. Soc. **A138**, 643 (1932).

Taking the quantum number u equal to 0, we have, apart from a constant factor in each solution,

$$\psi_{1l}=ik(l+1)P_{l+1}F_l, \qquad \psi_{3l}=-(\epsilon+1)(l+1)P_lG_l,$$
$$\psi_{2l}=ikP^1{}_{l+1}e^{i\varphi}F_l, \qquad \psi_{4l}=(\epsilon+1)P_l{}^1e^{i\varphi}G_l \tag{1}$$

and

$$\psi_{1l}'=iklP_{l-1}F_{-l-1}, \qquad \psi_{3l}'=-(\epsilon+1)lP_lG_{-l-1},$$
$$\psi_{2l}'=-ikP^1{}_{l-1}F_{-l-1}, \qquad \psi_{4l}'=-(\epsilon+1)P_l{}^1e^{i\varphi}G_{-l-1}. \tag{2}$$

The P_l^m are Legendre functions of $x=\cos\theta$; we use the ordinary unnormalized functions, not those defined by Darwin which Hulme uses. F_l, G_l, F_{-l-1}, G_{-l-1} are real and are defined by

$$G_l=F_l+iG_l, \qquad G_{-l-1}=F_{-l-1}+iG_{-l-1},$$

$$G_l=[(l-s)-i\alpha(\epsilon+1)/k]\rho^s\int_{-1}^{1}(1-u)^{s-ib+1}(1+u)^{s+ib}e^{i\rho u}du, \tag{3}$$

$$G_{-l-1}=[\alpha(\epsilon-1)/k+i(l-1-s')]\rho^{s'}\int_{-}^{1}(1-u)^{s'-ib+1}(1+u)^{s'+ib}e^{i\rho u}du,$$

where $\rho=kr$ and, as in Hulme's notation,

$$s=\{(l+1)^2-\alpha^2\}^{\frac{1}{2}}-1, \quad s'=\{l^2-\alpha^2\}^{\frac{1}{2}}-1.$$

These functions are, apart from notation and constant factors, just those of Hulme and are exact solutions of the Dirac equations in spherical coordinates. We now proceed to simplify these solutions by neglecting consistently terms of orders $(1/\epsilon^2)$ or (α^2/l^2) compared to those kept. Then apart from constant factors:

$$G_l=\{-i+(\alpha/2)(1-\epsilon^{-1})/(l+1)\}\rho^l(1+i(d/d\rho))S_l(\rho),$$
$$G_{-l-1}=\{1+i(\alpha/2)(1+\epsilon^{-1})/l\}\rho^{l-1}(1+i(d/d\rho))S_{l-1}(\rho) \tag{3'}$$

with

$$S_l(\rho)=S_l^*(\rho)=e^{i\rho}F(l+1-i\alpha,\ 2l+2,\ -2i\rho).$$

Write $\rho^lS_l(\rho)=R_l(\rho)$. Then from the recurrence formulae[7]

$$bF(a,\ b,\ x)=(b-a)F(a,\ b+1,\ x)+aF(a+1,\ b+1,\ x),$$
$$xF(a,\ b,\ x)=-(b-a)F(a-1,\ b,\ x)+(b-2a)F(a,\ b,\ x)+aF(a+1,\ b,\ x)$$

we find that

$$\rho^lS_l'(\rho)=-(2l+3)^{-1}\{1+\alpha^2/(l+1)^2\}R_{l+1}-\alpha(l+1)^{-1}R_l.$$

For our present purposes the term with $\alpha^2/(l+1)^2$ is to be neglected.

If now we insert the approximate values of F_l, G_l, F_{-l-1}, G_{-l-1} so found into (1) and (2) and also multiply the two approximate solutions by the respective factors

$$2^l(k/2\pi)e^{\pi\alpha/2}\Gamma(l+1-i\alpha)\{(2l+1)\,!\}^{-1}\{\epsilon(\epsilon+1)(l+1)\}^{-\frac{1}{2}}\{1-i(\alpha/2)(1-\epsilon^{-1})(l+1)^{-1}\}$$

and

$$2^l(k/2\pi)e^{\pi\alpha/2}\Gamma(l+1-i\alpha)\{(2l)\,!\}^{-1}\{\epsilon(\epsilon+1)l\}^{-\frac{1}{2}}\{1+i(\alpha/2l)(1-\epsilon^{-1})\};$$

neglecting small terms as before, we get

$$\psi_{1l}=-NP_{l+1}\{ik(l+1)K_{l+1}+i(\alpha/2)(\epsilon+1)(K_l+iK_{l+1})\},$$
$$\psi_{2l}=-N(l+1)^{-1}P^1{}_{l+1}e^{i\varphi}\{\text{same as for } \psi_{1l}\},$$
$$\psi_{3l}=NP_l\{(\epsilon+1)(l+1)K_l-i(\alpha/2)k(K_l+iK_{l+1})\}, \tag{1'}$$
$$\psi_{4l}=-N(l+1)^{-1}P_l{}^1e^{i\varphi}\{\text{same as for } \psi_{3l}\}$$

[7] Derived, in a different notation, by P. S. Epstein, Phys. Rev. **28**, 695 (1926).

and

$$\begin{aligned}
\psi_{1l}' &= N'P_{l-1}\{iklK_{l-1}+i(\alpha/2)(\epsilon+1)(K_l-iK_{l-1})\},\\
\psi_{2l}' &= -N'l^{-1}P^1{}_{l-1}e^{i\varphi}\{\text{same as for } \psi_{1l}'\},\\
\psi_{3l}' &= N'P_l\{(\epsilon+1)lK_l+i(\alpha/2)k(K_l-iK_{l-1})\},\\
\psi_{4l}' &= N'l^{-1}P_l^1e^{i\varphi}\{\text{same as for } \psi_{3l}'\},
\end{aligned} \tag{2'}$$

where $N=\{8\pi\epsilon(\epsilon+1)(l+1)\}^{-\frac{1}{2}}$, $N'=\{8\pi\epsilon(\epsilon+1)l\}^{-\frac{1}{2}}$

and

$$K_l=2^l(2/\pi)^{\frac{1}{2}}ke^{\pi\alpha/2}\Gamma(l+1-i\alpha)\{(2l+1)!\}^{-1}R_l(\rho).$$

Here K_l is a radial function normalized in the k-scale.[5] For $\alpha=0$, (1′) and (2′) become correct wave functions normalized in the k-scale. For $\alpha\neq0$, their normalization is inaccurate by factors of the form $1+0(\alpha^2/l^2)$; this is the sort of inaccuracy which they contain in other respects, also, and which we are neglecting.

We now proceed to form a linear combination of the approximate solutions (1′) and (2′), using coefficients which in the case $\alpha=0$ produce normalized plane wave solutions out of normalized spherical wave solutions and which therefore form a row of a unitary transformation matrix. These coefficients are, respectively:

$$C_l=i^lk^{-1}(4\pi)^{-\frac{1}{2}}(l+1)^{\frac{1}{2}} \quad \text{and} \quad C_l'=i^lk^{-1}(4\pi)^{-\frac{1}{2}}l^{\frac{1}{2}}.$$

Setting[8]

$$\varphi=\sum_{l=0}^{\infty}C_l\psi_l+\sum_{l=1}^{\infty}C_l'\psi_l',$$

we have

$$\begin{aligned}
\varphi_1&=-N''\{kS-i(\alpha/2)(\epsilon+1)S'\}, & \varphi_3&=N''\{(\epsilon+1)S-i(\alpha/2)kS'\},\\
\varphi_2&=-N''i(\alpha/2)(\epsilon+1)S''e^{i\varphi}, & \varphi_4&=N''i(\alpha/2)kS''e^{i\varphi},
\end{aligned}$$

where

$$N''=(2\pi)^{-\frac{1}{2}}\{2\epsilon(\epsilon+1)\}^{-\frac{1}{2}},$$

$$S=(\pi/2)^{\frac{1}{2}}k^{-1}\sum_{l=0}^{\infty}i^l(2l+1)K_lP_l,$$

$$S'=(\pi/2)^{\frac{1}{2}}k^{-1}\{\sum_{l=0}^{\infty}i^{l+1}P_l(K_{l+1}+K_{l-1})+K_0-iK_{-1}\},$$

$$S''=(\pi/2)^{\frac{1}{2}}k^{-1}\{(1+x)\sum_{l=1}^{\infty}i^l(2l+1)l^{-1}(l+1)^{-1}P_l^1K_l+P_1^1K_0\}.$$

K_{-1} has not yet been defined and its value is arbitrary. In deriving the form given for S'' we have used the recurrence formula

$$lP^1{}_{l+1}(x)+(l+1)P^1{}_{l-1}(x)=(2l+1)xP_l^1(x),$$

which holds for $l\geq1$ if we set $P_0^1=0$.

For S Gordon obtained the value[5]

$$S=e^{\pi\alpha/2}\Gamma(1-i\alpha)e^{i\rho z}F(i\alpha,\,1,\,i\rho(1-x)).$$

To evaluate S' and S'' we must use Gordon's relation[5, 9]

$$K_l=(k/2\pi i)e^{3\pi\alpha/2}\Gamma(1-i\alpha)\oint e^{i\rho s}[\rho(1-s)]^{-\frac{1}{2}}J_{l+\frac{1}{2}}[\rho(1-s)]s^{i\alpha-1}(1-s)^{-i\alpha}ds.$$

[8] This summation is extended over the ranges of l for which the solutions are valid. Terms containing P_0^1 are to be regarded as vanishing. Cf. reference 12.

[9] The contour is as specified in reference 5.

Letting this serve to define K_{-1}, we have $K_{-1}=-iK_0$. The evaluation of S' and S'' thus depends on evaluating the sums

$$\bar{S}'=(\pi/2)^{\frac{1}{2}}\sum_{l=0}^{\infty} i^{l+1}\cdot\sigma^{-\frac{1}{2}}[J_{l+\frac{1}{2}}(\sigma)+J_{l-\frac{1}{2}}(\sigma)]P_l(x),$$

$$\bar{S}''=(\pi/2)^{\frac{1}{2}}\sum_{l=1}^{\infty} i^{l}(2l+1)l^{-1}(l+1)^{-1}\sigma^{-\frac{1}{2}}J_{l+\frac{1}{2}}(\sigma)P_l^1(x),$$

where $\sigma=\rho(1-s)$ and on performing contour integrations. On using the recurrence formula

$$J_{n+1}(\sigma)+J_{n-1}(\sigma)=2n\sigma^{-1}J_n(\sigma)$$

we have

$$\bar{S}'=i\sigma^{-1}(\pi/2)^{\frac{1}{2}}\sum_{l=0}^{\infty} i^{l}(2l+1)\sigma^{-\frac{1}{2}}J_{l+\frac{1}{2}}(\sigma)P_l(x)=i\sigma^{-1}e^{i\sigma z};$$

and the contour integration gives

$$S'=e^{\pi\alpha/2}\Gamma(1-i\alpha)(1-x)e^{i\rho z}F(1+i\alpha,\,2,\,i\rho(1-x)).$$

To evaluate $\bar{S}''$ we use the relations

$$(\pi/2)^{\frac{1}{2}}i^{l}\sigma^{-\frac{1}{2}}J_{l+\frac{1}{2}}(\sigma)=\tfrac{1}{2}\int_{-1}^{1}e^{i\sigma t}P_l(t)dt \quad\text{and}\quad P_l^1(x)=(1-x^2)^{\frac{1}{2}}dP_l(x)/dx.$$

Now

$$\sum_{l=1}^{\infty}(l+\tfrac{1}{2})l^{-1}(l+1)^{-1}P_l(t)P_l(x)=\begin{cases}-\tfrac{1}{2}\ln[(1-t)(1+x)]+\ln 2-\tfrac{1}{2}, & t\leqslant x;\\ -\tfrac{1}{2}\ln[(1+t)(1-x)]+\ln 2-\tfrac{1}{2}, & t\geqslant x;\end{cases}$$

being just the Green's function in the extended sense for Legendre's equation.[10] For $-1+\delta<x<1-\delta$, $\delta>0$ the convergence is uniform and we can interchange differentiation, integration and summation. Then

$$\bar{S}''=(1-x^2)^{\frac{1}{2}}[i(2\sigma)^{-1}(1+x)^{-1}(e^{i\sigma z}-e^{-i\sigma})+i(2\sigma)^{-1}(1-x)^{-1}(e^{i\sigma z}-e^{i\sigma})].$$

On carrying out the contour integration one finds that the term $e^{i\sigma}$ contributes nothing, that in $e^{-i\sigma}$ just cancels the term $P_1^1K_0$ and we have

$$S''=e^{\pi\alpha/2}\Gamma(1-i\alpha)(1-x^2)^{\frac{1}{2}}e^{i\rho z}F(1+i\alpha,\,2,\,i\rho(1-x)).$$

Being continuous in x, this result holds without the restriction $-1+\delta<x<1-\delta$.

Thus the resulting approximate wave function is:

$$\begin{aligned}\varphi_1&=-\bar{N}\{kf-i(\alpha/2)(\epsilon+1)(1-\cos\theta)f'\},\\ \varphi_2&=-\bar{N}i(\alpha/2)(\epsilon+1)\sin\theta e^{i\varphi}f',\\ \varphi_3&=\bar{N}\{(\epsilon+1)f-i(\alpha/2)k(1-\cos\theta)f'\},\\ \varphi_4&=\bar{N}i(\alpha/2)k\sin\theta e^{i\varphi}f',\end{aligned}\tag{4}$$

where

$$\bar{N}=(2\pi)^{-\frac{1}{2}}\{2\epsilon(\epsilon+1)\}^{-\frac{1}{2}}e^{\pi\alpha/2}\Gamma(1-i\alpha),$$

$$f=e^{ikr\cos\theta}F(i\alpha,\,1,\,ikr(1-\cos\theta)),$$

$$f'=e^{ikr\cos\theta}F(1+i\alpha,\,2,\,ikr(1-\cos\theta)).$$

[10] Courant-Hilbert, *Methoden der Mathematischen Physik*, pp. 322–323 (2nd edition).

An identical repetition of the above arguments, starting with Hulme's functions for $u=-1$, leads to the second function:

$$\begin{aligned}\varphi_1'&=-\bar{N}i(\alpha/2)(\epsilon+1)\sin\theta e^{-i\varphi}f',\\ \varphi_2'&=\bar{N}\{kf-i(\alpha/2)(\epsilon+1)(1-\cos\theta)f'\},\\ \varphi_3'&=-\bar{N}i(\alpha/2)k\sin\theta e^{-i\varphi}f',\\ \varphi_4'&=\bar{N}\{(\epsilon+1)f-i(\alpha/2)k(1-\cos\theta)f'\}.\end{aligned}\tag{5}$$

The two functions (4) and (5) become, either for $\alpha\to 0$ or for $r\to\infty$, the ordinary plane wave functions for a free electron of positive kinetic energy and positive or negative spin component. Functions for negative kinetic energy

may be obtained from them by the transformation

$$\varphi_1\to\varphi_3,\quad \varphi_2\to\varphi_4,\quad \varphi_3\to-\varphi_1,\quad \varphi_4\to-\varphi_2,\quad \alpha\to-\alpha,$$

as is readily seen from the form of the wave equations.[11]

On substituting (4) or (5) in the wave equations,[11] we obtain as the terms which fail to cancel out in the left member quantities of orders

$$(\alpha/2\epsilon)\sin^2\theta/2,\quad (\alpha/2\epsilon)\sin\theta/2,\quad (\alpha^2/r)\sin^2\theta/2,$$

and

$$(\alpha^2/r)\sin\theta/2$$

compared to the wave functions themselves. Thus, for very large ϵ we are left, as in the case of the Born functions, with a discrepancy of order α^2; but for $\theta\to 0$, in the region where the Born functions fail, the discrepancy in the present case becomes vanishingly small.

The functions as given are normalized in the scale of k_x, k_y and k_z; those we have obtained here are for $k_x=k_y=0$, $k_z=k$. The functions for any other direction of k may be obtained by a rotation of coordinates of the type required by Dirac wave functions.[12] Apart from this the use of the functions is similar to that described for the nonrelativistic case by Sommerfeld.[13]

The set of functions thus obtained is not a complete orthogonal set when $\alpha\neq 0$, but in the solution of problems it is to be used as if it were such a set. This is explained as follows: In the exact solution of the sort of problem for which these functions are intended one is concerned with the evaluation of a sum of the form

$$\sum_{lu} V'_{n';\,lu}V_{lu;\,n},$$

where V and V' are interaction energies, and l, u are angular momentum quantum numbers designating the spherical coordinate wave functions; n and n' denote states of the electron. In problems such as the photoelectric effect, pair production and radiative impacts one has $V'=V$, $n'=n$; in other problems such as that of the scattering of very hard radiation this is not so. The use of the set of functions here derived is to be justified by the relation

$$\sum_{lu} V'_{n';\,lu}V_{lu;\,n}\approx\sum_{lu}(V'_{n';\,lu})'(V_{lu;\,n})'$$

$$=\sum_{\sigma}\int d\omega\cdot V'_{n';\,\theta\varphi\sigma}V_{\theta\varphi\sigma;\,n}.$$

Here $(V_{lu;\,n})'$ and $(V'_{n';\,lu})'$ are calculated with the modified wave functions typified by (1′) and (2′); and $V_{\theta\varphi\sigma;\,n}$ and $V'_{n';\,\theta\varphi\sigma}$ are calculated with the approximate wave functions typified by (4) and (5), suitably renormalized, $d\omega$ being an element of solid angle containing the direction $(\theta,\ \varphi)$ and σ denoting the two spins. The approximate equality of the first two members is based on the fact that only very large values of l contribute appreciably to the sums and that for large l the matrix elements calculated from (1′) and (2′) are presumably very nearly equal to those calculated with the exact functions; the equality of the second and third members follows from the unitary character of the transformation from the set of functions typified by (1′) and (2′) to the set typified by (4) and (5).

The approximate equality of two sums which is involved in the above argument cannot be regarded as established with certainty by the physical arguments given in the introduction. On the other hand it could be proved rigorously only by making special considerations for each individual problem, and in doing this it would be necessary to overcome a large part at least of the difficulties which inhere in the exact solution of these problems using spherical coordinates. Thus the type of function which we have here constructed is best regarded as the basis of a method which is admittedly only approximate and subject to possible failures, but physically reasonable and probably reliable for the cases for which it was devised.

The writer wishes to thank Professor J. R. Oppenheimer, who suggested the construction of these functions, for much helpful advice.

[11] For the Dirac wave equations completely written out in the form which is the basis of the present work, see for example H. R. Hulme, Proc. Roy. Soc. **A133**, 382 (1931). The equations are to be put into natural units as we have previously explained.

[12] C. G. Darwin, Proc. Roy. Soc. **A118**, 654 (1928).

[13] A. Sommerfeld, Ann. d. Physik **11**, 256 (1931).

Inelastic Collisions with Changes of Mass and the Problem of Nuclear Disintegration with Capture or Non-Capture of a Neutron or Another Nuclear Projectile

WILLIAM D. HARKINS AND DAVID M. GANS, *George Herbert Jones Laboratory, University of Chicago*

(Received April 13, 1934)

Relativity equations are developed for the relations involved in the disintegration of an atomic nucleus by bombardment with a nuclear projectile which is not captured in the process. Similar equations for velocities not too close to that of light are also developed; these are based on the rest-masses and the only relativity term is that involved in the change of mass produced by the collision ($E_m = c^2\Delta m$). The relativity equation for the velocity of the projectile is:

$$V_A = \frac{(k_C m_C v_C + k_D m_D v_D)^2 - c^2(k_C m_C + k_D m_D - m_B)^2 + 2c^2 k_A m_A (k_C m_C + k_D m_D - m_B)}{2k_A m_A (k_C m_C v_C + k_D m_D v_D)\cos\alpha}$$

while the similar equation for not too high velocities is:

$$V_A = \frac{[M^2 + 2m_A[E_C + E_D + c^2(m_C + m_D - m_B)]]}{2m_A M \cos\alpha}$$

in which M represents momentum, E is kinetic energy, m mass, v velocity, c the velocity of light, and A, B, C and D are the nuclei involved. If a γ-ray is emitted the expression between brackets in Eq. (16) contains in addition a term $E\gamma$. A careful analysis is made of the evidence which has formerly seemed to indicate that in the majority of disintegrations produced by neutrons the neutron is captured. The conclusion is reached that this evidence is valid. A similar analysis of the evidence for non-capture of the neutron indicates that this evidence is not valid. Thus the velocities given for the neutron as calculated by either Eq. (5′) or Eq. (16) are in general higher, when the nitrogen nucleus is disintegrated, than that of any known neutron. It is found that the curve which gives the relation between the number of disintegrations and the velocities of the neutrons which produce them, is practically the same for scattered as for non-scattered neutrons, provided both are assumed to disintegrate by capture. There seems to be no evidence which indicates that any nucleus has been disintegrated by bombardment of another nucleus without capture. Obviously this does not prove that non-capture disintegrations are non-existent.

I. INTRODUCTION

COLLISIONS between atomic nuclei may be elastic (Fig. 1), and since for such collisions both momentum and kinetic energy are conserved, the analysis is very simple. The relations involved in inelastic collisions are more complicated and less well defined. Some of the possible types of inelastic collisions are listed below.

1.

The nucleus of an atom may be excited by a non-capture collision of another nucleus.

$$A + B \rightarrow A + B^*.$$

The excited nucleus B^* may emit a γ-ray, or lose its excess of energy by disintegration, as, for example, by the emission of a positive or negative electron.

2.

The two nuclei may unite to form a single excited nucleus (AB^*) which may lose its excess energy by the emission of a γ-ray (continuous spectrum) or by disintegration to give a positive or negative electron (continuous spectrum).

$$A + B \rightarrow AB^*(+\gamma).$$

Excitations of this type are much less probable than those of type (1) and are often considered as "impossible" on account of the difficulty involved in (a) the taking up by AB of just the amount of kinetic energy which is available, and (b) meeting the simultaneous condition imposed upon the resultant velocity by the conservation of momentum. The probability of the occurrence of an excitation of this type without the emission of a γ-ray is very low since this requires resonance.

Objection may be raised to the assumption of the existence of the intermediate product AB^*. However, it may be assumed that this exists for the extremely minute time necessary for the exchange of A and B into C and D to take place. Furthermore, while it is often shown that the recombination of hydrogen atoms, except in multiple collisions, is extremely improbable, this is largely conditioned by the high symmetry, and certain other special circumstances which do not hold for all other pairs of atoms. Even with

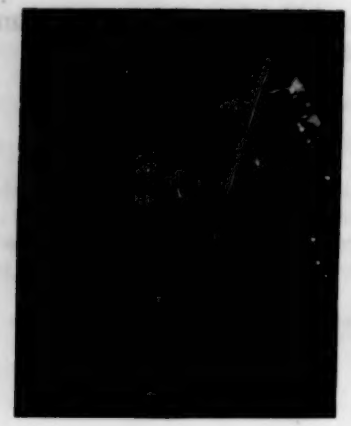

FIG. 1.

FIG. 2.

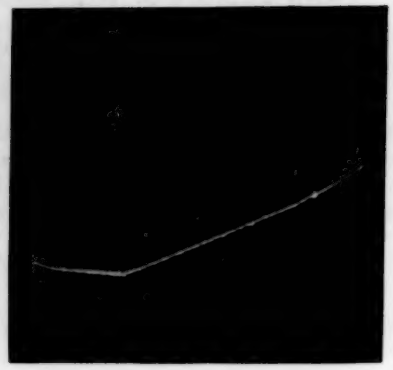

FIG. 3.

FIG. 1. Elastic collision of α-particle with argon nucleus.
FIG. 2. Disintegration of nitrogen ($_7{}^{14}N_0$) nucleus into oxygen ($_8{}^{17}O_1$) nucleus and proton ($_1{}^1H_{-1}$) by capture of α-particle ($_2{}^4He_0$).
FIG. 3. Disintegration of nitrogen ($_7{}^{14}N_0$) nucleus into a boron ($_5{}^{11}B_1$) nucleus and a helium ($_2{}^4He_0$) nucleus by capture of a neutron ($_0{}^1n_1$) from below. Angle ($\phi+\theta$) between visible tracks is 151°.

hydrogen atoms, it is possible to get combination by quadripole radiation. Pairs of nuclei seldom exhibit the high degree of symmetry shown by two hydrogen atoms.

3. Disintegrations by capture

$$A+B\rightarrow AB^*\rightarrow C+D.$$

The nuclei may unite to form an excited nucleus, with a life too short to be capable of measurement by any known method, which disintegrates into two or more nuclear particles. Such collisions are commonly designated as disintegrative-syntheses, or disintegrations by capture. Fig. 2 exhibits this type of collision for a case in which all of the nuclei which move with a high velocity give tracks which are visible in a Wilson chamber, while in Fig. 3 one of the particles involved is a neutron which leaves no visible track. There is evidence which indicates that in a part of the disintegrations of this type γ-rays are probably emitted.

An interesting type of disintegration by capture has been discovered recently by Irene Curie and F. Joliot.[1] This is found when boron, magnesium or aluminum is bombarded by α-rays. The reactions which they believe most probable for aluminum are

$$_{13}{}^{27}Al_1+{}_2{}^4He_0\rightarrow{}_{15}{}^{30}P_0+{}_0{}^1n_1$$

$$_{15}{}^{30}P_0\rightarrow{}_{14}{}^{30}Si_2+{}_1{}^0e_{-2}{}^+.$$

Curie and Joliot believe that $_7{}^{13}N_{-1}$ is formed from boron in a reaction similar to that of aluminum. This is of great interest, if true, since this would be the first known nuclear species other than the proton, which has an isotopic number less than zero.

The isotopic number (I) may be defined in terms of the Harkins-Masson formula, $(np)_Zn_I$, for any atomic nucleus, in which n represents a neutron and p, a proton, and Z is the atomic number. It was suggested by Harkins[2] that this might represent the composition of the nucleus, and this idea has been supported by Heisenberg[3] in several theoretical papers. If P is taken as the whole number closest to the atomic mass of the atom, and N is defined by the equation $P-Z=N$, then

$$I=P-2Z; \quad I=N-Z; \quad I=2N-P.$$

According to the idea suggested by Harkins as one possibility, and adopted in the theory of Heisenberg, N gives the total number of neutrons in the nucleus, and I gives the number of neu-

[1] Curie and Joliot, Comptes Rendus **198**, 254, 559 (1934).

[2] Harkins, Phil. Mag. **42**, 305–339 (1921); J. Am. Chem. Soc. **45**, 1427 (Table I, 1923).

[3] Heisenberg, Zeits. f. Physik **77**, 1–11 (1932); **78**, 156–164 (1932).

trons which are not associated with protons, or the number of "extra" neutrons.

Since a disintegration by capture and an elastic collision are alike in that in each the tracks are three straight lines which converge in a point, it is possible that some of the events which have been supposed to represent elastic collisions, as in Fig. 1, may actually be disintegrations. Thus let the reaction be

$$ {}_m{}^pA_r + {}_n{}^qB_s \rightarrow {}_{m+n}{}^{p+q}AB^*{}_{r+s} \rightarrow {}_m{}^pA_r' + {}_n{}^qB_s' $$
$$ {}_m{}^pA + {}_n{}^qB \rightarrow AB^* \rightarrow {}_m{}^pA' + {}_n{}^qB', $$

in which A' and B' have, respectively, the same charge and approximately the same mass as A and B, but do not contain the identical material. By sufficiently accurate work it would be possible to distinguish this from an elastic collision, provided the sum of the masses of A' and B' is not exactly that of A and B. If no change of internal energy is involved, there is no means known at present to determine whether a reaction of this type occurs, unless the scattering is sufficiently affected.

4. Disintegrations by non-capture (Fig. 5)

$$ A + B \rightarrow A + B^* \rightarrow A + C + D. $$

There is also the possibility that the nuclear projectile may not be captured; that is the two nuclei which meet at a high relative velocity may not unite, yet a nuclear disintegration may ensue.

While the mechanics of elastic collisions, and of disintegrations by capture, have both been given careful consideration, no attention has been paid to the relations involved in "disintegrations by non-capture." However, it is often assumed[4] as for example by Chadwick,[4] that disintegrations by non-capture have been found in the ejection of a proton from boron, or from aluminum (protons of 32 cm range) on bombardment by α-particles. More recently, however, Chadwick[5] seems to think that non-capture disintegrations have been found only when one of the particles is a neutron. Thus he states, "It seems probable that the neutron was not captured and that the ejected particle was a proton. If this view should prove correct, we have here the first example of a transmutation in which the bombarding particle is not captured." The evidence for non-capture disintegrations with neutrons in nitrogen, is considered by Langer[6] to be good, and that for capture disintegrations very weak. The point of view presented in this paper is exactly opposite: that is it is the evidence for capture which is strong.

II. Evidence for Disintegration by Capture

The evidence for the disintegration of a nitrogen nucleus by capture of an α-particle to give the following reaction

$$ {}_7{}^{14}N_0 + {}_2{}^4He_0 \rightarrow {}_8{}^{17}O_1 + {}_1{}^1H_{-1} $$

is so good as to be undisputed. This is due to the fact that in the photographs (e.g., Fig. 2) the track of every nucleus which has a high velocity is visible and the energy relations can therefore be determined with relatively great accuracy.

When the projectile is a neutron (Fig. 3) the evidence is less direct, since the track of a neutron is invisible. About 80 disintegrations of nitrogen nuclei by neutrons have been reported by Harkins, Gans and Newson,[7] who did not, however, consider the details of the evidence for disintegrations by capture.

Of the 80 pairs of photographs the best 28 pairs were measured with great care. Of these, 4 disintegrations found with a source of a different shape, were not included in considerations which follow. The source of the neutrons was nearly hemispherical in shape, with a horizontal diameter of 7 mm and a height of 4 mm. This was at the center of a Wilson chamber 17 cm in diameter, with an illuminated portion 2 cm high.

The first point of evidence which indicates capture is the fact that the plane of the two tracks of the disintegration particles passes through this source for 21 of the 24 events. The probability that this could be true by accident in the case of any specific disintegration was calculated from the distance of the point of disintegration from the center of the source (Fig. 5) and from the size of the source. The assumption was made that if normals through the center of the source are drawn to all of the

[4] Chadwick and Gamov, Nature, July 12, 1930; Chadwick, Constable and Pollard, Proc. Roy. Soc. **A130**, 463 (1930); Feather, Proc. Roy. Soc. **A136**, 709 (1932).
[5] Chadwick, Proc. Roy. Soc. **A142**, 21 (1933).
[6] R. M. Langer, Phys. Rev. **45**, 137 (1934).
[7] Harkins, Gans and Newson, Phys. Rev. **44**, 529 (1933).

planes which pass through this point, then the lines which represent these normals are distributed uniformly in space around the center of the source. The product of the 24 individual probabilities is found to be of the order of 10^{-22}. The probability that as many as 21 of the 24 planes should pass through the source was also calculated and found to be about 10^{-19}. The two fog tracks in each plane give an angle which in almost all cases points toward the source. Thus each plane exhibits a direction. If this direction is taken into account the probability is reduced from about 10^{-19} to about 10^{-25}.

It is found (Fig. 6) that the total number of disintegrations plotted as a function of the distance from the center of the source exhibit a linear relation up to a radius of about 45 mm beyond which the illuminated portion of the cloud chamber ceases to be cylindrical. A simple geometric theory agrees well with this except that it indicates a slight concavity toward the D axis. The line is displaced to the right on account of the fact that the platinum vessel which contains the source is 18 mm in diameter, and around this there is a certain amount of "dead" space in which only a part of the tracks are photographed. The intercept of the straight line with the x-axis is 14 mm from the center of the source, which gives the value of an apparent radius of the space not available for photography. One disintegration at 13 mm was found inside this region.

Early in the course of the work one of the photographed events which is coplanar with the source as, for example, that shown in Fig. 3, was selected for exact measurement and detailed study. A straight line (Fig. 4a) was drawn from the known position of the center of the course to the point B, and this was assumed to be the path of the neutron. The neutron was assumed to have been captured by the atom at B, which was a nitrogen atom. This would increase the mass from 14 to 15, then $x+y=7$; $u+z=15$, where x and y are whole numbers and represent the charges on the resulting nuclei C and D, while u and z are the whole numbers which represent their masses. For stable nuclei, except for protons $u \geqslant 2x$ and $z \geqslant 2y$.

The velocities of the nuclei C and D may be calculated from their ranges, provided the values of x, y, u and z are known.

The additional principle used in a determination of these values is that the momenta of C and D as resolved at right angles to the neutron path at B, must be equal in magnitude and opposite in sign. The best solution seemed to be given by

$$x=2 \quad u=4 \quad \text{or helium,}$$
$$y=5 \quad z=11 \quad \text{or boron.}$$

It was therefore considered that the reaction is

$$_7{}^{14}\mathrm{N}_0+{}_0{}^1n_1 \rightarrow {}_7{}^{15}\mathrm{N}_1 \rightarrow {}_5{}^{11}\mathrm{B}_1+{}_2{}^4\mathrm{He}_0.$$

If this same reaction is assumed for all of the other 23 disintegrations, then it is possible, by the principle of conservation of transverse momentum for C and D, to calculate for each event the direction of the neutron which would result in capture. The somewhat remarkable result is that for 20 of the remaining 23 disintegrations this line passes through the source. This reduces very greatly the already small (10^{-25}) probability that what occurred could have been given by chance. The total probability is of the order of 10^{-40}.

It is obvious that for any one of the 20 disintegrations indicated to occur by capture the neutron might have rebounded directly backward, even although the probability of this is extremely small, so that, so far as the evidence given above is concerned, any individual disinte-

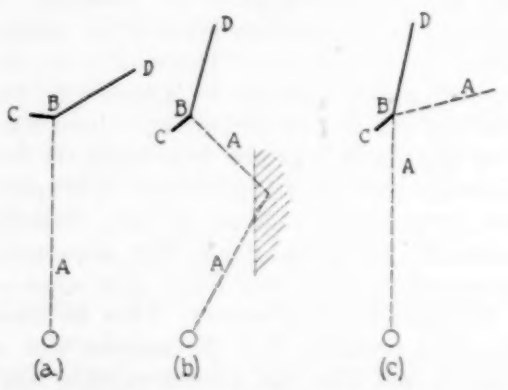

FIG. 4. (a) Diagram of disintegration of nucleus B by capture of projectile A directly from source; (b) diagram of the same disintegration by capture as for (a), except that projectile is first deflected by a nucleus in neighboring material; (c) diagram of disintegration of nucleus B by non-capture of projectile A directly from source.

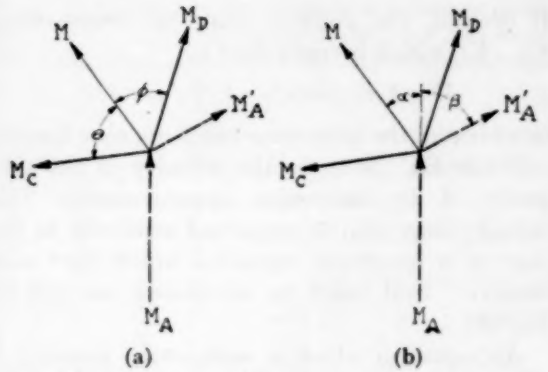

FIG. 5. Diagrams showing momentum vectors and defining angles in a disintegration by non-capture (Fig. 4c). M_C and M_D are not in general coplanar with M_A and M_A'. $M=M_C+M_D$ and $M_A=M+M_A'$.

Fig. 5b shows how the angle α is defined for events 20, 21 and 22, while for events 1, 6, 12 and 13 the value of α is zero (Fig. 4a).

gration may have occurred by non-capture. To determine whether this is possible it is essential to develop equations for the mechanics of such a process, which is, in general, associated with a change in the rest mass of the system. It is obvious that such equations are much more needed in connection with disintegrations which could not have been produced by the capture of a projectile directly from the source.

The largest error involved in the calculations used as a basis for the discussion of the evidence for non-capture is that due to the lack of accurate knowledge of the energy-range relations of ${}_5{}^{11}B_1$ and ${}_5{}^{10}B_0$.[8] However, the evidence for capture based upon the fact that the plane of the disintegration tracks passes through the neutron source for about 80 percent of the events recorded, is not affected by this error.

The fact that for about 70 percent of the events the vector which gives the vector sum of the momenta of the boron and helium atoms points directly away from the source, seems to indicate that the error involved in the range-velocity relations of the boron atoms is not very large.

III. Inelastic Nuclear Collisions with Changes of Mass

The mathematical relations involved in a collision in which the mass changes and the two nuclei unite, are comparatively simple, whether the nucleus thus formed remains intact for a moderate period of time or splits apart almost instantaneously to give a disintegration by capture.

The relations for a disintegration without capture (Figs. 4c and 5) are much less simple. A nuclear projectile A with a velocity $\mathbf{v}_A$ and a rest mass m_A strikes the nucleus B of mass m_B, which is at rest with reference to the frame of reference. The projectile A rebounds with the velocity $\mathbf{v}_A'$, and the same rest mass m_A. The nucleus B disintegrates into the nuclear particles C and D, with velocities $\mathbf{v}_C$ and $\mathbf{v}_D$ and rest masses m_C and m_D.

In general $m_C+m_D \neq m_B$ and the plane of $\mathbf{v}_C$ and $\mathbf{v}_D$ is different from that of $\mathbf{v}_A$ and $\mathbf{v}_A'$.

For any particle:

$$k_i=(1-v_i^2/c^2)^{-\frac{1}{2}} \tag{1}$$

in which c is the velocity of light. Then

$$k_i^2-k_i^2v_i^2/c^2=k_i^2(1-v_i^2/c^2)=1. \tag{2}$$

The rest masses of all of the particles involved are supposed to be known from positive ray or spectroscopic data. The velocities $\mathbf{v}_C$ and $\mathbf{v}_D$ (hence also k_C and k_D) of the disintegration particles may be calculated from the ranges of the visible tracks. The direction of $\mathbf{v}_A$, but not its magnitude, is supposed to be known, and is specified by the angle α between the direction of the initial momentum M_A of the projectile and the resultant momentum M of the disintegration particles C and D. The angles θ and ϕ (Fig. 5) are determined as described elsewhere.[7]

The relativity conservation equations for mass (3) and momentum (4) are

$$m_B+k_Am_A=k_A'm_A+k_Cm_C+k_Dm_D \tag{3}$$

$$k_Am_A\mathbf{v}_A=k_A'm_A\mathbf{v}_A'+k_Cm_C\mathbf{v}_C+k_Dm_D\mathbf{v}_D \tag{4}$$

in which the frame of reference is so chosen that $\mathbf{v}_B=0$, whence $k_B=1$.

The known quantities may be expressed in terms of the scalar K and the vector $\mathbf{W}$

$$K\equiv(k_Cm_C+k_Dm_D-m_B)/m_A=k_A-k_A', \tag{3'}$$

$$\mathbf{W}\equiv(k_Cm_C\mathbf{v}_C+k_Dm_D\mathbf{v}_D)/m_Ac$$
$$=k_A\mathbf{v}_A/c-k_A'\mathbf{v}_A'/c. \tag{4'}$$

[8] Harkins, Gans and Newson, reference 7, p. 536; Feather, Proc. Roy. Soc. **A142**, 689 (1933).

But by (2), (3′) and (4′)

$$k_A'^2 - k_A'^2 \mathbf{v}_A'^2/c^2 = 1 = (k_A - K)^2 - (k_A \mathbf{v}_A/c - \mathbf{W})^2$$

which reduces to

$$2k_A \mathbf{v}_A \cdot \mathbf{W} = c(W^2 - K^2) + 2k_A cK.$$

Now, since $\mathbf{v}_A \cdot \mathbf{W} = v_A W \cos \alpha$

$$v_A = [c(W^2 - K^2) + 2k_A cK]/2k_A W \cos \alpha. \quad (5)$$

For purposes of computation Eq. (4) may be expressed in the form:

$$v_A = [(F/k_A) + G]/J \cos \alpha \quad (6)$$

in which

$$G = 2cK = (2c/m_A)(k_C m_C + k_D m_D - m_B)$$

$$J = 2W = (2/m_A c)(k_C m_C v_C \cos \theta + k_D m_D v_D \cos \phi)$$

$$F = cJ^2/4 - G^2/4c.$$

Here F, G and $J \cos \alpha$ are calculated from the known quantities, and α is the angle between the direction of the projectile A and the resultant momentum of the disintegration particles C and D. Then, as a first approximation k_A is taken as unity and a preliminary value of v_A is calculated from Eq. (6). This value of v_A now gives a sufficiently accurate value of k_A to employ in Eq. (6), and a better value for v_A is calculated. If very great accuracy is desired, the calculation of k_A and of v_A may be repeated.

The velocity ($\mathbf{v}_A'$) of the projectile immediately after the collision may then be obtained from Eq. (3′), in which K and k_A are now known.

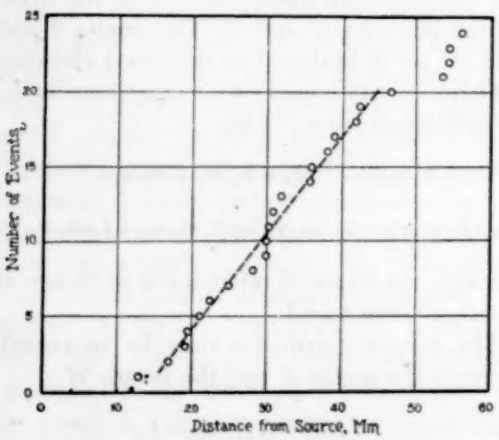

FIG. 6. Plot of the total number of disintegrations as a function of the distance from the center of the source. In general disintegrations at distances less than 14 mm are not visible, and so cannot be included.

If desired, the angle β may be found from Eq. (4′), which is equivalent to

$$W = k_A v_A \cos \alpha/c - k_A' v_A' \cos \beta/c$$

in which all the quantities but β are now known.

While Eq. (5) gives the velocity of the projectile A by successive approximation, this velocity may also be expressed explicitly as the root of a quadratic equation which does not, however, lend itself to calculation as well as Eq. (5).

An equation which is sufficiently accurate if the velocity is less than $c/6$ is derived below. The term E_m represents the rest mass which is derived from kinetic energy. If this is very small it may be negligible in comparison with the relativity corrections for velocity even if no velocity is greater than $c/6$. If this is true it does not mean that the equation fails, but merely that the approximate relations are given by the ordinary equations of mechanics.

In this derivation of the equation for v_A, m_X, v_X, M_X and E_X are the mass, velocity, momentum and kinetic energy of the particle X, and M is the resultant momentum of the particles C and D. The various angles involved are shown in Fig. 5, in which M_C and M_D are not in general coplanar with M_A and M_A'.

$$M = M_C \cos \theta + M_D \cos \phi \quad (7)$$

$$m_C + m_D = m_B + E_m/c^2 \quad (8)$$

$$E_A = E_A' + E_C + E_D + E_m \quad (9)$$

$$M \sin \alpha = M_A' \sin \beta \quad (10)$$

$$M \cos \alpha + M_A' \cos \beta = M_A. \quad (11)$$

Eliminating β from (10) and (11),

$$M_A^2 - M_A'^2 = 2M_A M \cos \alpha - M^2. \quad (12)$$

But by (9), $E_A - E_A' = E_C + E_D + E_m$ (13)

or $$M_A^2 - M_A'^2 = 2m_A(E_C + E_D + E_m). \quad (14)$$

Combining (12) and (14),

$$M_A = [M^2 + 2m_A(E_C + E_D + E_m)]/2M \cos \alpha \quad (15)$$

or

$$v_A = [M^2 + 2m_A(E_C + E_D + E_m)]/2m_A M \cos \alpha. \quad (16)$$

The velocity v_A' may be calculated by use of (14) since $M_A = m_A v_A'$, and the angle β determined from (10).

TABLE I. *Neutron velocities calculated from data on disintegration on the assumption of (A) non-capture and (B) capture.*
v_A (Initial velocity)$\times 10^{-9}$ cm sec.$^{-1}$ v_A' (Final velocity)$\times 10^{-9}$ cm sec.$^{-1}$

Event[a]	α	A. Non-capture							B. Capture
		Low velocity Eqs. (16) and (14); Relativity Eqs. (6) and (3′)					Elastic impact[d]		
		v_A (16)	v_A (6) I[b]	v_A (6) II[c]	v_A' (14)	v_A' (3′)	v_A	v_A'	
		a. Neutrons Directly from Source							
1	0°	5.54	5.51	5.49	3.66	3.71	1.01	0.88	1.89
6	0°	4.93	4.90	4.88	1.99	2.03	1.58	1.37	2.95
12	0°	5.35	5.22	5.18	0.66	0.85	2.52	2.18	4.70
13	0°	5.02	5.01	4.97	0.49	0.48	2.96	2.56	5.55
		b. Scattered Neutrons							
20	43°	7.70	7.65	7.62	6.46	6.49	1.37	1.27	1.93
21	47°	7.69	7.59	7.55	6.48	6.43	1.59	1.50	1.97
22	63°	10.22	10.20	10.03	9.33	9.26	3.10	3.02	2.65

[a] See Harkins, Gans and Newson, Phys. Rev. **44**, 533 (1933).
[b] Preliminary value (first approximation) by Eq. (6).
[c] Second approximation by Eq. (6).
[d] For equations, see Rutherford, Chadwick and Ellis, *Radiations from Radioactive Substances*. Macmillan, 1930, p. 241.

This equation might be modified to include the emission of a γ-ray, but unfortunately, the direction of emission of the γ-ray is not known. However, if the momentum of this ray, which for an energy of the order of 10 M.E.V. usually produces only a negligible effect, is neglected, the following approximate equation may be applied:

$$v_A = \frac{M^2 + 2m_A(E_C + E_D + E_m + E_\gamma)}{2m_A M \cos\alpha}. \quad (17)$$

IV. Relations for Disintegration by Non-Capture of a Neutron

Of the 24 disintegrations of a nitrogen nucleus, 3 are represented by tracks whose plane does not pass through the source. There are 3 disintegrations for which the plane passes through the source, but the orientation of the tracks in the plane indicates that the neutron could not have been captured provided it came in a straight line from the source. There are thus 6 which involved either (a) a deflection of the neutron in one of the walls of the chamber (Fig. 4b), and a subsequent disintegration by capture, or (b) a neutron which may have been scattered by the disintegration process which occurred with non-capture of the neutron (Fig. 4c).

In order to aid in a decision between these two possibilities (a) and (b), the five best of the nine photographs were taken for measurement. Data for all of the photographs are given by Harkins, Gans and Newson.[9] Feather does not give the data for the disintegrations of this type obtained by him so it is not possible to consider them here.

It was found in the case of event 26 that while the plane passed through the source, the orientation of the tracks was such as to prove that it cannot represent a non-capture disintegration by a neutron directly from the source. The necessary velocity (v_A) of a neutron directly from the source, if it were to produce a non-capture disintegration for event 28 was found to be greater than that of light if calculated by Eq. (16), and imaginary if by Eq. (6), and therefore also cannot be a non-capture disintegration by a neutron directly from the source.

In the three remaining cases, however, Table I shows it is just those few disintegrations that seem from qualitative phenomena to indicate a possibility of non-capture, which are shown by the application of the equations above to give improbably high velocities if non-capture is assumed. Thus the velocities (Table I) for non-capture are 7.5, 7.6 and 10 in units of 10^9 cm per sec., while the fastest neutron as yet discovered had a velocity of only 5.6,[10] and it has

[9] Harkins, Gans and Newson, reference 7, p. 533.
[10] Harkins, Gans and Newson, Phys. Rev. **43**, 584 (1933).

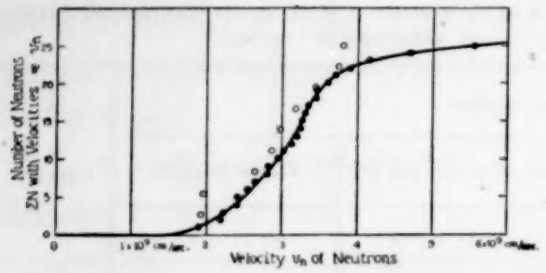

FIG. 7. Neutron velocities at impact for disintegration of $_7{}^{14}N_8$ by capture. Black circles represent events with neutrons directly from source. Open circles are for neutrons deflected prior to the disintegration.

been found that neutrons of velocities greater than 5.3 are extremely rare.[11] The obvious conclusion is that these are not disintegrations by non-capture but that they are caused by capture of neutrons which have experienced an earlier scattering by a close approach to an atomic nucleus in adjacent material.

Table I contains also a calculation of the velocity (v_A) of the neutron for events 1, 6, 12 and 13, which meet the criteria for capture but which are here recalculated as if by non-capture. It is thus assumed that the velocity (v_A') of the neutron just after the collision has exactly the opposite direction from the velocity (v_A) just before the collision.

In Fig. 7 the number of disintegrations is plotted against the neutron velocity for 25 disintegrations by capture of a neutron directly from the source (black circles), and for 9 disintegrations which are here assumed to occur by the capture of a previously scattered neutron (open circles). Since this is an integral curve the ordinates for the latter are multiplied by 25/9. If allowance is made for the inaccuracy introduced by the small number of disintegrations caused by scattered neutrons, it is seen that the form of the curve is very close to that given by the non-scattered neutrons, and that there is only an extremely slight shift of the curve toward lower velocities. This shift is to be expected since the initial scattering lowers the velocity of all of these neutrons. These relations give a further indication that all of the neutrons which produce disintegration are captured.

[11] Dunning, Phys. Rev. **45**, 590 (1934).

TABLE II. *Initial velocity of neutrons calculated on the assumption of non-capture disintegration by head-on collision (Eq. (16), $\alpha=0$) $v_A\times10^{-9}$ cm sec.$^{-1}$.*

Event	v_A	Event	v_A	Event	v_A	Event	v_A
1	5.54*	8	4.74	15	4.81	22	4.63
2	4.72	9	5.04	16	4.55	23	4.75
3	5.00	10	4.95	17	4.52	24	4.56
4	4.99	11	4.50	18	4.64	25	4.61
5	5.00	12	5.36	19	4.73	26	4.40
6	4.93	13	5.03	20	5.52	27	4.19†
7	5.26	14	4.73	21	5.34	28	4.70

* Maximum.
† Minimum.

Since it is possible that any one of the 28 disintegrations considered in this paper may have been caused by a head-on non-capture collision ($\alpha=0°$, $\beta=180°$) of a neutron with a nitrogen nucleus, the velocity (v_A) of each neutron has been calculated (Table II) on the basis of this assumption. In events 1 to 19 such a neutron would come directly from the source, and in events 20 to 28 it would be a deflected neutron. The lowest possible limit to the range of velocities is set by the fact that a neutron of velocity 3.7×10^9 cm sec.$^{-1}$ has a kinetic energy equal to that which is transformed into mass in the non-capture disintegration of nitrogen considered. The velocities of Table II give, for the kinetic energy of the neutron, a minimum slightly over 9 M.E.V. and a maximum of 16 M.E.V. These values are, as a whole, too high to be probable.

The general conclusion which is reached from all of the discussion presented in this paper is that there is no evidence which indicates that any nucleus has been disintegrated by bombardment with another nucleus without capture. This does not, of course, prove that non-capture disintegrations cannot occur, especially since the projectiles considered in this paper, although in general they have very high energies, nevertheless exhibit a much lower order of energy than those in cosmic rays.

The writers wish to thank Professor A. C. Lunn for his help in the mathematical analysis and to acknowledge a grant from the Alexander Dallas Bache Fund of the National Academy of Sciences, and a grant-in-aid of the National Research Council, which made possible this work and the earlier experimental investigations on which it is based.

Ionization of Air by Alpha- and Beta-Rays as a Function of Pressure

O. E. Polk, *Ryerson Physical Laboratory, University of Chicago*

(Received July 14, 1934)

Measurements of ionization of air by alpha-particles from polonium and by beta-rays excited by gamma-rays, were made under usual laboratory conditions. The ionization by beta-rays increased at a decreasing rate with increase in pressure, in accordance with results obtained in previous investigations. The ionization by alpha-particles decreased with increasing pressure, at first rapidly, then more slowly until, at 80 atmospheres, the value was approximately 5 percent of that at atmospheric pressure.

THE recent use of high pressure ionization chambers for measuring x-rays, gamma-rays and cosmic rays has raised anew the problem of ionization as a function of pressure. Many studies of ionization at pressures less than one atmosphere have been made.[1] At higher pressures, Erikson[2] performed pioneer experiments, using ionization by gamma-rays and working to pressures as great as 400 atmospheres. But with alpha-ray ionization almost no work seems to have been done until recent years.[3, 4, 5] The experiments of Erikson[2] and those of more recent investigators[4, 6, 7, 8, 9, 10] have shown that in air the ionization produced by beta-rays excited by gamma-rays is not proportional to the pressure but seems to approach a maximum at about 200 atmospheres and then decreases. With alpha-rays, it has long been known[1] that it is difficult to obtain a saturation ionization current, even at atmospheric pressure. Experiments by Steinke and Schindler[4] and Jacobsen and Madsen[5] have shown that at higher pressures the ionization by alpha-particles decreases to a small fraction of that at one atmosphere. Some discussion of the theory of these effects has been given by Rutherford,[1] Compton, Bennett and Stearns,[6] Bowen[8] and others.

For routine laboratory purposes, it was desirable to investigate, under usual laboratory conditions and with the same apparatus, the relationship of ionization of air by alpha-particles to that by beta-rays as a function of pressure. One occasion for making this comparison was the desire to learn how the residual radiation from the walls of an ionization chamber behaves as a function of pressure, the residual ionization being due to a mixture of alpha-, beta- and gamma-rays from radioactive impurities in the walls.

The apparatus used is a modification of that constructed and used by Bennett, Stearns and Compton[11] for the study of cosmic rays. It is shown diagrammatically in Fig. 1. The sources of ionization were: (*a*) beta-rays excited by gamma-rays; and (*b*) alpha-particles from polonium. The polonium was deposited electrolytically on a strip of platinum which was then placed at or near the center of the ionization chamber and about 2 millimeters from the electrode. A Lindemann electrometer, with sensitivity adjusted to 15 scale divisions per volt, was used to measure the ionization current. Two calibrated pressure gauges were used, one for pressures up to about 400 pounds per square inch, the other for higher pressures. The apparatus was left unshielded.

Beta-ray ionization at a given pressure was calculated as the difference between the value of the ionization current with the radium placed 1 meter from the electrode, then at infinity. In the latter case, the current was due to the effect of cosmic rays and local radiation. Alpha-ray

[1] Cf., e.g., E. Rutherford, *Radioactive Substances and their Radiations*, pp. 31–35 (1912).
[2] H. A. Erikson, Phys. Rev. **27**, 473 (1908).
[3] A. J. Dempster, Phys. Rev. **34**, 53 (1912).
[4] E. G. Steinke and H. Schindler, Naturwiss. **20**, 15 (1932).
[5] J. C. Jacobsen and C. B. Madsen, Naturwiss. **21**, 350 (1933).
[6] A. H. Compton, R. D. Bennett and J. C. Stearns, Phys. Rev. **39**, 873 (1932).
[7] R. A. Millikan and I. S. Bowen, Nature **128**, 582 (1932).
[8] I. S. Bowen, Phys. Rev. **41**, 24 (1932).
[9] J. W. Broxon, Phys. Rev. **42**, 321 (1932).
[10] J. J. Hopfield, Phys. Rev. **43**, 675 (1933).
[11] R. D. Bennett, J. C. Stearns and A. H. Compton, Phys. Rev. **41**, 119 (1932).

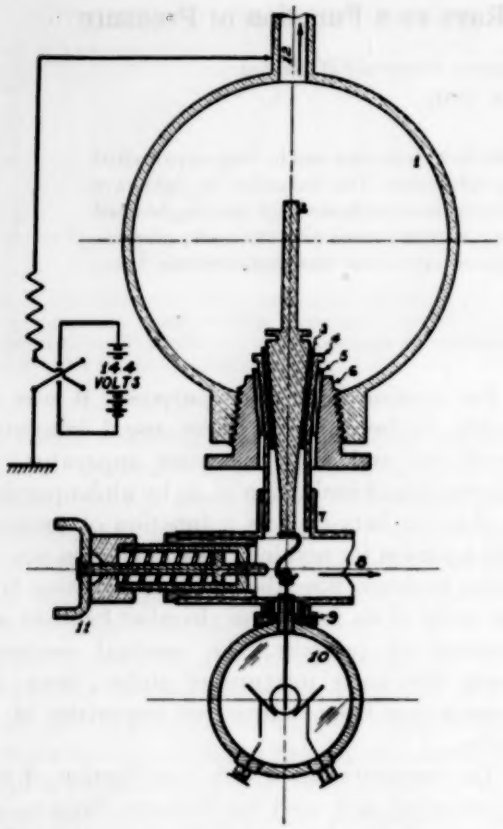

FIG. 1. Diagram of apparatus. 1, ionization chamber; 2, electrode; 3, amber cone; 4, brass cone; 5, rubber cone; 6, iron plug; 7, housing; 8, drying tube; 9, sponge rubber; 10, electrometer; 11, key; 12, inlet and gauges.

ionization was determined by measuring the difference in the values of the ordinates of two curves, the data for which were taken with, then without, polonium, respectively. In this manner the combined effect of cosmic rays, local radiation and contamination was eliminated. The data for beta-ray and alpha-ray ionization, calculated as indicated, are represented by Curve 1 and Curve 2, respectively, in Fig. 2. Curve 3 in Fig. 2 represents the ionization due to cosmic rays plus local radiation. The data for Curve 3 are multiplied by a factor of 10.

In general agreement with other investigations, the data show that, beginning at atmospheric

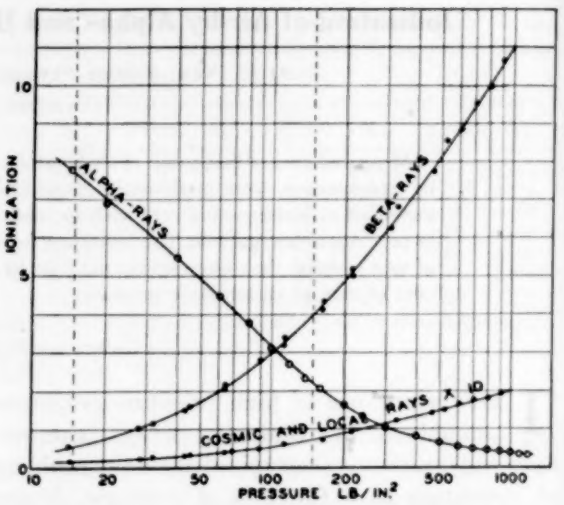

FIG. 2. Variation with pressure of the ionization due to alpha- and beta-rays.

pressure, ionization by beta-rays excited by gamma-rays increased at a diminishing rate with increase in pressure up to 60 atmospheres. On the other hand, ionization by alpha-particles from polonium, beginning at atmospheric pressure, at first decreased[4, 5] rapidly with increase in pressure, then more slowly until, at 80 atmospheres, about 5 percent of the initial value was reached. Saturation for the alpha-ray ionization was not attained.

These results indicate that in high pressure ionization chambers the wall effects due to alpha-rays are strongly though not completely suppressed relative to gamma-ray ionization. The relative importance of the beta-ray ionization from the walls is, on the other hand, not reduced by so great a factor as the pressure increases.

It is of interest to note that the form of the ionization-pressure curve for cosmic rays is similar to the beta-ray curve rather than to the alpha-ray curve. This supports the evidence from Wilson photographs that cosmic-ray ionization is due to particles of such high speed that the concentration of ions along their path is not high.

The writer wishes to thank Professor A. H. Compton for his suggestions in carrying out these experiments.

The Scattering of Lithium Ions by a Polycrystalline Nickel Surface

ANDREW LONGACRE, *Palmer Physical Laboratory, Princeton, New Jersey*

(Received July 13, 1933)

Positive ions scattered by a nickel target were measured both as to energy and quantity in various directions. The ions are scattered in a forwardly directed beam whose width at one-half the maximum intensity is about 45°. The direction of the maximum is independent of the incident energy and nearly so of the angle of incidence. The ratio of the most probable energy of the scattered ions to that of the incident ions is found to decrease as the total angle of scattering increases and to be independent of the energy or the angle of incidence. To a first approximation the energy distribution is found to be the same as that for projectiles of macroscopic size undergoing elastic impacts at a rough surface with a small coefficient of restitution.

THE investigation of the scattering of positive ions by a metal surface was undertaken at the same time by both Read[1] and Gurney[2] and has also been studied by Sawyer[3] and Woodcock.[4] The essential results found were that the ions were scattered in a forward direction and concentrated into a more or less well-defined beam. The position of the maximum concentration was associated by three investigators[1, 3, 4] with the specular direction while it was considered by the other[2] to be independent of that direction. It was also found that the mean energy of the scattered ions varies with the angle through which they are scattered.

The present work was undertaken to attempt to settle the question of association with specular reflection and to discover, if possible, any functional relation between the mean energy of the scattered ions and their direction.

THE APPARATUS

The apparatus was modeled somewhat after that used by Davisson and Germer[5] in their first electron diffraction experiments. The essential parts are shown in Fig. 1. The ion gun *G* and the target *T* rotated about the axis *O* that passed along the surface on the target perpendicular to the plane defined by the incident and collected beams. The outer walls of the gun, the target, the outer box of the collector *C*, *D*, and the frame supporting these were all of brass and interconnected, thus forming a field-free enclosure around the target.

The target *T* was a disk about 3.8 mm in diameter and 0.9 mm thick which had been cut from a piece of ordinary nickel rod. Although the polycrystalline surface had been highly polished by grinding with alundum and rouge, it lost this polish in the course of experimentation. Thus the results described are for a fine matte surface on three similar targets, numbered 1, 2 and 3. Precautions were always taken to keep the target clean. Also it was later heated to a bright red (1500°C) by radiation from the flat spiral tungsten filament *H* and thus thoroughly outgassed. To keep vapors from collecting on it during measurements it was kept at a dull red (500°C).

The inner box *C* of the collector was supported through its lead, so that the entire system of metallic connections between it and the electrometer was shielded from induction by an insulator supporting a difference of potential. The positive lithium ions were emitted thermionically from powdered spodumene[6] deposited on the small helical tungsten filament *F*.

The vacuum tube was in two sections which were connected by a large picein seal so that the apparatus might be easily removed for cleaning and reloading the source. Six long tubes extended from the under side of the larger section and enclosed the soft iron plungers which effected the changes in the positions of the gun and target. This section also had a Dewar seal holding a glass thimble near the metal parts. By keeping this filled with liquid air it served as a trap for vapors auxiliary to those traps in the vacuum system proper.

[1] G. E. Read, Phys. Rev. **31**, 629 (1928).
[2] R. W. Gurney, Phys. Rev. **32**, 467 (1928).
[3] R. B. Sawyer, Phys. Rev. **35**, 1090 (1930).
[4] K. S. Woodcock, Phys. Rev. **38**, 1696 (1931).
[5] C. Davisson and L. H. Germer, Phys. Rev. **30**, 750 (1927).
[6] K. T. Bainbridge, J. Frank. Inst. **212**, 317 (1931).

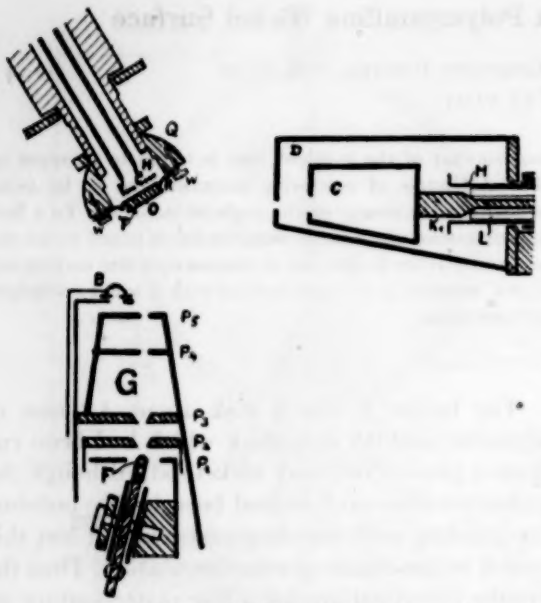

FIG. 1. 1.4 actual size.

The vacuum system consisted of a two-stage Pyrex mercury vapor pump backed by a Hy-Vac, a McLeod gauge, two liquid air traps and a Pirani gauge. The latter was as close to the tube as possible in order to detect fluctuations in pressure that might arise since the tube could not be baked out. The pumps were kept running continuously as long as the tube was assembled. The filament H (Fig. 1) was made to heat the entire tube until the walls in the immediate vicinity of the apparatus were about 50°C and no data were taken until the pressure remained below 10^{-5} mm of mercury. The mean free path of a positive ion with 100 or more volts kinetic energy is then greater than the 30 mm from the source to the collector.

THE PROCEDURE

Because of the construction of the apparatus the target carriage had to be clamped either to the gun or to the collector at an arbitrary angle before assembling it in the vacuum tube. Thus either the angle of incidence Φ, or the angle of scattering Θ, was determined. With Φ fixed and the acceleration voltages (V_{FA} between the filament F and the plate P_2, and V_{FG} between the filament F and the plate P_3 plus the rest of the metal parts) constant, two procedures were followed. The first led to a determination of the intensity distribution and consisted in measuring the current i as a function of the angle of scattering Θ when the retarding potential was kept zero. The second procedure led to a determination of the energy distribution. It consisted in measuring the current i to the collector C as the retarding potential V_{GS} between the boxes C, D was varied. The most probable energy E' of the ions scattered through the angle Θ was then obtained from the curve. By changing Θ and repeating, E' was measured as a function of Θ.

RESULTS AND DISCUSSION

Properties of the incident beam

Preliminary tests, with the target carriage removed, showed the incident beam to be relatively homogeneous as to energy (± 2.5 volts) and of small angular divergence ($<2°$). These properties vary somewhat with the relative values of V_{FA} and V_{FG}. The best conditions were found for V_{FA} equal to 0.1 V_{FG}. Also the most probable energy was 3 volts less than the value of V_{FG}.

Properties of the scattered ions

Table I is a summary of the twenty-four sets of data which were collected for the intensity distribution. The larger values for the breadth of curves 9 to 13 may be explained by referring to Fig. 1. For these curves the axis O inadvertently passed through the body of the target so that for large values of Φ, such as 70°, the entire beam was not incident upon the face of the target and some of the ions were scattered by the edge nearest the gun.

For ions with energies greater than 100 volts the position of the maximum does not seem to depend upon the incident energy. This is in accord with previous results.[1, 2, 3]

In regard to the connection between the position of the maximum and the specular angle the several investigators disagree. The data of Table I show that the angle of maximum scattering tends to remain constant rather than to vary with changes in the angle of incidence and therefore any association of this with the specular angle is probably fortuitous.

Four curves were obtained for constant Θ and varying Φ, which is analogous to part of Gurney's[2]

TABLE I. *Summary of data on intensity distribution. Columns 2 and 3 give the two accelerating potentials for maximum scattering in curves 12 to 24; column 5, angle of incidence; column 6, angle at maximum scattering; column 7, angular width to half maximum of scattered beam; column 8, angular position of mid-point of scattered beam.*

1	2	3	4	5	6	7	8
Curve No.	V_{FG} (volts)	V_{FA} (volts)	Target No.	Φ	Θ_{max} $\pm 2°$	Breadth at $I/I_{max}=0.5$	Middle point of breadth
1	186	186	1	70°	63°	55°	69°
2	195	193	1	70°	67°	40°	64°
3	180	100	2	68°	64°	40°	63°
4	180	100	2	72°	72°	35°	68°
5	180	100	2	67°	72°	30°	70°
6	180	100	2	71°	70°	35°	67°
7	150	100	2	71°	71°	30°	70°
8	180	100	2	49°	57°	45°	58°
9	250	100	3	70°	50°	70°	39°
10	250	100	3	70°	55°	75°	38°
11	200	100	3	70°	58°	55°	44°
12	300	30	3	70°	63°	90°	?
13	200	20	3	70°	55°	60°	49°
14	400	40	3	69°	65°	45°	60°
15	200	20	3	69°	65°	45°	58°
16	492	49	3	69°	67°	40°	62°
17	400	39	3	69°	69°	50°	60°
18	300	29	3	69°	67°	45°	61°
19	200	20	3	69°	66°	50°	61°
20	100	18	3	69°	63°	60°	55°
21	200	20	3	49°	63°	60°	54°
22	400	40	3	49°	72°	55°	56°
23	200	25	3	32°	63°	65°	51°
24	400	30	3	32°	55°	90°	?

work. The intensities observed are independent of both the incident energy and the arbitrary angles of scattering so they were plotted on a single graph (Fig. 2). The values of the radius vector are thus a measure of the relative efficiency of the scattering of ions as a function of the angle of incidence.

Data on the energy distribution were obtained, as described under "Procedure," for ions with

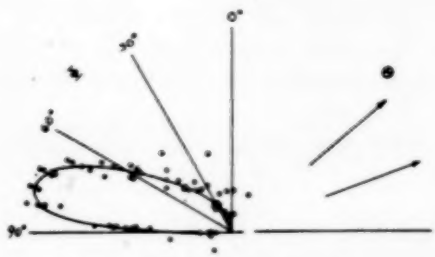

FIG. 2. $V_{FG}=200$ and 400 volts, $V_{FA}=20$ and 40 volts, respectively. $\Theta=70°$ and 50°, target No. 3.

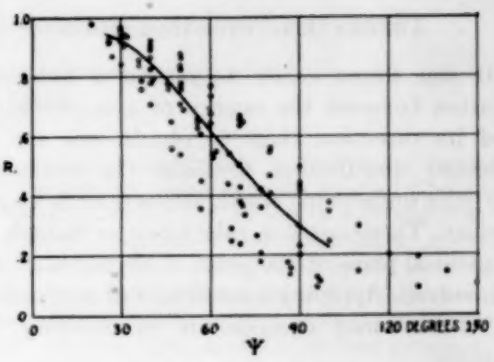

FIG. 3.

kinetic energies between 125 and 450 volts at angles of incidence near to 70° and 50°. The values of the ratio R of the most probable energy E' to the incident energy $E(V_{FG}^{-\frac{1}{2}})$ are plotted in Fig. 3 as a function of the total angle of scattering Ψ, where $\Psi=2\pi-(\Phi+\Theta)$. The heavy curve drawn through these points is a best curve obtained from averages. The spread of the points is so large that this curve would have little significance were it not for the fact that the points exist in sets in each of which R decreases as Ψ increases. Fig. 4 shows the family of curves corresponding to the data. It is to be observed that no distinction can be made between these on a basis of either the incident energy or the angle of incidence.

One set of retarding potential curves was taken for a constant angle of scattering, $\Theta=50°$, and the results are in all respects similar to those obtained with a constant angle of incidence. This is analogous to Gurney's[7] investigation with a mass-spectograph. His results are similar and his values of R would fall in the midst of the points below the curve in Fig. 2.

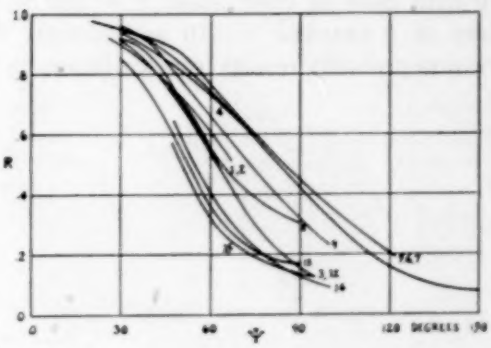

FIG. 4.

Theoretical Considerations

It was found easier to obtain a functional relation between the energy of a scattered ion and its direction than to obtain one for the intensity distribution. Consider the problem of particles undergoing elastic impacts with a rough surface. These impacts take place as though the tangential plane at the point of impact is all that is involved. Applying a coefficient of restitution b to the normal components of velocity one obtains:

$$R=(1-b)R^{\frac{1}{2}}\cos\Psi+b. \qquad (1)$$

The curves of Fig. 5 where $k=0$ are computed from this equation. However, with one or two

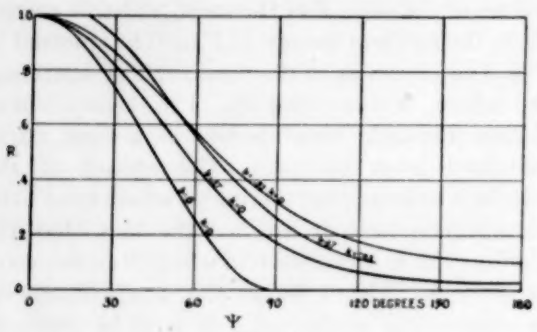

Fig. 5.

exceptions, no choice of b will make the curve of Eq. (1) fit the observed points perfectly. The introduction of a second parameter k, which may be thought of as expressing the effect of a charged layer on the surface of the target, gives a more complicated equation but makes it possible to obtain a better agreement with the experimental results. However, to represent all the experimental curves of Fig. 4 by theoretical curves it is necessary to use values of b ranging from 0 to 0.40 with most of them about 0.30 and to use values of k between -0.10 and $+0.01$. This variation probably results from variations in the target surface in different runs but makes the significance of b and k doubtful. It is to be emphasized that every effort was made to keep the surface clean, some data even being taken while the temperature of the target was greater than 850°C. It was further found possible to make an estimate of b and k for three curves published by Gurney.[7] These estimates fall within the limits given above.

Any attempt to extend this mechanism of scattering to the intensity distribution necessitates some assumptions concerning the roughness of the surface. However, this mechanism does provide that the incident energy will not effect this distribution.

For scattering outside of the plane of incidence one would expect a cosine law for the intensity when it is projected onto the plane through the normal and perpendicular to the incident beam. Gurney's two curves[8] become superimposed when so treated and therefore no further study was made of this.

Thus the scattering of positive ions by a metallic surface, to a first approximation, is the same as would be expected from a consideration of projectiles undergoing elastic impacts at a rough surface with a small coefficient of restitution.

In conclusion I wish to express my sincere thanks to Dr. K. T. Compton and to Professor H. D. Smyth for suggesting this problem and to Professors Smyth and Ladenburg for their continued interest throughout the work. Also I wish to express my appreciation for the assistance of R. T. Roberts in the taking of data, and to thank Mr. C. Stryker and Mr. L. Harris for their valuable assistance with the construction of the apparatus.

[7] Reference 2, p. 471, Figs. 3 and 4.
[8] Reference 2, p. 474, Fig. 8.

The Scattering of Hydrogen and Helium Beams in Mercury Vapor

R. M. ZABEL,* *Eastman Laboratory of Physics, Massachusetts Institute of Technology*

(Received April 6, 1934)

The scattering of beams of hydrogen molecules and helium atoms in mercury vapor has been investigated in the angular region from 5° to 65° at beam temperatures of 115°, 300° and 590°K. The results are expressed in terms of the number of molecules scattered per incident molecule, per cm path, per 10^{-3} mm of mercury at 0°C per unit solid angle in the direction θ to the original beam. The general shape, the absolute intensity and the change in shape of the helium scattering curves with change in beam temperature is in moderately good quantitative agreement with the quantum theory of scattering of rigid spheres as developed by Massey and Mohr. The scattering of hydrogen molecules, especially at low temperatures, shows some deviation from the results predicted by the same theory. In the case of both hydrogen and helium it is necessary to assume collision radii larger than the corresponding kinetic theory values in order to obtain the best agreement between the calculated and observed curves.

INTRODUCTION

RECENT developments in the quantum theory of scattering of atoms by Massey and Mohr[1] suggests the desirability of a detailed experimental study of scattering phenomena. Some notable advances have already been made in this field. Knauer[2, 3] first obtained curves showing the angular distribution of scattered molecules. His curves were confined in one case to angles above 22½° and in the other to angles less than 4°. The author[4] has previously studied the scattering of H_2 in H_2 and He in He. Fraser and Broadway[5, 6] find that the scattering of sodium and potassium in mercury vapor at angles of less than one degree is in agreement with the theory of Massey and Mohr.[1] The collision radii calculated on the basis of their results are approximately 2.5 times those obtained by viscosity measurements. In the results reported in this paper the scattering of beams of H_2 and He in Hg vapor has been investigated in the angular range from 5° to 65° with beam temperatures of 115°, 300° and 590°K.

APPARATUS

Fig. 1 shows the apparatus. The gas which forms the beam enters the beam system[7, 8] through tube A, which may be heated or cooled to produce various beam temperatures, and passes through three successive slits into the scattering chamber where it is detected by a Pirani[9] gauge. All important dimensions are given on the drawings.

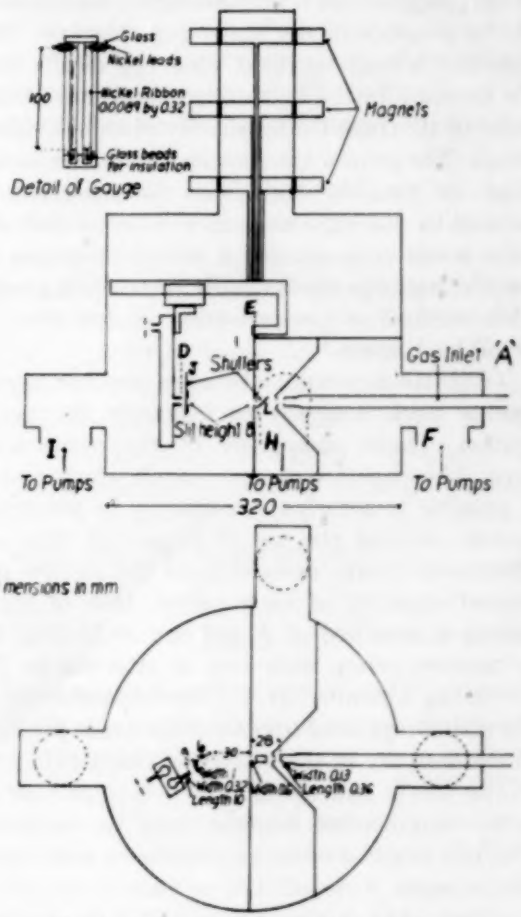

FIG. 1. Top and side view of apparatus.

* National Research Fellow.

[1] Massey and Mohr, Proc. Roy. Soc. **A141**, 434 (1933).
[2] Knauer, Zeits. f. Physik **80**, 80 (1933).
[3] Knauer, Naturwiss. **21**, 366 (1933).
[4] Zabel, Phys. Rev. **44**, 53 (1933).
[5] Fraser and Broadway, Proc. Roy. Soc. **A141**, 626 (1933).
[6] Broadway, Proc. Roy Soc. **A141**, 634 (1933).
[7] Knauer and Stern, Zeits. f. Physik **53**, 766 (1929).
[8] Ellett and Zabel, Phys. Rev. **37**, 1112 (1931).
[9] Ellett and Zabel, Phys. Rev. **37**, 1102 (1931).

To study completely the distribution of the molecules scattered from the beam the detector has three independent motions: (1) Rotation about D, the end of the channel entering the detector; (2) Rotation about E, the last slit of the beam system; (3) Variation of the distance between the detector and the last slit of the beam system. These motions make it possible to investigate the scattering from any point along the path of the beam. The three controls are operated by magnets.

The Pirani gauge used to detect the beam gives a deflection of 1 mm for a pressure change of 2×10^{-9} mm of Hg for H_2. The galvanometer sensitivity is $0.022\mu v$/mm. The greatest difficulty in the use of this gauge is encountered in constructing the beam and compensating gauges alike with sufficient accuracy so that the zero of the gauge system is not affected by fluctuations of the pressure in the scattering chamber. The difficulty is easily realized when one recalls that the pressure in the scattering chamber is of the order of 10^6 times the sensitivity of an individual gauge. The gauges are constructed as accurately alike as possible and final compensation is secured by placing a resistance in series with the more sensitive gauge and a second resistance in parallel with the more rapidly responding gauge. This method of compensation is described in detail by Knauer.[2]

To obtain as intense a beam as possible special pumps were designed to evacuate the beam system. These pumps are of the multinozzle type. They operate on apiezon oil which makes it possible to attach them directly to the beam system without the use of traps and thus use effectively a large percentage of the 70 liter per second capacity of each pump. One of these pumps is attached at F and one at H (Fig. 1). A mercury pump with trap is attached to the scattering chamber at I. The temperature of the trap is regulated to control the vapor pressure of the mercury in the scattering chamber.

The use of shutters J and L is important in order that correct readings may be obtained. The zero position of the galvanometer is obtained with shutter J closed. The motion of the galvanometer when shutter J is opened is the reading in any case. Four individual curves, shown in Fig. 2 are combined to give one scattering curve.

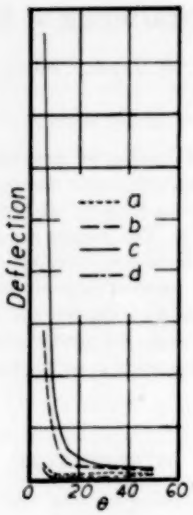

FIG. 2. Importance of shutters in obtaining scattering curves.

Curves (a) and (b) are taken with a low pressure in the scattering chamber (less than 10^{-5}), (a) with shutter L closed and (b) with shutter L open. Curve b then represents the scattering from the beam, scattering from the slit edges and the contribution of the flow of gas from the region between the second and third slits into the scattering chamber. Curve a taken with shutter L closed represents only the latter contribution. The subtraction of Curve a from Curve b represents the scattering due to the beam with low pressure in the scattering chamber. Similarly Curves c and d are taken with shutter L open and closed, respectively, but with the scattering pressure present in the chamber. Curve d may be positive or negative depending upon the gas flow through the third slit of the beam system. The algebraic subtraction of Curve d from c again gives the effect of the beam alone. Curve (c–d) obviously includes the effect of scattering from the beam and from the slit edges mentioned above. Hence Curve (b–a) multiplied by a factor which represents the decrease in intensity of the main beam when the scattering pressure is introduced into the scattering chamber must be subtracted from Curve (c–d) to obtain the scattering curve for the gas in the scattering chamber. The curve thus obtained multiplied by $\sin\theta$ to correct for the change in volume from which scattering may enter the

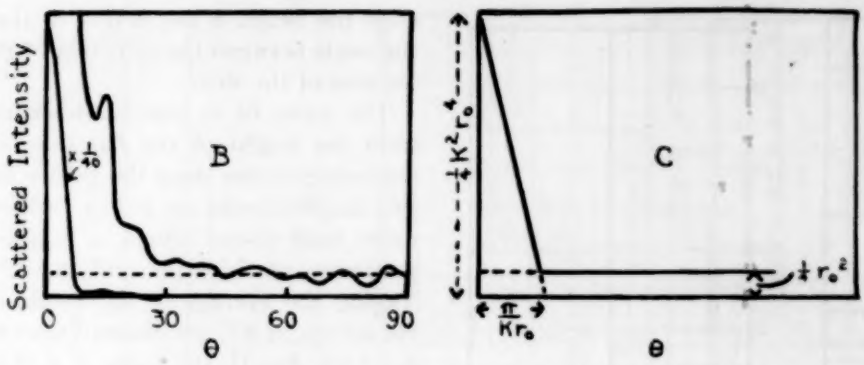

FIG. 3. Theoretical scattering curves of Massey and Mohr for dissimilar atoms.

gauge gives the relative scattering per unit solid angle.

THEORY

The quantum theory scattering curves for dissimilar atoms, assumed to be elastic spheres, as calculated by Massey and Mohr,[1] are shown in Fig. 3. The curves show the scattering per incident molecule per scattering molecule, per unit solid angle in the direction θ. B is the actual scattering curve and C is the easily calculated approximation used for comparison with experiment. The use of this approximation is partially justifiable because the small maxima and minima in the scattering curve will be smoothed out by the distribution of velocities in the beam. The r_0 referred to in Fig. 3 is the sum of the radii of the two colliding particles and $k=2\pi mv/h$ where m is the reduced mass $m_1m_2/(m_1+m_2)$, v is the relative velocity on collision, and h is Planck's constant. The additional assumption that the motion of the heavy mercury atoms may be neglected in comparison to the rapidly moving hydrogen molecules and helium atoms is made in order that the relative scattering curves, given in Fig. 3 in terms of relative coordinates, may be interpreted directly as scattering curves. In the least favorable case of He at 115°K the ratio of most probable velocity of the He atoms in the beam to the most probable velocity of the Hg in the scattering chamber is more than five and in the most favorable case of H_2 at 590°K the most probable velocity ratio is more than seventeen.

In order to obtain the resultant scattering curve for the Maxwellian distribution of velocities in the beam it is necessary to average weighted curves of type C Fig. 3 over the velocity range corresponding to the temperature of the beam. It is readily shown that the curves of type C drawn for different velocities sweep out the same volume when rotated about the axis of zero angle and hence must represent the same number of molecules. Multiplication of the height of a curve by a weight factor representing the abundance of atoms of that velocity in the beam, assuming a Maxwellian distribution, is therefore all that is necessary to assign the proper importance to the curve representing that velocity. Fig. 4 shows the group of single velocity curves properly weighted and the resultant scattering curve for He at 115°K. A single velocity curve is drawn every 10^4 cm per second throughout the velocity range in the beam. The horizontal line shown represents the sum of all the flat sections of the single velocity curves. A number of near vertical lines starting at angles less than 5° are not shown.

RESULTS

Fig. 5 shows the experimental results obtained in the scattering of beams of helium atoms and hydrogen molecules in mercury vapor at beam temperatures of 115°, 300° and 590°K. The curves show the number of molecules scattered per incident moledule, per cm path, per 10^{-3} mm of mercury at 0°C, per unit solid angle in the direction θ to the original beam. The scattering function $f(\theta)$ defined above is obtained by the relation

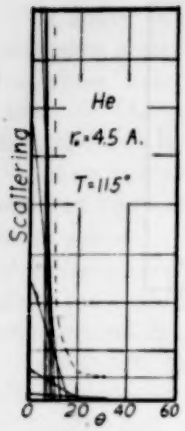

FIG. 4.

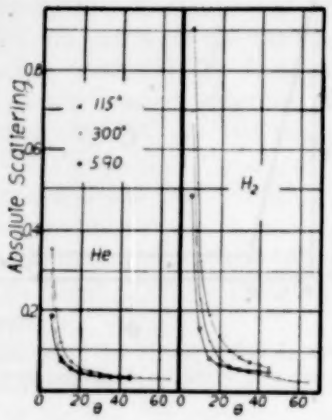

FIG. 5.

FIG. 4. Weighted monochromatic curves added to obtain curve to be expected with Maxwellian distribution of velocities.

FIG. 5. Number of scattered molecules per unit solid angle, per cm path length, per 10^{-3} mm of Hg at 0°C, per incident molecule as a function of angle for H_2 and He beams at temperatures of 115°, 300° and 590°K.

$$f(\theta)=c_1d_2\left[Ac_1d_1p\cdot 10^3\cdot\int\omega dx\right]^{-1}$$

$$=d_2\left[Ad_1p\cdot 10^3\cdot\int\omega dx\right]^{-1},$$

where d_1 is the deflection of the gauge in the main beam at its normal distance from the last slit of the beam system with the scattering pressure present in the scattering chamber, d_2 is the gauge deflection at an angle θ, c_1 is a constant relating the number of molecules incident on the gauge opening with the gauge deflection, A is the ratio of the area of the beam to the area of the gauge opening, p is the pressure in mm of Hg and ω is the solid angle of the slit system of the gauge as viewed from any increment of length dx along the path of the beam from which scattering may enter the gauge. Jordan and Brode[10] have shown that to a sufficient degree of accuracy

$$\int\omega dx=mnh/M(M-N)\sin\theta,$$

where m is the width of the gauge channel, M its distance from the beam, n the width of the defining slit near the beam and N its distance from the beam, h the height of the slits and θ the angle between the direction of the beam and the axis of the slits.

The value of r_0 may be determined directly from the height of the flat portion of the He scattering curves since the theory indicates that this height should be $\frac{1}{4}r_0^2$ or rather $\frac{1}{4}r_0^2\nu$ in the units used above where ν is the number of scattering particles per cm³ at 10^{-3} mm of Hg. Taking the average of the height of the three He curves at 45° we obtain $\frac{1}{4}r_0^2\nu=0.029$. Hence $r_0=5.6$A. For H_2 the value of r_0 obtained in the same way from the 590° curve since this is the only one which shows even a tendency to flatten out is 7.5A.

The majority of the curves are not extended beyond 45° because little new information seems to be obtained by doing so.

Fig. 6 shows the comparison between the experimental helium curve at 300°K and the theoretical curves calculated as previously described for various values of r_0. The classical value as obtained from viscosity measurements is $r_0=2.9$A. The proper ratio between the scattered intensity at large angles and at 10° is given by $r_0=4.5$A and is therefore choosen as the value best fitting the experimental results. There is obviously some degree of arbitrariness in the method to be adapted in choosing the r_0 value to fit the curves. In view of the rapid change of the theoretical curve with change in r_0, any other reasonable method would yield essentially the same result. It is interesting to note that the r_0 which best fits the shape of the curve is within 20 percent of the value obtained from the height of the flat portion. A somewhat larger value $r_0=7.5$A is plotted to show the rate at which the scattering curve changes with change in r_0.

Fig. 7 shows the experimental and theoretical curves for helium at various beam temperatures. For ease of comparison all curves are drawn with the flat portions (the 45° point in the case of the experimental curves) at the same level. The similarity between the experimental and theoretical curves in general shape and in trend with change in temperature is unmistakable.

Fig. 8 shows each of the corresponding theoretical and experimental curves plotted together to show the differences more clearly. The first

[10] Jordan and Brode, Phys. Rev. **43**, 112 (1933).

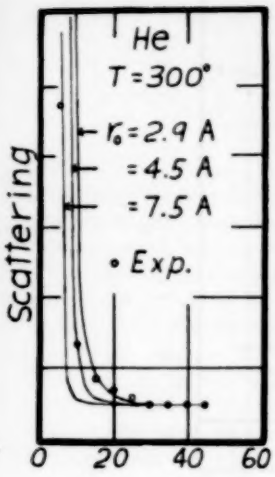

FIG. 6.

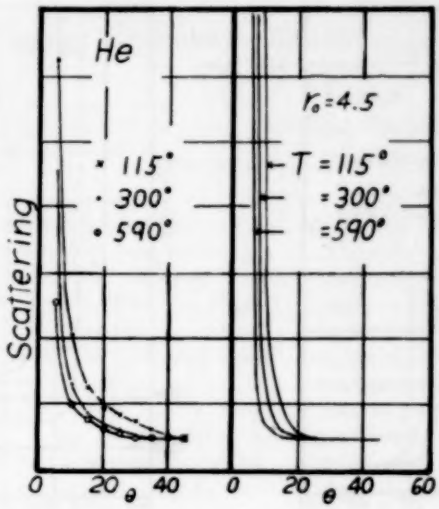

FIG. 7.

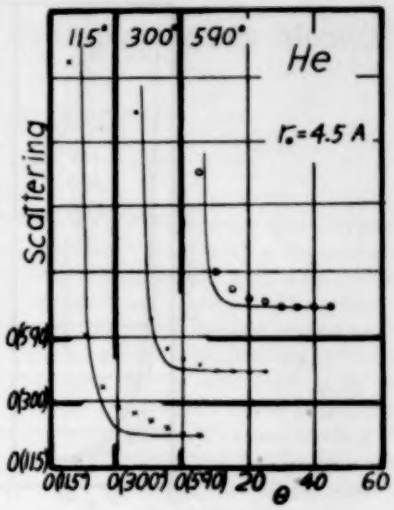

FIG. 8.

FIG. 6. Comparison of experimental scattering curve for He in Hg with theoretical curves calculated for $r_0 = 2.9$A, 4.5A and 7.5A.
FIG. 7. Trend of experimental and theoretical He curves with change in temperature.
FIG. 8. Comparison of experimental and theoretical He scattering curves. The solid lines represent the theoretical curves, the plotted points the experimental results.

suggestion which presents itself in connection with the differences in the curves is that there is appreciable multiple small angle scattering. To test this point curves were taken at two different pressures. Fig. 9 shows these curves. In taking Curve *e* the pressure in the scattering chamber was such that the mean free path of the helium beam was 4.5 cm and in Curve *f* the mean free path was 10.5 cm. A small effect due to multiple scattering is evident. Extrapolation to zero pressure indicates that further change in the curve will be small. All curves were taken with the longer mean free path.

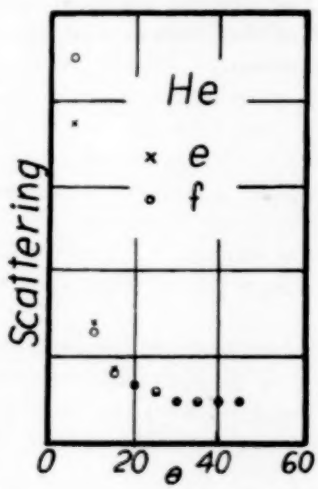

FIG. 9. He curves at different scattering pressures.

There is, however, good reason to believe that due to the size of the slits required to obtain an observable intensity the experimental point at 5° is not accurate. When the gauge is set to receive scattering at 5° it is obvious that the atoms received by the gauge may have been scattered through an angle somewhat larger or smaller than 5° although 5° will be the most probable. The probability that atoms will enter the gauge does not become zero until one reaches scattering angles of $1\frac{1}{2}$ and $8\frac{1}{2}$ degrees. Obviously the effect of this angular spread decreases rapidly in importance with increased scattering angle.

A considerable portion of the discrepancy between the theoretical and experimental curves in the region from 15° to 25° may be due to the fact that Curve C in Fig. 3 is not a sufficiently accurate approximation to the true results of the theory. It is obvious that the approximation would be poorest in the region of the transition from classical scattering to the intense small angle scattering.

Figs. 10 and 11 show the comparison between theory and experiment in the case of H_2. The r_0 value for the shape of the curve is chosen to fit

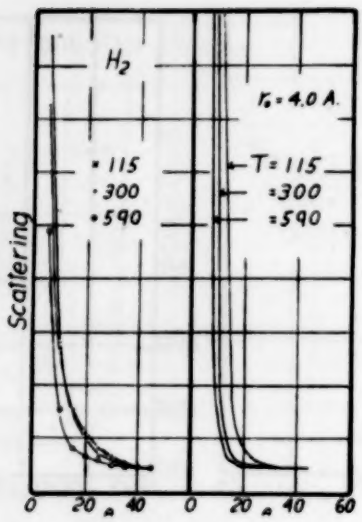

FIG. 10.

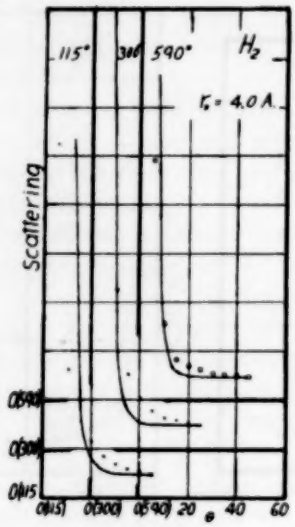

FIG. 11.

FIG. 10. Trend of experimental and theoretical H_2 curves with change in temperature.

FIG. 11. Comparison of experimental and theoretical H_2 scattering curves. The solid lines represent the theoretical curves, the plotted points the experimental results.

the 590° curve, again because of its semi-flat region. The value of 4.0A is markedly in disagreement with the value 7.5A previously obtained from the height of the flat portion. Hydrogen at low temperatures is obviously not in agreement with the theory. The general trend of the theoretical curves with change in temperature is not followed by the experimental curves in passing from 300° to 115°K. This discrepancy may be due to the molecular structure of one of the colliding particles which introduces complications not taken into account by the elastic sphere model or it is possible that an attractive force, tending to form a mercury-hydrogen compound, exists between the hydrogen molecules and mercury atoms which produces an increased distortion of the scattering curve at low temperatures. Massey and Mohr find that viscosity calculations for H_2 on the basis of their theory are not in agreement with experimental results at low temperatures. Obviously then H_2 should present a fruitful field for further theoretical study.

The writer wishes to thank Professors Slater and Morse for inspection of the manuscript and Mr. Neils Dall for his excellent work in the construction of the beam system and the gauge control mechanism.

The Quenching of Mercury Resonance Radiation by Hydrogen, Carbon Monoxide and Nitrogen

O. S. DUFFENDACK AND J. S. OWENS, *University of Michigan*

(Received July 10, 1934)

An investigation was made of the dependence upon the temperature of the quenching of mercury resonance radiation by hydrogen, carbon monoxide and nitrogen. The quenching by hydrogen was effectively independent of the temperature from 473°K to 973°K, but that by carbon monoxide and by nitrogen decreased with increasing temperature. This decrease was somewhat more marked in nitrogen than in carbon monoxide. These results show that the metastable $2\,^3P_0$ state of the mercury atom is involved in the quenching by carbon monoxide and by nitrogen, but not appreciably in the quenching by hydrogen. The quenching by hydrogen may be accounted for by a reaction involving the dissociation of the hydrogen molecule by collision with a $2\,^3P_1$ mercury atom, followed in a certain small fraction of the cases by the probable excitation by collision with a second $2\,^3P_1$ atom of the mercury hydride molecule so produced. The effective cross sections for energy transfer in the first process at the different temperatures are given. The quenching by carbon monoxide and by nitrogen may be accounted for by the transition $2\,^3P_1 \rightarrow 2\,^3P_0$ of the mercury atoms at gas collisions, by the return of some of the $2\,^3P_0$ atoms to the $2\,^3P_1$ state at subsequent gas collisions, and by the reduction of the remainder of them by several distinct processes to the $1\,^1S_0$ state. The effective cross sections for the different processes are given.

INTRODUCTION

SINCE the introduction of the concept of "Collisions of the second kind" by Klein and Rosseland[1] many attempts have been made under different conditions to evaluate both the probabilities of such collisions and the accompanying "effective cross sections for energy transfer."

From kinetic theory, the action cross section, q, for a collision may be interpreted as the product $\pi S_{12}^2\gamma$, where S_{12} is the sum of the effective radii of the colliding molecules and γ is the probability that the collision will result in a transfer of energy between the molecules at the distance S_{12} apart. Neither S_{12} nor γ, but only the product $S_{12}^2\gamma$, hereafter denoted by σ^2 and called the effective cross section, can be obtained directly from experiment. Also, according to modern quantum mechanics a "collision radius" cannot be distinguished physically from a "collision probability." Therefore only the quantity σ^2 will be sought in the various types of collisions.

The values obtained for these probabilities and effective cross sections depend to some extent upon the experimental conditions and to a large extent upon the theoretical treatment of the data as is shown by the results of the several analyses of the experimental observations of Stuart.[2]

Zemansky[3] applied Milne's[4] theory of the diffusion of resonance radiation, as modified by impacts of the second kind, to Stuart's data and found that a constant quenching efficiency could not be ascribed to each gas. Later, by means of a method more nearly suited to the requirements of Milne's theory, he[5] investigated the quenching by a number of gases. He assumed that at the gas pressures used only the quenching process D (Fig. 1) was present for H_2 and O_2, and only the primary quenching process E (Fig. 2) for CO, CO_2, H_2O, and N_2. From his experimental results he calculated a quantity σ_E^2, an "effective cross section for quenching." This σ_E^2 is an effective average over all the cross sections accompanying the various quenching transitions.

Modern quantum mechanics[6] has shown that the probability of energy exchange taking place at a collision depends upon the nature both of the colliding molecules and of the collision. The

[1] Klein and Rosseland, Zeits. f. Physik **4**, 46 (1921).

[2] Stuart, Zeits. f. Physik **32**, 262 (1925); Foote, Phys. Rev. **30**, 288 (1927); Gaviola, Phys. Rev. **33**, 309; **34**, 1049; **34**, 1373 (1929); **35**, 1226 (1930); Mitchell and Zemansky, *Resonance Radiation and Excited Atoms* (1934).

[3] Zemansky, Phys. Rev. **31**, 812 (1928).

[4] Milne, J. Lond. Math. Soc. **I**, 40 (1926).

[5] Zemansky, Phys. Rev. **36**, 919 (1930).

[6] Kallmann and London, Zeits. f. physik. Chemie **B2**, 207A (1929); Morse and Stueckelberg, Ann. d. Physik **9**, 579 (1931); Stueckelberg, Helv. Phys. Acta **5**, 370 (1932).

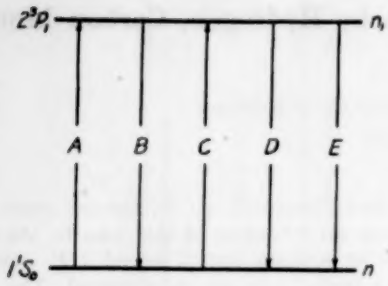

FIG. 1.

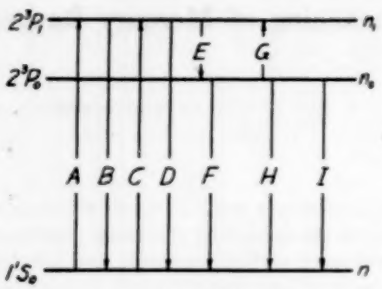

FIG. 2.

Transition processes of the mercury atom.

FIG. 1. Transitional diagram for the quenching by hydrogen.

A—Absorption of λ2437
B—Spontaneous emission of λ2537
C—Reabsorption of λ2537 within the mercury vapor.
D—Dissociation of the hydrogen molecule by collision with a $2\,^3P_1$ mercury atom.
E—Excitation by collision with a second $2\,^3P_1$ mercury atom of the mercury hydride molecule produced by *D*.

FIG. 2. Transitional diagram for the quenching by carbon monoxide and by nitrogen.

A—Absorption of λ2537
B—Spontaneous emission of λ2537
C—Reabsorption of λ2537 within the mercury vapor.
D, E, F, G—Transitions of the mercury atoms produced by collisions with gas molecules.
H—Transition of the $2\,^3P_0$ mercury atom independent of the gas pressure, probably mercury molecule formation.
I—Diffusion to the walls.

nature of the collision depends primarily upon whether or not the transition of the excited molecule is optically allowed. Thus, in order for a quenching cross section to have more meaning than that of a kind of average one over the whole reaction, the actual processes taking place must be determined and a cross section calculated for each. No attempt to do this was made in any of the work mentioned above.

Samson[7] studied the effect of temperature and of nitrogen pressure upon the decay of the afterglow of mercury resonance radiation in a mixture of mercury vapor and nitrogen. He took into account all the transition processes shown in Fig. 2 with the exception of H, and evaluated the "effective temperature cross section," which corresponds to σ_E^2, for each process involving the collisions of excited mercury atoms with nitrogen molecules. Thus his values of effective cross sections have more meaning than any of the previous ones.

Upon the basis of the present experimental work, the quenching by hydrogen is taken to be a two-step reaction involving, as most important, the processes *A*, *B*, *C*, *D* and *E* in Fig. 1. The processes *A*, *B*, *C*, *E*, *F*, *G*, *H* and *I* in Fig. 2 are the ones used in the analysis of the quenching by carbon monoxide and by nitrogen. Effective cross sections are calculated for each process.

[7] Samson, Phys. Rev. **40**, 940 (1932).

EXPERIMENTAL APPARATUS AND METHOD

The purpose of this experiment was to determine the type of reaction taking place between the excited mercury atoms and the foreign gas molecules by an investigation of the dependence of the quenching upon both the foreign gas pressure and the temperature.

The apparatus assembly was similar to that of Stuart.[2] The primary λ2537 radiation from a special source was absorbed by mercury vapor at a pressure of 0.28 mm in a quartz cell. The resonance radiation which passed back through the incident window of the cell in a direction nearly parallel to that of the primary radiation was photographed.

The experimental cell was a quartz cylinder, 5.3 cm long and 3.5 cm in diameter, with plane quartz windows sealed on each end. It was connected to the liquid mercury source for the mercury vapor by an electrically heated quartz tube. The cell was enclosed in an electric furnace, provided with quartz windows. The temperature of the furnace could be accurately controlled up to 1070°K. The temperature of the liquid mercury source for the mercury vapor in the cell was held at 100°C by means of a thermostatic relay.

Two important improvements over the technique of Stuart were utilized, *viz.*, a constant primary light source and an improved method of

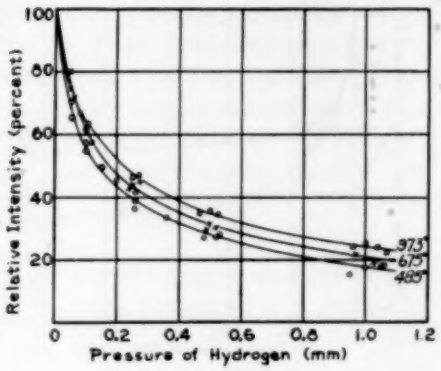

FIG. 3.

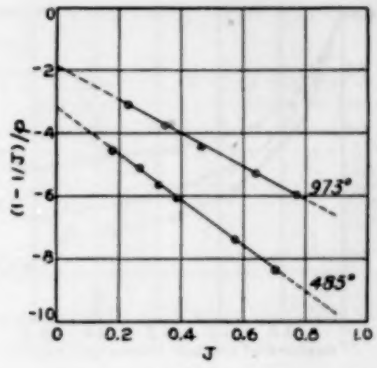

FIG. 4.

FIG. 3. Quenching by hydrogen. The curves are drawn from the theory and the plotted points represent experimental observations.
FIG. 4. Quenching by hydrogen. $(1-1/J)/p$ as a function of J.

intensity calibration of the photographic plates. The light source was a 30 m.a. glow discharge in a mixture of argon at 8.0 mm pressure and mercury vapor at 0.0004 mm pressure. The low mercury vapor pressure insured a very narrow λ2537 line having a strong core, thus eliminating the necessity for a resonance lamp. The variation in the intensity of the λ2537 line over a period of twelve hours was found to be less than one percent. A chlorine filter placed between the source and the resonance cell absorbed all the radiation from λ2600 to λ4358,[8] thus preventing the stepwise excitation of the 2^3P_2 state.

Plate blackenings, obtained with a self-recording microphotometer of the Moll type, were translated into light intensities by the use of a step-diaphragm as described by Hansen.[9]

Great care was taken to insure extreme purity of the gases used. Hydrogen was admitted to the system by diffusion through an electrically heated platinum cylinder. Nitrogen and carbon monoxide were generated on an auxiliary system, transferred to the quenching system, and carefully purified by conventional means. Subsequent tests showed that both the latter gases were spectroscopically pure.

The experimental procedure was as follows: A photograph was taken with pure mercury vapor in the resonance vessel. Then a series of photographs were taken on the same plate with varying pressures of foreign gas, each pressure change being made very slowly, and the mercury vapor pressure allowed to reach equilibrium before the following exposure. The temperature was kept constant during this time. Then a Hansen calibration pattern was photographed on the plate. This entire procedure was repeated for a series of temperatures of the resonance vessel from 473°K to 973°K.

Tests were made of the effects of variations in all of the experimental operations involved and showed that the probable experimental error did not exceed two percent for the procedure finally adopted. This high degree of accuracy was essential in order that the determination of the processes taking place in the quenching by hydrogen should be significant.

EXPERIMENTAL RESULTS

The experimental results are given in Tables I, II and III and in Figs. 3 to 6. The latter are curves showing the relative intensity J of the resonance radiation as a function of the foreign gas pressure p in mm of mercury. The plotted points were experimentally determined and the curves are drawn in accordance with the theory given below.

For hydrogen, Fig. 3, the results show that, in the temperature range investigated, the quenching by hydrogen is nearly independent of the temperature, while the quenching by carbon monoxide and by nitrogen decreases as the temperature is increased. This variation with temperature is more marked in nitrogen than in carbon monoxide. A brief investigation of the

[8] Oldenberg, Zeits. f. Physik **29**, 328 (1924).
[9] Hansen, Zeits. f. Physik **29**, 356 (1924).

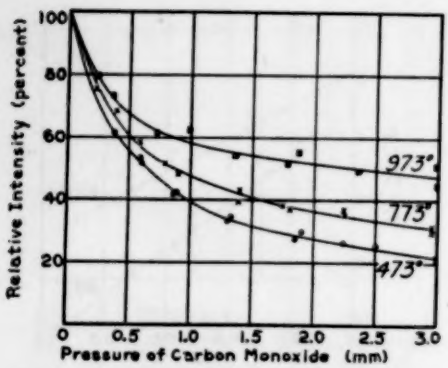

FIG. 5. Quenching by carbon monoxide.

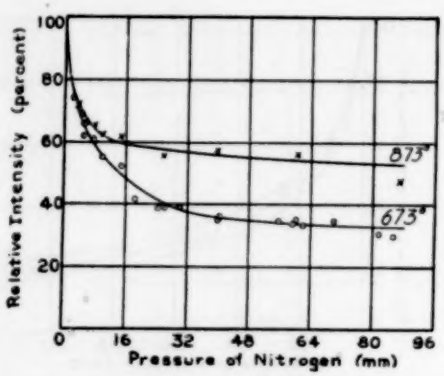

FIG. 6. Quenching by nitrogen.

quenching by nitrogen at 973°K indicated that the intensity of the resonance radiation decreased only to 85 percent of its original value even at a pressure of 90 mm of nitrogen. This result is in qualitative agreement with that of Cario and Franck.[10]

DISCUSSION AND INTERPRETATION OF RESULTS

Quenching by hydrogen

Upon the basis of the results of Franck and Cario,[11] the dissociation of the hydrogen molecule has always been regarded as the fundamental process in the quenching of mercury resonance fluorescence by hydrogen. Several types of reactions involving this dissociation have been advanced,[12] of which the two-step process postulated by Beutler and Rabinowitsch[13] is the most probable.

Since the quenching by hydrogen was found to be practically independent of the temperature, the effect of the mercury metastable $2\,^3P_0$ state is negligible. Otherwise the quenching action should markedly decrease with increasing temperature due to the rapid increase with temperature of the reverse transition $2\,^3P_0 \rightarrow 2\,^3P_1$.

Heretofore, the hydrogen quenching reaction has been simply assumed to comprise only the one step.

$$Hg' + H_2 \rightarrow Hg\ H + H + K.E.$$

However, from the quenching experiments one may determine whether there occurs a one-step reaction involving only one excited mercury atom or a two-step reaction, each step having a definite probability, involving two excited mercury atoms. This latter type of process proved to be the most probable on the basis of the excellent agreement between the theoretical curves obtained from it and the experimental quenching curves.

The calculation of J as a function of p is carried out on the basis of a two-step reaction:

$$(1) \qquad Hg'_{(2\,^3P_1)} + H_2 \rightarrow Hg\ H + H + K.E.$$

$$(2) \qquad Hg'_{(2\,^3P_1)} + Hg\ H \rightarrow Hg\ H' + Hg + K.E.$$

The statistical processes are shown in Fig. 1.

n, n_1 = concentrations of the mercury atoms in the $1\,^1S_0$ and $2\,^3P_1$ states, respectively.

n is approximately the total concentration of the mercury atoms.

p = pressure of hydrogen in mm of mercury.

A = Einstein coefficient of spontaneous emission of $\lambda 2537$.

$B = AK$, where K is a constant proportional to the intensity of the incident radiation.

$\rho(\nu)d\nu$ = radiation density of a frequency between ν and $\nu + d\nu$ within the $\lambda 2537$ line.

$b(\nu)\rho(\nu)d\nu dt$ = probability that a $1\,^1S_0$ atom will absorb a quantum in the frequency range between ν and $\nu + d\nu$ in time dt.

k_1 = number of effective collisions per second per excited atom at 1 mm hydrogen pressure producing transition D in Fig. 1.

$k_2 n_1^2$ = number of transitions per second at 1 mm hydrogen pressure corresponding to transition E in Fig. 1.

In the steady state,

$$dn_1/dt = 0 = Bn + n\int_0^\infty b(\nu)\rho(\nu)d\nu - An_1 - pk_1 n_1 - pk_2 n_1^2.$$

[10] Cario and Franck, Zeits. f. Physik **37**, 619 (1926).
[11] Franck and Cario, Zeits. f. Physik **11**, 161 (1922).
[12] Compton and Turner, Phil. Mag. **48**, 360 (1924); Hulthen, Zeits. f. Physik **32**, 32 (1925).
[13] Beutler and Rabinowitsch, Zeits. f. physik. Chemie **B8**, 403A (1930).

If we assume, as did Samson,[7] that $\rho(\nu)$ at any point is chiefly due to the radiating atoms in its vicinity, we may represent the absorption term by Ln_1, where L is an unknown constant. Then $P=A-L$ is the "resultant radiation coefficient" for the cell and each volume element in it. Then

$$0=Bn-(P+pk_1+pk_2n_1)n_1.$$

If $n_1^{(p)}$ and $n_1^{(o)}$ are the concentrations of the $2\,^3P_1$ atoms in the presence and absence, respectively, of hydrogen, the ratio of the intensity I of the resonance radiation at any given hydrogen pressure to the intensity I_0 in pure mercury vapor is then

$$J=\frac{I}{I_0}=\frac{n_1^{(p)}}{n_1^{(o)}}$$

$$=\frac{-(P+pk_1)+[(P+pk_1)^2+4pk_2AKn]^{\frac{1}{2}}}{2pk_2(AK/P)n}. \quad (1)$$

Although it is impossible to carry out a rigorous calculation for P for the present experimental apparatus, an approximate value for it may be obtained by consideration of the absorption coefficient of the mercury vapor for both the primary and resonance λ2537 radiation and of the geometry of the apparatus. This value is $P=0.2A=1.82\times10^6$. The use of this same value at all the temperatures may be justified by the fact that at all the temperatures all of the incident light quanta are absorbed. The only effect of temperature change is to change slightly the depth of penetration of the incident light.

By means of (1) the values of the k_1 and k_2K may be obtained from the quenching data. The values taken for these quantities are average ones obtained from all the quenching data at each temperature. The effective cross section Σ_1^2 for the first process is obtained by equating the total number of collisions of the second kind per cm³ per second experimentally determined to the total number of collisions within the distance Σ_1 given by a Maxwellian distribution of velocities.[7] Hence

$$k_1=(2N\Sigma_1^2/p_1)(2\pi kT/\mu)^{\frac{1}{2}} \quad (2)$$

where μ = reduced mass for mercury and hydrogen; T = absolute temperature; k = Boltzmann's constant; N, p = hydrogen concentration and pressure, respectively. The results are given in Table I.

TABLE I. *Values of k_1, Σ_1^2 and k_2K for the quenching of mercury resonance radiation by hydrogen.*

T°K	$k_1\times10^{-8}$ from (1)	$\Sigma_1^2\times10^{16}$ from (1)	$k_2K\times10^{18}$ from (1)	$k_1\times10^{-8}$ from	$\Sigma_1^2\times10^{16}$ curves	of	$k_2K\times10^{18}$ Fig.	4
485	5.80	4.06	4.78	5.74	4.02		4.77	
530	5.85	4.28	4.92	5.91	4.33		4.88	
675	4.87	4.02	5.39	4.82	3.97		5.62	
973	3.47	3.44	6.91	3.44	3.41		6.86	

Confirmatory evidence that the quenching by hydrogen is a two-step reaction is obtained by plotting the quantity $(1-1/J)/p$ as a function of J.* If the quenching is a one-step reaction, this curve should be a horizontal straight line with the constant value of $(1-1/J)/p=-k_1/P$. If it is a two-step reaction, this curve should be a straight line with intercept $-k_1/P$ at $J=0$ and slope $-k_2AKn/P^2$. The present experimental data plotted in this manner gave excellent straight lines of the latter type as shown in Fig. 4. The constants calculated from these curves are shown in the last three columns of Table I. The close agreement between the constants obtained by these two methods indicates the accuracy with which they were determined.

Since the quenching by hydrogen does apparently decrease slightly with increase of temperature, this fact might be attributed to the presence of the metastable $2\,^3P_0$ state of mercury in the quenching reaction. However, this state has not been considered in the analysis of the quenching by hydrogen for several reasons. First, the experimental results show that any influence of this state upon the quenching must be very slight. Second, the energy of the $2\,^3P_0$ atom, as well as that of the $2\,^3P_1$ atom, is sufficient to dissociate the hydrogen molecule. Third, the inclusion of the effect of this state in the analysis so complicates the equations that an accurate solution becomes impossible, and, in view of its small effect, consideration of this state was omitted.

Quenching by carbon monoxide and by nitrogen

Since the quenching by carbon monoxide and by nitrogen decreases with increasing temperature and that by hydrogen is effectively independent of the temperature, there is an essential difference between the quenching reactions in the

* This method was suggested by Professor A. E. Ruark.

two cases. This difference is due to the differences in their dissociation energies and in their critical potentials.

The primary process in the quenching by carbon monoxide and by nitrogen must be the reduction of the $2\,^3P_1$ mercury atom to the $2\,^3P_0$ metastable state by collision with a gas molecule. The energy difference, 0.218 volt, between these states is given to the gas molecule, and probably is transformed into vibrational energy.

If all the metastable atoms so produced were returned to the normal state by gas collisions or by diffusion to the walls, the quenching process should be that of a one-step reaction. However, the experimental data point to the occurrence of another process which partially neutralizes the effect of the quenching collisions. This process is taken to be the return of $2\,^3P_0$ atoms to the $2\,^3P_1$ state by gas collisions.

A priori, the transition $2\,^3P_0 \rightarrow 2\,^3P_1$ of the mercury atom may be produced by either one or both of the following types of collisions: (A) Collisions of the first kind with high speed gas molecules; (B) Collisions of the second kind with gas molecules having vibrational energy. The fraction of all collisions in which there is sufficient energy to produce the transition $2\,^3P_0 \rightarrow 2\,^3P_1$ is, for the two cases:

$$\text{(A)} \qquad F_a = (1+\epsilon/kT)e^{-\epsilon/kT}, \tag{3}$$

where ϵ is the energy difference between the $2\,^3P_1$ and $2\,^3P_0$ states.[14]

$$\text{(B)} \qquad F_b = e^{-E/kT}, \tag{4}$$

where $E(\geqq\epsilon)$ is the energy of a vibrational state of the gas (this will be the first vibrational state of nitrogen or carbon monoxide). For both gases, $F_b < F_a$. In fact $F_b < 0.2F_a$ from 291°K to 973°K.

The quenching action never entirely disappears at high temperatures because of the return of some metastable atoms to the normal state by diffusion to the walls, by gas collisions,[15] or by processes independent of the pressure of the foreign gas. Since the effect of the first two of these processes should be less in nitrogen than in carbon monoxide, the quenching action should more nearly disappear in nitrogen. This fact was experimentally observed.

[14] Tolman, *Statistical Mechanics*, The Chemical Catalogue Company, New York.
[15] Gaviola, Phil. Mag. **6**, 1167 (1928).

The general expression derived for the quenching by carbon monoxide and by nitrogen is similar to that of Magliano and Gaviola[16] and gives at high pressures essentially the same expression as does an adaptation of Samson's[7] theory to quenching. The statistical processes are shown in Fig. 2.

n, n_1, n_0 = concentrations of mercury atoms in the $1\,^1S_0$, $2\,^3P_1$, and $2\,^3P_0$ states, respectively.
N = concentration of foreign gas molecules.
k_1, K_1, k_0, K_0 = numbers of effective collisions per second per excited atom at 1 mm gas pressure producing the respective transitions E, D, G, F shown in Fig. 2.
H_0n_0 = number of $2\,^3P_0 \rightarrow 1\,^1S_0$ transitions, corresponding to H in Fig. 2, per second produced by any processes independent of the foreign gas pressure.
$dn_0/(p+p_0)$ = loss per cm³ per second of $2\,^3P_0$ atoms by diffusion to the walls, corresponding to transition I in Fig. 2.
p = pressure of foreign gas in mm of mercury.
p_0 = pressure of mercury vapor in mm of mercury.

The diffusion of $2\,^3P_1$ atoms is not considered because their natural lifetime is too short to permit them to reach the walls before radiating.

Here, as in the quenching by hydrogen, $P = A - L$ is the resultant radiation coefficient. In the steady state by equating the number of transitions both to and from the $2\,^3P_1$ and the $2\,^3P_0$ states, we have

$$Bn + pk_0n_0 = (P + pk_1 + pK_1)n_1, \tag{5}$$

$$pk_1n_1 = (pk_0 + pK_0 + H_0 + d/(p+p_0))n_0. \tag{6}$$

Thus

$$\frac{n_0}{n_1} = R = \left[\frac{k_0+K_0}{k_1} + \frac{H_0}{pk_1} + \frac{d}{pk_1(p+p_0)}\right] - 1. \tag{7}$$

If thermal equilibrium exists between the $2\,^3P_0$ and $2\,^3P_1$ states

$$k_1 = k_0\alpha = k_0(q_0/q_1)e^{\epsilon/kT}, \tag{8}$$

q_0 and q_1 are the statistical weights of the $2\,^3P_0$ and $2\,^3P_1$ states, respectively. Due to the rapid interchange of atoms between these states, the deviation from thermal equilibrium will be small, especially in the case of nitrogen.

Then from (5), (7) and (8)

$$J = \frac{I}{I_0} = \frac{n_1^{(p)}}{n_1^{(0)}} = \left[1 + \frac{p}{P}K_1 + \frac{p}{P}k_1\left(1 - \frac{R}{\alpha}\right)\right]^{-1} \tag{9}$$

[16] Magliano and Gaviola, Univ. Nac. La Plata, Estudio Ciencias 5, No. 93, 479 (1931).

(9) is the general expression for the quenching by carbon monoxide and by nitrogen.

(a) For low pressures of the foreign gas—we may for such low gas pressures that diffusion to the walls will destroy most of the $2\,^3P_0$ atoms put $R/\alpha \ll 1$ in (9) and obtain

$$J=[1+(p/P)(k_1+K_1)]^{-1}. \tag{10}$$

(b) For high pressures of the foreign gas—neglecting diffusion in (7), the substitution of (7) into (9) gives

$$J=\left[1+\frac{k_1k_0H_0}{P(k_0+K_0)^2}+\frac{p}{P}\left(K_1+\frac{k_1K_0}{k_0+K_0}\right)\right]^{-1}. \tag{11}$$

From (10) and (11) the curve of $1/J$ against p is seen to have two straight line portions, one at very low pressures and the other at high pressures, the latter having the smaller slope.

On the basis of the equations given, the values of neither k_1 nor K_1, but of only k_1+K_1 can be obtained from the experimental data. Samson[7] found that nitrogen apparently produced the transition $2\,^3P_1 \rightarrow 1\,^1S_0$, corresponding to K_1, with an appreciable probability, but only with stimulated emission of λ2537. Such a process would not, therefore, be detected in quenching experiments. On the basis of both this fact and the impossibility, on the basis of any known energy transfer, to attribute to a radiationless transition $2\,^3P_1 \rightarrow 1\,^1S_0$, produced by carbon monoxide or by nitrogen, a probability comparable with that of the transition $2\,^3P_1 \rightarrow 2\,^3P_0$, K_1 has been neglected in this analysis. The value of k_1 then obtained does not depend upon the assumption of thermal equilibrium between the $2\,^3P_0$ and $2\,^3P_1$ states.

Curves of $1/J$ as a function of p are given in Fig. 7 for carbon monoxide at 473°K and at 973°K and in Fig. 8 for nitrogen at 673°K and 873°K. In Table II are given the values of k_1, K_0, and H_0, obtained from these curves, and of the respective corresponding effective cross sections Σ_1^2, Σ_0^2, and S_0^2. The latter are calculated from the following formulas.[7]

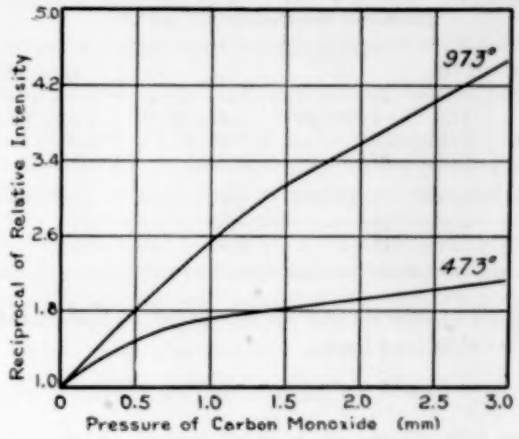

FIG. 7. $1/J$ as a function of the pressure of carbon monoxide.

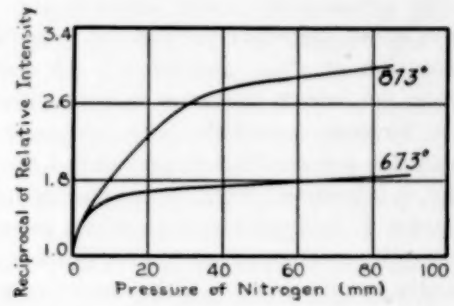

FIG. 8. $1/J$ as a function of the pressure of nitrogen.

$$k_1=(2N\sigma_1^2/p)(2\pi kT/\mu)^{\frac{1}{2}}, \tag{12}$$

$$K_0=(2N\Sigma_0^2/p)(2\pi kT/\mu)^{\frac{1}{2}}, \tag{13}$$

$$H_0=2nS_0^2(2\pi kT/\mu)^{\frac{1}{2}}. \tag{14}$$

The values of k_0 and of the corresponding

TABLE II. *Constants for the quenching of mercury resonance radiation in CO and N_2.*

Gas	T°K	k_1	σ_1^2 cm^2	K_0	Σ_0^2 cm^2	H_0	S_0^2 cm^2
CO	473	3.05×10^{8}	7.40×10^{-16}	4.62×10^{4}	1.12×10^{-17}	9.17×10^{4}	1.60×10^{-16}
	773	2.60	8.06	12.4	3.85	37.1	8.29
	973	1.96	6.82	9.65	3.36	33.0	8.28
N_2	473	2.52×10^{8}	6.12×10^{-17}	4.25×10^{3}	1.03×10^{-19}	3.84×10^{4}	6.71×10^{-17}
	673	2.73	7.91	6.16	1.78	21.5	44.8
	873	2.52	8.33	6.55	2.16	20.7	49.1

TABLE III. *Values of k' and σ_0^2 in the quenching of mercury resonance radiation in CO and N_2.*

Gas	T°K	k_0	$\sigma_{0(a)}{}^2$ cm^2	$\sigma_{0(b)}{}^2$ cm^2
CO	473	4.30×10^{4}	3.49×10^{-16}	7.72×10^{-15}
	773	29.7	5.66	4.84
	973	43.6	5.68	3.62
N_2	473	3.56×10^{3}	2.89×10^{-17}	9.59×10^{-16}
	673	18.9	4.98	7.81
	873	41.6	6.39	6.24

effective cross section σ_0^2 are given in Table III. σ_0^2 is calculated from

$$k_0=(2N\sigma^2{}_{0(x)}/p)(2\pi kT/\mu)^{\frac{1}{2}}F_{(x)}. \qquad (15)$$

The two values of σ_0^2 correspond to the two values as given by (3) and (4), of F. The subscripts to σ_0^2 correspond to those of F.

In the temperature range investigated the values of all of the effective cross sections, with the exception of $\sigma^2{}_{0(b)}$, and of σ_1^2 for carbon monoxide, for energy transfer at gas collisions tend to increase somewhat with temperature. The probable process H_0, independent of the gas pressure, is considered to be the combination of a $2\,{}^3P_0$ and a $1\,{}^1S_0$ atom into an excited mercury molecule. S_0^2, corresponding to this process, has apparently a real variation with temperature for which, due to the present incomplete knowledge of the dependence upon the temperature of the rates of bimolecular reactions, no reason can yet be assigned.

Previous investigations[17] have indicated that no simple relationship exists between the dipole character and the election affinity of a gas and its quenching efficiency. The much greater quenching efficiency of carbon monoxide than of nitrogen may probably be accounted for upon the following basis.

(1) The discrepancy Δ between the amount of energy which the mercury atom gives up in the transition $2\,{}^3P_1\rightarrow2\,{}^3P_0$ and that which the gas molecule may take up as vibrational energy is smaller for carbon monoxide (+0.047 volt) than for nitrogen (+0.070 volt). Since kinetic energy must be supplied at collision, σ_1^2, as defined, intrinsically contains the factor $e^{-\Delta/kT}$. The greater variation with temperature of this factor for nitrogen than for carbon monoxide may account roughly for the difference between the variation with temperature of σ_1^2 for nitrogen and of σ_1^2 for carbon monoxide.

(2) The probability for the destruction of $2\,{}^3P_0$ atoms by collisions of the second kind with carbon monoxide is very much greater than that with nitrogen.

This explanation accounts also for the greater dependence upon the temperature of the quenching by nitrogen than of that by carbon monoxide.

Calculations have shown that the neglect of the loss of $2\,{}^3P_1$ atoms by diffusion to the walls could cause a maximum error of only 10 percent in the evaluation of the quenching constants. The random errors in this evaluation may amount to about 15 percent in the case of carbon monoxide and to about 20 percent in the case of nitrogen.

In conclusion, the authors wish to express their appreciation to Professor G. E. Uhlenbeck for his interest in the work and for his advice in the preparation of the theoretical portion of it.

[17] Mannkopf, Zeits. f. Physik **36**, 315 (1926); Stuart, reference 2; Zemansky, reference 5.

Asymmetry of Collector Currents

R. D. Rusk and A. L. Peckham, *Mount Holyoke College, South Hadley, Massachusetts*

(Received January 26, 1934)

The two unsymmetrical components of current to a collector in mercury vapor were separarely measured from the anode and the cathode directions. A collector taking current from both directions would receive the approximate sum of these unsymmetrical components. Sets of readings at different positions in an arc type of discharge show that both random electron currents and random positive ion currents are greater to the cathode face of the collector than to the anode face except in a region near the cathode where exactly the reverse is true. Determinations of space potentials and electron energies were not greatly affected by the asymmetry of the currents but determinations of electron concentrations were and the results indicate a region of maximum concentration from which positive ions and electrons may diffuse or drift in both directions. From a consideration of the rate of absorption of the primary beam a value of the mean free path is obtained and the region of maximum ionization appears at approximately this distance from the cathode.

Introduction

In several recent papers[1, 2] on the subject of measurements with collector electrodes the assumption has been stated or implied that the energy distribution of the electrons or ions is essentially isotropic. This ideal state may be approximated under certain conditions as, for example, in a uniform positive column which is shielded from the primary electrons emitted by the filament but, in general, the nature of current flow in a gas demands an essential asymmetry which may differ considerably in different regions of a discharge and which may appreciably affect collector measurements. Especially in discharges between a hot cathode and an anode not far removed, as in some recent experiments, the asymmetry may be considerable. Such a lack of symmetry may be due in part to a beam of primary electrons from the cathode, a drift of one or more groups of electons or positive ions in an electric field or diffusion of one or more groups of electrons or positive ions in the direction of a decreasing concentration gradient. The following measurements with a suitable collector give information regarding these factors.

In the present experiment, in order to study the differences between the random and drift currents in the two main directions of a discharge tube, a double collector with two plane faces separated by mica insulation was used. These two faces were kept at the same relative potential and the experimental tube was so arranged that the relative distances of the anode, cathode and collector could be continuously varied. Langmuir has used a single plane collector[3] backed with mica insulation and has found that when turned toward the cathode the current-voltage characteristic showed a marked rise due to reception of the primary beam. He also noted that when faced toward the axis of the tube the primary beam was lacking but the other groups of carriers appeared as before. An advantage of the double collector is that approximately simultaneous sets of readings for the two faces may be taken at any one collector position thus minimizing the effect of variations in the discharge.

Apparatus

The collector which was used for most of the current determinations consisted of two plane circular faces of nickel, each having an area of 9.6 mm² and a thickness of 0.15 mm. These were fixed at the end of a small bore glass tube. The mica insulation between the two faces extended beyond them in a circular ring 1 mm in width. This double probe or collector was suspended so as to be raised or lowered by a winch operating through a ground glass joint, the faces moving along the axis of the tube. Electrical connection was made to these faces by a double spiral of baked-enamel wire. The arc was maintained between an oxide coated filament[4] and the surface of a mercury column of adjustable height in a tube of 32 mm diameter. The whole was connected in the usual manner

[1] Sloane and Emeleus, Phys. Rev. **44**, 333 (1933).
[2] Druyvesteyn, Zeits. f. Physik **64**, 781 (1930).
[3] Langmuir, Phys. Rev. **26**, 592 (1925).
[4] Courtesy of Westinghouse Electric Company.

to a condensation pump and McLeod gauge and the customary electrical circuits were employed. Both collector faces were connected to the same source of variable potential, and it was so arranged that the current to either face might be measured. Varying the potential on one face while the other was kept constant did not appreciably affect currents to the other and gave results of no importance other than that the insulation between the faces could thereby be tested. As the hot filament kept the temperature of the tube somewhat higher than the temperature of the mercury surface the vapor pressure was that due to the temperature of the mercury. This temperature though not directly measured was kept uniformly close to 45°C as indicated by a thermometer inside a small insulating jacket surrounding the mercury column. The discharge was run over considerable intervals of time in order to get steady conditions and it was found possible to check results satisfactorily by repetition. The edge corrections for the collector electrode faces were omitted because they appeared to be very small and, in considering the differences between the currents to the separate faces, they would presumably cancel.

Current-Voltage Curves and Their Interpretation

Typical current-voltage characteristic curves for the two faces, which we may call the cathode face (*C.F.*) and the anode face (*A.F.*) are shown in Fig. 1 and their sum is shown by the dotted curve. These measurements were made at a distance of 10 mm from the cathode and the curves are members of a series taken at different positions with the anode 45 mm from the filament, with 10 milliamperes flowing through the arc and with fifty volts on the anode. The collector potentials were measured with respect to the center of the cathode. It is interesting to note the large difference between the potentials for which the currents to the two faces are zero. These so-called floating potentials, which an insulated collector would assume and at which it would receive zero current, are 21 volts and 47 volts for the cathode and anode faces, respectively, and 38.5 volts for a collector receiving the sum of the two currents. Differing from each other by 26 volts, only that potential indicated by the anode face is anywhere near the neighborhood of space potential. These differences decreased with increasing distance from the cathode.

The marked rise of the current-voltage characteristic for the cathode face of the collector at a little above zero potential as seen in Fig. 1

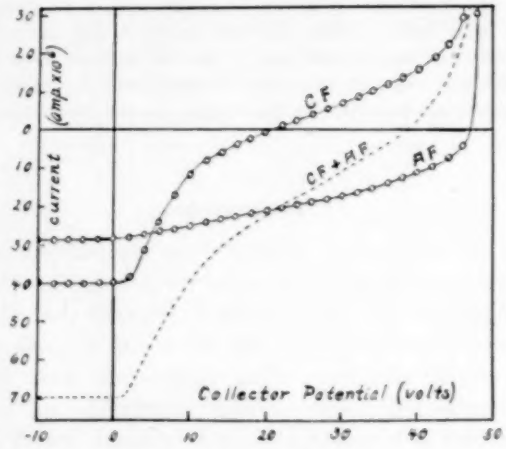

Fig. 1. Current-voltage characteristics for the two collector faces at 10 mm distance from the cathode.

indicates reception of the primary electrons from the filament. These electrons having been accelerated through the cathode fall region have sufficient energy to penetrate the sheath about the collector when the latter is in the neighborhood of fifty volts negative to space. That these primary electrons have a distribution of velocities has been noted by previous observers[5] and although the present curves show them being received over a considerable voltage range, they nevertheless represent a very definite and distinct group. The values of the current due to this group must be subtracted as corrections from current readings at higher voltages in order to obtain true current values due to scattered electron groups of lower energies. An approximate value for this correction may be obtained by taking the difference in ordinates between the prolonged adjacent branches of the curve for a mean value of the primary current. All electron current values must of course be corrected for the positive ion current and, as in the present experiment the positive ion current

[5] Langmuir and Jones, Phys. Rev. **31**, 389 (1928).

was quite constant for each curve, the electron currents could most easily be determined by simply taking the ordinate above this level.

Current-voltage characteristic curves corrected for the primary electron beam and plotted semi-logarithmically are shown in Figs. 2, 3 and 4 for three different positions in the discharge. These curves uniformly exhibit two distinct parts below space potential, the two parts having totally different slopes yet each being essentially rectilinear between the transition portions and each therefore representing an entirely different electron group.

There is little evidence for the existence of a large number of different Maxwellian electron groups and the present curves may be taken to represent two general groups of scattered electrons, one a comparatively small group scattered about a relatively high mean energy value, and the other a comparatively large group scattered about a relatively low mean energy value. The former group which is fed by the primary beam and which is in process of scattering we may call the secondary group and the latter group in which the scattering process has been largely completed we may call the slow group.

The first part of the curve in Fig. 3 showing currents to the cathode face (*C.F.*) of the collector represents secondary electrons scattered about a mean energy value of 33 volts with a concentration of 3.8×10^{7} per cc, while the

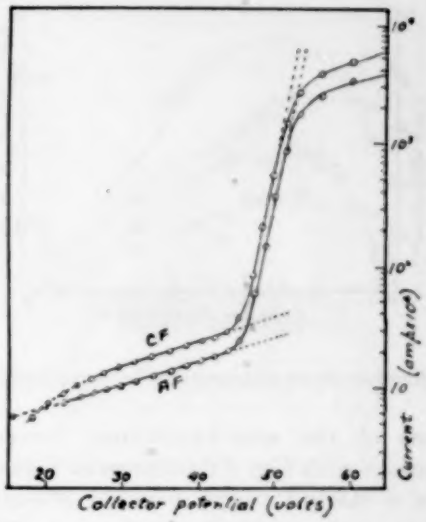

FIG. 3. Semi-logarithmic characteristics at 10 mm distance from the cathode.

second portion of the curve represents the slow group of electrons scattered about a mean energy value of 1.9 volts with a concentration of 1.1×10^{10} per cc. Similarly the curve for currents to the anode face (*A.F.*) shows the secondary electrons scattered about a mean energy value of 35 volts with a concentration of 2.6×10^{7} per cc and the slow group scattered about a mean energy value of 1.9 volts with a concentration of 0.9×10^{10} per cc. These energies are readily determined from the slopes of the straight

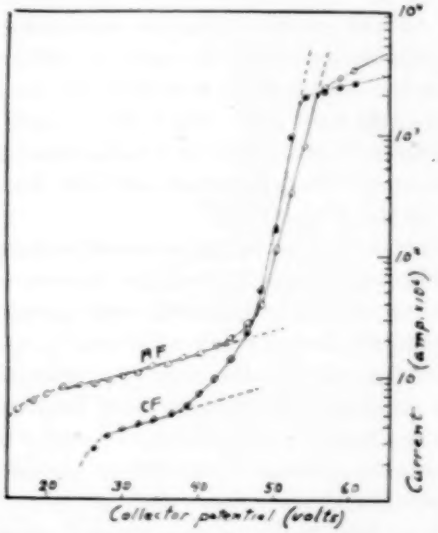

FIG. 2. Semi-logarithmic characteristics at 2.5 mm distance from the cathode.

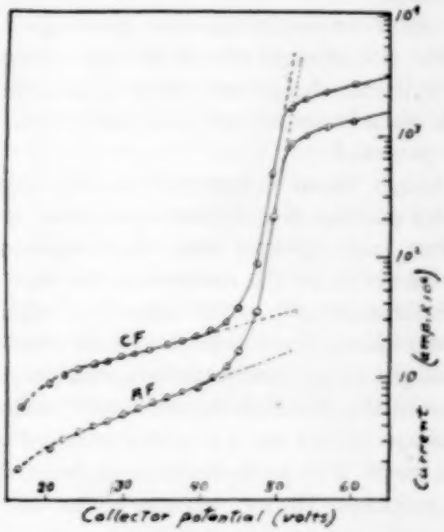

FIG. 4. Semi-logarithmic characteristics at 35 mm distance from the cathode.

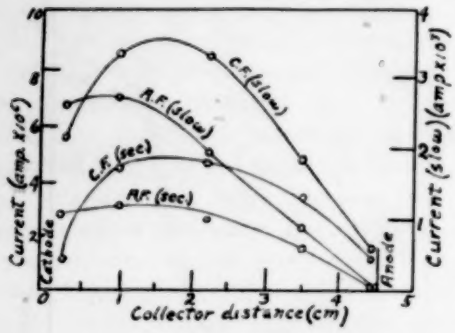

FIG. 5. Random electron currents to the two collector faces.

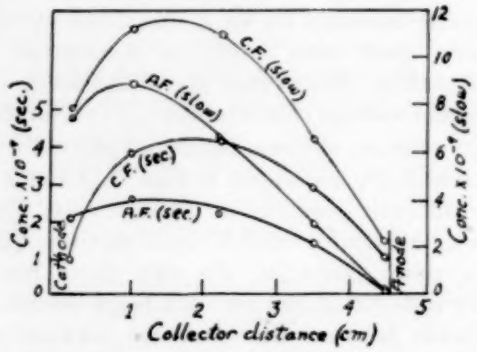

FIG. 6. Concentrations of slow electrons and secondaries.

portions of the semi-logarithmic curves.[6] In comparison with Fig. 3 the curves of Figs. 2 and 4 show a marked variation in the strengths of currents to the two collector faces at different collector positions, while the slopes of the straight portions of the curves and hence the energies are seen to vary but slightly, either for the two faces or for different positions of the collector. Nor were determinations of space potential different for the two faces by more than a fraction of a volt except very near the cathode as in Fig. 2 where the curve of currents to the cathode face became less distinctive in character as might be expected. In Fig. 2 it is also seen that near the cathode the secondary currents to the anode face are considerably greater than to the cathode face, while in the other curves the reverse is true, the difference increasing toward the anode. As the area of the collector was only about one-eightieth the cross section of the tube, it is thought that it did not appreciably disturb the discharge and there was never any visible disturbance except at several volts above space potential.

Although mean energy values for any one collector position do not show variations between the two faces greater than the experimental error, however, as the currents to the two faces vary systematically so do also the calculated concentrations. These concentrations should not be thought of as concentrations exactly at the surface of the electrode or its sheath but rather as average values for a region extending as far as the mean free path distance in front of the collector face. Hence, although the distance between the collector faces may be negligibly small, the distances between these regions may be appreciable and, as a drift due to any kind of gradient is represented by more electrons or positive ions crossing unit area in one direction than in the other per unit of time, the collector measures this drift.

Nearer the cathode where the primary beam was stronger the characteristic curve of the current to the anode face showed a slight rise similar to that of the cathode face. This was probably due to primary electrons elastically scattered but, at the same time, if the average energy of the secondary electron group is high and if the group is Maxwellian, an appreciable number of these may also reach the collector. If primary current values are read from the curve to the cathode face at potentials for which there is an appreciable secondary current as given by the current curve to the anode face, then a correction should be made by subtracting this current to the anode face from the current to the cathode face and, where the cathode and anode faces receive different intensities of secondary current, this amount should first be multiplied by the proper ratio.

In calculating the electron concentrations from the semi-logarithmic curves the current values for the secondary and slow electron groups were extrapolated to space potential and, to get the current due only to the slow electron group at space potential, corrections must be made for both the primary and secondary currents. Curves representing current values thus obtained for the secondary and slow electron groups are shown in Fig. 5. The corresponding concentrations are shown in Fig. 6.

[6] Darrow, *Electrical Phenomena in Gases*, p. 351.

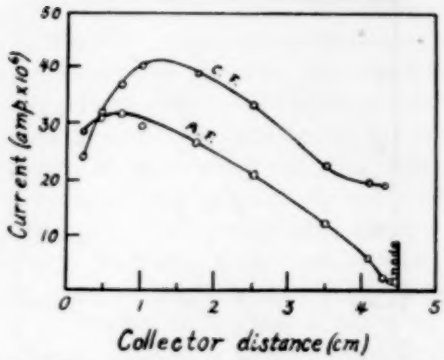

FIG. 7. Random positive ion currents to the two collector faces with an arc current of 10 m.a.

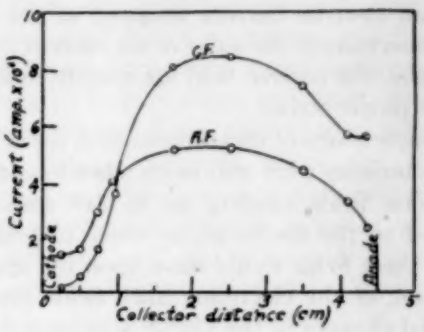

FIG. 8. Random positive ion currents to the two collector faces with an arc current of 1.0 m.a.

In Fig. 1 it is seen that the positive ion current is considerably greater to the cathode face than to the anode face. Two very simple explanations at once suggest themselves. The collector electrode may cast a "shadow," though none is visible, or else there may be a real drift of positives in the anode direction either with or against a field. The collector, of course, does intercept the primary beam and any other agency following an essentially rectilinear path from cathode to anode but if the difference in currents were due to such an effect it should increase in the direction of the cathode. However, just the opposite is true as may be seen from the data of Fig. 7 which represents random positive ion currents to the anode and cathode faces of the collector taken from a separate set of readings at nine different collector positions in which only the positive ion branch of the curve was measured in order to obtain more readily the variation with position. Indeed it is seen that in a region near the cathode the relative magnitudes of the currents to the two faces are reversed and the collector evidently measures a real drift. This reversal is even more clearly seen in the curves of Fig. 8 which were taken with one-tenth the usual current through the arc and it is especially to be noted that the point of intersection has moved farther from the cathode.

Langmuir[7] has considered the possibility, in a different type of tube, of the positive ions drifting toward the cathode thus causing more ions to strike the anode face of a spherical collector than the cathode face. Visual observations of the thickness of the sheath, however, failed to show that the effect on the sheath was significant. In the present experiment such asymmetry would be zero for the region where the two curves of Fig. 8 intersect but would increase in both directions from it. This region might be expected to correspond closely to a region of maximum concentration but it always appeared somewhat nearer to the cathode. The curves of Fig. 6 represent concentrations of both the secondary electron group and the slow group as calculated from the currents to the separate faces of the collector. All of these curves show that the concentrations attain a maximum value and though such values are not sharply marked they indicate the existence of a region of maximum ionization from which it appears that electrons and positive ions may diffuse in both directions. For a discharge with one-twentieth as much current flowing through the tube, the concentrations of the slow electron group decreased proportionately but the concentrations of the secondary group decreased much less and the energies did not change appreciably.

In a field-free space all groups would diffuse freely toward the anode from the region of maximum concentration but actual measurements under the conditions mentioned showed a reverse e.m.f. of 4 to 5 volts total between the anode and the region of maximum ionization, the gradient increasing near the anode. Electrons were therefore diffusing against this field and positive ions were moving with it. The ratio of the random electron current to the total current through the tube was greater than twenty to one in the region of maximum concentration but the

[7] Langmuir, Gen. Elec. Rev. **27**, 812 (1924).

random electron current dropped at the anode to almost exactly the value of the current through the tube, the reverse field apparently limiting it to the proper value.

Complete sets of measurements of the collector characteristics were also made when longitudinal magnetic fields ranging up to 240 gauss were applied to the discharge, in order to find what effect these fields would have upon the apparent grouping of the electrons. Such fields produced marked changes in the visible appearance of the discharge and the collector electrode cast a sharply defined visible shadow in the direction of the anode. Under such conditions the asymmetry of the collector currents was considerably changed and it became especially difficult to distinguish between electrons of the primary and secondary groups incident upon the cathode face of the collector.

In the presence of the strongest magnetic field the positive ion currents to both collector faces increased by a small amount. So also did the currents due to the slow electron group and the secondary current to the anode face of the collector. These small increases were due partly to the fact that the discharge was restricted to a smaller area of cross section by the magnetic field. On the other hand the ratio of the secondary currents to the cathode and anode faces appeared to increase by as much as four or five times, the random distribution at the cathode face being completely disturbed. Measurements in the shadow indicated, in spite of the presence of large numbers of positive ions and slow electrons, that recombination was a negligible factor in producing luminosity.

Mean Free Paths

Mean free paths for the primary electrons in a discharge have been calculated by Langmuir and Jones[8] from data obtained at varying gas pressures and fixed electrode distances and Maxwell[9] has used a movable Faraday cage for similar measurements. In the present experiment data were obtained by keeping the vapor pressure constant and varying the positions of the collector electrode. Values of the primary current

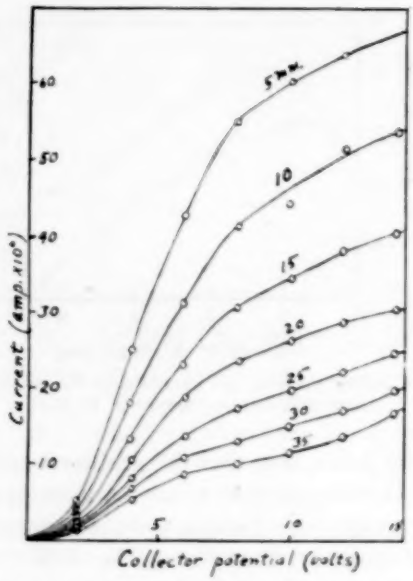

FIG. 9. Primary electron currents showing variation with energy and distance.

for which the energy loss is not too great when plotted as a function of the distance from the cathode thus give a decay curve to which the simple Langevin equation $i = i_0 e^{-(x/l)}$ may be applied and, if plotted semi-logarithmically, the points lie on a straight line. The mean free paths so obtained under present conditions ranged from extremes of 1.5 to 1.9 cm and averaged close to the kinetic theory value for 45°C. This marks the approximate distance from the cathode to the region of maximum ionization previously mentioned.

Discussion

The curves of Fig. 9 represent a separate set of current-voltage characteristics showing the rise in current due to the primary beam and its variation with electrode distance. The primary beam has a velocity distribution due in part to varying initial velocities and to the voltage drop in the filament, if to no other reason, and the current usually began to rise *sharply* at from 1 to 2 volts positive with respect to the filament although this rise might have been expected to occur at nearer zero potentials. At potentials more than 4.9 volts higher than this, the curves change rapidly in slope and the transition to

[8] Langmuir and Jones, Phys. Rev. **31**, 401 (1928).
[9] Maxwell, Proc. Nat. Acad. Sci. **12**, 509 (1926).

those portions of the curves representing the more completely scattered or secondary group becomes noticeable. Because there are several types of inelastic collisions by which the electrons may lose energy and because of the velocity distribution of the primary electrons, this transition is complex and gradual. In the secondary group electrons are continually passing from higher to lower energy states and, in view of this and the many constraints present in the tube, it is surprising that this group appears to be so near a purely random or Maxwellian distribution as is evidenced by the straightness of the semi-logarithmic plot.

In the same year that Killian[10] suggested the possibility of an excess of high speed electrons to explain effects he observed, Druyvesteyn shortly after suggested a deficiency of electrons with speeds higher than the mean as compared with a true Maxwellian distribution in order to explain the deviation of his curves from the rectilinear. This result he obtained by a double differentiation of his curves. The experimental conditions were different in the two cases but, because the mechanism for increasing energies is evidently much less effective than the mechanism for reducing energies by inelastic collisions, the latter effect in a discharge would seem more probable. Druyvesteyn's data, however, were taken with a discharge between a hot filament and anode with a quite short wire collector under conditions in which the presence of secondary and most likely primary electrons could scarcely be either avoided or corrected for. Curves similarly deviating from the rectilinear have been called the "*S*" type by Seeliger and Hirchert[11] and the deviation has been ascribed by them to impurities in the gas or on the walls of the tube.

The present authors have used a quite short unshielded wire collector near the cathode, of the type used by Druyvesteyn, and have obtained curves in mercury vapor similar to those obtained by him in argon and neon. But when the same discharge was studied with the double plane collector described above the separate electron groups became more distinctly marked. Further study with another collector, a double wire collector, the two wires nine millimeters long separated by a mica strip, gave results similar to the plane collector except for a smaller apparent primary current. Effects were also studied at different spacings of anode and cathode. So long as the spacing was sufficient for a definite positive column to form and so long as the collector was in that region the curves retained their usual character, but in a more typical glow type of discharge or with the short wire collector and with spacings of much less than the electron mean free paths, there was much less differentiation of electron groups. The electrode spacings in Druyvesteyn's experiments were not large and the curves of his Fig. 6 show considerable variation for different collector positions. It seems, in view of the type of discharge and the kind of collector used, that at least part of the curvature he obtained may have been due to the asymmetry of the discharge.

In conclusion, it appears that although energies of secondary or slow electrons vary but slightly when measured from different directions, the concentrations may differ greatly and the energy transfer per second across unit area will likewise vary. Hence energy distributions may be far from isotropic and the deviations may appreciably affect certain types of results. It also appears that, in the discharge studied, a region of maximum ionization occurs at a distance from the cathode of the order of magnitude of the mean free path for the electron, from which electrons and positive ions migrate in both directions.

[10] Killian, Phys. Rev. **35**, 1238 (1930).
[11] Seeliger and Hirchert, Ann. d. Physik **11**, 817 (1931).

The Significance of J. Clay's Ionization Depth Data in Relation to the Nature of the Primary Cosmic Radiation

W. F. G. SWANN, *Bartol Research Foundation, Swarthmore, Pennsylvania*

(Received August 11, 1934)

THE latitude and directional effects in cosmic radiation necessitate the existence of charged particles entering our atmosphere with energies greater than 10^{10} electron-volts. These particles, if of electron type, would, in passage through the atmosphere, lose but a fraction of their energy, so that they would arrive at the earth's surface with energies comparable with 10^{10} volts.

The latitude and directional effects necessitate the assumption that about 14 percent of the rays observed at sea-level are of energy greater than 10^{10} volts. On the other hand, it has been frequently asserted that cloud-chamber experiments show far fewer rays than this number with energies comparable with the amount in question.

In a former communication[1] the writer has pointed out that harmonization of the cloud-chamber experiments and the latitude and directional effects in these matters necessitates the assumption that corpuscular rays of sufficiently high energy (energy comparable to 10^{10} volts) do not ionize in the sense of producing ions at the rate of about 50 in each centimeter of their path at atmospheric pressure. It is inferred, however, that they do produce from time to time showers of secondary rays of lower energy. These showers perpetuate the directions of the non-ionizing primaries, and hand on these directional characteristics in Geiger counter experiments. They would hand them on even in cloud-chamber experiments, where, however, the secondary rays would reveal themselves only with the actual energies they possessed, i.e., with energies smaller than those of the primaries. The writer has further given theoretical reasons to substantiate the reasonableness of an absence of ordinary ionization in the case of very high energy primaries.[2] He has also pointed out[3] that the existence of such a state of affairs would result in a diminution of ionization in a vessel with increase of depth of the vessel below the surface of the medium (say water) until a depth was reached at which the primary rays had lost enough energy to bring them into the region of energy in which they could ionize. Below this depth, the observed ionization in the vessel should show an increase followed by a decrease to zero in a range comparable with that representative of the total range of ionization of the primary particles in the medium.

In a recent communication,[4] J. Clay has found, at great depths, an increase of ionization followed by a sharp decrease to zero, the whole phenomenon being in harmony with the predictions cited above. The object of the present note is to call attention to this fact and to trace its significance in somewhat greater detail. Fig. 1 represents a reproduction of Clay's curve. The ordinates represent relative values of the ionization at the depths given by the abscissae.

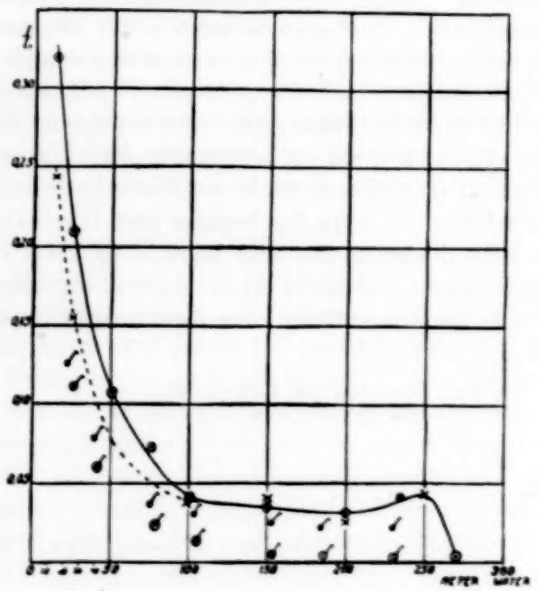

FIG. 1.

[1] W. F. G. Swann, Phys. Rev. **43**, 945 (1933).

[2] W. F. G. Swann, Phys. Rev. **44**, 943 (1933); J. Frank, Inst. **217**, 59 (1934). Also, W. F. G. Swann and A. Bramley. Phys. Rev. **41**, 393 (1932).

[3] W. F. G. Swann, Military Engineer, Vol. XXVI, No. 146, 116–120, March–April, 1934. See in particular p. 120.

[4] J. Clay, Physica **1**, 363 (1934).

It will be observed that there is a hump at 250 meters followed by a relatively sharp fall to zero at about 270 meters.

Statement of Hypothesis and Development of Consequences

For simplicity we shall consider the case of a corpuscular radiation of definite energy of such amount that the corpuscles can travel a distance L in the medium before their energy becomes reduced to the point at which ordinary ionization commences. After the energy has fallen to the region characterized by ionization, we shall suppose that the particle completes its range in a further distance l, in which distance it ionizes in the ordinary manner. For convenience we shall consider the atmosphere as compressed to a layer of the density of the medium under consideration (water), and shall picture it as lying on top of that medium, and forming part of it. We shall denote by h the distance below the surface and by θ the angle from the vertical. We shall suppose that the number of primary rays falling within the solid angle $\sin\theta d\theta d\varphi$ is

$$J = J_0 \cos^2\theta \sin\theta d\theta d\varphi,$$

$\cos^2\theta$ being the usually accepted empirical approximation to the result represented more exactly by the Gold formula, and φ being measured, of course, in the plane perpendicular to the vertical.

Consider an ionization chamber of volume V filled with gas at one atmosphere pressure. Then if q is the ionization per centimeter of path of the primary rays in the region of energy where they ionize, and if Q is the number of ions produced per second in the vessel by the primary rays, Q will be zero if $h>L+l$. Between the values of h given by $L+l$, and L the value of Q will be

$$Q_1 = 2\pi VqJ_0 \int_0^{\theta_1} \cos^2\theta \sin\theta d\theta,$$

where $\cos\theta_1 = h/(L+l)$. For $h<L$, the value of Q is

$$Q_2 = 2\pi VqJ_0 \int_{\theta_2}^{\theta_1} \cos^2\theta \sin\theta d\theta,$$

where $\cos\theta_1 = h/(L+l)$, $\cos\theta_2 = h/L$. Thus

$$Q = 0 \quad \text{for } h>L+l, \tag{1}$$

$$Q = Q_1 = \frac{2\pi}{3} VqJ_0\left[1 - \frac{h^3}{(L+l)^3}\right] \text{ for } L<h<L+l, \tag{2}$$

$$Q = Q_2 = \frac{2\pi}{3} VqJ_0\left[\frac{h^3}{L^3} - \frac{h^3}{(L+l)^3}\right] \text{ for } h<L. \tag{3}$$

We notice that for $h<L$, Q *increases* with increase of h, and proportionally to the cube. For $L<h<L+l$, Q decreases with increase of h, again in cubic fashion. The curve for Q plotted against h thus rises to a maximum (or rather to a highest value) at $h=L$, and then falls to zero at $h=L+l$. The general shape of the curve is such as is qualitatively indicated by the dotted curve of A, B, C of Fig. 2. To obtain the complete

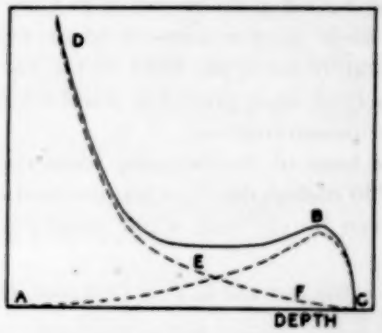

Fig. 2.

ionization in the vessel we must superpose upon this a curve which, according to our hypothesis would be produced by the showers generated by the primaries. If the rate of production of showers decreases with decrease of energy of the rays, attaining a sensibly zero value by the time the energy has reached the value at which ionization begins, we may expect to obtain a curve such as that qualitatively represented by the dotted curve D, E, F of Fig. 2. The combination of these two curves to the full curve thus gives a result similar to that shown by Clay's graph. On the basis of our hypothesis we should associate the point at 250 meters depth in Clay's curve with the point B of Fig. 2, and, the point where Clay's curve cuts the horizontal axis at 270 meters should be associated with the point C of Fig. 2. The total range of ionization would thus correspond to a path of 20 meters in water. Now according to the theoretical

curves quoted by P. M. S. Blackett and G. P. S. Occhialini,[5] as obtained from the theoretical work of Bethe,[6] the energy loss, in ionization, per centimeter of path in water for rays of the order of 10^9 volts energy and of the electron type is about 2.5×10^6 volts per centimeter of path.[7] This gives 5×10^9 volts energy loss in 20 meters of water. Anderson's experimental data on absorption lead to an energy loss of 8×10^9 volts in 20 meters of water. It is a significant fact that the calculations of A. Bramley and the writer, based on the writer's theory already cited, suggests 10^{10} as the energy at which ionization should cease. The figures are not of course intended to give more than orders of magnitude; but, viewed in this light, it is of considerable interest to note that the magnitudes 5×10^9 to 8×10^9 volts found from Clay's curve on the basis of the present ideas represents approximately an upper limit to the energies of rays observed in appreciable numbers in cloud chamber measurements.

On the basis of the foregoing ideas the ionization at 250 meters depth is representative of the value given by (2) with h put equal to L. This value is, approximately, $2\pi VqJ_0l/L$. On the other hand, the ionization which would be obtained at the surface of the medium if all of the primary rays were capable of ionizing there would be $2\pi VqJ_0/3$. Since our interpretation combined with Clay's curve gives l/L of the order of 20/280, we see that if all of the primary rays ionized at the surface of the medium, or let us say at the earth's surface, with the normal ionization efficiency, they would produce $(1/3)\times(1/14)$, i.e., about 5 times the ionization observed at 250 meters. But the ionization observed at 250 meters is only about one-twentieth of that observed at the earth's surface. Hence, it is necessary to assume that, at the earth's surface there are 20/5, i.e., 4 times as many rays as there are primaries. In other words, each ray is responsible for 4 shower rays at the earth's surface, and this number would be still further reduced if some of the surface ionization were caused by other ionization agencies, such as photons or their secondaries. The foregoing considerations render it possible that the showers concerned involve only one or two secondaries. In conclusion it may be added that we would hesitate to extend the ideas here involved in too great detail to the higher regions of the atmosphere. However, as appears from the foregoing, the main relevant facts are discussable in terms of a comparison of the ionization at the earth's surface with that at great depths.

[5] P. M. S. Blackett and G. P. S. Occhialini, Proc. Roy. Soc. **A139**, 699 (1933).

[6] Bethe, Ann. d. Physik; Zeits. f. Physik **76**, 293 (1932).

[7] Bethe's theory would of course become invalid for energies higher than those where ionization ceases; but, it would represent an approximation of the truth for lower energies.

LETTERS TO THE EDITOR

Prompt publication of brief reports of important discoveries in physics may be secured by addressing them to this department. Closing dates for this department are, for the first issue of the month, the twentieth of the preceding month; for the second issue, the fifth of the month. The Board of Editors does not hold itself responsible for the opinions expressed by the correspondents.

Negative Protons in the Nucleus?

In an attempt to construct a building-up scheme for atomic nuclei heavier than A^{38}, the writer[1] has pointed out that, in the field of A^{38}, a neutron is apparently not as stable as a configuration of mass $+1$ and charge -1. This configuration was supposed to be a neutron plus an electron. However, the possibility of its being a negative proton does not seem to be excluded, especially since there appears to be evidence[2] for the existence of such particles among the cosmic rays. Gamow[3] has mentioned the possibility that negative protons may be constituents of the nucleus. In this note, we wish to investigate the matter somewhat more in detail, and in particular to call attention to a certain regularity in the isotope pattern which may show how the negative protons become incorporated into the nucleus.

Let us consider the isotope pattern of zinc, which is more or less typical for heavy elements with even atomic number. The known isotopes have mass numbers (M) equal to 64, 66, 67, 68 and 70, respectively. The vacancy at $M=65$ is filled by Cu^{65}, and that at $M=69$ is filled by Ga^{69}. That is, if an odd mass number is vacant at the lighter end of the pattern, then there is a stable isotope of the same mass number, but with atomic number one less. If the vacancy is at the heavier end, then a stable isotope of the same mass number exists, but with atomic number greater by one. (The word "vacancy" applies only to mass numbers between the two known extremes, e.g between 64 and 70 in the above case.) An application of this rule accounts for the following isotopes: Cl^{37}, K^{39}, K^{41}, V^{51}, Mn^{55}, Co^{59}, Cu^{65}, Ga^{69}, Ga^{71}, As^{75}, Br^{79}, Br^{81}, Rb^{85}, Nb^{93}, Rh^{103}, Ag^{107}, Ag^{109}, In^{113}, In^{115}, Sb^{121}, I^{127}, Cs^{133}, Pr^{141}, Eu^{153}, Tb^{159}, Tu^{169}, Cp^{175} and Re^{185}. Assuming the general validity of the rule, one can predict the isotopes Nb^{95}, Ma^{97}, Ma^{99}, I^{125}, I^{129}, Cs^{135}, Il^{145} and Ir^{191}. Indeed, although the experimental information is still rather insufficient for definite prediction, it is not unlikely that several elements, including indium, antimony and iodine, will be found to have three odd isotopes.

On the assumption that negative protons do exist in the nucleus, we may re-formulate the above rule. According to our view, the sequence Zn^{64}, Cu^{65}, Zn^{66}, Zn^{67}, Zn^{68}, Ga^{69}, Zn^{70} may be obtained by the successive addition to Zn^{64} of a negative proton, a positive proton, a neutron, another neutron, a positive proton, and a negative proton. For a given (even) atomic number, the most stable particle of mass unity in the field of one of the lighter isotopes is either a neutron or a negative proton; the most stable one in the field of one of the heavier isotopes is either a neutron or a positive proton. For the lighter isotopes of such an element, a positive proton cannot be added until a negative proton has already been added; for the heavier isotopes, the reverse is true. It may be that we shall have to have more information about the masses of the isotopes heavier than A^{38} before the underlying reasons for the above rules become apparent.

Finally, if this model be essentially correct, one would expect the nuclear spins to be integral or half-integral according as the mass number is even or odd (and not as suggested in reference 1).

JAMES H. BARTLETT, JR.

Cambridge, England,
July 24, 1934.

[1] J. H. Bartlett, Jr., Phys. Rev. **42**, 145 (1932).
[2] E. J. Williams, Phys. Rev. **45**, 729 (1934).
[3] G. Gamow, Phys. Rev. **45**, 728 (1934).

Ruled Grating Wave-Length of the Copper $K\alpha_1$ Line

The existence of a discrepancy of about 0.25 percent between x-ray wave-lengths as measured by ruled and crystal gratings has been confirmed by many investigators. In all of the measurements in which this discrepancy has been observed the x-rays which were incident on the ruled grating were collimated by slits. In the original experiment of Compton and Doan[1] a calcite crystal and a slit were used to collimate the x-rays and separate a particular wave-length. While no great accuracy was claimed for these initial results (0.4 percent) the wave-length obtained was about 0.1 percent lower than the crystal values. Wadlund[2] using a similar arrangement in a more precise determination obtained results which agreed well with the crystal values. He estimated his error to be about 0.08 percent. Since no explanation has been given of the discrepancy between ruled and crystal grating values as found by all the other observers it was thought worth while to repeat the experiments in which a crystal and slit were used for collimating the x-rays before they fell on the ruled grating.

The disposition of the apparatus is shown in Fig. 1. The apparatus is essentially the same as that previously used[3] except the two collimating slits have been replaced by a calcite crystal and one slit. The accurate adjustment of the plateholders and the grating was accomplished exactly as previously described. The cleaved surface of

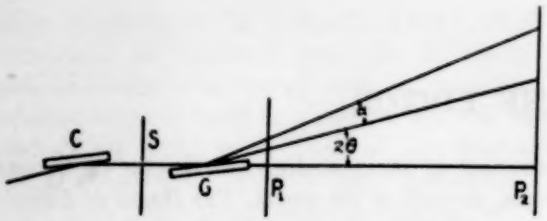

FIG. 1. Schematic diagram of apparatus. *C*, calcite crystal; *S*, slit 0.01 mm; *G*, grating ruled 143 lines per mm; P_1, P_2 photographic plates. The distance from P_1 to P_2 was 1843 mm.

the calcite crystal was placed parallel to the axis of rotation of the grating and then the slit was adjusted until the $K\alpha_1$ line from the crystal was parallel to the surface of the grating. The spectral line was made to pass over the axis of rotation of the grating by displacing the slit and x-ray tube in a horizontal plane. The crystal was then moved in a direction perpendicular to its surface until the x-rays from the most intense portion of the focal spot passed through the slit. In this adjustment only the intensity of the $K\alpha_1$ line was considered.

The grating used had 143 lines per mm and was coated with a thin layer of silver. The silver coating increased the angle of total reflection and also increased the intensity of the diffracted spectra. The direct and reflected $K\alpha_1$ line was recorded on x-ray plates placed in each plateholder. The diffracted lines were recorded only on the second plate. All of the lines were much wider than those obtained with the two-slit method of collimation. The increased width is due to the divergence of the x-ray beam reflected by the crystal which is much greater than that obtained when narrow slits are used. A representative plate is shown in Fig. 2. The separations of the lines on the plates

FIG. 2. Representative photograph. *D* is the direct beams of the α_1 and α_2 lines, *R* is the reflected α_1 line, *O* designates the first and second orders of the α_1 line.

were first measured with the plate in one direction and then remeasured with the direction of the plate reversed. On account of the width and low density of some of the lines it was difficult to make the two sets of measurements agree to better than 0.005 mm. Repeated measurements were made on most of the plates.

Since the x-rays were first reflected from a crystal, the intensity of each wave-length was reduced. This together with the dispersion introduced by the crystal decreased the intensity of the lines on the photographic plates by at least a factor of five over that obtained when slit collimation was used. The increased time of exposure made it difficult to maintain the apparatus in good adjustment and this was probably the cause of the fluctuation in the results from different plates.

The wave-length values were calculated from the equation

$$n=2d \sin [(2\theta+\alpha)/2] \sin (\alpha/2),$$

where θ is the angle between the surface of the grating and the direction of the incident beam, α is the angle between the reflected and diffracted beams, and d is the grating space. The errors introduced by the divergence of the x-rays were calculated and taken into account.

The results obtained from 27 sets of plates are shown in Table I. It will be noticed that on some plates the second order was not recorded. There is a considerable difference between the first and second order results but this probably represents the limited precision of the present results rather than indicating any dependence of the wave-length on the order of diffraction. The average of the results is in good agreement with the results that have been obtained using slits for collimating the incident x-rays. The crystal value of this wave-length was 1.5367A which is obtained from the grating constant[4] of calcite $d_{\infty}=3.02810$A. Even with the wide fluctuation of the above results not a single one came as low as the crystal value. Thus it appears that the agreement between ruled and crystal values as obtained in the previous measurements by this method was due to some consistent undetected error.

TABLE I.

Plate No.	1st Order	Weight	2nd Order	Weight
1	1.5406	4		
2	1.5437	3		
3	1.5408	4		
4	1.5410	3		
5	1.5396	3		
6	1.5401	4	1.5403	2
7	1.5428	4	1.5387	3
8	1.5438	4		
9	1.5398	4		
10	1.5424	4	1.5382	3
11	1.5406	4		
12	1.5405	4	1.5402	3
13	1.5410	3	1.5395	3
14	1.5429	3	1.5427	2
15	1.5395	1	1.5392	3
16	1.5420	3	1.5421	2
17	1.5406	3	1.5425	1
18	1.5382	1	1.5410	2
19	1.5408	2	1.5399	3
20	1.5386	2		
21	1.5400	2		
22	1.5418	2	1.5397	1
23	1.5424	1		
24	1.5432	1		
25	1.5444	1		
26	1.5425	1		
27	1.5429	1		
weighted mean	1.5413		1.5401	
	0.299%		0.221%	

P. F. GOTTLING
J. A. BEARDEN

Rowland Physical Laboratory,
Johns Hopkins University,
July 28, 1934.

[1] A. H. Compton and R. L. Doan, Proc. Nat. Acad. Sci. **11**, 598 (1925).
[2] C. P. R. Wadlund, Phys. Rev. **32**, 841 (1928).
[3] J. A. Bearden, Phys. Rev. **37**, 1210 (1931).
[4] J. A. Bearden, Phys. Rev. **38**, 2089 (1931).

Purification and Spectroscopic Evidence for He_2^3

Following the procedure outlined in a previous letter[1] deuterium was circulated through a large canal-ray discharge tube. The discharge ran at an average of 75 kv and 10 m.a. exhibiting an intense canal-ray beam which was, however, of a slightly green color due to a trace of mercury vapor which had entered the system. The discharge tube was filled twice and each time a run of 4 hours was made. After this treatment the two samples, which amounted to 5 cc at N.T.P. of deuterium and its disintegration products, were combined together and sealed off in a bulb having a magnetic break seal.

After transportation to the Massachusetts Institute of Technology it was sealed by means of the magnetic break-off to a purifying apparatus designed by one of us (W.D.U.) for the isolation of small quantities of helium. After flushing the entire apparatus with air-free oxygen the gas mixture was introduced and purified. The complete process used is described by Paneth and Peters.[2] Owing to the inaccuracy of McLeod gauge measurements with such small quantities of gas a modified Pirani-Stern manometer system developed by Paneth and Urry[3] was used to measure the quantity of helium contained in the sample.

It was found after purification that 1.1×10^{-5} cc at N.T.P. of gas remained. From the nature of the purifying process this could be only helium and neon, and the lines due to these gases were the only ones which could be observed spectroscopically. The spectroscopic examination was made with a calibrated D-77 Hilger spectrograph. The gas was compressed into a capillary tube 0.000132 sq. cm in internal cross section and the discharge was excited by means of a leak-tester in contact with an external electrode of thin copper wire wound around the gas-filled space. An estimate of the intensities of the helium and neon lines showed that the neon was present to at most ten percent of the mixture (see Paneth and Peters). The neon present was presumably of atmospheric origin and had diffused through the hot glass during sealing off from the canal-ray tube or had been driven out of the walls or metal parts of the apparatus during the bombardment process. A certain amount of ordinary atmospheric helium would be expected to be associated with this neon. As the neon-to-helium ratio in air is 18 : 5 an amount of helium equal to $0.28\times0.1\times1.1\times10^{-6}$ cc or about 3×10^{-7} cc was probably present as an impurity. No appreciable amount of helium can have been introduced during the purifying process for a control run the previous day agreed with weekly controls over a period of two years in giving only about 10^{-8} cc of neon and helium in atmospheric proportions. Atmospheric helium is therefore expected to be present to the extent of at most three percent, and neon to a maximum of ten percent; hence at least 9.6×10^{-6} cc at N.T.P. was the helium disintegration product from the deuterium reaction. Previously reported[4] results obtained with the mass-spectrograph from samples which have been subjected to the same canal-ray bombardment have shown this helium to be of mass three. None of the helium isotope of mass four has ever been found by the mass-spectrograph in these samples except when it has been deliberately admitted to the analyzing apparatus for comparison purposes. The three percent attributed to atmospheric helium in this sample is too small an amount to have been detected and identified as of mass four by the mass-spectrograph.

The quantitative agreement between the amount of helium isolated from this sample and the He^3 peak obtained with the mass-spectrograph is also satisfactory. The estimate by the latter method of the He^3 content of comparable samples varies from about 10^{-4} to 10^{-5} cc at N.T.P. depending on the discharge conditions. Because of the trace of mercury vapor present in the discharge from which this helium was isolated there is reason to believe that the discharge conditions were not the optimum ones. As it has not as yet been possible to measure the number of D-D collisions during a run no quantitative estimate of the yield can be given, though it is certainly very large.

In an attempt to remove the helium from the purifying system the specimen was lost. It is hoped that with future samples the mass may be further verified by a thermal-conductivity method and the spectroscopic characteristics such as fine structure and isotopic shift studied. We are indebted to the Princeton Department of Chemistry for supplying us with the deuterium used.

G. P. Harnwell
H. D. Smyth

Palmer Physical Laboratory,
Princeton, N. J.

Wm. D. Urry

Research Laboratory of Physical Chemistry,
Massachusetts Institute of Technology,
Cambridge, Mass.

August 11, 1934.

[1] Harnwell, Smyth, Van Voorhis and Kuper, Phys. Rev. **45**, 655 (1934).
[2] Paneth and Peters, Zeits. f. physik. Chemie **134**, 353 (1928).
[3] Paneth and Urry, Zeits. f. physik. Chemie **152**, 110 (1931).
[4] Bleakney, Harnwell, Lozier, Smith and Smyth, Phys. Rev. **46**, 81 (1934).

The Production of Radioactive Oxygen

Since the preliminary report[1] from this laboratory on the radioactivity induced in certain substances by deuton bombardment, the apparatus has been changed so as to bring the ion beam outside the apparatus through a thin aluminum window. Both solid and gaseous targets can be exposed to the beam, and then removed to a quartz-fiber electroscope for measurement of the induced activity. For these experiments 1 microampere of 2 million-volt deutons was used.

With this arrangement, carbon and aluminum targets were bombarded and found to give the activities already reported.[1] When a carefully cleaned platinum target was bombarded in air, a much smaller but accurately measurable positron activity with a half-life of 126 ± 5 sec. was observed. Both clean and oxidized copper targets gave the same effect. When the target was bombarded in N_2 gas the same activity was found, but it was not present when O_2, H_2 or A were used. In CO_2 an activity of the same

magnitude was observed, decaying with the characteristic 10 minute half-life of deuton activated carbon.

It is apparent that these effects are due to atoms of the gas, activated in the space between the window and the target and driven onto the target by recoil. This interpretation is supported by the observation of an activity with a period characteristic of the aluminum in the window when the space was evacuated. To show more conclusively that nitrogen is responsible for this 126 second activity, nitrogen gas was bombarded, transferred to a bulb, and its gamma-ray (positron annihilation) activity measured. From an empirical calibration of the chamber for gamma-rays, this experiment showed that approximately 1 nitrogen atom is activated per million incident deutons.

A solid KNO_3 target did not show the expected large effect, probably because the active oxygen is not tightly held in the nitrate lattice, as it is in platinum.

A chemical separation showed that the active constituent is oxygen. The N_2 gas was activated, mixed with some O_2 and an excess of H_2 and passed over heated platinized asbestos. The oxygen, present as NO_2, N_2O or O_2, was reduced to H_2O and collected in a $CaCl_2$ drying tube, the residual gases being collected in a previously evacuated bulb. The active constituent was found to go entirely into the drying tube. In a check run with the platinized asbestos cold the activity went into the collecting bulb. The probable nuclear reactions are:

$$ {}_7N^{14}+{}_1H^2-{}_8O^{15}+{}_0n^1 \qquad (1) $$

$$ {}_8O^{15}-{}_7N^{15}+{}_1e^+. \qquad (2) $$

The neutrons given by reaction (1) were found to be produced in the activating process in about the expected numbers. The maximum energy of the positrons from the radioactive process (2) estimated from their absorption in aluminum, is about 1.7 million volts.

M. Stanley Livingston
Edwin McMillan

Radiation Laboratory,
Department of Physics,
University of California,
Berkeley, California,
August 1, 1934.

[1] Henderson, Livingston and Lawrence, Phys. Rev. **45**, 428 (1934).

The Annihilation of the Proton

The experiments of Anderson, Millikan, Neddermeyer and Pickering[1] and Gilbert[2] on the production of showers indicates that the immediate cause of the spray of negative and positive electrons observed in cloud photographs of the showers are gamma-rays. The high energy gamma-rays on striking a nuclear field lose their energy by generating a number of high energy pairs, negative and positive electrons. The origin of these hard gamma-rays is obscure. Experiments indicate that these high energy photons are probably not produced by electrons impinging on the nucleus. There then remains the possibility that their formation arises from the annihilation of matter, in a somewhat similar way to that suggested by Jeans[3] in his paper on the origin of cosmic rays. We shall give in this note an approximate expression for the probability $P(\eta)$ of the following process. A high energy proton strikes a nuclear Coulomb field of atomic number Z and is converted into a gamma-ray and a positive electron of energy ηc.

In treating this problem we have followed the method suggested by Fermi for the analysis of the beta-ray problem. We shall suppose that the wave function μ of the proton is changed into the wave function ϕ of a neutral particle and at the same time a positron and a photon of energy $h\nu$ appear in the field. According to Heisenberg we should consider the proton and the neutral particle as two separate states of the particle described through an inner coordinate ρ:

$\rho=+1$ for the neutral particle,
$\rho=-1$ for the proton.

The passage from the proton to the neutral particle is determined through the operators $Q=\begin{vmatrix}0 & 1\\ 0 & 0\end{vmatrix}$ and $Q^*=\begin{vmatrix}0 & 0\\ 1 & 0\end{vmatrix}$ which operate on the coordinate ρ appearing in the Hamiltonian of the proton and the neutral particle. The Hamiltonian function for the problem is composed of three terms, the energy H_1 of the proton and neutral particle, the energy H_2 of the photon and positron and finally the coupling energy between the two sets of particles, H_3.

$$ H_1=(1+\rho)N/2+(1-\rho)P/2, $$

where N and P are the energy operators for the neutral particle and proton, respectively. The wave functions for the positron in the central field Ze are designated by the symbol ψ_ν. In carrying out the calculations, the vector potential a of the radiation field is analyzed into a system of plane waves $a=\Sigma_i q^i a_i$. We shall assume, following Fermi, that the coupling term is effective only at small distances and can be represented by the expression

$$ H_3=g\{Q\psi(x)\phi(x)+Q^*\psi(x)\phi(x)\}-e(\alpha a), $$

where the coordinates of the proton and neutral particle are taken at the position of the proton. If the proton changes into a neutron and positron the neutron represents one of the neutral particles but if the mass of the proton is annihilated we shall assume the neutral particle is a neutrino. We have attempted in this way to give a mathematical description of a process which we recognize may be only crudely represented by such a mechanism. In the annihilation problem the failure of the conservation laws will be taken care of by the energy given to the neutrino.

On the basis of calculations performed with this Hamiltonian, we have arrived at the following results. The positrons are distributed in energy near their maximum energy $\eta_0 c$ according to a law very similar to that with which we are familiar in beta-particle emission from radioactive nuclei in the same region. The total probability of annihilation per nucleus $P=\int_0^{\eta_0} P(\eta)d\eta$, where $\eta_0 c$ is the maximum energy possible for the positron, varies as $(\eta_0)^5$ and is practically independent of the atomic number of the nucleus with which it collides.

The accuracy of these results is limited by a number of considerations: (1) the field of the nucleus is not represented by a Coulomb field for all distances; (2) the wave functions for the nucleus is unknown; (3) the interaction of the positron and neutrino has been taken in a form similar to that given by Fermi in his treatment of the beta-ray spectrum. All these difficulties appear in the current theories of the beta-ray spectrum of the radioactive elements;[4] and finally (4) the change of a proton into a positron and neutrino is taken as the representation of the annihilation of the proton. Processes in which there is such a large change in mass occur may possibly not be represented by such simple quantum mechanical considerations. However, the agreement of the theory with experiment in the case of the beta-ray spectrum makes us hopeful that this theory of the annihilation of the proton may fairly well represent the facts.

According to these ideas, part of the primary cosmic rays are protons which on striking the outer atmosphere are converted in the majority of cases into a photon and a positron. Until the proton strikes a nucleus and is converted into a photon and a positron, it loses its energy gradually by primary ionization along its path. As we have mentioned, the probability of this type of collision in which there occurs the annihilation of the mass of the proton, is proportional per nucleus to the fifth power of the maximum energy possible for the positron but is independent of the atomic number of the nucleus with which it makes the collision. The secondary gamma-rays produced in this collision and which are responsible for the showers should be absorbed per nucleus proportionally to the square of the atomic number of the nuclei in the medium in which the showers are produced. However, the rate of absorption of these gamma-rays should be independent of their energy.[5] The observations of Kunze[6] on the rate of ionization of the high energy particles in cosmic rays support the view that these particles are protons.

ARTHUR BRAMLEY

Bartol Research Foundation
of the Franklin Institute,
August 12, 1934.

[1] Anderson, Millikan, Neddermeyer and Pickering, Phys. Rev. **45**, 352 (1934).
[2] Gilbert, Proc. Roy. Soc. **A144**, 559 (1934).
[3] Jeans, Nature **116**, 861 (1925).
[4] Fermi, Zeits. f. Physik **88**, 161 (1934); Bramley, Phys. Rev. **45**, 901 (1934); Tamm, Nature **133**, 981 (1934); Iwanenko, Nature **133**, 981 (1934).
[5] Oppenheimer and Plesset, Phys. Rev. **44**, 53 (1933).
[6] Kunze, Zeits. f. Physik **83**, 1 (1933); Williams, Phys. Rev. **45**, 729 (1934).

A Second-Order Calculation of He I $2s2p\ ^{1,3}P$

Lennard-Jones[1] gives the following formula for the energy of a perturbed system:

$$E_k=\epsilon_k+A_{kk}+\frac{1}{\epsilon_k}\int\psi_k v^2\psi_k d\tau-\frac{1}{\epsilon_k}A_{kk}^2+\sum_{j\neq k}\frac{\epsilon_j A_{kj}^2}{\epsilon_k(\epsilon_k-\epsilon_j)} \quad (1)$$

where ϵ_k is the zero-order energy and ψ_k the corresponding wave function, $A_{kk}=\int\psi_k v\psi_k d\tau$ is the first-order correction to the energy ($=e^2/r_{12}$ in the present application) being the perturbing potential, $A_{kj}=\int\psi_k v\psi_j d\tau$, and the series extends over all discrete and continuous states of the system. It is to be expected that the series will be small for discrete states far beyond the first ionization limit ($E_k\ll 0$) since the greatest contributions to the summand will come from neighboring portions of the continuum, which will give approximately equal positive and negative values. For low states, the series will not be negligible, (cf. Table I) since most of its terms will then have the same sign, i.e., positive in (1). The series has been neglected in the present calculations.

TABLE I.

Term (cm $^{-1}$)	(calc)	(obs[2])	(obs[3, 7])	(obs[4])	(calc[4])
$1s2p\ ^1P$	21944	27176			
^3P	26114	29224			
$2s2p\ ^1P$	−288350				−296118
^3P	−269807		−273663	−296859	−274526

The application of (1) to He I $1s2p\ ^{1,3}P$ and $2s2p\ ^{1,3}P$ gives the four term-values of Table I, second column. The next two columns show the experimental values for $1s2p$ and a possible experimental value for $2s2p\ ^3P$. The fourth column gives Hylleraas' value for the latter term, derived on an assumption which he himself discredits. The last column presents recent theoretical results of Fender and Vinti; the relative reliability of the latter and the present results cannot be estimated until the publication of the details of their procedure, and especially their approximate orthogonalizing of the wave functions for $2s2p$ to those of all lower states, discrete and continuous.

An interesting point arises concerning the choice of the zero of energy in the Lennard-Jones formula (1): an arbitrary constant C can be added to E_k and ϵ_k. The effect of C is, ultimately, to change the respective values of the last three of the five terms on the right of (1), while, of course, leaving their sum invariant. For $C\to\infty$, (1) becomes the usual formula for the second-order energy. For a certain C_0, the series vanishes; but unfortunately the problem of finding C_0 turns out to be equivalent to that of evaluating the series in (1).

It may not be out of place here to point out that two lines, λλ320.392 and 322.517A in the He spectrum as measured by Kruger,[7] (which are identified by him as He I $1s2p\ ^3P-2p^2\ ^3P$ and $1s2p\ ^1P-2p^2\ ^1D$) have the wave-number separation of He I $1s2p\ ^{1,3}P$.

WILLOUGHBY M. CADY*

California Institute of Technology,
August 9, 1934.

[1] J. E. Lennard-Jones, Proc. Roy. Soc. **A129**, 598 (1930).
[2] Bacher and Goudsmit, *Atomic Energy States*, p. 220.
[3] K. T. Compton and J. C. Boyce, J. Frank. Inst. **205**, 497 (1928).
[4] E. Hylleraas, Zeits. f. Physik **69**, 361 (1931).
[5] F. G. Fender and J. P. Vinti, Phys. Rev. **46**, 77 (1934).
[6] A. H. Rosenthal, Zeits. f. Astrophys. **1**, 115 (1930).
[7] P. G. Kruger, Phys. Rev. **36**, 855 (1930).
* National Research Fellow.